

Multi-modal Energy Consumption Modeling and Eco-routing System Development

Jinghui Wang

Dissertation submitted to the Faculty of the
Virginia Polytechnic Institute and State University
in partial fulfillment of the requirements for the degree of

Doctor of Philosophy
in
Civil Engineering

Hesham A. Rakha, Chair
Linsey C. Marr
Pamela Murray-Tuite
Ihab El-Shawarby

June 8, 2017
Blacksburg, Virginia

Keywords: Multi-modal, Eco-routing, Energy Consumption, Greenhouse Gas Emissions,
Vehicle Specific Power, Intelligent Transportation System, Advanced Traveler Information
System

Copyright©2017, Jinghui Wang

Multi-modal Energy Consumption Modeling and Eco-routing System Development

Jinghui Wang

ABSTRACT

A door-to-door trip may involve multiple traffic modes. For example, travelers may drive to a subway station and make a transfer to rail transit; alternatively, people may also start their trips by walking/cycling to a bus/subway station and then take transit in most of the trip. A successful eco-route planning thus should be able to cover multiple traffic modes and offer intermodal routing suggestions. Developing such a system requires to address extensive concerns. The dissertation is a building block of the multi-modal energy-efficient routing system which is being developed and tested in the simulation environment before real applications. Four submodules have been developed in the dissertation as partial fulfillment of the simulation-based system: energy consumption modeling, subway system development, on-road vehicles dynamic eco-routing, and information effect on route choice behavior. Other submodules such as pedestrian/bicycle modeling will be studied in the future.

Towards the research goal, the dissertation first develops fuel consumption models for on-road vehicles. Given that gasoline light duty vehicles (LDVs) and electric vehicles were modeled in previous studies, the research effort mainly focuses on heavy duty vehicles (HDVs). Specifically, heavy duty diesel trucks (HDDTs) as well as diesel and hybrid-electric transit buses are modeled. The models are developed based on the Virginia Tech Comprehensive Power-based Fuel consumption Modeling (VT-CPFM) framework. The results demonstrate that the model estimates are highly consistent with field observations as well as the estimates of the Comprehensive Modal Emissions Model (CMEM) and MOtor Vehicle Emissions Simulator (MOVES). It is also found that the optimum fuel economy cruise speed ranges between 32 and 52 *km/h* for the tested trucks and between 39 and 47 *km/h* for the tested buses on grades varying from 0% to 8%, which is significantly lower than LDVs (60-80 *km/h*).

The dissertation then models electric train dynamics and energy consumption in support of subway simulation system development and trip energy estimation. The dynamics model varies throttle and brake level with running speed rather than assuming constants as was done by previous studies, and the energy consumption model considers instantaneous energy regeneration. Both models can be easily calibrated using non-engine data and implemented in simulation systems and eco-transit applications. The results of the dynamics modeling demonstrate that the proposed model can adequately capture instantaneous acceleration/deceleration behavior and thus produce realistic train trajectories. The results of the energy

consumption modeling demonstrate that the model produces the estimates consistent with the National Transit Database (NTD) results, and is applicable for project-level analysis given its ability in capturing the energy consumption differences associated with train, route and operational characteristics.

The most suitable simulation testbed for system development is then identified. The dissertation investigates four state-of-the-art microsimulation models (INTEGRATION, VISSIM, AIMSUM, PARAMICS). Given that the car-following model within a micro-simulator controls longitudinal vehicle motion and thus determines the resulting vehicle trajectories, the research effort mainly focuses on the performance of the built-in car-following models from the energy and environmental perspective. The vehicle specific power (VSP) distributions resulting from each of the car-following models are compared to the field observations. The results demonstrate that the Rakha-Pasumathy-Adjerid (RPA) model (implemented in the INTEGRATION software) outperforms the Gipps (AIMSUM), Fritzsche (PARAMICS) and Wiedemann (VISSIM) models in generating accurate VSP distributions and fuel consumption and emission estimates. This demonstrates the advantage of the INTEGRATION model over the other three simulation models for energy and environmental analysis.

A new eco-routing model, comprehensively considering microscopic characteristics, is then developed, followed by a numerical experiment to test the benefit of the model. With the resulting eco-routing model, an on-road vehicle dynamic eco-routing system is constructed for in-vehicle navigation applications, and tested for different congestion levels. The results of the study demonstrate that the proposed eco-routing model is able to generate reasonable routing suggestions based on real-time information while at the same time differentiate eco-routes between vehicle models. It is also found that the proposed dynamic eco-routing system achieves lower network-wide energy consumption levels compared to the traditional eco-routing and travel time routing at all tested congestion levels. The results also demonstrate that the conventional fuel savings relative to the travel time routing decrease with the increasing congestion level; however, the electric power savings do not monotonically vary with congestion level. Furthermore, the energy savings relative to the traditional eco-routing are also not monotonically related to congestion level. In addition, network configuration is demonstrated to significantly affect eco-routing benefits.

The dissertation finally investigates the potential to influence driver behavior by studying the impact of information on route choice behavior based on a real world experiment. The results of the experiment demonstrate that the effectiveness of information in routing rationality depends upon the traveler's age, preferences, route characteristics, and information type. Specifically, information effect is less evident for elder travelers. Also, the provided information may not be contributing if travelers value other considerations or one route significantly outperforms the others. The results also demonstrate that, when travelers have limited experiences, strict information is more effective than variability information, and that the faster less reliable route is more attractive than the slower more reliable route; yet the difference becomes insignificant with experiences accumulation. The results of the study will be used to enhance system design through considering route choice incentives.

Multi-modal Energy Consumption Modeling and Eco-routing System Development

Jinghui Wang

GENERAL AUDIENCE ABSTRACT

A door-to-door trip may involve multiple traffic modes. For example, travelers may drive to a subway station and make a transfer to rail transit; alternatively, people may also start their trips by walking/cycling to a bus/subway station and then take transit in most of the trip. A successful eco-route planning thus should be able to cover multiple traffic modes and offer intermodal routing suggestions. Developing such a system requires to address extensive concerns. The dissertation is a building block of the multi-modal energy-efficient routing system which is being developed and tested in the simulation environment before real applications. Four submodules have been developed in the dissertation as partial fulfillment of the simulation-based system: energy consumption modeling, subway system development, on-road vehicles dynamic eco-routing, and information effect on route choice behavior. Other submodules such as pedestrian/bicycle modeling will be studied in the future.

Towards the research goal, the dissertation first develops fuel consumption models for on-road vehicles. Given that gasoline light duty vehicles (LDVs) and electric vehicles were modeled in previous studies, the research effort mainly focuses on heavy duty vehicles (HDVs) including heavy duty diesel trucks (HDDTs) as well as diesel and hybrid-electric transit buses. The model estimates are demonstrated to provide a good fit to field data.

The dissertation then models electric train dynamics and energy consumption in support of subway simulation system development and trip energy estimation. The proposed dynamics model is able to produce realistic acceleration behavior, and the proposed energy consumption model can provide robust energy estimates that are consistent with field data. Both models can be calibrated without mechanical data and thus easily implemented in complex frameworks such as simulation systems and eco-transit applications.

The most suitable simulation testbed for system development is then identified. The dissertation investigates four state-of-the-art microsimulation models (INTEGRATION, VIS-SIM, AIMSUM, PARAMICS). The results demonstrate that INTEGRATION outperforms the other three simulation models for energy and environmental analysis. Also, INTEGRATION is able to generate measures of effectiveness (MOEs) for electric vehicles, which makes it more competitive than the state-of-the-art counterpart.

A dynamic eco-routing system is then developed in the INTEGRATION simulation environ-

ment. The built-in eco-routing model of the system comprehensively considers microscopic characteristics and is demonstrated to generate reasonable routing solutions based on real-time information while at the same time differentiate vehicle models. The system is able to provide routing suggestions for both conventional gasoline/diesel and electric vehicles. The testing results demonstrate that the proposed eco-routing system achieves network-wide energy savings compared to the traditional eco-routing and travel time routing at all tested congestion levels. Also, network configuration is demonstrated to significantly affect eco-routing benefits.

The dissertation finally investigates the potential to influence driver behavior by studying the impact of information on route choice behavior based on a real world experiment. The results of the experiment demonstrate that the effectiveness of information in routing rationality depends upon the traveler's age, preferences, route characteristics, and information type. Specifically, information effect is less evident for elder travelers. Also, the provided information may not be contributing if travelers value other considerations or one route significantly outperforms the others. The results also demonstrate that, when travelers have limited experiences, strict information is more effective than variability information, and that the faster less reliable route is more attractive than the slower more reliable route; yet the difference becomes insignificant with experiences accumulation. The results of the study will be used to enhance system design through considering route choice incentives.

Acknowledgements

With my heart full of gratitude, I would like to give most special thanks to my advisor, Dr. Hesham A. Rakha, for his contribution to my dissertation and continuous financial support during my Ph.D. study. Dr. Rakha has always been encouraging me not only in academic research but also in career planning. Without his assistance, I would not have made the level of achievements that I have made today. He is a highly respectful advisor with excellent professional experiences and great academic accomplishments which I want to achieve in the future. I have learned a lot from his knowledge and attitude of facing life. I also would like to thank my advisory committee members, Dr. Linsey C. Marr, Dr. Ihab El-Shawarby, Dr. Pamela Murray-Tuite, for their invaluable advice and recommendations. Special thanks go to my colleagues, Ahmed Elbery, Karim Fadhloun, and Mariska van Essen for their contributions to my dissertation.

I would like to thank other colleagues, Dr. Jianhe Du, Dr. Hao Yang, Dr. Hao Chen, Boon Teck Ong, Mohamed Abdelmegeed, Ran Tu, Arash Jahangiri, Raj Kishore Kamalanathsharma and many others, for their friendship. It was a great pleasure to work with all of you. I also want to thank all of the projects and funding sponsors that support my dissertation work, such as the Mid-Atlantic Universities Transportation Center (MAUTC), Department of Energy ARPA-E Program, the TranLIVE University Transportation Center.

Finally, I would like to thank my parents for their endless love and support throughout my life. Their understanding and encouragement nourish my success.

Contents

List of Figures	x
List of Tables	xii
1 Introduction	1
1.1 Problem Statement	2
1.1.1 Energy Consumption Modeling	3
1.1.2 Subway System Modeling	3
1.1.3 Microsimulation Testbed	4
1.1.4 Eco-routing Study for In-vehicle Applications	4
1.1.5 Effect of Route Information on Route Choice Behavior	5
1.1.6 Conclusions	6
1.2 Research Scope	6
1.3 Research Objectives	7
1.4 Research Contributions	7
1.5 Dissertation Layout	8
2 Literature Review	11
2.1 Energy Consumption and Emission Modeling	11
2.1.1 Conventional Gasoline and Diesel Vehicle	11
2.1.2 Plug-in Electric Vehicle	14
2.1.3 Electric Train	15
2.2 Railway Simulation and Dynamics Modeling	17
2.3 Traffic Microscopic Simulation Models	20
2.4 Eco-routing Systems	22
2.5 Effect of Route Information on Route Choice Behavior	24
2.6 Summary	26
3 Heavy Duty Diesel Vehicles Fuel Consumption Modeling	29
3.1 Introduction	30
3.2 Modeling Framework	30
3.3 Heavy Duty Diesel Truck Fuel Consumption Modeling	31
3.3.1 Data Preparation	32
3.3.2 Model Development	33

3.3.3	Model Validation	42
3.4	Diesel and Hybrid-Electric Bus Fuel Consumption Modeling	46
3.4.1	Data Preparation	46
3.4.2	Model Development	46
3.4.3	Model Validation	54
3.5	Conclusions	56
4	Electric Train Dynamics and Energy Consumption Modeling	57
4.1	Introduction	57
4.2	Dynamics Modeling	58
4.2.1	Fadhloun-Rakha Traction Dynamics Model	58
4.2.2	Hay Brake Dynamics Model	60
4.2.3	Proposed Dynamics Model	60
4.2.3.1	Acceleration Modeling Approach	61
4.2.3.2	Resistance Force Module	62
4.2.3.3	Throttle Discretization Procedure	62
4.2.3.4	Deceleration Modeling Approach	62
4.2.4	Data Preparation	65
4.2.5	Model Calibration	67
4.2.5.1	Acceleration Model Calibration	67
4.2.5.2	Deceleration Model Calibration	68
4.2.6	Model Validation	68
4.2.6.1	Acceleration Modeling Results	69
4.2.6.2	Deceleration Modeling Results	70
4.2.7	Simulation Test	70
4.3	Energy Consumption Modeling	73
4.3.1	Tractive Power and Tractive Effort	73
4.3.2	Starting Tractive Effort	75
4.3.3	Regenerative Braking Efficiency	76
4.3.4	Model Calibration	76
4.3.5	Model Validation	81
4.3.6	Discussion of Modeling Results	84
4.4	Conclusions	87
5	Comparison of car-following Models: An Energy and Environmental Perspective	89
5.1	Introduction	89
5.2	State-of-the-practice Car-following Models	90
5.2.1	Wiedemann Model	91
5.2.2	Gipps Model	93
5.2.3	Fritzsche Model	94
5.2.4	Rakha-Pasumarthy-Adjerid Model	95

5.3	Test Scenario	98
5.3.1	Field Data Preparation	99
5.3.2	Numerical Simulation	99
5.3.3	Comparison of VSP Distribution and Vehicle Dynamics	100
5.4	Results for VSP Distribution and Vehicle Dynamics	102
5.4.1	VSP Distribution	102
5.4.2	Acceleration Behavior	102
5.4.3	Root Mean Square Error	104
5.5	Fuel Consumption and Emissions	106
5.6	Discussion	111
5.7	Conclusions	112
6	Eco-routing Formulation and System Development for On-board Navigation Applications	115
6.1	Link Cost Function	115
6.2	Eco-routing Model	119
6.3	Numerical Experiment	120
6.3.1	Sample Network	120
6.3.2	Test Scenario	122
6.3.3	Results Analysis	123
6.4	Dynamic Eco-routing System	126
6.4.1	INTEGRATION Framework for Traffic Assignment	127
6.4.2	System Architecture	128
6.4.3	System Testing	131
6.4.3.1	System Testing in Sample Network	131
6.4.3.2	System Testing in Real World Network	134
6.5	Conclusions	141
7	Effect of Dynamic Route Information on Driver Route Choice Behavior	143
7.1	Experimental Design	143
7.2	Results Analysis	145
7.3	Conclusions	151
8	Conclusions and Recommendations for Further Research	154
8.1	Dissertation Conclusions	154
8.2	Recommendations for Further Research	157
	Bibliography	159

List of Figures

Figure 3.1	Vehicle power vs. fuel consumption functional form (truck)	34
Figure 3.2	Fuel consumption vs. cruise speed at different grade levels (truck concave model)	35
Figure 3.3	Impacts of vehicle weight on the optimum fuel economy cruise speed at different grade levels (truck concave model)	36
Figure 3.4	Model performance vs. order of magnitude of the second-order parameter (truck model)	38
Figure 3.5	Fuel consumption vs. cruise speed at different grade levels (truck convex model)	39
Figure 3.6	Impacts of road grade on the optimum fuel economy cruise speed (truck convex model)	40
Figure 3.7	Impacts of vehicle weight on the optimum fuel economy cruise speed at different grade levels (truck convex model)	41
Figure 3.8	Instantaneous truck model validation	43
Figure 3.9	Impact of cruise speed on truck fuel consumption levels: VT-CPFM vs. CMEM	44
Figure 3.10	CO ₂ estimation using fuel consumption rate (HDDT 1)	45
Figure 3.11	Model performance vs. order of magnitude of the second-order parameter (bus model)	49
Figure 3.12	Fuel consumption vs. cruise speed at different grade levels (bus model)	51
Figure 3.13	Impacts of road grade on the optimum fuel economy cruise speed (bus model)	52
Figure 3.14	Impacts of vehicle weight on the optimum fuel economy cruise speed at different grade levels (bus model)	53
Figure 3.15	Impact of cruise speed on fuel consumption levels: a. conventional diesel bus; b. hybrid-electric bus	55
Figure 4.1	Variation of throttle level as a function of speed	59
Figure 4.2	Dynamic brake characteristics	61
Figure 4.3	Piecewise feature of braking dynamics	64
Figure 4.4	The driving cycle for the MAX Blue Line	66
Figure 4.5	Instantaneous model validation (acceleration)	69

Figure 4.6	Model evaluation: acceleration versus speed and acceleration versus distance	70
Figure 4.7	Instantaneous model validation (deceleration)	71
Figure 4.8	Model evaluation: deceleration versus speed and deceleration versus distance	71
Figure 4.9	Instantaneous simulation test	72
Figure 4.10	A simplified representation of the MAX light rail traction system . .	77
Figure 4.11	Portland MAX light rail vehicle	78
Figure 4.12	Regenerative braking efficiency varies as a function of the deceleration level	82
Figure 4.13	The driving cycle for the Chicago Brown line	83
Figure 4.14	Chicago Brown Line: speed and electric power on the entire cycle . .	85
Figure 4.15	Instantaneous acceleration levels	87
Figure 5.1	Regime of car-following models	93
Figure 5.2	Desired speed distribution	100
Figure 5.3	Comparison of VSP and acceleration distributions: (a) VSP distribution and (b) Acceleration distribution	103
Figure 5.4	Maximum acceleration behavior (m/s^2)	105
Figure 5.5	Root mean square error	106
Figure 5.6	Relative difference of VSP distribution RMSE between RPA and other car-following models	107
Figure 5.7	Root mean square error (after model calibration)	112
Figure 5.8	Maximum acceleration behavior (m/s^2)(after model calibration) . . .	113
Figure 6.1	Comparison of vehicle power between vehicle models	117
Figure 6.2	A sample network	121
Figure 6.3	INTEGRATION framework for the dynamic eco-routing system . . .	130
Figure 6.4	QNET sample network configuration	131
Figure 6.5	Doha network configuration	136
Figure 6.6	Electric energy consumption vs. cruise speed	139
Figure 7.1	Logical- and inertial- choice rates over trials.	147
Figure 7.2	Participants choice patterns without vs. with route information. . . .	148
Figure 7.3	Logical- and inertial- choice rates over participants.	149
Figure 7.4	Logical- and inertial- choice rates over trips	150
Figure 7.5	Choice rates with strict information vs. with range information . . .	151
Figure 7.6	Choice rates with risky-fast scenario vs. safer-fast scenario	152

List of Tables

Table 2.1	Four identified driver behavioral types	27
Table 3.1	Heavy duty diesel truck vehicle-specific information	32
Table 3.2	Parameters required for truck model calibration	33
Table 3.3	Truck concave model	34
Table 3.4	Truck convex model	37
Table 3.5	Comparison of truck model performance	42
Table 3.6	The performance of truck CO_2 models	45
Table 3.7	Tested bus specifications	47
Table 3.8	Parameters required for bus model calibration	48
Table 3.9	Bus fuel consumption model	50
Table 3.10	Comparison of bus model performance	54
Table 4.1	Throttle discretization procedure	63
Table 4.2	Rolling stock characteristics	65
Table 4.3	Description of model parameters	74
Table 4.4	Test train characteristics	78
Table 4.5	Track information for the MAX Blue Line	79
Table 4.6	Parameter set for starting tractive effort	81
Table 4.7	Track information for the Chicago Brown Line	83
Table 4.8	Validation on Energy Prediction	84
Table 4.9	Sensitivity of model predictions to railcar empty weight	86
Table 4.10	Sensitivity of model predictions to the number of railcars	86
Table 4.11	Sensitivity of model predictions to road grade	86
Table 5.1	Testing vehicle characteristics	100
Table 5.2	Model parameter values for Gipps, Fritzsche and Wiedemann	101
Table 5.3	MOVES energy/emission rate (model year: 1999)	108
Table 5.4	MOVES energy/emission rate (model year: 2015)	109
Table 5.5	The FC/EM estimation error (%) by numerical simulation	110
Table 5.6	Comparison of simulated fuel consumption error (%) between MOVES and VT-CPFM	111
Table 6.1	Network characteristics	121

Table 6.2	Tested vehicle specifications	122
Table 6.3	Link energy cost	124
Table 6.4	Path energy cost	125
Table 6.5	Comparison of eco-routes	126
Table 6.6	Network-wide impacts of the proposed eco-routing system (sample network: QNET)	133
Table 6.7	Impacts of congestion levels (sample network: QNET)	135
Table 6.8	Network-wide impacts of the proposed eco-routing system (Doha network)	138
Table 6.9	Impacts of congestion levels (Doha network)	140
Table 7.1	Trip characteristics	146

Chapter 1

Introduction

The transportation sector has become a major contributor to energy use and greenhouse gas (GHG) emissions not only in the United States but worldwide. As reported by [1, 2], transportation activities account for 28% of the total U.S. energy use and 33.4% of CO_2 emissions (CO_2 is the majority of GHG emissions). Globally, 27% of the world primary energy consumption and one-third of CO_2 emissions are contributed by the transportation sector [3]. Climate change and deteriorating dwelling environment stimulate numerous efforts on environmentally sustainable transportation systems, such as improving vehicle engine efficiency, developing alternative fuels, reducing the vehicle miles traveled (VMT), and enhancing traffic operational efficiency. Intelligent transportation system (ITS) technologies have been widely utilized to reduce energy use and emissions by improving traffic operational efficiency.

One of the major successes in ITS during the past decade is the advanced traveler information systems (ATIS). ATIS is basically the system that acquires, analyzes, and presents information to assist surface transportation travelers in moving from a starting location (origin) to their desired destinations [4]. Relevant information may include locations of incidents, weather and road conditions, optimal routes, recommended speeds, and lane restrictions. In particular, starting from the early 2000's, online trip planning services became increasingly available and quickly started to be an integral part of route planning, especially for private users [5]. The majority of the commercial routing services primarily offer the route with either shortest distance or minimum travel time between an origin and a destination. The shortest distance route is typically calculated based on the physical lengths of network roadways. The minimum travel time route is usually generated based on speed limits of different road types. Recently, more advanced services have been developed that are capable of using real time information to provide optimum routes so that enable drivers to avoid congestion and incidents.

Nonetheless, either shortest distance or minimum travel time routing may not always be the best from an energy and environmental perspective. For example, although the shortest distance route minimizes the VMT of a trip, it may result in more energy use and GHG

emissions per unit distance if congestion occurs on the route. Likewise, vehicles running on the minimum travel time route may produce higher unit-distance energy and emission levels given traveling at high speeds. Also, there may be cases that travel time-based routing results in longer distance traveled. A recent study by Ahn and Rakha [6] demonstrated that significant improvements to energy and air quality could be achieved when motorists rather traveled on the arterial route (shorter distance) at moderate speeds, although it incurs additional travel time compared to the faster freeway route (travel time routing). Given the limitations of distance and travel time routing in terms of environmental sustainability, an innovative routing concept, known as eco-routing, has been proposed recently [7, 8] in response to rising energy costs and increased environmental concerns. An eco-routing system is designed specifically to minimize trip energy consumption and emission levels.

A door-to-door trip may involve either one traffic mode or sometimes multiple modes. For example, travelers may drive by themselves throughout a trip, or first drive to a subway station and then make a transfer to rail transit; alternatively, people may also start their trips by walking/cycling to a bus/subway station and take transit in most of the time of the trip. Therefore, a successful eco-route planning should be able to compute energy consumption for multiple traffic modes and offer inter-modal routing suggestions. Furthermore, for private car or truck drivers who can choose routes randomly, eco-routing systems are anticipated to generate routing suggestions based on real time information, so that vehicles can be routed dynamically. In-vehicle eco-routing applications are also expected to differentiate eco-routes between vehicle models given their differences in energy consumption behavior. Developing such a system in reality requires to address extensive concerns such as multi-modal energy consumption modeling, eco-routing algorithm development, public transit and non-motorized traffic system design, and travelers responses to received route information.

The dissertation is a building block of the multi-modal energy-efficient routing system which is being developed and tested in a micro-simulation environment before it can be used in real applications. Basically, four sub-modules are developed in the dissertation as partial fulfillment of the system: energy consumption modeling, subway system development, on-road vehicles eco-routing, and information effect on route choice behavior. Other sub-modules such as pedestrian and bicycle modeling will be investigated in the future study.

1.1 Problem Statement

This section presents the research gap relative to the proposed study in five aspects: energy consumption modeling, subway system development, traffic micro-simulation testbeds, eco-routing systems for in-vehicle applications, and effect of route information on route choice behavior.

1.1.1 Energy Consumption Modeling

Towards the research goal, simple, accurate and efficient energy consumption models relative to each motor traffic mode are first needed. Numerous models have been developed from macroscopic to mesoscopic to microscopic levels. The macroscopic and mesoscopic models such as MOBILE [9], Emission Factors (EMFAC) [10], and the VT-Meso model [11], however, may produce unreliable estimates given that they are incapable of accounting for transient vehicle behavior. Instead, microscopic models are better suited to adequately incorporate the elements associated with a wide range of dynamic characteristics. Most of the prevalently-used microscopic models such as comprehensive modal emissions model (CMEM), Motor Vehicle Emissions Simulator (MOVES), VERSIT+^{micro}, the passenger car and heavy duty emissions model (PHEM), vehicle transient emissions simulation software (VeTESS), EMissions from Traffic (EMIT), and the VT-Micro, however, either produce poor model predictions or cannot be easily calibrated or implemented in complex frameworks (e.g. traffic simulation software, in-vehicle and smartphone eco-routing and eco-driving applications).

To overcome these shortcomings in the modeling practice, Rakha et al. developed a modeling framework, known as the Virginia Tech Comprehensive Power-based Fuel consumption Model (VT-CPFM), which can be calibrated using publicly available data or using the data that can be readily collected by non-engine instrumentation (e.g. GPS) [12]. The VT-CPFM model has been calibrated for light duty vehicles (LDVs); however, it has not been extended to model heavy duty diesel vehicles (HDDVs) such as transit buses and trucks. This study partly aims to develop the HDDVs fuel consumption model.

All of the above-mentioned models were developed for conventional gasoline and diesel vehicles. Towards electric vehicles, Fiori et al. developed the modeling approach, known as the Virginia Tech Comprehensive Power-based Energy consumption Model (VT-CPEM), which also can be easily calibrated to specific vehicle models and used in traffic simulation software, in-vehicle and smartphone eco-routing and eco-driving applications [13]. The VT-CPEM framework is applied to model electric trains in this study for rail energy estimation.

1.1.2 Subway System Modeling

For the subway system module, a railway simulation model is proposed to be developed and combined with the train energy model to estimate railway trip energy consumption. A dynamics model is the essential component to develop the simulation system given that longitudinal dynamics characterizes the motion of rolling stock vehicles in the direction of the track and thus determines acceleration/deceleration behavior.

The majority of the existing train dynamics models, however, cannot either capture realistic acceleration/deceleration behavior (e.g. [14, 15, 16, 17]) or be easily calibrated given the need of considerable mechanical data for model calibration (e.g. [18, 19, 20]). Unrealistic

acceleration behavior may result in incorrect simulated vehicle trajectories which cause bias in energy estimation [21, 22, 23]. Consequently, developing an accurate and efficient train dynamics model is essential to enhance the robustness of a railway simulation system.

1.1.3 Microsimulation Testbed

As mentioned before, the proposed system is developed and tested in a microsimulation environment. Microsimulation model is considered because macro- and meso- simulation models are incapable of modeling instantaneous vehicle motions and thus may cause the bias in energy estimation. Which microsimulation model would be better suited to serve as the testbed is thus another issue that needs to be deliberately concerned. The applicability of a simulation model in this regard highly depends on the accuracy of the simulated vehicle trajectories and the built-in energy consumption model. A suitable simulation model should be able to adequately capture realistic vehicle motions and to accurately estimate energy consumption. In addition, the simulation testbed is also expected to easily model large transportation network and simultaneously can assign traffic dynamically.

1.1.4 Eco-routing Study for In-vehicle Applications

For private cars and trucks which do not have fixed routes, the routing system is anticipated to generate route guidance in real time, so that vehicles en route can be re-routed with the evolution of network traffic conditions using in-vehicle navigation tools.

The majority of the existing eco-routing systems, however, are not able to dynamically update link costs and thus eco-routes based on real time information. Specifically, these systems calculate eco-routes by every vehicle's departure from the origin of a trip; namely, each vehicle is provided with the optimum route at the beginning of the trip and travels on the suggested route until it arrives at the destination. Upon these systems, the vehicles en route cannot be re-routed to other routes even though the traffic conditions on the original routes environmentally deteriorate. In reality, however, traffic conditions on a road network evolve in real time. The pre-trip optimum route may be no longer the best when a vehicle is en route. Traveling on the original optimum route throughout may instead result in more energy use. Although transit buses and rail trains cannot be re-routed in real time, private cars and trucks routing should be able to adapt to the ever-changing traffic conditions. It is worth mention that Rakha et al. [24] developed an agent-based dynamic eco-routing system which updated eco-routes by every vehicle's departure from a link. The system, however, assumes that all vehicle models have the same link energy cost and eco-route, which is not realistic in reality given that energy behavior significantly differs between vehicle models.

Eco-route calculation is based on the shortest path algorithm which requires the availability of link energy cost factors. Accordingly, the accuracy of link cost factors significantly

determines the validity and robustness of resulting eco-routes. Before an eco-route can be calculated, link costs should be estimated or updated. Vehicle energy consumption are affected by many factors including traffic conditions (e.g. speed, acceleration, congestion level), road attributes (road type and vertical grade), and vehicle characteristics (vehicle type and weight). Most of the existing eco-routing systems, however, cannot comprehensively incorporate these factors into link cost functions. For example, the early studies, such as [25, 26, 27, 28, 29, 30], modeled traffic assignment at a macroscopic level, which either assumed fixed link-specific emission factors or utilized the average speed as the input of link cost function. These systems cannot capture the impact of dynamic characteristics (e.g. speed and grade variation) and vehicle specifications on energy estimation, so that are not suitable for operational level analysis such as evaluating the energy and environmental impact of ITS deployment. A recent study [31] developed a mesoscopic approach which successfully incorporated road grade and vehicle type into the system modeling. The system, however, cannot account for the impact of within-link grade and speed variation on energy estimation. It has been demonstrated that failing to capture these microscopic characteristics may result in incorrect eco-routing suggestions [6]. Accordingly, developing a link cost function, comprehensively considering microscopic elements, would be an important enhancement of the eco-routing study. A recent study [24] successfully incorporated microscopic elements into route planning through estimating and accumulating second-by-second fuel consumption to achieve link-level fuel cost; however, the study, as mentioned before, was not able to differentiate link costs and eco-routes between vehicle models.

How to formulate link cost and the eco-routing problem which can comprehensively consider microscopic elements and dynamically route vehicles in real time while simultaneously differentiate vehicle models? This question remains to be answered by this study.

1.1.5 Effect of Route Information on Route Choice Behavior

In reality, travelers may not completely conform to the received route information. Empirical research found that the factors considered by travelers in route choice decision-making were not unitary [32]. Numerous attributes were found to be important considerations such as travel time, trip distance, average speed, and the number of traffic signals. Therefore, investigating how travelers response to route information would provide significant implications to enhance the design of the system in order to maximize the eco-routing benefit.

Despite numerous research efforts in this regard, most of the attempts were based on either simulator or stated preference approach. In the simulator surroundings, respondents make decisions in a digital and virtual environment. Stated preference, alternatively, is an investigative approach in which respondents are given questionnaires to make choices hypothetically. Both approaches are performed under fictitious conditions and may not adequately capture actual choice behavior. Consequently, a real world case study is needed to address the realistic route choice behavior when travelers are informed.

1.1.6 Conclusions

In a nutshell, this dissertation addresses the following questions:

1. How to develop energy consumption models for HDDVs and electric trains based on the VT-CPFM and VT-CPEM frameworks, respectively?
2. How to model train dynamics to build a railway simulation system?
3. Which micro-simulation model would be better suited to serve as a modeling tool to evaluate eco-routing strategies?
4. How to formulate the link cost and eco-routing problem that is able to comprehensively consider microscopic elements and route private cars and trucks in real-time while at the same time differentiate between vehicle models?
5. With the resulting link cost and eco-routing model as well as the selected simulation testbed, how to develop and test the eco-routing system?
6. How would route information affect travelers route choice behavior in the real world?

1.2 Research Scope

The study of the dissertation is not a complete package but a building block of the multi-modal eco-routing system. Specifically, the study develops some of the submodules including multi-modal energy consumption models, railway simulation system, dynamic eco-routing system for in-vehicle applications, and the route information effect on route choice behavior. Other submodules such as pedestrian and bicycle modeling will be studied in the future. It should be noted that the proposed system focuses on minimizing energy consumption and GHG emissions (CO_2). The routing solutions on minimum pollutant emissions such as hydrocarbon (HC), carbon monoxide (CO) and nitric oxides (NO_x) are not investigated in this study. Furthermore, as a preliminary study, this dissertation employs energy consumption as the single objective (the minimum CO_2 route is identical to the minimum energy route given that CO_2 is linearly related to energy consumption [12]) without considering the constraints from other factors such as travel time. In addition, conventional gasoline and diesel vehicles as well as all-electric vehicles and trains are tested in this study; other vehicle types (e.g. hybrid electric vehicle (HEV), compressed natural gas (CNG) vehicle) remain to be included and tested in the future.

1.3 Research Objectives

Given the above-mentioned research gaps, the research effort presented in this dissertation attempts to develop some of the submodules of the multi-modal eco-routing system. Towards this goal, several objectives are addressed:

1. Develop the HDDV and electric train energy consumption model which can be easily calibrated and implemented in traffic simulation software and in-vehicle eco-routing and eco-driving applications.
2. Develop a railway simulation system by introducing a state-of-the-art dynamics model.
3. Identify the best microscopic simulation model in which the proposed system can be developed and tested.
4. Formulate the link energy cost function and eco-routing problem in support of the private car and truck dynamic eco-routing as an in-vehicle application of the multi-modal energy-efficient system.
5. Develop and test the dynamic eco-routing system in the simulation environment.
6. Investigate the effect of route information on route choice behavior based on a real world experiment in order to provide significant implications to enhance the design of the proposed system in the future.

1.4 Research Contributions

To achieve the state-of-the-art on the proposed study, the major contributions of this dissertation are addressed hereinafter:

1. The dissertation comprehensively investigates the existing research efforts on energy consumption modeling, railway microsimulation and dynamics, eco-routing study, microscopic traffic simulation model, effect of route information on route choice behavior, and offers an in-depth synthesis of the relevant literature.
2. The research constructs real world transit bus trajectory and fuel consumption dataset, and develops the VT-CPFM-based HDDVs fuel consumption model and VT-CPFM-based electric train model.
3. The study develops a state-of-the-art train dynamics model which can be calibrated without mechanical engine data and easily implemented in railway simulation systems.

4. The research also compares the performance of the state-of-the-art traffic microsimulation software in terms of energy and environmental analysis, and identifies the simulation model which produces the lowest prediction error in vehicle trajectories and energy consumption to be served as the testbed for the proposed system.
5. Furthermore, the dissertation formulates the link energy cost function and eco-routing problem based on the VT-CPFM and VT-CPEM models, which adequately includes microscopic elements and is able to serve real time eco-routing application while at the same time to differentiate eco-routes between vehicle models.
6. With the resulting link cost and eco-routing model as well as the selected simulation testbed, the dissertation develops and tests the private car and truck dynamic eco-routing system as an exemplary application of the multi-modal eco-routing system. The system is tested by comparing the resulting network-wide measures of effectiveness (MOEs) with those derived from traditional dynamic eco-routing [24] and the travel time routing methods.
7. The research also constructs a route choice dataset based on a real world experiment, and investigates how drivers make route choice decision when they are informed with dynamic route information.

1.5 Dissertation Layout

In achieving the research objectives, the dissertation is composed of eight chapters. The first chapter provides an overview of the problem and identifies research scope, objectives and contributions. The second chapter provides a synthesis of the literature on energy consumption and emissions modeling, railway simulation and dynamics, eco-routing study, traffic microsimulation model, effect of route information on route choice behavior, and identifies research needs that are to be addressed. The third chapter introduces the VT-CPFM framework and develops fuel consumption models for HDDVs (i.e. heavy duty truck and transit bus). The fourth chapter develops electric train energy consumption and dynamics models in support of railway simulator development and trip energy estimation. The fifth chapter identifies the best microsimulation testbed through comparing the model performance in terms of energy and emissions analysis. The sixth chapter formulates the link energy cost and eco-routing problem, and develops and tests the private car and truck dynamic eco-routing system in the selected simulation testbed. The seventh chapter investigates the effect of route information on route choice behavior. Finally, the last chapter gives the concluding remarks of the dissertation and provides several recommendations for further research.

The main contents of this dissertation have been published or are under review in journals and/or conferences as listed below:

Journal Publications

1. **Wang, J.** and Rakha, H. Electric Train Energy Consumption Modeling. *Journal of Applied Energy*, 2017.
2. **Wang, J.** and Rakha, H. Convex Fuel Consumption Model for Diesel and Hybrid Buses. *Transportation Research Record: Journal of Transportation Research Board*, 2017.
3. **Wang, J.** and Rakha, H. Fuel Consumption Model for Conventional Diesel Buses. *Journal of Applied Energy*, 2016.
4. **Wang, J.** and Rakha, H. Hybrid-Electric Bus Fuel Consumption Modeling: Model Development and Comparison to Conventional Buses. *Transportation Research Record: Journal of Transportation Research Board*, 2016.
5. **Wang, J.** and Rakha, H. Fuel Consumption Model for Heavy Duty Diesel Trucks: Model Development and Testing. *Transportation Research Part D: Transport and Environment*. (In Review).
6. **Wang, J.** and Rakha, H. Empirical Study of Effect of Dynamic Travel Time Information on Driver Route Choice Behavior. *Transportation Research Part F: Traffic Psychology and Behaviour*. (In Review).
7. **Wang, J.**, Rakha, H., and Fadhloun, K. Comparison of car-following Models: A Vehicle Fuel Consumption and Emissions Estimation Perspective. *Transportation Research Part D: Transport and Environment*. (In Review).
8. **Wang, J.** and Rakha, H. Train Dynamics Model for Rail Transit Simulation System. *Transportation Research Part C: Emerging Technologies*. (In Review).
9. **Wang, J.** and Rakha, H. An Eco-Routing Model for Multi-Modal Transportation Systems. (Working Paper).
10. **Wang, J.**, Rakha, H., and Elbery, A. Dynamic Multi-modal Eco-routing System: Model Development and Testing. (Working Paper).

Conference Proceedings

1. **Wang, J.**, Rakha, H., and Fadhloun, K. Comparison of car-following Models: A Vehicle Fuel Consumption and Emissions Estimation Perspective. Presented at *96th Transportation Research Board Annual Meeting*, Washington D.C., 2017.

2. **Wang, J.** and Rakha, H. Convex Fuel Consumption Model for Diesel and Hybrid Buses. Presented at *96th Transportation Research Board Annual Meeting*, Washington D.C., 2017.
3. **Wang, J.** and Rakha, H. Heavy Duty Diesel Truck Fuel Consumption Modeling. Presented at *95th Transportation Research Board Annual Meeting*, Washington D.C., 2016.
4. **Wang, J.** and Rakha, H. Hybrid-Electric Bus Fuel Consumption Modeling: Model Development and Comparison to Conventional Buses. Presented at *95th Transportation Research Board Annual Meeting*, Washington D.C., 2016.
5. **Wang, J.** and Rakha, H. Impact of Dynamic Route Information on Day-to-Day Driver Route Choice Behavior. Presented at *94th Transportation Research Board Annual Meeting*, Washington D.C. 2015.

Selected Technical Reports

1. Witten, T., Samuel, A., Guerrero, I., Alden, A., Rakha, H., **Wang, J.**, Chen, H. et al. Transit Bus Routing On Demand: Developing an Energy-Saving System. Federal Transit Administration (FTA 0704-0188), 2015.
2. Rakha, H., **Wang, J.**, and Abdelmegeed, M. Fuel Consumption and Emissions Model for Heavy Duty Diesel Trucks: Model Development and Testing. Mid-Atlantic Transportation Sustainability UTC, 2016.
3. Rakha, H., **Wang, J.**, and Abdelmegeed, M. Energy Consumption and Emissions Modeling. TranLIVE UTC, 2016.

Chapter 2

Literature Review

This chapter presents extensive literature to further address the research needs and establish the basis for the proposed research effort. First, the modeling work on energy and emissions is introduced in order to identify the best model for the proposed eco-routing system. Secondly, the literature on railway simulation and dynamics is reviewed. Thirdly, the chapter compares the most state-of-the-practice microscopic traffic simulation software in terms of energy and environmental analysis. Furthermore, the existing eco-routing systems are comprehensively investigated, which sheds light on the limitations of these research efforts and enlightens the significance of the proposed study. Finally, the studies relative to the effect of route information on route choice behavior are presented.

2.1 Energy Consumption and Emission Modeling

As mentioned in section 1.1.1, macroscopic and mesoscopic models may produce unreliable estimates given their inability in accounting for transient vehicle behavior. Alternatively, microscopic models are able to generate robust model estimates through addressing the details in instantaneous vehicle motions, and thus are applied in this study. This section mainly focuses on the research efforts relative to microscopic models. Review effort is presented for conventional fossil fuel-powered vehicles as well as electric vehicles and trains respectively.

2.1.1 Conventional Gasoline and Diesel Vehicle

There are several key microscopic models for conventional vehicles, including CMEM, PHEM, EMIT, VT-Micro, VeTESS, MOVES, VERSIT+^{micro}, VT-CPFM. The review effort mainly focuses on these models.

CMEM was originally developed at the University of California (UC) at Riverside, along with

researchers from the University of Michigan and Lawrence Berkeley National Laboratory. This model is a physically power-based model that separates the entire modeling process into different components which consist of a power demand model, an engine speed estimator, a fuel rate model, an engine-out emission component and an after-treatment component [33]. The first three components are used to generate fuel consumption rate. The CMEM-based fuel consumption model requires the input of engine data (e.g. engine speed) to generate model estimates. Therefore, the model can be calibrated only when the engine data is available, which makes the calibration work difficult and thus limits its popularization to new vehicle models. The requirement of engine data also restricts the extensive use of the model in complex frameworks such as traffic simulation software. Another issue of the model is that the model characterizes fuel consumption as a linear function of vehicle power, which may produce a bang-bang type of control. The bang-bang control may arise when the partial derivative of fuel consumption with respect to the vehicle power is not a function of vehicle power [12, 34], suggesting that drivers accelerate at full throttle to reduce acceleration time and minimize their trip fuel consumption levels.

Another model, which also requires the input of engine speed and torque for model development, is the PHEM modeling framework [35]. Similar to CMEM, PHEM also cannot be easily calibrated given the need of engine data and is difficult to popularize to new vehicle models.

Massachusetts Institute of Technology (MIT) researchers developed a simple statistical model, known as EMIT [36], to estimate instantaneous emissions and fuel consumption for light-duty composite vehicles. The model uses instantaneous speed/acceleration and vehicle specifications as input variables and is easy to calibrate and implement. However, the model was calibrated and validated only for two composite LDVs under the level grade condition. Further efforts are needed to model other vehicle categories and include road grade as an explanatory variable. In addition, the model cannot cover a wide range of real world driving conditions given that it was calibrated using very limited data.

Another statistical model (VT-Micro) was developed in 2004 by Virginia Tech researchers, characterizing fuel consumption as a polynomial combination of speed and acceleration. The original VT-Micro model was developed using chassis dynamometer data for nine LDVs, and then was expanded to more vehicle categories including 60 LDVs and trucks [37]. The model predictions were compared against laboratory measurements, producing the prediction error of fuel consumption within 2.5%. The major limitation of the model is that the calibration work requires massive on-road data collection, which would significantly increase monetary and time costs to calibrate new vehicle models.

VeTESS [38] was developed for a European project, known as DECADE, to capture dynamic engine behavior and to predict instantaneous fuel consumption and emissions. The model evaluates engine speed and torque from the forces acting on the vehicle, and can adequately predict fuel consumption and emissions. The major limitation of the model is that it considers only one vehicle at a time and one journey at a time. Also, model calibration requires a

large amount of engine tests. If an engine type or its emissions control equipment is updated, the engine test must be repeated for the new engine. This demonstrates that the model is not suitable for mass simulation of hundreds of vehicle types, and also not easily used in traffic simulation system and ITS applications.

Environmental Protection Agency (EPA) also developed a microscopic model, known as MOVES which has been widely used in the United States for energy and environmental analysis at different levels: national, state and project. The up-to-date version of the model is MOVES 2014. The input of the model is instantaneous vehicle speed and acceleration as well as road grade and vehicle specifications, without any engine data required. To generate MOVES estimates, the operating modes, defined discretely based on vehicle speed, acceleration and vehicle specific power (VSP) [39], need to be calculated. MOVES cannot model specific vehicle models, and provides less accurate model estimates at an instantaneous level compared to CMEM and VT-Micro given the discrete operating mode definition [40]. Furthermore, the use of the model requires massive user inputs for each scenario run and significantly increases the time required to run multiple scenarios and large networks [40, 41], which is not suitable for real time applications.

VERSIT+^{micro} is another microscopic model which was developed in Netherlands to simulate the emissions of CO_2 , NO_x and PM_{10} as well as energy consumption [42]. The inputs of the model are instantaneous speed and acceleration which can be easily collected using non-engine instrumentation. The model also accounts for the impact of vehicle type and road gradient on the model estimates. It is worth mention that VERSIT+^{micro} can be easily linked to complex frameworks such as traffic simulation models so that allows for evaluation of effectiveness of transportation measures (e.g. signal coordination and speed control) in improving energy efficiency and air quality. However, the model assumes that energy/emissions are the linear dependence on vehicle speed, which is not correct in reality and may lead to model estimation bias. Also, the linear relationship, as mentioned before, may result in the bang-bang type of control.

To overcome the shortcomings of the above-mentioned models, Rakha et al. [12] developed the VT-CPFM modeling framework which characterizes fuel consumption as a second-order polynomial function of vehicle power, circumventing the bang-bang control problem. The model can be calibrated using publicly available data without massive field data collection. The validity of the model has been tested using both standard driving cycles [12] and on-road measurements [43]. Also, given the simple model specification, the model is ideal for implementation within traffic simulation software, in-vehicle or smartphone applications. The model was originally developed for gasoline LDVs, yet it has not been extended to HDDVs before this study. Chapter 3 presents the HDDVs modeling effort in detail.

2.1.2 Plug-in Electric Vehicle

Energy consumption models can be divided into two categories: forward models and backward models [44]. As demonstrated by [13], models that compute the tractive contribution required at the wheels and “work backward” towards the engine are called “backward models”; alternatively, models that start from the engine and work with transmitted and reflected torque are called “forward models”. The use of forward models requires extensive internal engine data. These models are very complex and characterized by slow execution time and high computer memory. Backward models, however, achieve reliable evaluation of vehicle energy consumption based on drive cycle and vehicle characteristic data, without the need to input engine data. In addition, they are characterized by fast computational times and low memory usage, and can be easily implemented in traffic simulation model and ITS applications [45]. The backward modeling approach is thus recommended for the proposed study.

Macroscopic and mesoscopic electric energy models, similar to conventional fuel models, also do not allow for addressing the differences of electric power consumption associated with microscopic characteristics. For example, the aggregated values are not able to reflect difference in energy consumption that results from traveling on one route with frequent acceleration and deceleration and cruising on another route with constant speed if both trips have identical average speed. Accordingly, the electric energy model used for ITS applications (e.g. eco-routing navigation) should be able to consider microscopic elements.

A number of models have been developed to estimate plug-in electric vehicle energy consumption. For example, Hayes et al. [46] developed a simplified energy model to quantify the impact of battery degradation on the total vehicle energy consumption. The model is able to recognize the differences of energy consumption resulting from various routes, driving conditions, and driving cycles. Muratori et al. [47] proposed a model to estimate the total energy consumption associated with private cars of the United States. The model was used to evaluate the impact of plug-in electric vehicles on the electric power grid. Another effort [48] developed an analytical model which characterized energy power as a function of vehicle velocity, acceleration and road grade. The model is able to differentiate energy use on different routes and under different driving patterns. Specifically, the results of the study demonstrated that electric vehicles were more efficient when driving on in-city routes than driving on freeway routes. Some of the studies incorporated energy regeneration into the modeling practice. Abousleiman et al. [49] evaluated the energy consumption of an electric vehicle considering a constant regenerative braking efficiency. Hayes et al. [50] developed an energy consumption model based on EPA coast-down parameters by assuming that all the available regenerative energy was returned to the battery as long as the regenerative power level is 20 kW or less. Many other efforts have been made on electric energy modeling such as [51, 52, 53, 54]. Despite these models, most of them cannot either accurately model vehicle transient behavior, or model energy regeneration at a microscopic level, or easily to be implemented in traffic simulation software and ITS applications.

To overcome the above-mentioned modeling shortcomings, Fiori et al. [13] developed a backward microscopic energy consumption model, known as VT-CPEM, which included instantaneous speed/acceleration, vehicle specification and road gradient as the explanatory variables. The model can be easily calibrated using non-engine data and also implemented in the following applications: in-vehicle or smartphone eco-driving and eco-routing systems, and transportation microsimulation software. It is worth mention that the model can address the energy regeneration microscopically by characterizing regenerative efficiency as an exponential function of instantaneous deceleration level, as formulated in Equation (2.1),

$$\eta_{re}(t) = \begin{cases} \frac{1}{e^{\frac{\alpha}{|a(t)|}}}, & \forall a(t) < 0 \\ 0, & \forall a(t) \geq 0 \end{cases} \quad (2.1)$$

where η_{re} is the regenerative efficiency (%), a is the acceleration level (m/s^2), and α is the model coefficient. Equation (2.1) demonstrates that energy can be regenerated only during braking ($a < 0$). The resulting regenerative efficiency is used to calculate recovered energy ($P_{recovery}$) as illustrated in Equation (2.2) with $P_{available}$ the total available negative power to be regenerated (kW).

$$P_{recovery}(t) = P_{available}(t) \times \eta_{re}(t) \quad (2.2)$$

The electric power consumption is computed using Equation (2.3):

$$P(t) = \left(ma(t) + mg \cdot \cos(\theta) \cdot \frac{C_r}{1000} (c_1 v(t) + c_2) + 0.5 \rho_{air} A_f C_D v^2(t) + mg \cdot \sin(\theta) \right) \cdot v(t) \cdot \frac{1}{1000 \eta_d} \quad (2.3)$$

where P is the electric power consumption in kW , m is the vehicle mass in kg , g is the gravitational acceleration which equals $9.8066 m/s^2$, θ is the road grade angle, C_r , c_1 and c_2 are rolling coefficients (unitless), v is the vehicle speed in m/s , ρ_{air} is the air density at the sea level ($1.2256 kg/m^3$), A_f is the frontal area of a vehicle (m^2), C_D is the drag coefficient (unitless), and η_d is the driveline efficiency. The model has been demonstrated to produce robust energy estimates that are consistent with field observations.

Given the robustness in energy estimation and the simplicity in model specification, the VT-CPEM model is applied to electric vehicle eco-routing in the proposed study.

2.1.3 Electric Train

Electric trains are widely used in urban subway systems. A subway, put simply, is a train and the tunnel through which the train runs. A subway train consists of several connecting cars that contain durable seats as well as poles and straps for people to hold on to when the

train is full [55]. The trains, known as rolling stock, are complex given that they include a traction and dynamics system that highly impact energy consumption. For example, the traction system determines how the propulsive force is generated and provided to move a train forward; and the dynamics system determines how a train is accelerated or decelerated thus affecting train transient behavior that highly impacts instantaneous energy consumption. Also, the brake system determines whether the braking power is regenerated to be used or wasted as heat. For regenerative braking, the brake energy can be recovered by converting kinetic energy into a form that can be either immediately used or stored until needed; however, other brake systems, such as dynamic braking, dissipate electric energy as heat rather than using it. Other train characteristics, such as car empty weight, number of axles per rail car and drag coefficient significantly affect the forces acting on a train and thus are also important parameters in energy modeling.

In addition to the train itself, there are several other rail system components, such as track infrastructure and passenger loading, affecting the tractive/braking forces acting on the train. For instance, a good condition track (good rails and cross ties) decreases the starting tractive effort [56]; while a track with steep grades and large curvature results in high resistance forces [56, 57]; and passenger loading affects the total railcar weight and thus acting forces. These factors should also be incorporated into the energy modeling framework.

The most widely available measures for rail (either electric or diesel-electric train) energy consumption are those estimated on an annual gross average basis. Specifically, Equation (2.4)-(2.6) present the modeling approach, where E_p , E_s and E_v are the energy consumed per passenger kilometer ($kWh/P \cdot km$), per seating kilometer ($kWh/S \cdot km$) and per vehicle kilometer ($kWh/V \cdot km$), respectively; E is the annual energy consumption of a rail transit system in kWh ; M_p , M_s and M_v are total passenger kilometers, seating kilometers and vehicle kilometers, respectively; C is the train seating capacity and β is the line loss factor associated with the train transmission system. The parameters in the models are readily available from the National Transit Database (NTD) [58, 59, 60]. Despite the effortless acquisition of the aggregated measurements, they are not capable of representing the differences in energy consumption associated with route and vehicle characteristics, passenger loading, speed profiles and weather and track conditions, and thereby not suitable for project-level analysis.

$$E_p = \frac{E}{M_p \times \beta} \tag{2.4}$$

$$E_s = \frac{E}{M_s \times C \times \beta} \tag{2.5}$$

$$E_v = \frac{E}{M_v \times \beta} \tag{2.6}$$

Research efforts have thus focused on developing a modeling framework sensitive to the aforementioned system characteristics. An early study conducted by Mittal [61] proposed an analytical method to estimate energy consumption sensitive to speed, train configuration and passenger load. However, the method used average speed for energy prediction without considering speed fluctuation. The model also did not incorporate an energy regeneration module. Some of the state-of-the-art models [62, 63, 64, 65, 66, 67] considered an average constant regenerative braking energy efficiently that mainly depended on the train's average speed. The major limitation is that these models cannot capture vehicle transient behavior and model energy regeneration at a microscopic level. Although some of these simplified models have been used to develop energy-optimized strategies [68, 69, 70, 71, 72, 73], the validity of the resulting strategies is questionable given the models' inadequacy in instantaneous energy prediction. The National Cooperative Rail Research Program (NCRRP) [74] designed a passenger rail simulation framework which incorporated route and train characteristics, speed, passenger load and regenerative braking into the energy modeling practice. The framework, however, is an excel-based tool and cannot be implemented in more complex frameworks, such as traffic simulation software, smartphone eco-driving and eco-routing systems. Furthermore, the energy prediction within the framework also considers average speed and a constant regenerative efficiency. A recent study [57] initiated a bottom-up modeling framework sensitive to acceleration behavior by incorporating second-by-second speed profiles. Nonetheless, the model cannot generate instantaneous energy regeneration because it assumes a constant regenerative efficiency. The model is also an excel-based tool and thus does not allow for integration in complex frameworks. Other models, such as [75, 76, 77], are also not suitable for ITS applications due to their complexity in model specification.

To the authors' best of knowledge, although there have been numerous studies on modeling train electric power consumption, these studies were of limited application. They either cannot model train transient behavior or fail to capture energy regeneration at a microscopic level or are not simple enough to be implemented within complex systems. The dissertation partially attempts to fill this void and, for the first time, relates energy regeneration with the instantaneous deceleration level in rail transit energy modeling.

2.2 Railway Simulation and Dynamics Modeling

Numerous simulation programs have been developed and widely used to support the sustainability (e.g. safety, comfort, efficiency, environment) of the off-the-shelf railway systems. Based on the level of simulation detail, railway simulators can be classified into two categories: discrete and continuous. The discrete-event simulation, such as [78, 79, 80, 81, 82], models the operation of the rail system as a discrete sequence of events in time, which assumes no change in the system between consecutive events (e.g. assume constant speed over the track segment between two stations). Such simulators fail to capture the instant acting forces and thus acceleration/deceleration behavior, and thus cannot adequately emulate

the details of train motion and effectively design and test various strategies (e.g. environmentally optimal operation, speed control, passenger comfort improvement) which require the acquisition of the continuous state of train activities. Continuous simulation, however, tracks the system dynamics over time, and thus can instantly model the train movement. Nonetheless, existing continuous simulators, such as [16, 17], cannot emulate realistic train dynamics given a lack of accurate dynamics models to mathematically and dynamically characterize the throttle and brake input. For instance, Nash et al. [16] assumed that a train always accelerated at full throttle, which overestimates acceleration levels overall. Consequently, incorporating an accurate and efficient train dynamics model is needed for realistic acceleration/deceleration behavior from the railway simulation perspective.

The application of dynamics models to address acceleration behavior in railway systems has been found in some literature. The typical equation used to estimate tractive effort for acceleration analysis is illustrated in Equation (2.7)[83], with N and N_{max} the typical and maximum throttle notch respectively, and P_{max} the maximum engine power and v the vehicle speed. The traction of locomotives or rolling stock vehicles, known as throttle notch, is controlled discretely. Namely, the typical throttle notch N varies discretely with train power conditions. It is difficult to determine a relationship between the throttle notch and engine output power without the assistance of train manufacturers. Although some of the studies [84, 85, 86] have accounted for the impact of throttle notch on force profiles, yet no analytical expressions so far are available. This void highlights the need to mathematically characterize throttle input as a function of train motion data (e.g. speed) which can be easily measured using non-engine instrumentation such as Global Positioning Systems (GPSs).

$$F_t = \left(\frac{N}{N_{max}} \right)^2 \frac{P_{max}}{v} \tag{2.7}$$

Towards this goal, the achievements on motor vehicle dynamics may provide valuable insights. Searle [87], one of the pioneers using dynamics model for acceleration prediction, linked vehicle motion to the ratio of engine power to vehicle weight by introducing a constant acceleration efficiency that accounts for external resistance forces and the losses in the transmission. The model assumes the acting force to be a constant and thus cannot account for the change of dynamics with vehicle operational conditions. To enhance vehicle dynamics modeling, Rakha et al. [88, 89] developed a standard dynamics model considering the impact of vehicle speed on tractive force, yet failing to capture the realistic driver throttle input given the assumption that vehicles always accelerate at full throttle. An enhancement to the standard model was proposed by Rakha et al. [90] through introducing a constant throttle input level. Nonetheless, recent studies by Fadhloun et al. [91, 92] found that the driver throttle level input varied as a hyperbolic function of the ratio of vehicle speed to the facility desired speed. The model was demonstrated to generate a better match of acceleration behavior to field observations than other dynamics models. The proposed dynamics model for acceleration counterpart was thus developed based on Fadhloun et. al's modeling

framework which is described in section 4.2.1.

For deceleration estimation, researchers have either empirically or mathematically addressed train dynamics. Hay [56] presented empirical results, indicating that the brake force linearly increased up to the maximum level with the increasing speed at the low speed level (smaller than 10 *km/h*), and fluctuated at the vicinity of the maximum force level within a specific speed range (10-30 *km/h*), then decayed at relatively high speed levels (larger than 30 *km/h*). Namely, they assumed the brake force to be a piecewise linear function of speed. A later study by Iwnicki et al. [83] confirmed Hay’s results and further demonstrated that the modern locomotive design ensured a constant brake force at the maximum force level. In addition to empirical experiments, many mathematical models have been developed in the field of mechanical engineering [14, 15, 18, 19, 20]. These models, however, cannot be easily calibrated and used in simulators or control systems given that the model calibration requires considerable mechanical data that are not easily accessible without seeking assistance from train manufacturers. For instance, the model in Equation (2.8), developed by Perpinya et al. [14], requires 10 mechanical parameters ¹ as the model inputs to estimate the brake force, which significantly limits the model application in transportation systems. Hay [56] developed a simple brake force model that characterizes the brake force as a function of braking ratio, the weight of rolling stock, the efficiency of the brake lever system, and the coefficient of friction between the wheel and the brake shoe. The coefficient of friction is the only variable in the model that dynamically changes as a function of speed levels, and needs to be functionally determined. Given the simplicity in model specification, Hay’s model was used to develop the proposed deceleration model.

$$F_{b,i} = \left[\left(\frac{\pi \cdot d_{bc}^2 \cdot p_{bc,i}}{4} - F_R \right) \cdot i_c - R_{sa} \right] \cdot i_l \cdot n_{\Delta} \cdot n_{bc} \cdot f(P_s, v_i) \cdot \eta_{br} \quad (2.8)$$

To quantify the coefficient of friction, earlier studies [93, 94] tested various train fleets and generated experimental curves to determine the magnitude of the coefficient of friction at each speed level, yet without mathematical generalization. This limits the use of the results by other researchers once the empirical brake data is not available. Some of the researchers [14, 95, 96, 97, 98] mathematically developed functions to analytically compute the coefficient of friction, demonstrating that it strongly depends on the instantaneous running speed, the applying force on a brake shoe and the surface contact pressure. However, these models also require the measurement of mechanical data for model calibration and implementation. Thus, a simple modeling framework is needed in order to ensure that the use of the model

¹ d_{bc} brake cylinder diameter, $p_{bc,i}$ the instantaneous relative air pressure in the brake cylinder, F_R and R_{sa} the resistance force due to the brake cylinders back spring and to the self-adjusting mechanism incorporated in the piston rod respectively, i_c the central brake rigging, i_l the amplification ratio of the brake rigging vertical levers, n_{Δ} the number of triangular axles, n_{bc} the number of brake cylinders of the vehicle, f the coefficient of friction between the wheel and the brake shoe, η_{br} the mechanical efficiency of the brake rigging.

requires only non-mechanical data (e.g. speed) that can be measured directly using non-engine instrumentation.

In summary, an accurate, simple and efficient longitudinal dynamics model is needed to capture typical train acceleration and deceleration behavior and develop railway simulation systems. The model will also support the planning, management and control of railway transportation systems, such as designing and testing cruise control strategies [99, 100], optimizing rail signal timings [101], evaluating eco-friendly strategies [102, 103, 104].

2.3 Traffic Microscopic Simulation Models

This section investigates the applicability of the most state-of-the-art traffic microsimulation models for energy and environmental analysis, and identifies the model which is better suited to serve as the testbed for the proposed study. As mentioned hereinbefore, the applicability of a simulation model for energy and environmental analysis highly depends on the accuracy of the simulated vehicle trajectories and the embedded energy/emissions model. The car-following model of a simulator controls longitudinal vehicle motions and thus determines the resulting vehicle trajectories [21, 22, 23, 105]. Therefore, the review efforts in this section mainly focus on the built-in car-following function and energy/emission model of each simulator. The key microsimulation models include VISSIM, CORSIM, AIMSUM, PARAMICS, INTEGRATION.

VISSIM is a microscopic, time step- and behavior-based simulation model developed to analyze the full range of functionally classified roadways and public transportation operations [106]. The model was first developed in 1970s and can simulate multiple traffic modes such as LDVs, buses, light rail, heavy rail, trucks, pedestrians, and bicyclists. With the integrated dynamic traffic assignment module, VISSIM can generate assignment results dynamically over time for either an aggregated O-D matrix or an individual vehicle. The basic traffic model ruling the movement of vehicles was developed by Rainer Wiedemann in 1974 [107] which is a psycho-physical model. The steady-state car-following behavior of the Wiedemann model is constituted by the Pipes model [108], while the non-steady state behavior is jointly determined by four discrete regimes and a linear acceleration model. VISSIM has been demonstrated by a recent study [109] that the system generates unrealistic vehicle trajectories that are inconsistent with field observations, given the inadequacy of the Wiedemann model in capturing acceleration behavior [21]. Furthermore, the built-in energy/emissions model, PHEM, provides predictions that are less accurate than those derived from the state-of-the-art models such as CMEM, VT-Micro and VT-CPFM [110].

CORSIM, developed and maintained by U.S. Federal Highway Administration (FHWA), is a microscopic simulation model designed for the analysis of freeways, urban streets, and corridors or networks. The model integrates a conventional traffic assignment module with two optimization algorithms: the user equilibrium assignment and the system optimal as-

segment [111]. CORSIM combines the NETSIM and FRESIM models into an integrated package to characterize the car-following behavior. Both NETSIM and FRESIM can be reverted to the Pipes model, and simulate traffic behavior at a microscopic level with detailed representation of individual vehicles and their interactions with their physical environment and other vehicles [112]. Accordingly, both VISSIM and CORSIM incorporate the Pipes model as their core component of the car-following model. In addition, CORSIM uses the VeTESS model for energy/emissions estimation, which allows for energy and environmental analysis relative to very limited number of vehicles and engines [38].

AIMSUM is an integrated transport modeling system, developed and marketed by Transport Simulation Systems (TSS) in Barcelona, Spain. The model stands out for the exceptionally high speed of its simulations and for fusing travel demand modeling, static and dynamic traffic assignment with mesoscopic, microscopic and hybrid simulation – all within a single software application. The embedded dynamic traffic assignment module is able to route a portion of the vehicles along pre-defined OD routes. The system uses the Gipps car-following model [113] to control longitudinal vehicle motions. The vehicle trajectories derived from the Gipps model have been demonstrated to be more consistent with field measurements compared to the Wiedemann and Fritzsche models [23]. However, the system applies the VERSIT+^{micro} model for energy/emissions estimation which, as mentioned before, may result in prediction bias and the bang-bang type of control given the linear relationship between fuel consumption and speed.

Another prevalently-used microscopic simulation package is PARAMICS which was developed at the Edinburgh Parallel Computer Center in Scotland. The model simulates the individual components of traffic flow and congestion, and presents its output as a real-time visual display for traffic management and road network design [114]. PARAMICS also offers wide area vehicle routing with dynamic feedback. The vehicle movement of the model is principally controlled by the Fritzsche car-following model [115] which was demonstrated by the recent study [23] to generate high simulation error in vehicle trajectories. The energy/emissions model in PARAMICS, CMEM as mentioned before, is not easily calibrated for new vehicle models given the need of engine test, and thus cannot be extensively implemented in traffic simulation software. Although it has been used by PARAMICS, the engine test has to be repeated for the new integrated vehicle models.

The INTEGRATION system is an agent-based microscopic traffic assignment and simulation software [116, 117, 118], conceived as an integrated simulation and traffic assignment model and performs traffic simulations by tracking the movement of individual vehicles every deci-second [24]. There are many different variations to the system's routing logic. Some of these techniques are static and deterministic while others are stochastic and dynamic. The car-following behavior of the system is characterized by the Rakha-Pasumarthy-Adjerid (RPA) model which consists of three components: Van Aerde steady-state car-following model [119, 120], collision avoidance model [121, 122] and vehicle dynamics model [88, 90]. It has been demonstrated that the RPA model can adequately capture both steady-state and non-steady-state car-following behavior [90, 112, 122, 123, 124]. In addition, INTEGRA-

TION has incorporated three microscopic energy/emissions models, known as VT-Micro, VT-CPFM and VT-CPEM, to generate environmental measures of effectiveness (MOEs). The VT-CPFM and VT-CPEM models, as discussed in section 2.1.1, can generate highly accurate energy estimates and also outperforms the other state-of-the-art models in terms of its simplicity in calibration and implementation.

In conclusion, most of the above-mentioned micro-simulators are capable of assigning traffic dynamically. For VISSIM and PARAMICS, the built-in car-following models have been demonstrated to provide unrealistic vehicle trajectories, and the energy/emissions models are not easily calibrated and implemented in ITS applications given the need of engine test. The car-following model within AIMSUM generates more accurate vehicle trajectories compared to VISSIM and PARAMICS; however, the built-in energy/emissions model, VERSIT+^{micro}, may result in estimation bias and the bang-bang control problem. INTEGRATION incorporates accurate energy/emissions models which can be calibrated using non-engine data and easily used by traffic simulation model and ITS applications. It is worth mention that the VT-CPEM model recently has been included. This enables INTEGRATION to generate MOEs relative to electric vehicles, which also makes it more competitive than the state-of-the-art counterparts. However, its validity of the simulated vehicle trajectories in terms of energy/emissions analysis has not been investigated yet, although the adequacy of car-following behavior has been demonstrated.

2.4 Eco-routing Systems

The commonly used User Equilibrium (UE) and System Optimum (SO) traffic assignment algorithms utilize minimum travel time or the marginal travel time respectively as a generalized cost to assign traffic flows over a network. However, given that UE and SO assignments are estimated based on travel time, energy consumption and emissions of UE and SO conditions may not achieve their optimum solutions. Several researchers have attempted to enhance traffic assignment methods from the energy and environmental perspective.

Tzeng et al. [25] developed a multi-objective (travel time, distance, and emissions) traffic assignment method, and produced various solutions that minimize CO emissions constrained by the other two objectives. The method assumed that link traffic flow was the only explanatory variable of CO emission. Namely, the link emission cost is a constant relative to speed/acceleration, vehicle type and road attribute. This is not correct in reality given that traffic conditions, road and vehicle characteristics significantly affect energy/emissions estimation. Furthermore, the method was developed for the transportation planning purpose and thus not suitable for real time navigation applications. A similar study was conducted by Nagurney et al. [26, 27] who developed a multi-class and multi-criteria traffic network equilibrium model with an environmental criterion. The model also made a constant assumption on link-specific emission factors.

Rilett et al. [28, 29] developed a macroscopic traffic assignment system with environmental considerations. Specifically, the system aimed to minimize CO emission which was estimated using average speed and link length as explanatory variables. The system outperforms Tzeng’s method by incorporating average speed and link length into the emission model, and is suitable for the planning purpose. Nonetheless, the system assumed that vehicles traveled at a constant rate on each link of their journey and that the grades on the roadways were 0%, failing to capturing the impact of within-link speed and grade variation on emissions. This may result in incorrect optimal solutions for operational level programs such as dynamic routing system.

Another macroscopic traffic assignment system was developed in 2002 by Sugawara and Niemeier [30]. The method also used average speed CO emission factors developed by the California Air Resources Board (CARB). The results of the study demonstrated that the emission-optimized trip assignments could reduce system-level vehicle emissions moderately compared to time-dependent UE and SO solutions, and was most effective when the network is under low to moderately congested conditions, saving up to 30% of total CO emissions. The results also demonstrated that the emission-optimized assignments became less effective when the network was highly congested, achieving emission saving of only 8%. Also, it was found that less traffic was assigned to freeway routes under minimum emission assignment given that emission levels became very high at high speeds.

Barth et al. [8, 31] presented an eco-routing navigation system that combined a microscopic energy/emissions model (CMEM) with a large vehicle activity database to create functional relationships between link-based energy/emission factors and a set of link-based explanatory variables (e.g. speed and road grade). The link-level energy consumption was characterized as a polynomial function of speed and grade as formulated in Equation (2.9):

$$\ln(f_k) = \beta_0 + \beta_1 v_k + \beta_2 v_k^2 + \beta_3 v_k^3 + \beta_4 v_k^4 + \beta_5 g_k \quad (2.9)$$

where f_k is the fuel consumption of link k , v_k is the link average speed, g_k is the link-specific road grade, and $\beta_{(\cdot)}$ are the model coefficients. According to Equation (2.9), the link cost function uses the average speed and grade as the inputs of the model without considering their within-link variation. Furthermore, the regression analysis may cause an unexplainable random error to the model estimates. In addition, this navigation system generates eco-routes only at the beginning of a trip; namely, vehicles en route cannot be re-routed to other routes even though the traffic conditions on the original route environmentally deteriorate.

Nie et al. [125] incorporated some of the microscopic factors (e.g. between-link acceleration and idling delay) into their eco-routing model. The model basically assumed that vehicles accelerated/decelerated only when they were traveling from one link to another. This assumption, however, also excludes the impact of within-link speed fluctuation. Another limitation of the model is the exclusive of the effect of road grade. Additionally, the model was developed based on the CMEM model which requires engine data for model calibration and implementation, and thus is not easily integrated into traffic simulation models and ITS

applications.

Rakha et al. [24, 126] developed and tested an agent-based eco-routing system in the simulation environment that comprehensively considered microscopic elements and was able to dynamically update link costs and eco-routes based on real time information. The system is essentially a feedback traffic assignment method that utilizes the fuel costs experienced by vehicles running on each link for eco-routes update. Link costs and eco-routes update is triggered by every vehicle's departure from its origin or from a link, and each vehicle is assigned individually based on routing suggestions. A major issue of the system is that it may generate unrealistic routing suggestions when there are multiple vehicle models in the network, given the assumption that different vehicle models have the identical link-specific fuel cost. In reality, however, different vehicle models may have different energy consumption behavior. For example, under the same traffic and road conditions, a heavy duty truck may produce significantly higher fuel consumption level than a passenger car. Furthermore, the results of the recent studies [12, 127, 128] imply that the optimum fuel economy cruise speed varies with vehicle models, demonstrating that optimum routes may be different between vehicle models. According to Rakha's eco-routing system, all vehicle models in the network have the same optimum route given the identical link-specific fuel cost. Consequently, this dynamic eco-routing system is not applicable to real world road networks in which there may be hundreds of vehicle models.

In summary, most of the existing eco-routing systems either do not comprehensively include microscopic elements, or cannot dynamically update eco-routes for the vehicles en route, or are unable to differentiate eco-routes between vehicle models. These systems thus cannot adequately generate realistic routing suggestions for in-vehicle navigation applications. To overcome these shortcomings, the dissertation develops an innovative eco-routing framework as being a submodule of the multimodal energy-efficient system.

2.5 Effect of Route Information on Route Choice Behavior

As captured in the "hot stove" effect [129], individuals were not inclined to select options associated with high variability, although these might actually provide larger benefits. Considering uncertainty, people do not have perfect knowledge of the gains that could be accrued and the loss associated with risking changing habitual choices. Prospect Theory [130] explicitly and thoroughly describes this psychological behavior that risk-seeking behavior would likely exhibit in the loss domain rather than in the gain domain. In relation to route choice, katsikopoulos et al. [131] verified the results of Prospect Theory through a simulated experiment in which participants were provided with the information of travel time variability, indicating that risk aversion emerged in the gain domain (alternative route is faster but riskier) while risk seeking emerged in the loss domain (alternative route is slower but

riskier). Accordingly, drivers repeatedly make illogical choices due to the risk aversion in the gain domain. Information is expected to reduce the uncertainty and enhance rational behavior partially by leading travelers to risk seeking in the gain domain. katsikopoulos et al. [131, 132] revealed that the provided information supported for choice rationality and reduced inertia.

The behavioral effect of route information on route choice behavior has been incrementally studied both from a theoretical and practical standpoint. Ben et al. [133] thoroughly investigated the combined effects of information and driving experience on route choice behavior using a simulated experiment. The results provided evidence to suggest that the expected benefit of information is achieved only if drivers lacked long-term experience. Based on this study, a discrete choice model with Mixed Logit specifications was developed to accurately describe the respondents' learning process under the provision of real-time information [134]. Further, Ben et al. [134] also demonstrated that information provided on average travel time resulted in different responses compared to information on travel time variability, which remained to be verified. Using a simulation- and a stated preference-based approach, numerous attempts were made to econometrically address the various behavioral mechanisms of drivers' route choice with real-time information. The studied behavioral mechanisms involved logical choice [133, 134], inertia choice [135], switching behavior [136, 137, 138] and habit and learning [139, 140]. Specifically, Karthik et al. [135] demonstrated that users experiences decreased inertia behavior in day-to-day variation. Route information was demonstrated by many studies to effectively move route choice towards rationality [133, 134, 136, 138, 141, 142, 143], however, the effect of information strongly depends on other factors, such as personal traits, trip characteristics, and other decision considerations. From the personal trait perspective, Jou et al. [136] concluded that elderly travelers would be less likely to switch due to the habitual and risk-averse effects, and male travelers would be more likely to switch to the best route. Also, trip characteristics and traveler preferences were proved by Polydoropoulou et al. [137] significantly to affect route switching and compliance with information. However, few of the existing studies have characterized the information effect of the details of trip characteristics, such as directness of the route, number of intersections, conflicts with non-motorized traffic.

Although previous attempts provided econometric and empirical generalizations, most were based on simulator and stated preference approaches. In the simulator surroundings, however, respondents make decisions in a digital and virtual environment. Stated preference is an investigative approach in which respondents are given questionnaires to make choices hypothetically. Both approaches are performed under fictitious conditions and may not accurately capture actual choice behavior. Consequently, an in-field case study is needed. To the author's best knowledge, this study, is the first attempt at addressing this need using dynamic travel time information, which differs from the previous real-world experiments (e.g. [144, 145, 146, 147]) that conducted experiments for a short time period (e.g. several days) and did not capture the day-to-day variation of route choice behavior using the learning mechanism that accounts for information effects. As a follow-up test of Tawfik and Rakha's

experiment (in which information was not available) [148], participants were provided with real time information during test driving.

Drivers' responses to information may differ based on personal characteristics, demographics, preferences and choice situations [149, 150]. Nonetheless, few studies so far have attempted to quantitatively investigate such discrepancy. Tawfik et al. [140] developed a latent class choice model by classifying personal traits and choice situations into four behavioral groups as illustrated in Table 2.1. The results demonstrated that the model outperformed traditional hierarchical models in predicting realistic behavior. However, Tawfik et al.'s study did not consider information effect. Accordingly, this study attempts to investigate the information effect considering different participants and choice situation characteristics in order to provide significant implications to enhance the design of the routing system.

In general, given the incomplete picture of the existing studies, more attempts are justified. The dissertation thus initiates a real world case study to provide a better understanding of underlying effects of route information on route choice behavior.

2.6 Summary

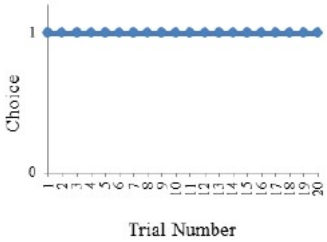
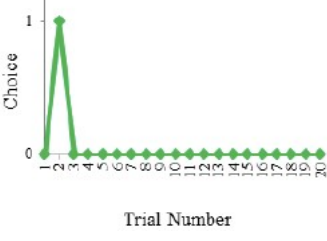
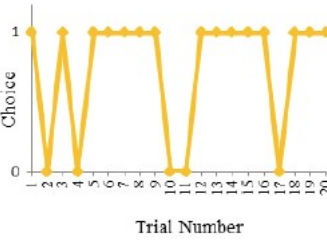
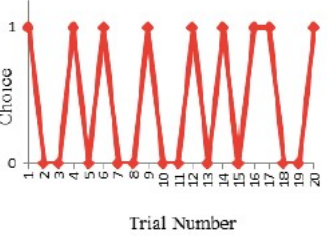
The review effort first demonstrates that the VT-CPFM and VT-CPEM modeling frameworks outperform the other state-of-the-art models in terms of either robustness in energy estimation or simplicity in model calibration and implementation. The frameworks are thus used in this dissertation to model HDDV and electric train energy consumption.

The literature relative to railway simulation and dynamics modeling demonstrates that existing efforts on dynamics modeling either cannot adequately capture realistic acceleration/deceleration behavior given the constant assumption on throttle or brake level, or require extensive mechanical engine data for model calibration and implementation, which limits their popularization in simulation applications. It is important to develop an accurate, simple and efficient longitudinal dynamics model to characterize typical train acceleration/deceleration behavior in support of the proposed subway system model.

Furthermore, the state-of-the-art traffic microsimulation models were investigated in order to identify the better suited model to serve as the testbed for the proposed eco-routing system. Five commonly used microsimulation models were reviewed: VISSIM, CORSIM, AIMSUM, PARAMICS, and INTEGRATION. The results demonstrate that INTEGRATION outperforms the other models in terms of the accuracy and simplicity of the built-in energy consumption and emissions models (VT-CPFM and VT-CPEM). However, the validity of INTEGRATION simulated vehicle trajectories for energy and environmental analysis needs to be investigated and compared with the other microsimulation models.

The literature relative to eco-routing studies demonstrates that most of the existing eco-routing systems may generate incorrect link costs and eco-routing solutions given their in-

Table 2.1: Four identified driver behavioral types

Behavior Type	Typical Behavior	Type Description
1	 <p>A line graph with 'Choice' on the y-axis (0 to 1) and 'Trial Number' on the x-axis (1 to 20). The data points are all at the value of 1, forming a horizontal line.</p>	<p>A driver starts by arbitrarily selecting a route, is apparently satisfied with the experience, and continues making the same choice for the entire 20 trials.</p>
2	 <p>A line graph with 'Choice' on the y-axis (0 to 1) and 'Trial Number' on the x-axis (1 to 20). The choice is 1 for trial 1 and 0 for all subsequent trials from 2 to 20.</p>	<p>A driver starts by arbitrarily selecting a route, is apparently not satisfied with the experience, tries the other route, and decides that the first route was better. The driver makes a choice after trying both routes and does not change afterwards.</p>
3	 <p>A line graph with 'Choice' on the y-axis (0 to 1) and 'Trial Number' on the x-axis (1 to 20). The choice is 1 for trials 1, 3, 5, 7, 9, 11, 13, 15, 17, 19 and 0 for trials 2, 4, 6, 8, 10, 12, 14, 16, 18.</p>	<p>A driver switches between the two alternative routes over the duration of the experiment. The driver, however, drives on one route more than the other route. This reflects his/her preference for the selected route.</p>
4	 <p>A line graph with 'Choice' on the y-axis (0 to 1) and 'Trial Number' on the x-axis (1 to 20). The choice alternates between 1 and 0 every trial, starting with 1 on trial 1.</p>	<p>A driver switches between the two alternative routes over the duration of the experiment. The driver drives both routes with approximately equal percentages. This reflects a lack of preference towards any of the alternatives.</p>

ability in capturing microscopic characteristics. Also, most of them are not able to route vehicles en route in real time, except for one of the systems [24] which, however, assumes that all vehicle models had the same eco-route. This is unrealistic in reality given that energy consumption behavior significantly differs between vehicle models. The major concern of this dissertation is thus to develop an innovative eco-routing system that is able to comprehensively consider microscopic elements and route vehicles in real time while at the same time differentiate vehicle models. The proposed eco-routing system is developed for in-vehicle navigation applications as being an integral of the multimodal energy-efficient routing system.

Finally, the review effort relative to information effect on route choice behavior demonstrates that the majority of the research efforts in this regard are based on simulation and stated preference approaches. Both approaches are performed under fictitious conditions and may not adequately capture realistic route choice behavior. Consequently, a real world case study is designed in this dissertation.

Chapter 3

Heavy Duty Diesel Vehicles Fuel Consumption Modeling

This chapter is based on the papers listed below:

1. Wang, J. and Rakha, H. Convex Fuel Consumption Model for Diesel and Hybrid Buses. *Transportation Research Record: Journal of Transportation Research Board*, 2017.
 2. Wang, J. and Rakha, H. Fuel Consumption Model for Conventional Diesel Buses. *Journal of Applied Energy*, 2016.
 3. Wang, J. and Rakha, H. Hybrid-Electric Bus Fuel Consumption Modeling: Model Development and Comparison to Conventional Buses. *Transportation Research Record: Journal of Transportation Research Board*, 2016.
 4. Wang, J. and Rakha, H. Fuel Consumption Model for Heavy Duty Diesel Trucks: Model Development and Testing. *Transportation Research Part D: Transport and Environment*. (In Review).
-

This chapter aims to develop conventional HDDVs fuel consumption model based on the VT-CPFM modeling approach. The resulting models will be used to estimate HDDVs trip fuel costs and eco-routes. Truck and transit bus are modeled in this study as the most typical representatives of HDDVs.

3.1 Introduction

Although HDDVs make up only a fraction of the total vehicle population, they are major contributors to GHG emissions in the transportation sector. For example, heavy duty diesel trucks (HDDTs) account for 22.8% of the total CO₂ production [2]. Also, bus fuel consumption had been continually increasing from 827 million gallons/year to 2,059 million gallons/year between 1960 and 2012 as reported by the U.S. Bureau of Transportation Statistics (BTS). HDDVs are receiving increasing attention from legislators, the government and society at large. For example, in September 2011, the National Highway Traffic Safety Administration (NHTSA) and the U.S. Environmental Protection Agency (EPA) jointly promulgated the first-ever federal regulations mandating improvements in fuel economy of heavy-duty commercial vehicles [151]. Furthermore, researchers have been committed to developing road eco-freight [152, 153, 154, 155] and eco-transit programs [156, 157] in order to support “green transportation” policy making.

A simple, accurate and efficient fuel consumption model is needed to provide robust fuel estimates in support of quantifying potential reductions in fuel consumption and emission levels induced by implementing eco-freight or eco-transit strategies. As mentioned in section 2.1, the VT-CPFM model outperforms the other state-of-the-art models so that is applied for HDDVs modeling.

3.2 Modeling Framework

Rakha et al. [12] developed two VT-CPFM frameworks (VT-CPFM-1 and VT-CPFM-2) for LDVs each of which is a two-regime model and characterizes fuel consumption as a second-order polynomial function of vehicle power. The use of a second-order model ensures that a bang-bang control does not result from the application of the model. Furthermore, a model higher than a second-order model cannot be calibrated using standard drive cycles given the complexity of the higher order model. Consequently, a second-order model achieves a good trade-off between model accuracy and applicability. However, only VT-CPFM-1 is utilized to develop the model in this study given that VT-CPFM-2 requires engine gear data which is typically not available. The VT-CPFM hereinafter refers to the VT-CPFM-1 model.

The VT-CPFM modeling framework is illustrated in Equation (3.1) with P the vehicle power (kW) and α_0 , α_1 , and α_2 the vehicle type-specific model coefficients. The power function

is formulated by Equation (2.3). A second-order polynomial function was used to model the positive power condition in order to circumvent the bang-bang type of control [12]. For the negative power condition, fuel consumption is a constant which equals the idling fuel rate. The model has been validated for LDVs by Park et al. [43] using real world data, demonstrating a good model fit to field measurements.

$$FC(t) = \begin{cases} \alpha_0 + \alpha_1 P(t) + \alpha_2 P(t)^2, & \forall P(t) \geq 0 \\ \alpha_0, & \forall P(t) < 0 \end{cases} \quad (3.1)$$

It should be noted that the model coefficients, α_0 , α_1 , and α_2 , can be calibrated using publicly available data using Equation (3.2)-(3.4):

$$\alpha_0 = \frac{P_{fmp} \omega_{idle} d}{22164(HV)N} \quad (3.2)$$

$$\alpha_2 = \frac{(F_{city} - F_{hwy} \frac{P_{city}}{P_{hwy}}) - (T_{city} - T_{hwy} \frac{P_{city}}{P_{hwy}}) \alpha_0}{P_{city}^2 - P_{hwy}^2 \frac{P_{city}}{P_{hwy}}} \quad (3.3)$$

$$\alpha_1 = \frac{F_{hwy} - T_{hwy} \alpha_0 - P_{hwy}^2 \alpha_2}{P_{hwy}} \quad (3.4)$$

Here P_{fmp} is the idling fuel mean pressure (400,000 *Pa*); d is the engine displacement (*l*); HV is the fuel lower heating value (43,000,000 *J/kg* for gasoline and 43,200,000 *J/kg* for diesel); N is the number of engine cylinders; ω_{idle} is the engine idling speed (*rpm*); F_{city} and F_{hwy} (*liters*) are the fuel consumed for the EPA city and highway drive cycles (*mpg*); P_{city} , P_{city}^2 , P_{hwy} , P_{hwy}^2 are the sum of the power and power squared over the EPA city- and highway- cycle respectively; T_{city} and T_{hwy} are the duration of EPA city and highway drive cycles (*s*). Most of the parameters are related to either physical characteristics of the vehicles or fuel type, and stated as specifications by vehicle manufacturers. Nonetheless, the HDDVs standard driving cycles and the relevant fuel economy data cannot be obtained given that EPA does not require HDDVs to report the cycle-specific fuel economy data. Consequently, instead of using publicly available data, the HDDVs models were calibrated based on in-field data.

3.3 Heavy Duty Diesel Truck Fuel Consumption Modeling

This section presents the procedure and results of HDDTs fuel consumption modeling.

Table 3.1: Heavy duty diesel truck vehicle-specific information

Make/Model	Model Year	Engine Make/Model	Rated Power (hp)	Engine Size (l)	Vehicle Mass (kg)
International/ 9800 SBA	1997	Cummins/M11-330	330	10.8	7182
Freightliner/ D120	1997	DDC/C-60	360/400	12.7	7758
Freightliner/ D120	1997	Cummins/N14	370/435	14	7029
Freightliner/ C-120	1997	Cummins/N14	370/435	14	7623
Freightliner/ C-120	1998	DDC/C-60	370/430	12.7	8028
Freightliner/ FDL 120	1999	DDC/C-60	470	12.7	8118
Freightliner/ FDL 120	1999	DDC/C-60	360	12.7	8118
Freightliner/FLD 120	2001	CAT/C-15	475	14.6	7092

3.3.1 Data Preparation

The data used for model development were collected and provided by the University of California (UC) at Riverside. The modeling effort aimed to test the applicability of the VT-CPFM framework to modeling the HDDTs within diverse vehicle-technology categories. The recruited trucks differ in a wide range of vehicle specifications. A total of eight trucks were randomly recruited from used vehicle fleets in Southern California within test categories by vehicle model year and engine model/displacement, and a balance between horse power and manufacturers was attempted. The detailed vehicle information is presented in Table 3.1. For simplicity, the eight trucks, from the top to the bottom of Table 3.1 are respectively denoted as HDDT1, HDDT2, HDDT3, HDDT4, HDDT5, HDDT6, HDDT7, HDDT8.

To adequately measure real-world fuel consumption and emission levels, UC Riverside developed a mobile emissions research laboratory (MERL) that contains all instrumentation that is normally found in a regular vehicle emission laboratory. MERL weighs approximately 45,000 lbs and could serve as a truck load, so that it is capable of capturing the transient fuel consumption and emissions of a truck pulling it when the truck is being tested. Further details of MERL can be found in [158, 159].

The HDDT test was conducted by the Center for Environmental Research and Technology at UC Riverside on the roadways in California’s Coachella Valley involving long, uninterrupted stretches of road, approximately at sea level. All trucks were tested using standard fuel from the same source. The data were recorded at a frequency of 1 Hz and a total of 238,893 seconds of data were gathered with a collection of 8 parameters for each truck, including CO_2 , CO, HC, NO_x , velocity, fuel rate, engine speed and elevation. For more details on data collection procedure, the reader is recommended to see [158]. It should be noted that the primary goal of this section is to model fuel consumption and CO_2 emissions, and modeling CO, HC and NO_x emissions is out of the scope of this research effort.

The raw fuel consumption rates were in g/s and then converted to l/s in order to use the VT-CPFM framework to develop the proposed model. Also, the unit of velocity was converted from mi/h to km/h for the modeling purpose. Upon comparing second-by-second CO_2 emissions with engine control unit (ECU) data (i.e. velocity, fuel rate and engine speed), a time delay was detected. Consequently, a time alignment was needed to synchronize the

Table 3.2: Parameters required for truck model calibration

Parameter	Value	Source
Drag coefficient (C_D)	0.78	[88]
Altitude correction factor (C_h)	NA^a	Computed from field data
Vehicle frontal area (A_f)	10.0 m^2	Computed from truck dimensions
Vehicle speed (v)	NA^a	Measured in field
Mass (m)	NA^a	Manufacturer website
Rolling coefficient (C_r)	1.25	[88]
c_1	0.0328	[88]
c_2	4.575	[88]
Road grade (G)	NA^a	Computed from field data
Acceleration (a)	NA^a	Computed from field data
Driveline efficiency (η)	0.94	[88]

^aThe parameter is not a single value.

raw data. Since fuel rates have a strong relationship with emissions, they were utilized to determine the value of the required time shift. The proper time shift was determined through a cross-correlation analysis by which the correlation coefficients between CO_2 and fuel data were estimated by a correlation function for a range of lag times. The lag times with the highest correlations were selected as the optimal events. It should be noted that the CO_2 emission data collected for two of the trucks (HDDT 4 and HDDT 5) were invalid due to an error in the emission sensors of MERL during data collection, and the CO_2 model thus did not cover these vehicles.

3.3.2 Model Development

Each tested truck was individually modeled. Table 3.2 gives a generalization of the model inputs along with their sources. Some of the variables are capable of being gathered in the field (e.g. vehicle speed), and some can be obtained from either the literature or manufacturer websites (e.g. drag coefficient, vehicle mass).

As demonstrated by Figure 3.1, the empirical fuel consumption points to a concave function of vehicle power for the positive power condition. The model was calibrated with general linear regression analysis, and modeling results are summarized in Table 3.3. The second-order parameters (α_2) are negative, demonstrating that fuel consumption indeed varies as a concave polynomial function of vehicle power and that exhibits a mild growth with the increasing power. This is similar to the transit bus model developed by the author of the dissertation [41, 160].

Nonetheless, the concave model may produce unrealistic driving recommendations as demon-

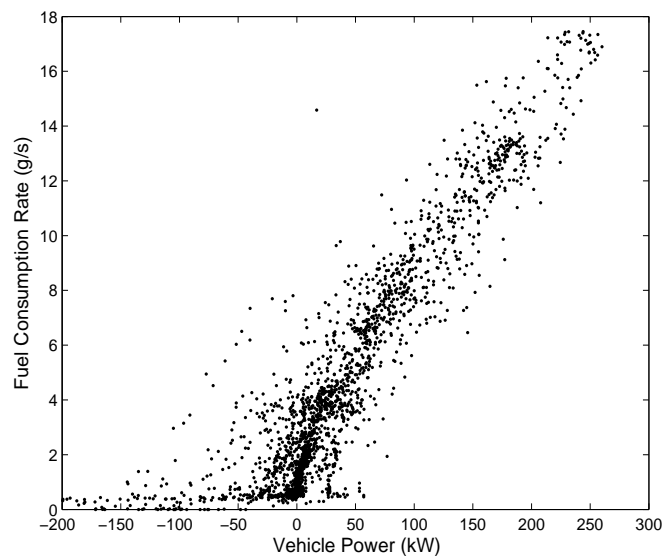


Figure 3.1: Vehicle power vs. fuel consumption functional form (truck)

Table 3.3: Truck concave model

Truck classification	α_0	α_1	α_2
HDDT 1	1.13E-03	1.11E-04	-1.71E-07
HDDT 2	1.88E-03	1.01E-04	-1.27E-07
HDDT 3	1.56E-03	1.09E-04	-1.24E-07
HDDT 4	1.42E-03	1.03E-04	-1.22E-07
HDDT 5	1.38E-03	1.10E-04	-1.64E-07
HDDT 6	1.02E-03	1.06E-04	-9.28E-08
HDDT 7	9.18E-04	1.06E-04	-8.75E-08
HDDT 8	2.02E-03	8.78E-05	-3.33E-08

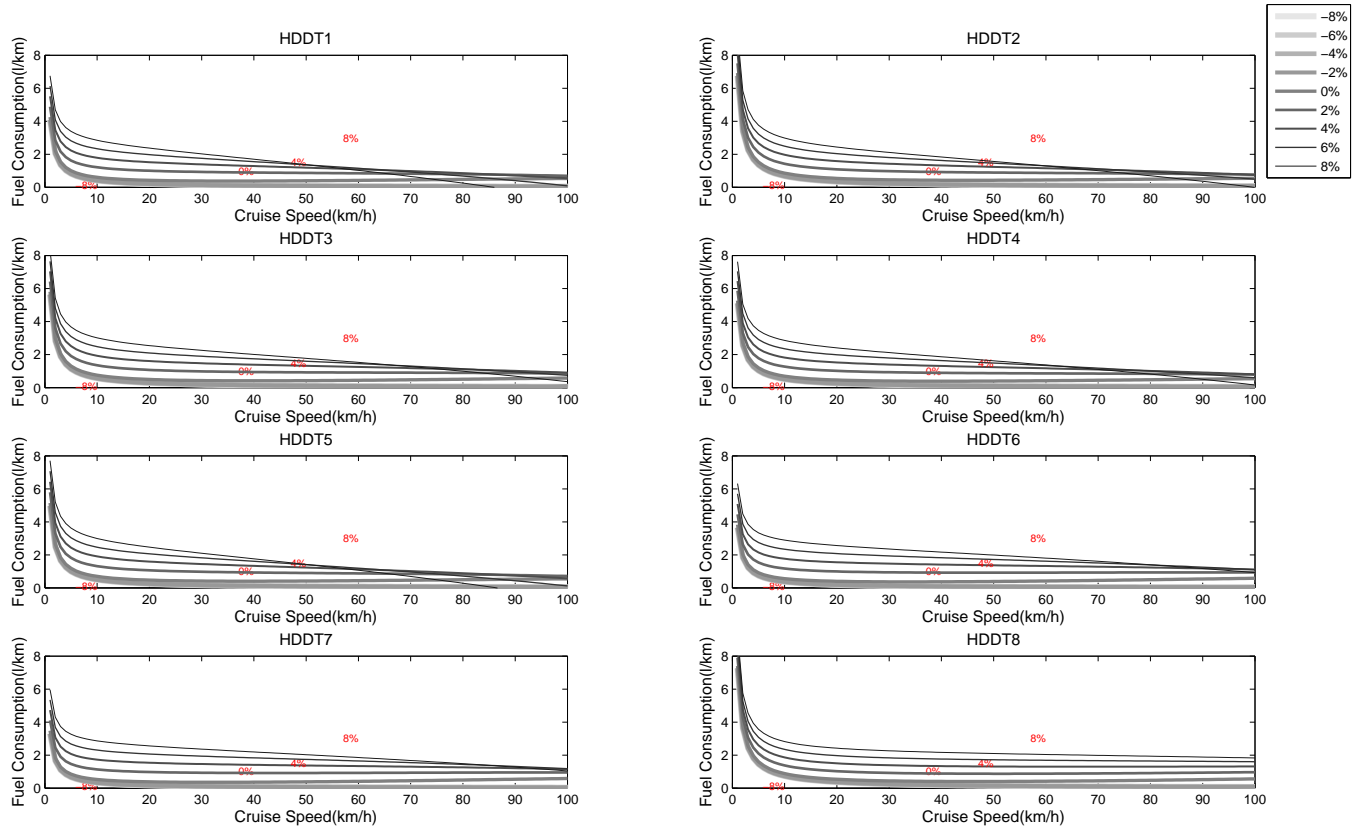


Figure 3.2: Fuel consumption vs. cruise speed at different grade levels (truck concave model)

stated by the sensitivity of estimated optimum fuel economy cruise speed to road grade and vehicle weight, as illustrated in Figure 3.2 and Figure 3.3, respectively. The road grade varies from -8% to 8% with a span of 2%, and the vehicle weight varies from 17,000 *kg* to 38,000 *kg* by having a identical span of 1000 *kg*. Figure 3.2 characterizes the variation of fuel consumption over cruise speed at different grade levels, demonstrating that the optimum fuel economy cruise speed increases with the rising gradients. This implies that drivers have to maintain a higher speed on steeper roads to minimize their fuel consumption levels, which is not realistic in reality. Figure 3.3 also gives unrealistic results that heavier vehicles result in higher optimum cruise speeds, implying that, drivers of heavier vehicles, compared to those driving lighter vehicles, are recommended to achieve higher cruise speed to minimize their fuel consumption levels. Given that the concave model generates a mild increase of fuel consumption with the growth of vehicle power, the unrealistic driving recommendations cannot be avoidable.

Given the deficiency of the concave model, an enhancement was considered to make the model

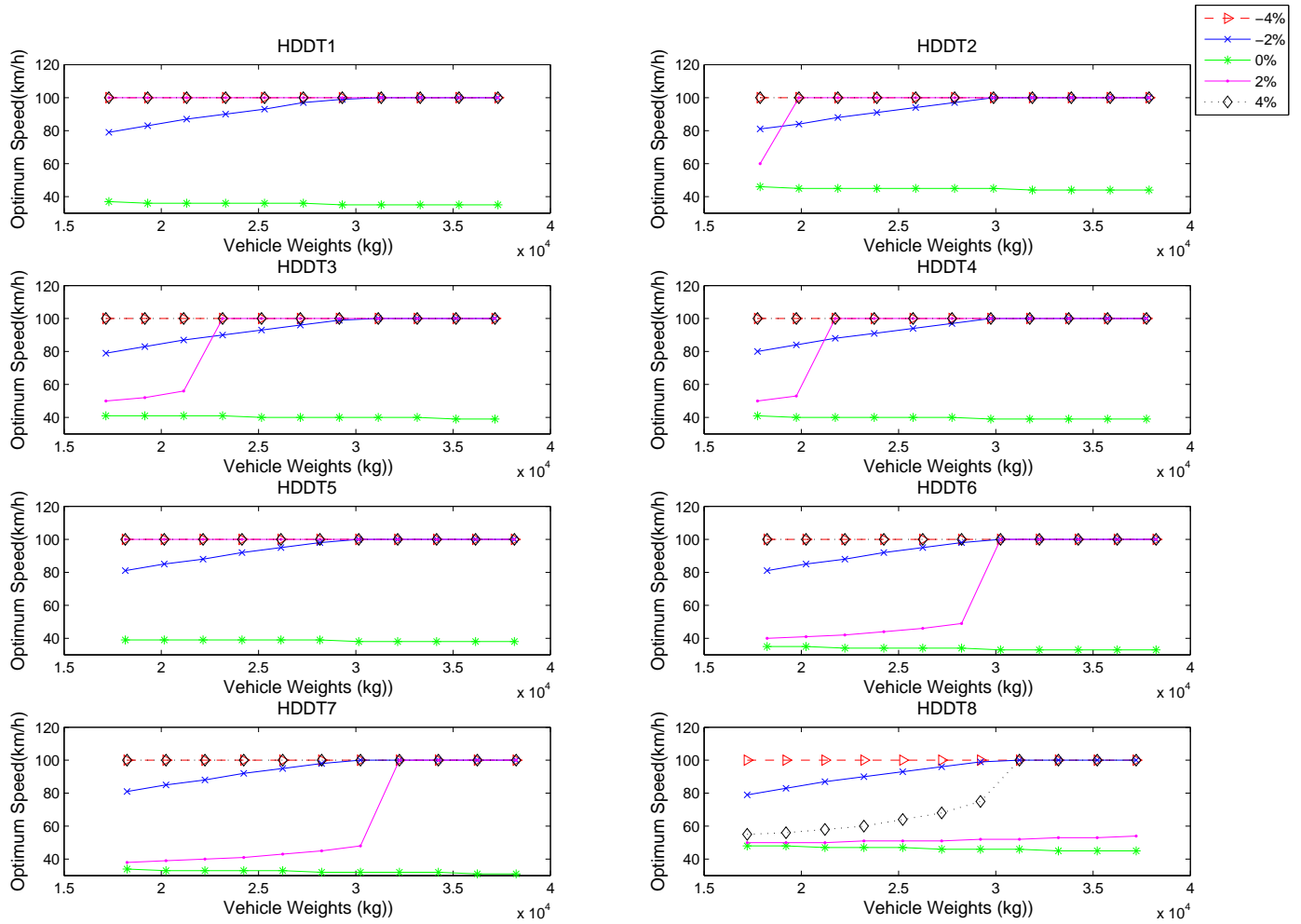


Figure 3.3: Impacts of vehicle weight on the optimum fuel economy cruise speed at different grade levels (truck concave model)

Table 3.4: Truck convex model

Truck classification	α_0	α_1	α_2
HDDT 1	1.56E-03	8.10E-05	1.00E-08
HDDT 2	2.48E-03	7.14E-05	1.00E-08
HDDT 3	2.26E-03	7.82E-05	1.00E-08
HDDT 4	1.80E-03	7.96E-05	1.00E-08
HDDT 5	2.02E-03	7.59E-05	1.00E-08
HDDT 6	1.45E-03	8.48E-05	1.00E-08
HDDT 7	1.31E-03	8.63E-05	1.00E-08
HDDT 8	2.16E-03	7.98E-05	1.00E-08

more applicable in reality. The convex model had been developed for LDVs and validated to be capable of generating reasonable driving instructions in existing eco-driving and eco-routing systems [24, 161, 162]. Consequently, the model was alternatively developed for the tested trucks (linear model has not been considered given that it produces the bang-bang control).

To develop a convex model, the order of magnitude of the second-order parameter, which impacts the degree of convexity of the function, needs to be determined. Basically, a lower order of magnitude generates estimates of the convex model less consistent with those of the concave model. However, a higher order of magnitude, although more accurate, is very similar to a linear model. A trade-off is thus needed between the accuracy of the model and the degree of convexity. The performance of the convex model in terms of R^2 values has been comprehensively investigated by varying the order of magnitude from $1E - 05$ to $1E - 11$, as illustrated in Figure 3.4. For each model, the R^2 value increases with the growth of the order of magnitude, while the performance achieves little improvement when the coefficient is higher than $1E - 08$. Consequently, $1E - 08$ was considered as the best order of magnitude in balancing the model performance and the degree of convexity of the model. The convex model is summarized in Table 3.4.

The effects of road grade and vehicle weight on the optimum fuel economy cruise speed were also evaluated for the convex model. As illustrated in Figure 3.5, the model produces a bowl-shaped curve as a function of cruise speed and higher road grades result in higher fuel consumption levels, which is similar to LDVs. Specifically, Figure 3.6 reveals that, when moving downhill, high cruise speeds can minimize fuel consumption levels, yet not recommended for safety purposes. For uphill, steeper roads result in lower optimum cruise speeds, implying that drivers have to reduce their cruise speed to minimize their fuel consumption levels with an increase in the road gradient.

Heavier vehicles, as demonstrated in Figure 3.7, have higher optimum cruise speeds when moving downhill while lower when moving uphill. It should be noted that, in Figure 3.7a, optimum cruise speeds remain constant with an increase in vehicle weight when the road grade is -8%, -6% and -4%. This is because the sensitivity analysis was performed only for the

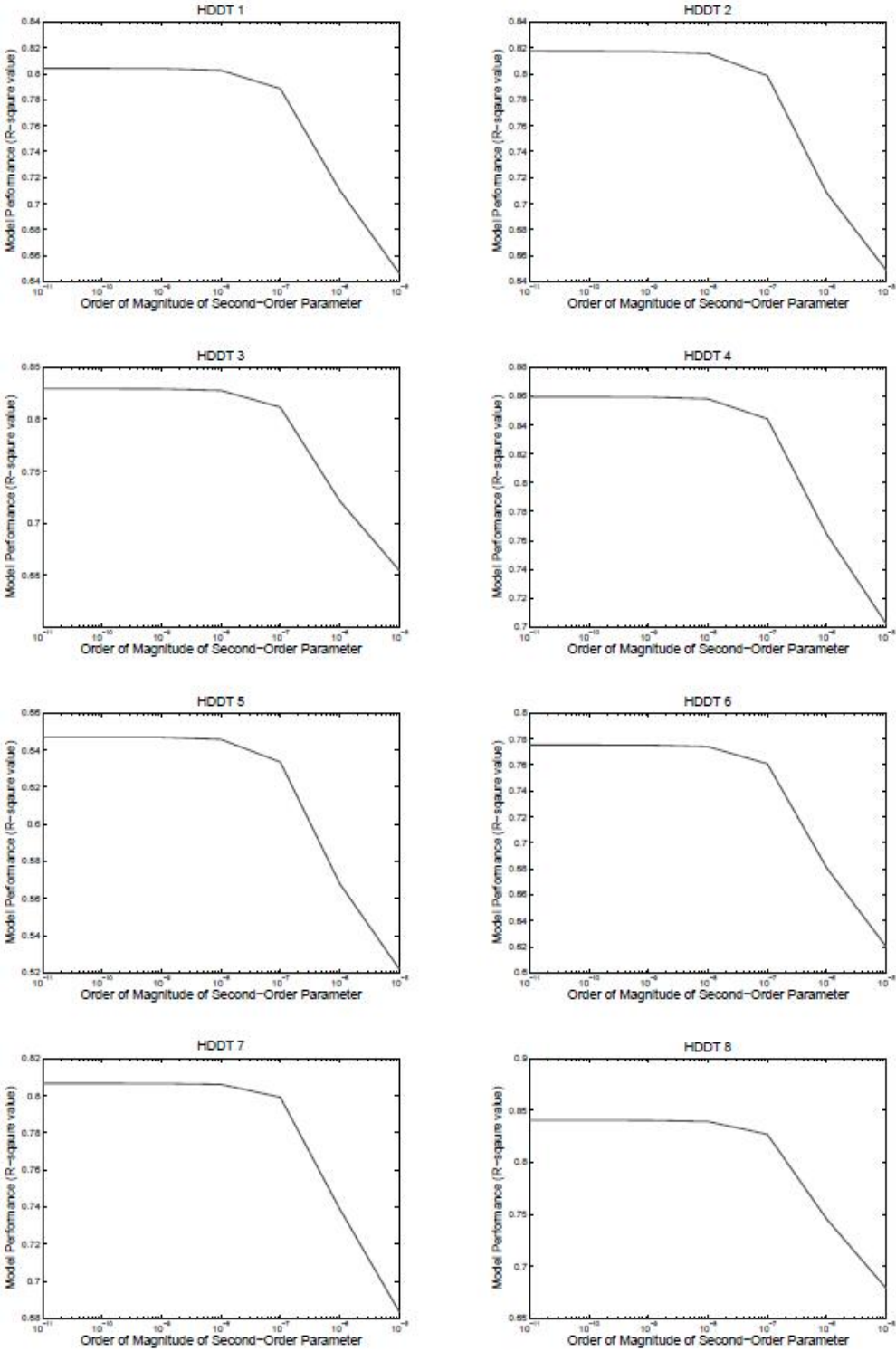


Figure 3.4: Model performance vs. order of magnitude of the second-order parameter (truck model)

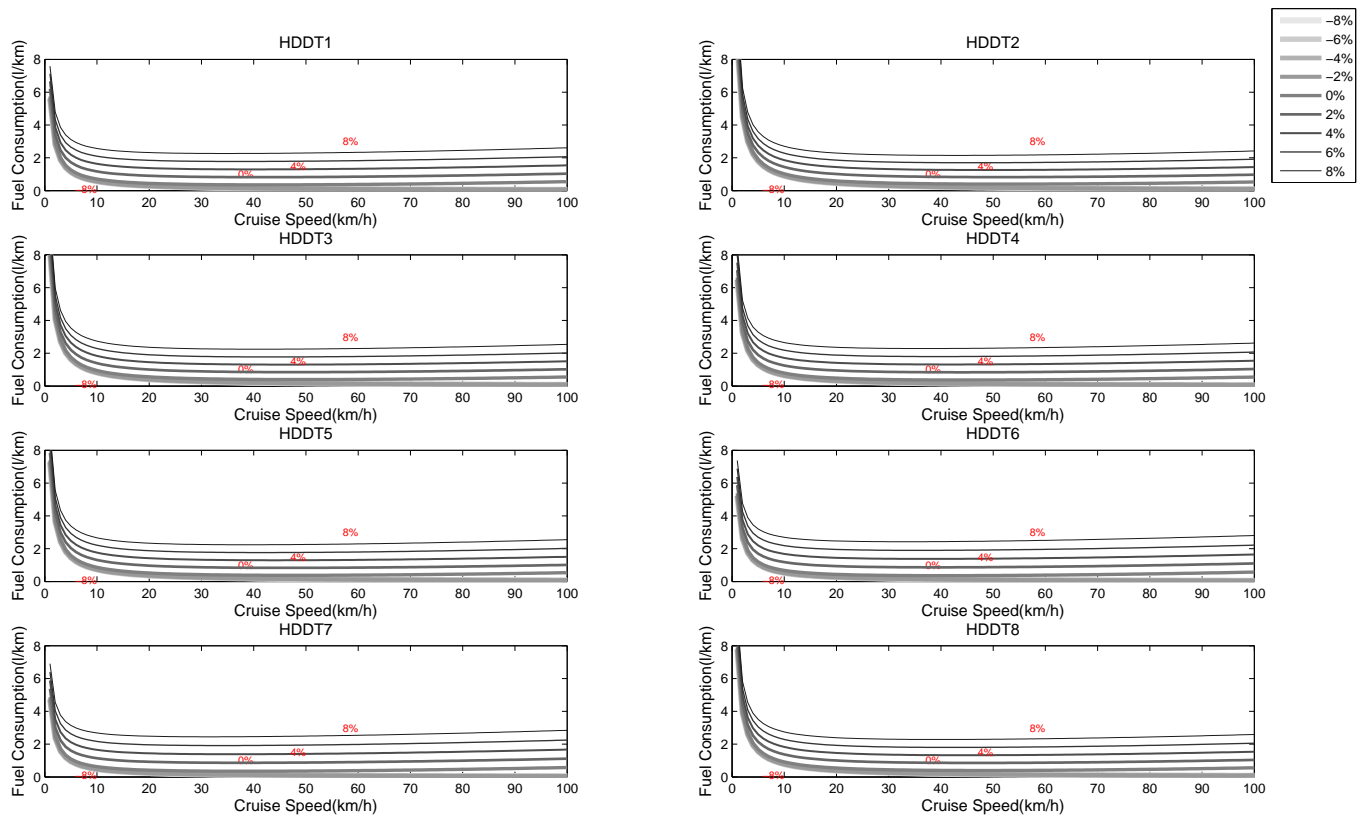


Figure 3.5: Fuel consumption vs. cruise speed at different grade levels (truck convex model)

speed range of 0-100 km/h and the optimum cruise speeds already reached the maximum level when vehicle weights were at a low level (e.g. 17,000 kg). Furthermore, Figure 3.7b clearly demonstrates that the optimum cruise speeds are more sensitive to vehicle weight at higher grade levels. In short, the convex model can provide reasonable driving recommendations and thus be applicable to eco-driving and eco-routing systems.

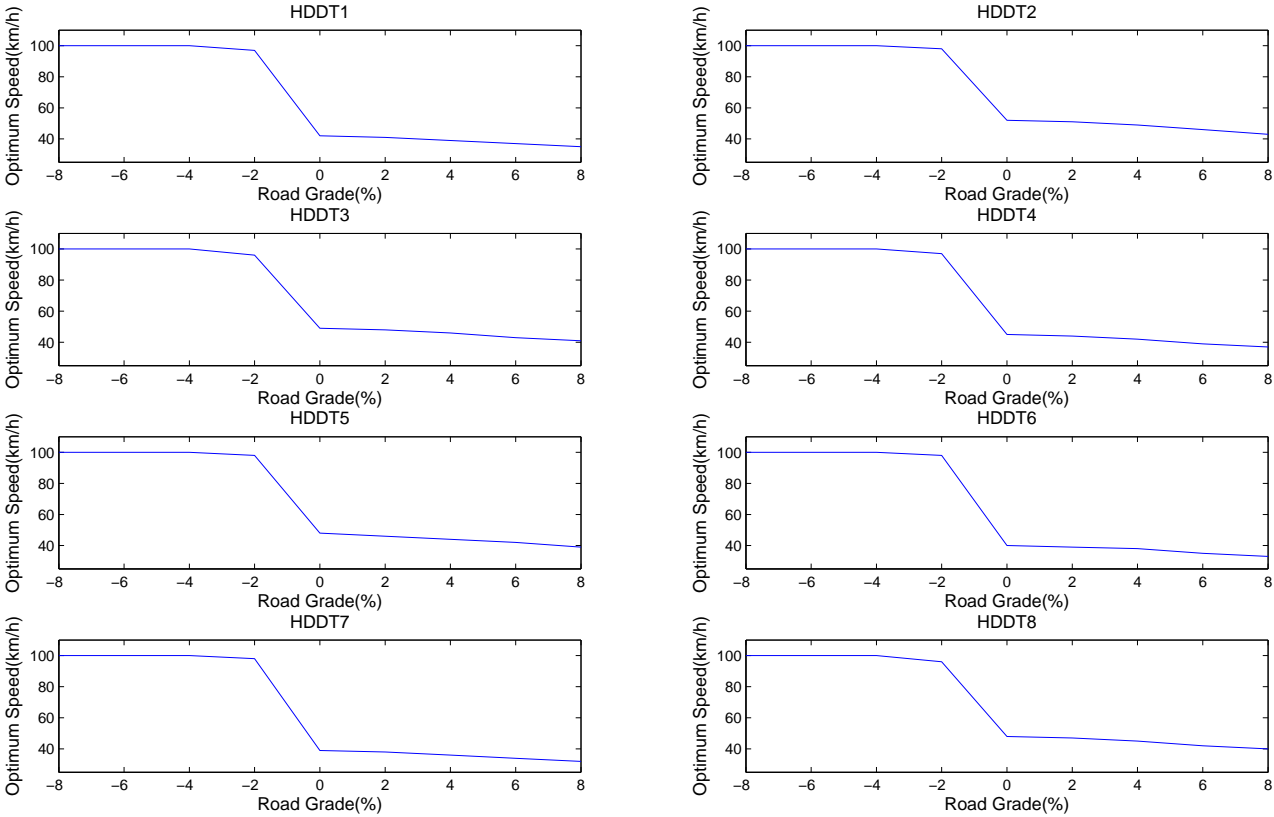
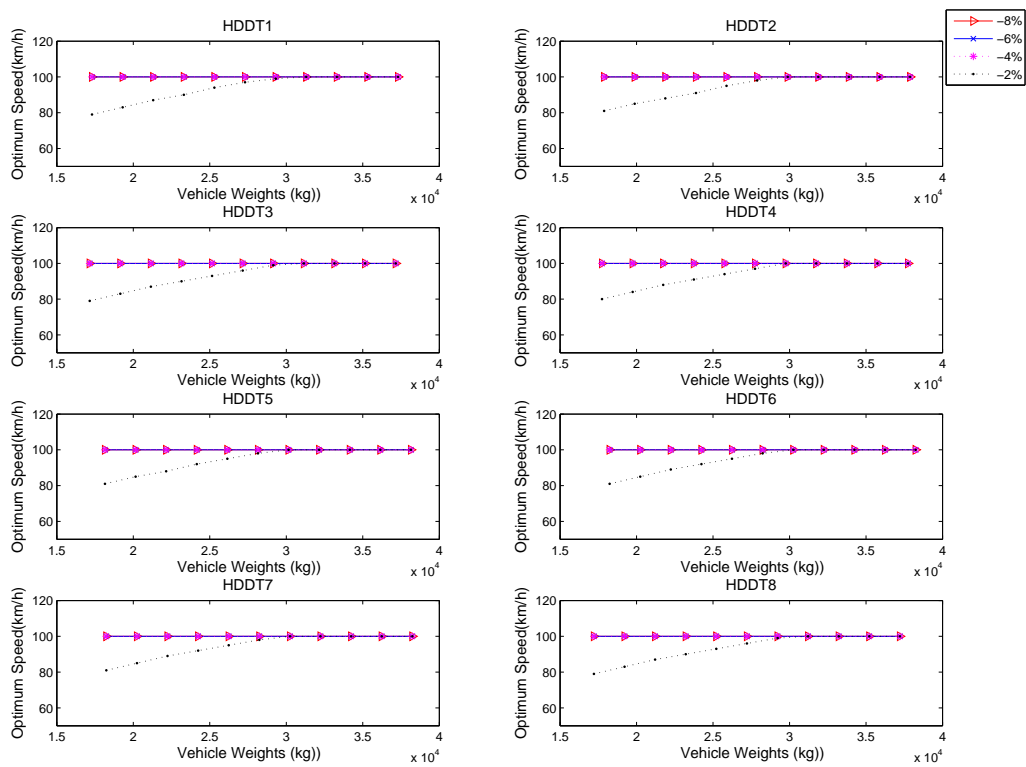
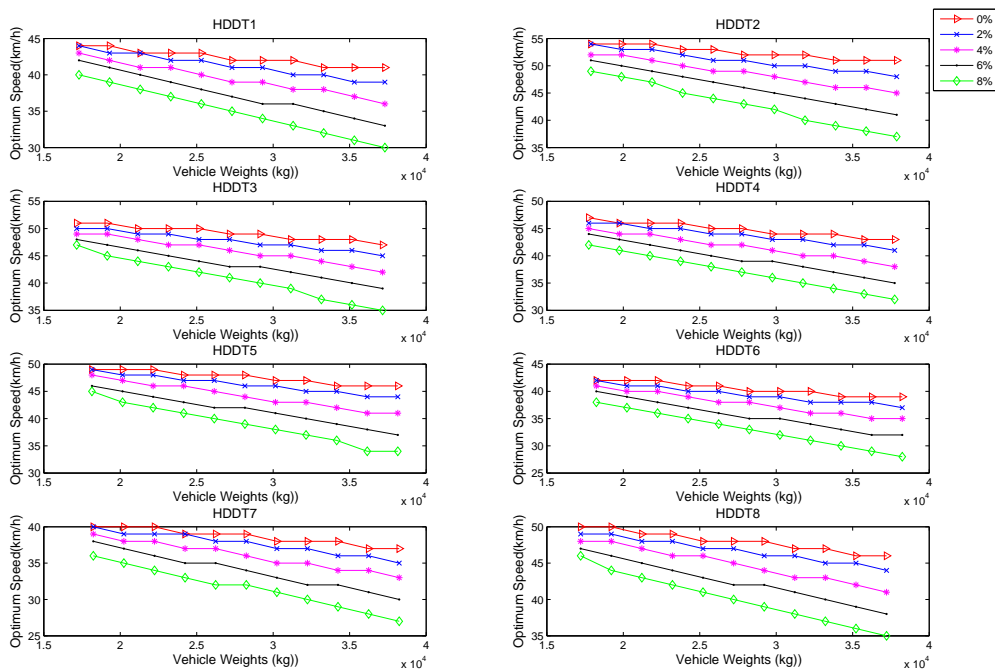


Figure 3.6: Impacts of road grade on the optimum fuel economy cruise speed (truck convex model)



(a) downhill



(b) uphill

Figure 3.7: Impacts of vehicle weight on the optimum fuel economy cruise speed at different grade levels (truck convex model)

Table 3.5: Comparison of truck model performance

Truck classification	VT-CPFM (concave)		VT-CPFM (convex)		CMEM		MOVES	
	R^2	Slope	R^2	Slope	R^2	Slope	R^2	Slope
HDDT 1	0.82	0.93	0.80	0.87	0.87	0.78	0.72	0.42
HDDT 2	0.83	0.81	0.81	0.76	0.87	0.75	0.76	0.39
HDDT 3	0.84	0.92	0.83	0.81	0.90	0.78	0.77	0.42
HDDT 4	0.87	0.91	0.86	0.88	0.90	0.77	0.78	0.42
HDDT 5	0.66	0.75	0.64	0.69	0.71	0.65	0.57	0.39
HDDT 6	0.78	0.89	0.77	0.86	0.83	0.72	0.72	0.38
HDDT 7	0.81	0.82	0.81	0.78	0.85	0.64	0.74	0.35
HDDT 8	0.84	0.86	0.84	0.84	0.89	0.79	0.78	0.43

3.3.3 Model Validation

A rigorous validation procedure was designed using an independent dataset. The validation process was firstly initiated by comparing the model estimates with field measurements along with CMEM and MOVES estimates at an instantaneous level. Furthermore, the variation of fuel estimates over cruise speed was compared between the proposed model and CMEM. Finally, CO₂ emissions were computed using fuel estimates and validated against in-field measurements.

Figure 3.8 provides two example illustrations of the instantaneous model validation, demonstrating that the model estimates in general provide a good agreement with in-field measurements as well as CMEM and MOVES predictions by following the peaks and valleys of the fuel rates. Specifically, Table 3.5 statistically summarizes the performance of different models. Basically, CMEM performs the best in terms of R^2 values, whereas it produces a bang-bang type of control. Although convex models have a slightly lower R^2 value compared to concave models, they can provide realistic driving recommendations. MOVES performs the worst among the models given that it is designed for conformity use instead of instantaneous analysis; however, it can reflect a large proportion of transient fuel consumption behavior by producing relatively high R^2 values.

Based on the slopes of the regression lines between model estimates and field measurements, all of the models tend to underestimate fuel consumption levels by having slopes smaller than 1.0, while the VT-CPFM model produces better approximation to measurements with higher slope values than CMEM and MOVES. MOVES has extremely low slope values given that the MOVES database has no trucks as heavy as the combination of the test truck plus the MERL trailer. The researchers at UC Riverside used MERL to collect data which was accounted for as part of truck load, which makes the total truck load extremely high.

In validating the proposed model, the variation of fuel predictions over cruise speed was also compared against CMEM results, as illustrated in Figure 3.9 which gives one example result. The two models have highly consistent bowl shaped curves as a function of cruise speed,

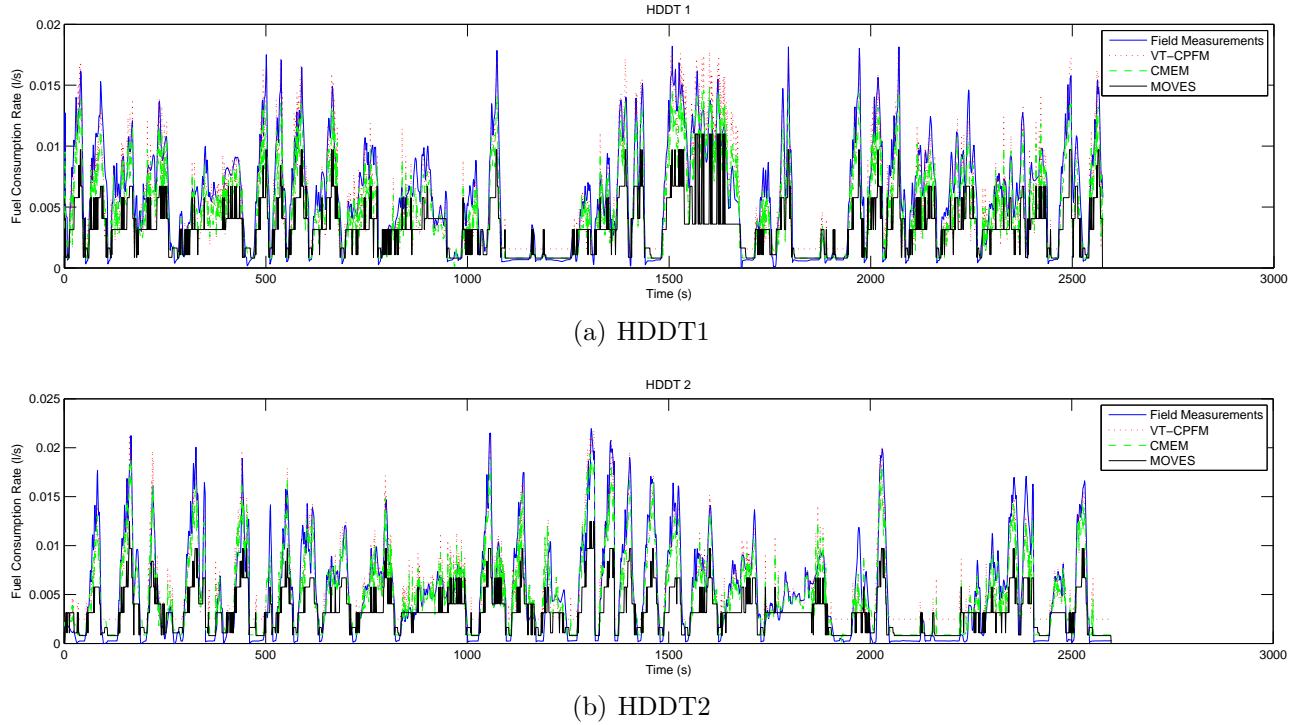


Figure 3.8: Instantaneous truck model validation

demonstrating that the proposed model can produce robust fuel estimates. Specifically, the optimum cruise speed ranges between $32\sim 52\text{ km/h}$ (lower than LDVs: $60\sim 80\text{ km/h}$) for all of the test trucks varying the grade level from 0% to 8%, and moves towards the negative direction with the increase of vehicle load and grade level.

The validation effort was also conducted for CO_2 estimation. CO_2 basically can be estimated from the carbon balance equation using the fuel consumption, HC and CO estimates. Given that the magnitude of CO_2 emissions is significantly higher than HC and CO emissions, the fuel consumption level is thus the primary factor that affects CO_2 emissions. As demonstrated in [12], CO_2 emission is linearly related to fuel consumption. Equation (3.5) was used to capture the relationship between CO_2 and fuel predictions. The model was first calibrated for each truck individually with CO_2 in g/s and fuel consumption in l/s , and the resulting model coefficient (θ) values were then averaged over individual models to generate the average model given that the relationship between CO_2 and fuel consumption is only relevant to fuel type rather than vehicle type. The average θ value was found to be 2070. CO_2 estimates were demonstrated to be consistent with field measurements, as the example results illustrated in Figure 3.10. The results of other validation efforts are summarized in Table 3.6 which has an R^2 values ranging between 0.74 and 0.85. In general, the model provides reliable CO_2 predictions. Noticeably, the model cannot be validated for HDDT 4 and HDDT 5 due to a lack of valid CO_2 field data, and the model performance is thus not

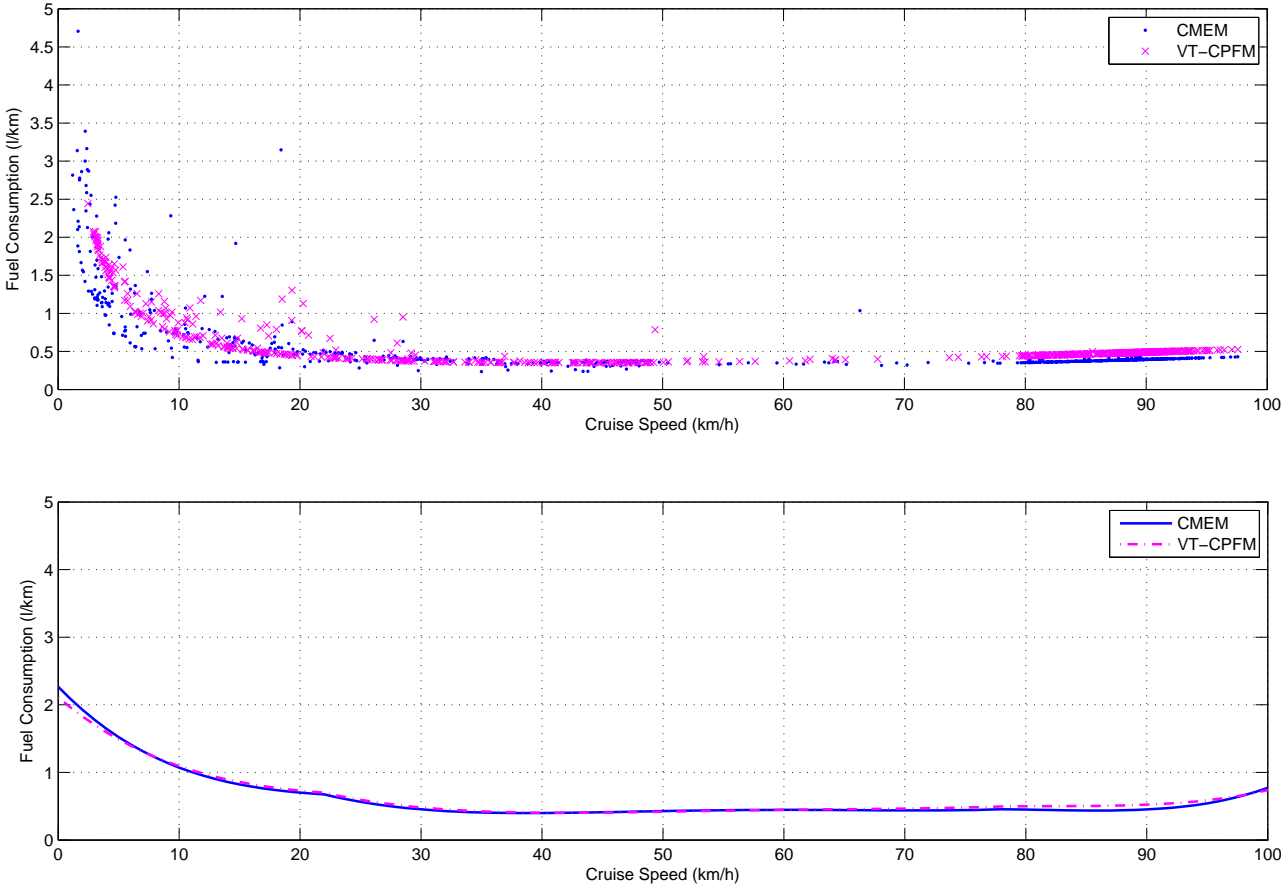


Figure 3.9: Impact of cruise speed on truck fuel consumption levels: VT-CPFM vs. CMEM

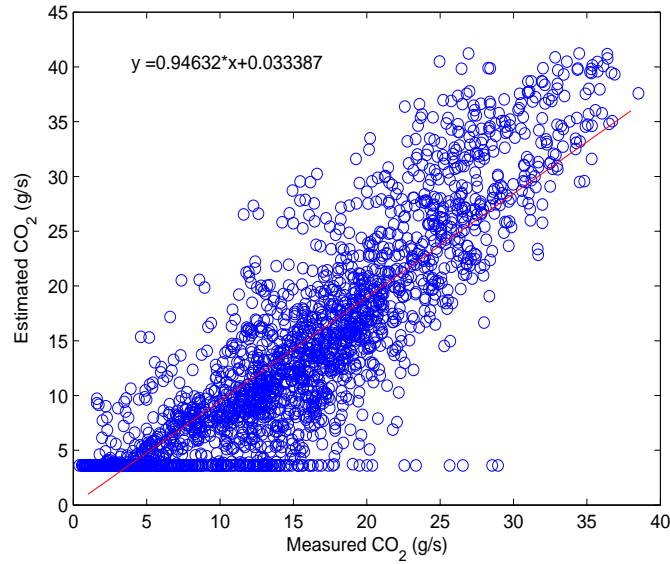


Figure 3.10: CO₂ estimation using fuel consumption rate (HDDT 1)

discussed for these vehicles.

$$\theta = \frac{CO_2(t)}{FC(t)} \tag{3.5}$$

Table 3.6: The performance of truck CO₂ models

Truck Classification	Coefficients of determination (R^2)	Slope
HDDT 1	0.78	0.95
HDDT 2	0.85	0.72
HDDT 3	0.81	0.82
HDDT 4	NA ^a	NA ^a
HDDT 5	NA ^a	NA ^a
HDDT 6	0.74	0.73
HDDT 7	0.81	0.65
HDDT 8	0.79	0.82

^aCO₂ model cannot be validated due to the invalid CO₂ in-field measurements.

3.4 Diesel and Hybrid-Electric Bus Fuel Consumption Modeling

This section presents the procedure and results of fuel consumption modeling for conventional diesel and hybrid-electric transit buses. The resulting models will be used to estimate bus trip energy consumption in support of door-to-door trip energy estimation.

3.4.1 Data Preparation

The field data were collected by test driving the buses around the town of Blacksburg, Virginia. The test was conducted on two types of roads: US 460 (highway with a speed limit of 65 mi/h (104 km/h)) and local streets with speed limits ranging between 25 mi/h and 45 mi/h (40–72 km/h) in order to cover a wide range of driving conditions. The test routes comprised a variety of uphill and downhill sections, and thus provided a suitable environment to test different engine load conditions.

A total of 22 transit buses (14 diesel buses and 8 hybrid buses) were tested under similar ambient temperature conditions to minimize the impact of other external factors on the data. Specifically, the diesel buses were classified into four series (19XX, 62XX, 630X, and 632X). The hybrid buses were categorized into two series (601X and 602X). Within the same series, buses have identical vehicle properties, as illustrated in Table 3.7 in which bus specifications were provided.

The Hydraulics + Electrical + Mechanical (HEM) logger was used for data acquisition given its portability and capability of collecting data autonomously without any maintenance. The data were collected from ignition-on to ignition-off, and saved on a microSD card to be uploaded to a server via Wi-Fi. Up to 46 parameters were collected, six of which were employed for the proposed study: time stamp, vehicle speed, fuel consumption rate, latitude, longitude, and altitude. The data were recorded at a frequency of either 2 Hz or 5 Hz and converted to a second-by-second basis. 75% of the data set of each bus was taken for calibration and 25% for validation.

3.4.2 Model Development

Each bus was individually modeled, resulting in an individual parameter set. The parameter sets for all buses in the same series were then averaged to generate a composite (series) model. Table 3.8 summarizes the parameters needed for model development. Some of the parameters, such as rolling resistance coefficient and driveline efficiency, were obtained from the literature; others were estimated based on the field data. It should be noted that the total mass of the bus is the sum of the vehicle curb weight and passenger load which is

Table 3.7: Tested bus specifications

Bus series number	Model year	Make and model	Length (ft)	Engine model	Horsepower (hp)	Empty weight (lbs.)	Fuel type
19XX	2009	New Flyer SR-1360 D40LFR	40	ISL-07	250-330	28,300	Diesel
62XX	2012	New Flyer SR-1614 XD35	35	ISL-2010	280-330	26,750	Diesel
630X	2013	New Flyer SR-1733 XD35	35	ISL-2010	280-330	26,750	Diesel
632X	2013	New Flyer SR-1734 XD60	60	ISL-2010	280-330	39,675	Diesel
601X	2010	New Flyer Hybrid SR-1439 DE40LFR	40	ISL-07	280	31,140	Hybrid
602X	2010	New Flyer Hybrid SR-1440DE60LFR	60	ISL-07	330	45,860	Hybrid

Table 3.8: Parameters required for bus model calibration

Parameter	Value	Source
Drag coefficient (C_D)	0.78	[88]
Altitude correction factor (C_h)	NA^a	Computed from field data
Vehicle frontal area (A_f)	$6.824 m^2$	Computed from truck dimensions
Vehicle speed (v)	NA^a	Measured in field
Mass (m)	NA^a	Computed from field data
Rolling coefficient (C_r)	1.25	[88]
c_1	0.0328	[88]
c_2	4.575	[88]
Road grade (G)	NA^a	Computed from field data
Acceleration (a)	NA^a	Computed from field data
Driveline efficiency (η)	0.94	[88]
Ridership	NA^a	Measured in field

^aThe parameter is not a single value.

computed as the product of the ridership and the average weight of an individual passenger. In this study, 179 lb (81.5 kg) was assumed to be the average passenger weight. Road grade was computed using Equation (3.6) with $Elv(\cdot)$ the altitude at t and $t + \Delta t$ respectively and $D(\cdot)$ the distance a bus travels in one second. The measured elevation data was corrected using GIS given the unsatisfied measurement accuracy.

$$G(t) = \frac{Elv(t + \Delta t) - Elv(t)}{\sqrt{(D(t + \Delta t) - D(t))^2 - (Elv(t + \Delta t) - Elv(t))^2}} \quad (3.6)$$

Given the limitation of the concave model as discussed in section 3.3, fuel consumption should be restricted to a convex function of vehicle power. To develop a convex model, the order of magnitude of the second-order parameter, which impacts the degree of convexity of the model, needs to be determined. Basically, a lower order of magnitude suggests a higher degree of convexity and results in larger difference between the model estimates and field measurements given that empirical fuel consumption points to a concave function of vehicle power. A higher order of magnitude, however, results in an asymptotically linear model that produces a bang-bang type of control. Accordingly, a trade-off is necessarily achieved between the accuracy of the model and the degree of convexity. The performance of the convex model is thoroughly investigated by varying the order of magnitude from 1E-05 to 1E-11, as demonstrated by Figure 3.11. Each bus series shows similar behavior, as R^2 increases with the growth of the order of magnitude up until 1E-08, beyond which the model achieves little improvement. 1E-08 is thus taken as the best compromise between model accuracy and the degree of convexity, resulting in the convex model shown in Table 3.9.

The effects of road grade and vehicle load on fuel consumption as it varies with cruise speed, have been analyzed. As demonstrated by Figure 3.12, the model, in general, represents

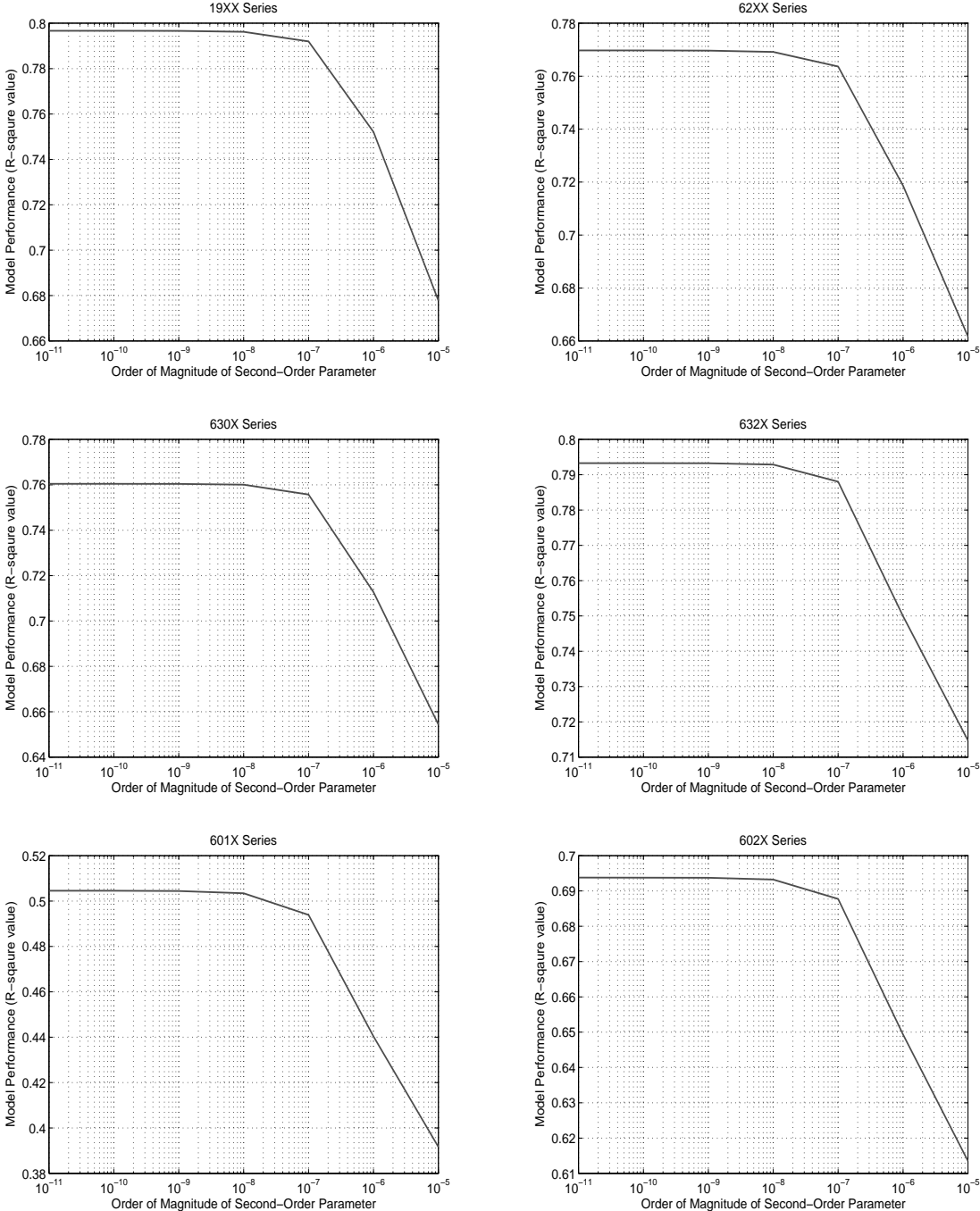


Figure 3.11: Model performance vs. order of magnitude of the second-order parameter (bus model)

Table 3.9: Bus fuel consumption model

Bus series number	α_0	α_1	α_2
19XX	1.66E-03	8.68 E-05	1.00E-08
62XX	1.13E-03	5.69 E-05	1.00E-08
630X	9.76E-04	6.44 E-05	1.00E-08
632X	1.41E-03	8.21 E-05	1.00E-08
601X	1.00E-03	5.18 E-05	1.00E-08
602X	1.38E-03	6.22 E-05	1.00E-08

fuel consumption as a bowl-shaped function of vehicle speed at non-negative grade levels, suggesting that optimum cruise speeds are achieved within the lower bound and upper bound of the speed range. Specifically, Figure 3.13 characterizes the optimum cruise speed as it varies with road grade, demonstrating that higher uphill grades result in a lower optimum cruise speed, whereas steeper downhill roads require a higher cruise speed to minimize fuel consumption level (which is not recommended for safety purposes).

Figure 3.14 summarizes the impact of vehicle load on the optimum cruise speed. Basically, heavier vehicles accrue lower optimum speeds when moving uphill and higher when moving downhill. It is worth noting that, as demonstrated by Figure 3.14b, the optimum speeds remain constant with an increase in vehicle weight when the road grade is -4% , -6% and -8% . This is attributed to the fact that the analysis is performed only for the speed range of $0 - 100 \text{ km/h}$, and, at these grade levels, the optimum speeds reach the maximum level at a low vehicle load. In addition, the optimum speeds are demonstrated by Figure 3.14b (uphill) to be more sensitive to vehicle load at higher grade levels.

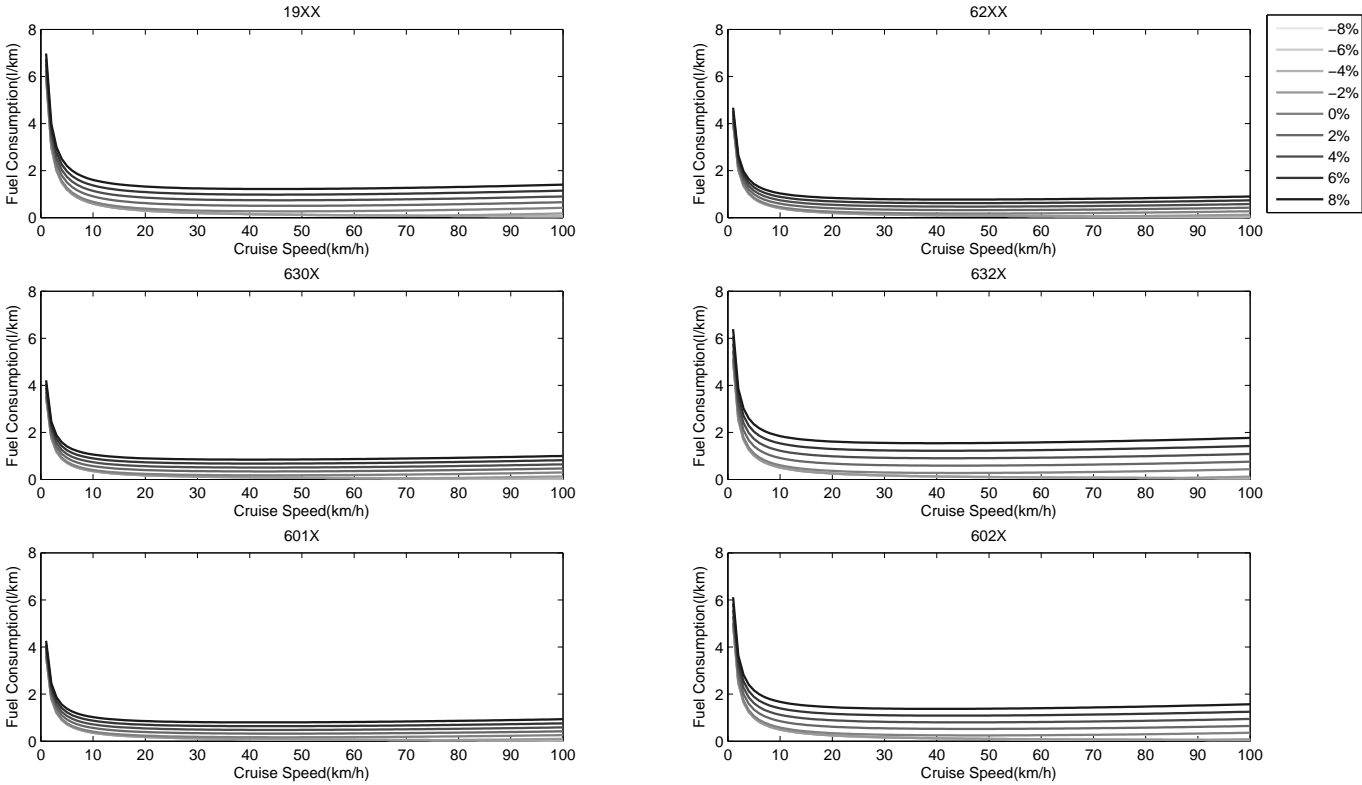


Figure 3.12: Fuel consumption vs. cruise speed at different grade levels (bus model)

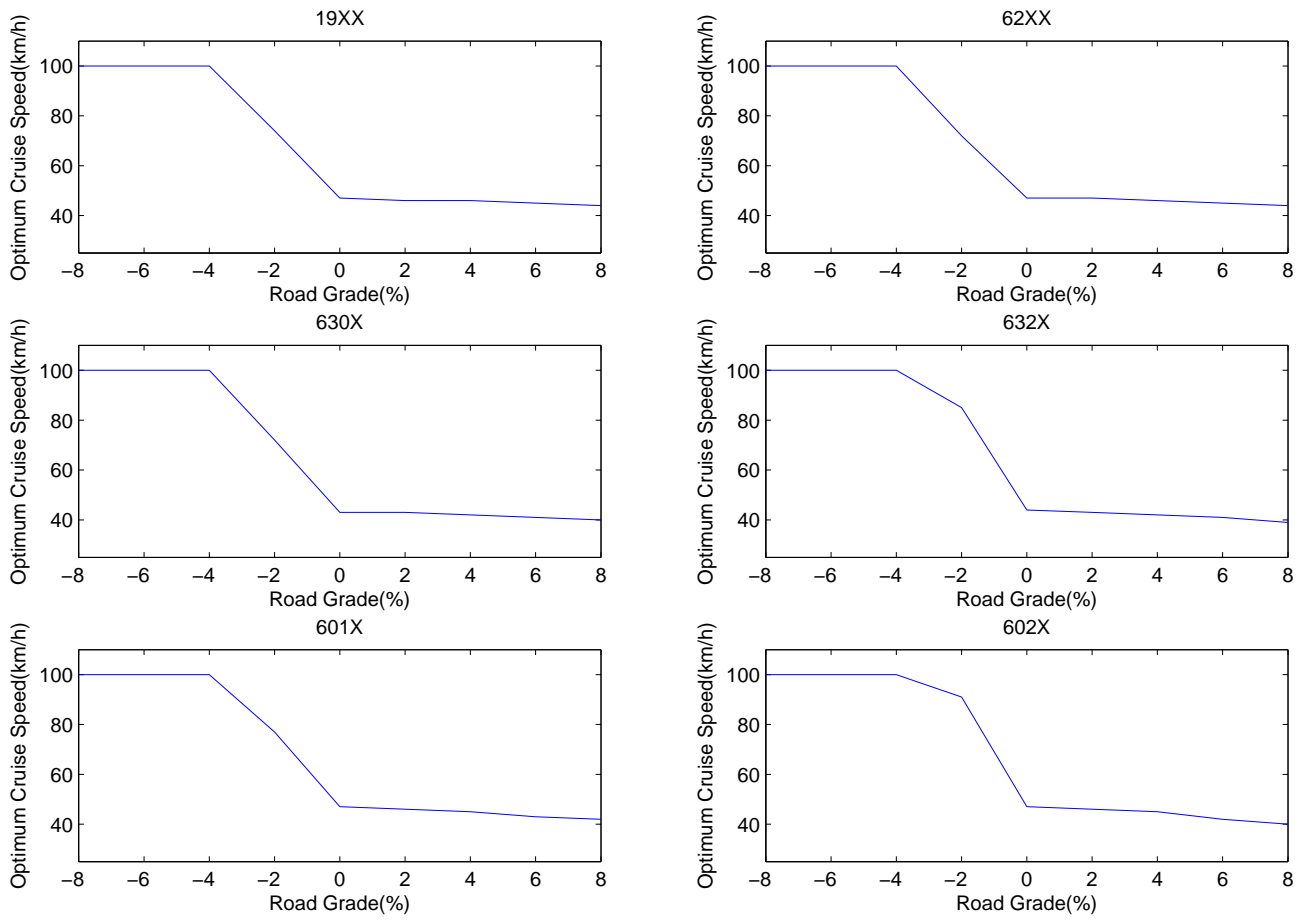
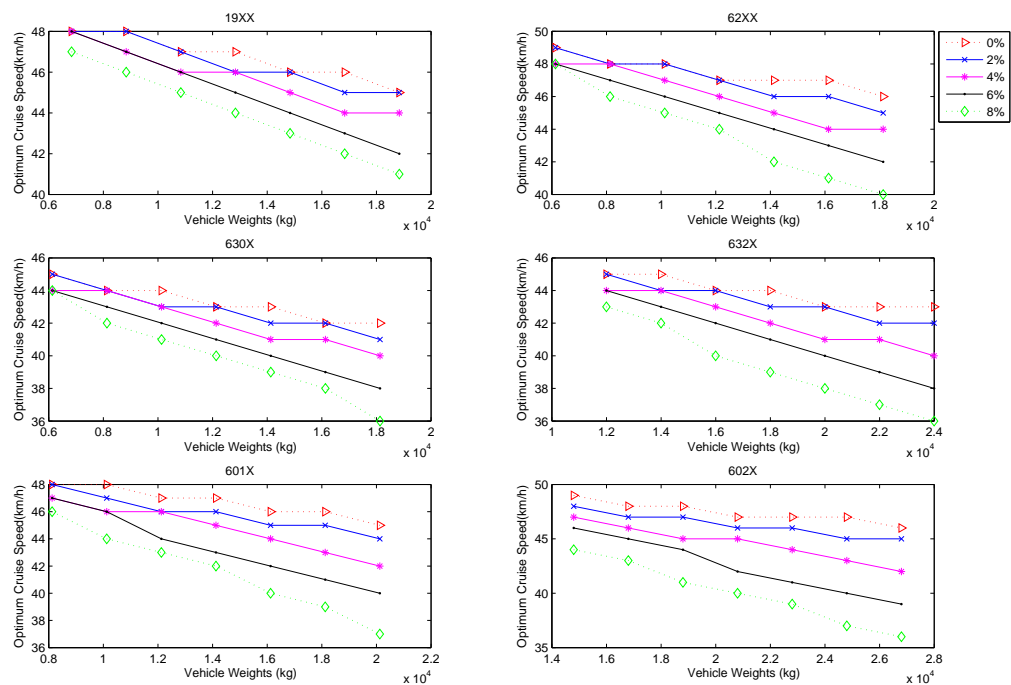
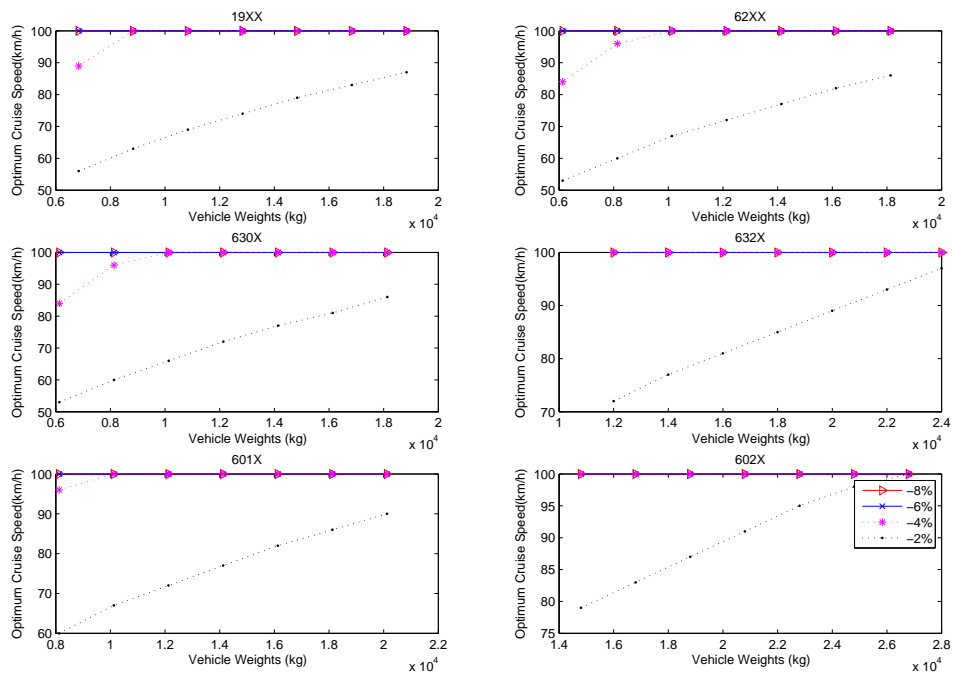


Figure 3.13: Impacts of road grade on the optimum fuel economy cruise speed (bus model)



(a) downhill



(b) uphill

Figure 3.14: Impacts of vehicle weight on the optimum fuel economy cruise speed at different grade levels (bus model)

Table 3.10: Comparison of bus model performance

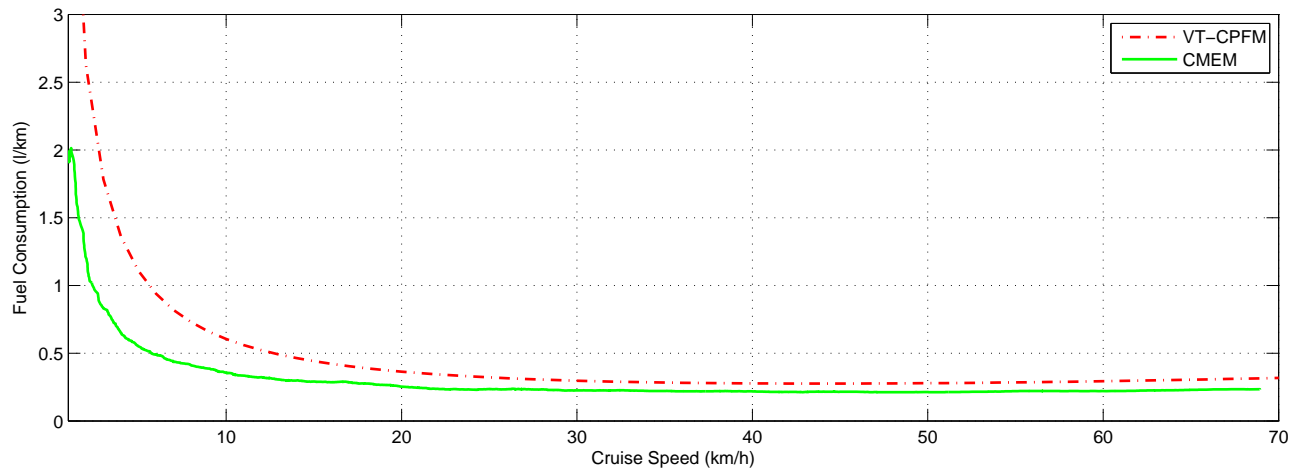
Bus Series Number	VT-CPFM (concave)		VT-CPFM (convex)		CMEM		MOVES	
	R^2	Slope	R^2	Slope	R^2	Slope	R^2	Slope
19XX	0.81	0.78	0.82	0.81	0.81	0.66	0.74	0.82
62XX	0.78	0.77	0.80	0.88	0.80	0.76	0.74	1.20
630X	0.75	0.83	0.76	0.75	0.72	0.73	0.68	1.06
632X	0.79	0.80	0.80	0.85	0.80	0.69	0.70	0.60
601X	0.63	0.79	0.63	0.75	0.63	0.67	0.57	1.13
602X	0.69	0.90	0.69	0.90	0.70	0.82	0.67	0.76

3.4.3 Model Validation

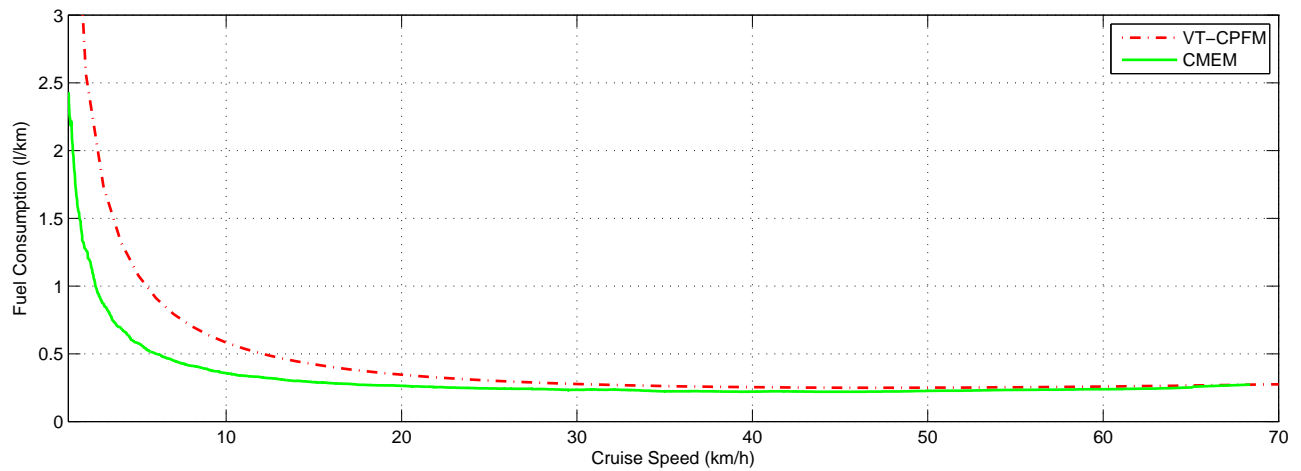
The validation efforts were made using the data set independent of calibration. The fuel estimates resulted from each series model were compared against the field measurements of a real bus in that series as well as the predictions from CMEM, MOVES, and the concave model. Furthermore, the variation of fuel consumption with cruise speed was also tested and compared with the results derived from CMEM.

As summarized in Table 3.10, VT-CPFM and CMEM can generate approximately accurate estimates by having proximate R^2 values; however, CMEM produces a bang-bang type of control and also cannot be easily calibrated and implemented given the need of engine data for model calibration. The convex model does not entail a significant decrease of R^2 compared to the concave model, demonstrating that the model maintains precision in enabling realistic driving recommendations. MOVES produces the least accurate estimates given that it is designed for conformity use instead of instantaneous analysis. Furthermore, the slopes of the regression lines of model estimates versus field measurements demonstrate that VT-CPFM and CMEM, in general, underestimate fuel consumption levels, while VT-CPFM can provide better estimates by having higher slope values. MOVES generates an underestimate for some series while overestimating for others, which is explained by the fact that the buses employed by the MOVES database are a composite of numerous bus categories rather than the specific type used in this study.

In validating the model, a comparison was made to CMEM, as demonstrated in Figure 3.15, which illustrates two example results. The proposed model generates an optimum cruise speed consistent with CMEM and produces the same bowl-shaped curve as a function of cruise speed. Specifically, the optimum cruise speed ranges between 39 and 47 km/h (lower than LDVs: 60–80 *km/h*) for all of the tested buses varying grades from 0% to 8%, and decreases with the rise of grade and vehicle load.



(a)



(b)

Figure 3.15: Impact of cruise speed on fuel consumption levels: a. conventional diesel bus; b. hybrid-electric bus

3.5 Conclusions

This chapter develops the fuel consumption models for HDDTs, conventional diesel and hybrid-electric buses, circumventing the bang-bang type of control in the modeling practice. Given a lack of publicly available data, the models were calibrated using field data. Eight trucks and six bus series (four diesel series and two hybrid series) were tested. The validation efforts were made by comparing the model estimates against field measurements as well as the predictions of CMEM and MOVES.

The results demonstrate that the predictions of the VT-CPFM model are consistent with field observations as well as the estimates of CMEM and MOVES, and that the model can provide realistic driving suggestions in control systems. The optimum fuel economy cruise speed ranges between 32 and 52 *km/h* for tested trucks and between 39 and 47 *km/h* for tested buses on grades varying from 0% to 8%, and decreases with the rise of grade and vehicle load. This demonstrates that steeper uphill roads and heavier vehicles result in a lower optimum cruise speed, which is justified in reality. These optimum cruise speeds are significantly lower than those for LDVs (60-80 *km/h*).

Given the simple model specification, the VT-CPFM model can be readily calibrated without any engine data which typically are not available, and easily implemented in traffic microsimulation software and in-vehicle or smartphone eco-routing and eco-driving systems.

Chapter 4

Electric Train Dynamics and Energy Consumption Modeling

This chapter is based on the papers listed below:

1. Wang, J. and Rakha, H. Electric Train Energy Consumption Modeling. *Journal of Applied Energy*, 2017.
2. Wang, J. and Rakha, H. Train Dynamics Model for Rail Transit Simulation System. *Transportation Research Part C: Emerging Technologies*. (In Review).

4.1 Introduction

The urban transportation system has been deteriorating with regards to the environment given the higher residential density and travel demand, growth in automobile ownership and worsening of traffic conditions. Many cities, especially metropolis areas, are served by a mixture of multiple traffic modes comprised of passenger cars, transit buses, trucks and rail transit. Accordingly, to reduce city-wide energy consumption and GHG emissions, not only are effective strategies required for each mode, but also integrated strategies considering the interaction of these modes are required. To enable the efficient and cost-effective design and testing of new strategies, a multi-modal energy-efficient system is being developed.

As aforementioned, system development requires the design of multiple submodules. This chapter focuses on subway electric train dynamics and energy consumption modeling. The developed models will support the overall modeling framework in estimating rail-induced energy consumption, and designing and testing eco-friendly strategies customized to urban

rail transit systems, such as energy-efficient timetables [163, 164] and eco-speed control [165, 166].

4.2 Dynamics Modeling

The proposed model was developed based on Fadhloun-Rakha's [91] and Hay's modeling framework [56]. Consequently, their theoretical backgrounds are necessarily introduced to give a general picture of the modeling approach.

4.2.1 Fadhloun-Rakha Traction Dynamics Model

The dynamics model for estimating acceleration can be mathematically generalized by Equation (4.1), with a the acceleration level (m/s^2), M the total vehicle mass (kg), F_t the tractive effort (N) and R the resistance force (N) which is the combination of rolling, grade and aerodynamic resistive forces. The tractive effort is constrained by the maximum tractive effort to ensure that it does not approach infinity at low speeds, as formulated in Equation (4.2), where η is the the mechanical efficiency of the transmission and gear, P_{max} is the maximum engine power (kW), u is the vehicle speed (mi/h), 1.61 is the unit conversion factor from mi/h to km/h , μ is the coefficient of friction between tire and road surface for motor vehicles (or between the wheel and the track for trains), M_{ta} is the vehicle mass on the tractive axle (kg), g is the gravitational acceleration ($9.8066 m/s^2$), λ is the throttle level ($0 \leq \lambda \leq 1$) which was assumed to be either 1 [88, 89] or a constant reduction [90] before Fadhloun et al.'s study [91]. It should be noted that the coefficient of friction μ is different from the aforementioned coefficient of friction f that quantifies the friction between the wheel and the brake shoe.

$$a = \frac{F_t - R}{M} \quad (4.1)$$

$$F_t = \min(3600\eta\lambda \frac{P_{max}}{(u \cdot 1.61)}, \mu M_{ta}g) \quad (4.2)$$

It is well known that delivered engine power is sensitive to the throttle level, which itself is empirically demonstrated by [91] to hyperbolically vary with the ratio of vehicle speed to the desired speed, demonstrating, in Figure 4.1, that the throttle level first increases up to the maximum throttle level with the increasing speed and then decreases when the speed approaches the facility desired speed. The hyperbolic throttle function is presented in Equation (4.3):

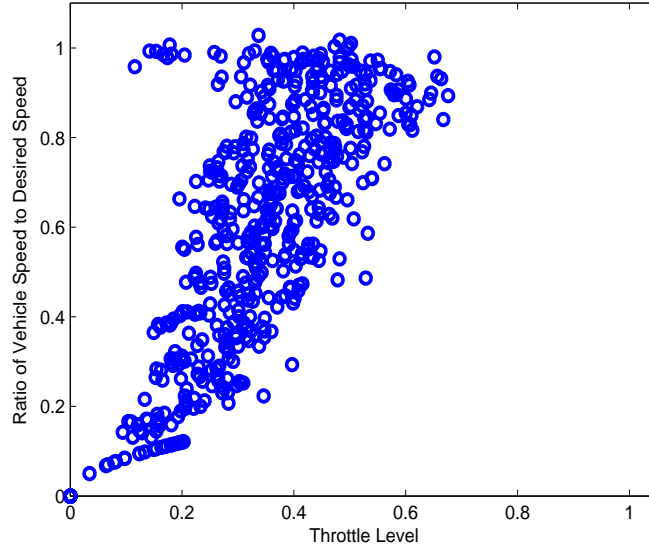


Figure 4.1: Variation of throttle level as a function of speed

$$\lambda\left(\frac{u}{u_d}\right) = \begin{cases} \frac{\frac{u}{u_d}}{t_1 + \frac{t_2}{1 - \frac{u}{u_d}} + t_3 \frac{u}{u_d}}, & 0 \leq u \leq u_m \\ \max\left(\frac{\frac{u}{u_d}}{t_1 + \frac{t_2}{1 - \frac{u}{u_d}} + t_3 \frac{u}{u_d}}, \lambda^*\right), & u_m < u \leq u_d \end{cases} \quad (4.3)$$

where u_d is the facility desired speed (mi/h), u_m is the speed at the maximum throttle (mi/h), t_1, t_2 , and t_3 are model parameters to be calibrated, and λ^* is the minimum throttle that is allowed when achieving the desired speed to avoid zero throttle during free driving (zero throttle cannot maintain the desired speed). λ^* can be estimated by assuming that acceleration equals zero when the desired speed is achieved, as illustrated in Equation (4.4). The first term of the numerator in Equation (4.4) is the tractive force at the desired speed, and the second term $R(u_d)$ is the resistance force (N) at the desired speed. Other parameters in the function were earlier defined.

$$\frac{\min(3600\eta\lambda^* \frac{P_{max}}{(u_d \cdot 1.61)}, \mu M_{tag}) - R(u_d)}{M} = 0 \quad (4.4)$$

The Fadhloun-Rakha dynamics model has been demonstrated to address typical acceleration behavior more accurately than other dynamics and kinematics models [167, 168, 169, 170] by introducing the variable throttle mechanism into the modeling framework, and thus is employed as the basis to model train dynamics in this chapter. Noteworthy here is that rail

trains are controlled by several discrete throttle notches; resulting in the throttle changing abruptly from one level to another with the running speed rather than varying continuously as is the case with motor vehicles. A discretization procedure is thus needed for the model to capture discrete events, which is introduced in section 4.2.3.

4.2.2 Hay Brake Dynamics Model

The general dynamics modeling framework for deceleration estimation is presented in Equation (4.5) based on the Newton Motion Law, with a_d the deceleration (m/s^2), F_b the brake force (N), R and M defined earlier. According to [56], the brake force is linearly related to the coefficient of friction between the wheel and the brake shoe, as illustrated in Equation (4.6), with R_b the braking ratio (constant for passenger trains), W the weight per rail car (lb), e the efficiency of the brake lever system (usually 90-95%), and f the coefficient of friction between the wheel and the brake shoe. The model implies that the brake force varies with speed similar to $(e \times f)$ given a constant $R_b W$ for a specific train type. $e \times f$ is treated as a variable, specified as the coefficient of friction f hereinafter. In addition, the application of the model requires an upper bound constraint on the friction force (μM_{tag}) to avoid wheel slippage.

$$a_d = \frac{F_b + R}{M} \tag{4.5}$$

$$F_b = R_b W e f \tag{4.6}$$

Based on the studies by [56, 83], the brake force is a piecewise function of train speed, as illustrated in Figure 4.2. In general, the brake force first increases to the maximum retardation with increasing speed, and is limited at the steady force level within a specific speed range, then decays at high speed levels. As demonstrated in [83], the early locomotive design does not have the steady force region, while designers have been trying to achieve full dynamics brake force at as low velocity as possible so that the regions of maximum retardation become large in modern locomotive packages (different curves in Figure 4.2 represent different locomotive packages). Given the empirically piecewise features of the brake force, the coefficient of friction f should also be a piecewise function of train speed. The proposed modeling framework is analytically addressed in section 4.2.3.

4.2.3 Proposed Dynamics Model

The modeling framework was developed for acceleration and deceleration respectively. As was mentioned, the acceleration model was developed based on Fadhloun-Rakha's throttle

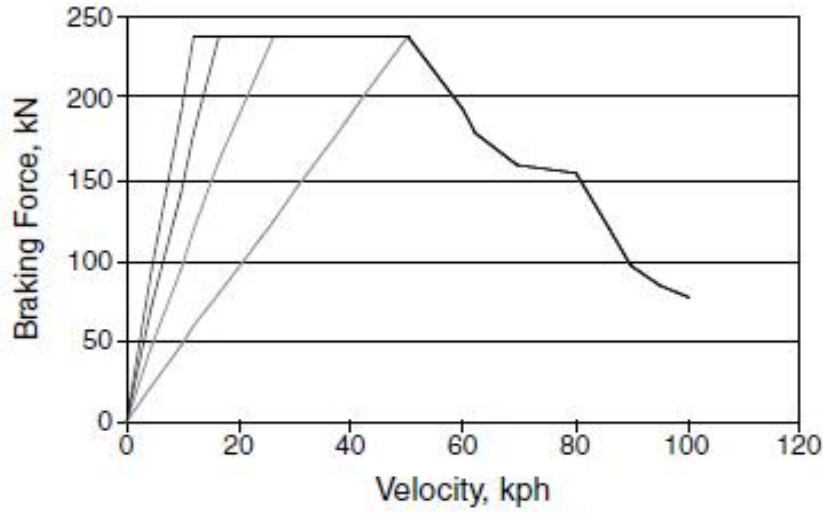


Figure 4.2: Dynamic brake characteristics

function by a combination of discretization procedure, and deceleration was characterized as a piecewise function of running speed.

4.2.3.1 Acceleration Modeling Approach

Acceleration is generally computed based on the Newton Law of Motion, as formulated in Equation (4.7) in which the tractive force F_t is estimated using Equation (4.8) and instantaneously varies with train speed and throttle level. It is noteworthy that m in the two models is the weight per rail car (kg) instead of total train weight (unlike M in Equation (4.1) refers to the total vehicle weight), given that the Electric Multiple Units (EMUs) tested in this study enclose electric traction motors within each of the carriages so that each rail car is self-propelled. It is unlike the trains propelled by a single locomotive. In addition, the mass of the railcar is fully acted on the tractive axles for EMUs, so that the weight acting on the tractive axles (M_{ta} in Equation (4.2)) equals the railcar mass (m). Other parameters in the models were defined earlier.

$$a(t) = \frac{F_t(t) - R(t)}{m} \quad (4.7)$$

$$F_t(t) = \min\left(3600\eta\lambda(t)\frac{P_{max}}{(u(t) \cdot 1.61)}, \mu mg\right) \quad (4.8)$$

4.2.3.2 Resistance Force Module

The resistance force acting on a train is demonstrated in Equation (4.9) in which the first four terms are the modified Davis equation [171] where w_p is the weight per railcar axle (*tons*) consisting of empty railcar weight and total passenger weight, K is train drag coefficient, n_p is the number of axles per rail car, θ is the track gradient (%), 1000 is the mass unit conversion from *kg* to *ton*, and 4.4482 is the unit conversion coefficient from *lb* to *N*. Given that the Davis equation generates the resistance force in *lbs*, the unit conversion (4.4482) is necessary for the model to be integrated into the dynamics model.

$$R(t) = \left[\left(0.6 + \frac{20}{w_p} + 0.01u(t) + \frac{Ku(t)^2}{w_p n_p} + 20\theta \right) \right] \times \frac{m}{1000} \times 4.4482 \quad (4.9)$$

4.2.3.3 Throttle Discretization Procedure

The continuous throttle function in Equation (4.3) cannot directly capture train discrete throttle notches. A discretization procedure is thus introduced to the modeling framework.

According to [83], the discrete throttle level λ_d can be computed by $(\frac{N}{N_{max}})^2$ as demonstrated in Equation (2.7). However, it is difficult to address how λ_d or N relates to train operation conditions (e.g. speed) without the being reported by the engine manufacturer. Accordingly, the Fadhloun-Rakha model was first used to generate the continuous throttle level, which was then discretized to approximate the discrete events. Specifically, the continuous throttle λ estimated by Equation (4.3) was instantaneously compared to each level of the discrete throttle λ_d , and the discrete throttle that minimized the difference between λ and λ_d was selected as the final throttle level for the time instant. Assuming that there are $(N_{max} + 1)$ notches, resulting in the discrete throttle levels: $\lambda_{d(1)}, \lambda_{d(2)}, \dots, \lambda_{d(N_{max})}, \lambda_{d(N_{max}+1)}$, the discretization procedure is presented in Table 4.1.

4.2.3.4 Deceleration Modeling Approach

Deceleration behavior is mathematically addressed in Equation (4.10); again, m refers to the weight of each railcar (*kg*). The brake force F_b in the model is formulated using a combination of Hay's model and the friction force constraint (μmg), as illustrated in Equation (4.11) with f the ($e \times f$) as mentioned in Section 4.2.2. Other parameters were defined earlier.

$$a_d(t) = \frac{F_b(t) + R(t)}{m} \quad (4.10)$$

Table 4.1: Throttle discretization procedure

Procedure DISCRETIZATION (time duration of driving cycle: T ; time instant: t ; discrete notch level: i ; the difference between λ and λ_d : D)

for all $t \leftarrow 1, 2, \dots, T$ **do**

if $u(t) \leq u_m$, instant speed smaller than the speed at the maximum throttle

$$\lambda(t) \leftarrow \frac{\frac{u(t)}{u_d}}{t_1 + \frac{t_2}{1 - \frac{u(t)}{u_d}} + t_3 \frac{u(t)}{u_d}}$$

else

$$\lambda(t) \leftarrow \min\left(\frac{\frac{u(t)}{u_d}}{t_1 + \frac{t_2}{1 - \frac{u(t)}{u_d}} + t_3 \frac{u(t)}{u_d}}, \lambda^*\right)$$

end if

for all $i \leftarrow 1, 2, \dots, N_{max} + 1$ **do**

$D(i) \leftarrow |\lambda(t) - \lambda_d(i)|$

end for

$Index \leftarrow \min(D)$, find the minimum-difference discrete throttle

$\lambda(t) \leftarrow \lambda_d(Index)$, discretized final throttle

end for

end procedure

$$F_b(t) = \min(R_b W f(t), \mu m g) \quad (4.11)$$

Dynamic braking is usually controlled as a continuous mode rather than a discrete notch [83]. Thus, a continuous brake function was proposed by characterizing the coefficient of friction (f) as a piecewise function of train speed. The piecewise feature of the brake force is not only suggested by the literature (as shown in Figure 4.2), but also empirically confirmed by this study. Figure 4.3 presents the empirical relations in the domains of coefficient of friction (f) versus speed and brake force versus speed. Basically, the braking dynamics is a three-stage piecewise function of speed with a linear feature for the first stage, a steady level for the second phase and an approximately exponential decay mechanism for the last stage. The modeling framework for the coefficient of friction is represented in Equation (4.12), where θ , u_1 , u_2 , β are model parameters to be calibrated. It should be noted that u_1 , u_2 are the critical speeds (mi/h) at which the model specification would be changed.

$$f(t) = \begin{cases} \theta u(t), & 0 \leq u(t) < u_1 \\ \theta u_1, & u_1 \leq u(t) < u_2 \\ \theta u_1 e^{-\beta(u(t)-u_2)}, & u(t) \geq u_2 \end{cases} \quad (4.12)$$

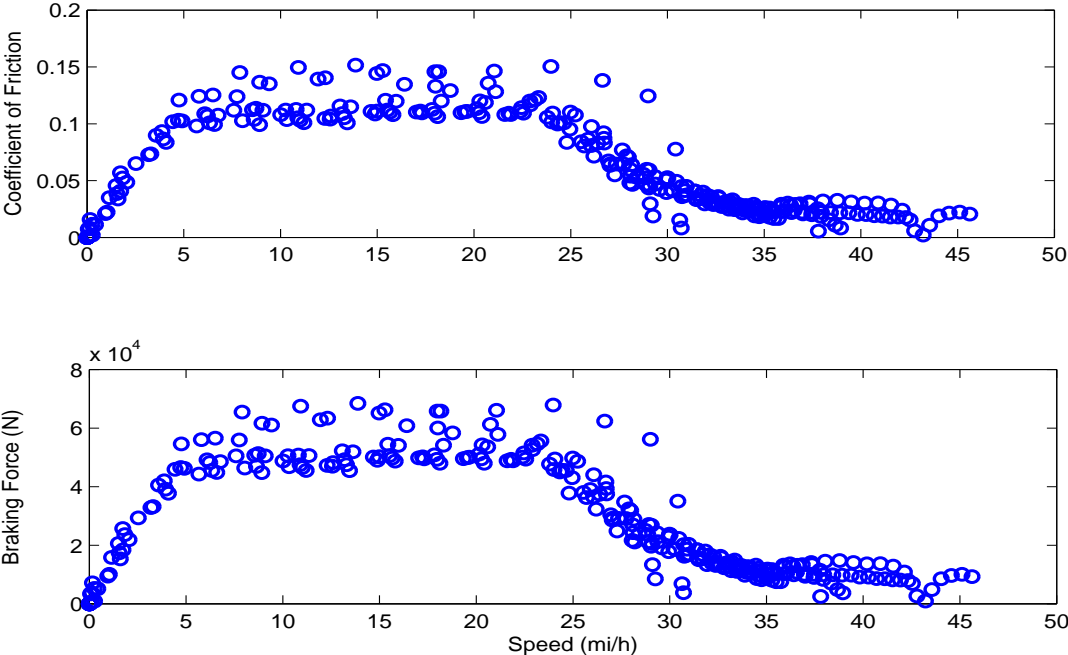


Figure 4.3: Piecewise feature of braking dynamics

Table 4.2: Rolling stock characteristics

Parameter	Values	Data source
Weight of empty railcar	54.5 <i>tons</i>	Manufacturer website
Number of axles per railcar (n_p)	6	Manufacturer website
Drag coefficient (K)	0.07 ([56])	Literature
Seating capacity per railcar	64	Manufacturer website
Daily passenger loading	43%	Transit agency or National Transit Database
Number of cars per train	2	Transit agency
Mechanical efficiency (η)	0.96 ([56])	Literature
Maximum engine power (P_{max})	580 <i>kW</i>	Manufacturer website
Braking ratio (R_b)	0.9 ([56])	Literature
Coefficient of friction (μ)	0.2 ([56])	Literature

4.2.4 Data Preparation

The model calibration and testing require comprehensive data including rolling stock information, train trajectory, and route characteristics. The data were provided by researchers at Georgia Tech who requested the data from the Tri-County Metropolitan Transportation District of Oregon (TriMet), the public agency that operates mass transit in the Portland Metropolitan area. TriMet responded with the information for the Metropolitan Area Express (MAX) Blue Line where the train trajectories were collected instantaneously.

The test train was representative of the typical train fleet in the Portland light rail transit system. The information on the rolling stock is summarized in Table 4.2, which presents the main characteristics of the test train and related parameters for use in the dynamics model. Some of the information (e.g. the weight per empty rail car, the number of axles per car, the maximum power, seating capacity) can be easily obtained from manufacturer websites. The drag coefficient, mechanical efficiency, braking ratio and the coefficient of friction between the wheel and the track were based on recommended values suggested in the literature for electric passenger trains. The information on passenger loading can be acquired from either the transit agency or a national transit database. Noticeably, the weight per rail car (W and m) in the dynamics model requires to include passenger weights in addition to the weight of the empty car.

The test section covers an entire trip of the MAX Blue Line from the starting station to the terminus with a total distance of 32.4 *miles*. The vertical layout of the section demonstrates a combination of upgrade (up to 4.3%) and downgrade (up to -4.5%) sections. The train was tested on 115-lb good rails with good cross ties at normal temperature on sunny days. The test was conducted under normal operational conditions, given that it is technically impossible to perform an on-site test in a continuous acceleration/deceleration mode. The trajectory data were collected by TriMet using GPS equipment and recorded on a second-by-

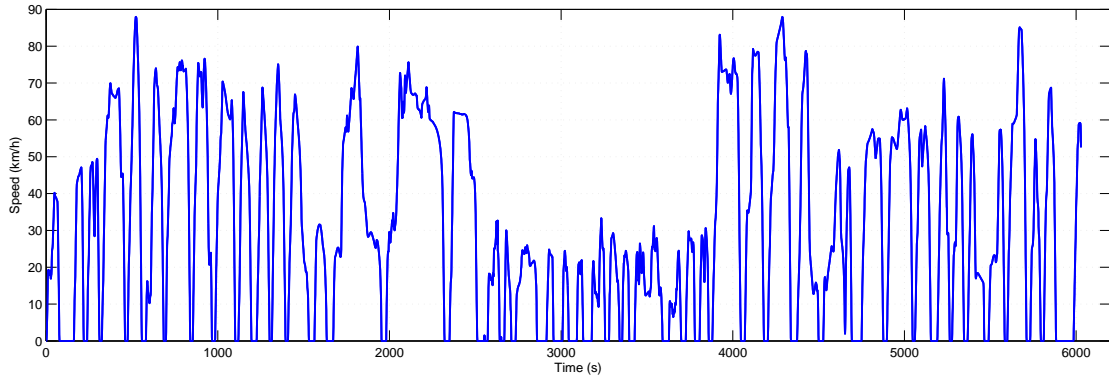


Figure 4.4: The driving cycle for the MAX Blue Line

second basis, which enables the characterization of detailed train dynamics. As illustrated in Figure 4.4, the trip driving cycle lasts for approximately 6000 s. In addition, the information on route characteristics was provided in terms of station name, milepost and elevation in order to generate the track segment-specific grade as the input of the train dynamics model.

Given that the train was tested in normal operational conditions, identifying acceleration and deceleration events was not a straightforward process. Specifically, the train may occasionally decelerate or cruise while starting from a station and accelerating to the target speed. Similarly, a train may accelerate or cruise while decelerating from the target speed to a complete stop at the next station. To accurately model the train dynamics behavior, the straightforward acceleration and deceleration events were identified respectively using the train trajectories.

There are 47 micro-trips (a micro-trip refers to the trip from one complete stop to the next) for the driving cycle in Figure 4.4. The acceleration event for each micro-trip was recognized by continuously tracking the trajectories from the complete stop at the starting point to the time instant when a cruise or deceleration event occurred, so that the trajectories refined from each micro-trip captured only acceleration events. Likewise, the deceleration event for each micro-trip was identified by tracking the trajectories backward from the complete stop at the ending point to the moment when a cruise or acceleration event occurred. Neither the acceleration events starting from a non-complete stop nor the deceleration events ending at a non-complete stop were selected. The events lasting only a few seconds (e.g. < 10 seconds) were removed in order to ensure sufficient data samples in each event, resulting in a total of 42 acceleration events and 11 deceleration events.

The constructed acceleration and deceleration datasets were respectively divided into two sections, 70% of each dataset was used for model calibration and 30% for validation purposes.

4.2.5 Model Calibration

The model was calibrated and tested only for light rail electric trains given a lack of data for other classifications, but the modeling framework would be applicable to the entire train fleet.

4.2.5.1 Acceleration Model Calibration

Based on the modeling framework introduced in Section 4.2.3.1, a total of three parameters need to be calibrated: t_1 , t_2 , t_3 . The three parameters are mathematically related to the maximum throttle level (T_m) and the ratio of speed (u) to the segment target speed (u_d) at the maximum throttle (specified as α_m hereinafter), as illustrated in Equation (4.13-4.15). The functions were determined through implementing boundaries on the partial derivative of throttle with respect to the ratio $\frac{u}{u_d}$, see [92]. The mathematical transformation clarifies the physical implications of t_1 , t_2 , t_3 . On the one hand, the parameters affect the maximum throttle that would be implemented; on the other hand, they manipulate the critical $\frac{u}{u_d}$ ratio (α_m) beyond which throttle would commence to decrease. This implies that the parameter values may be sensitive to driver behavior. However, the train manipulation is significantly less heterogeneous compared to motor vehicles. In addition, the functions enable the conversion from calibrating t_1 , t_2 , t_3 to calibrating t_1 , T_m , α_m , simplifying the calibration given that the ranges of α_m and T_m are deterministic ($\alpha_m, T_m \in [0, 1]$).

$$0 \leq t_1 \leq \frac{2\alpha_m - 1}{\alpha_m T_m} \quad (4.13)$$

$$t_2 = \frac{(1 - \alpha_m)^2}{2\alpha_m - 1} t_1 \quad (4.14)$$

$$t_3 = \frac{1}{T_m} - \frac{t_1}{2\alpha_m - 1} \quad (4.15)$$

Model calibration work can be formulated as a constrained non-linear optimization problem, as illustrated in Equation (4.16). The objective is to minimize the sum of the squared error (E) between the estimated (\hat{u}) and observed (u) speeds for each observation i . The constraints ensure that the estimated speeds and distances (\hat{x}) satisfy the system of the first-order ordinary differential equations (ODEs) in addition to the non-negativity constraints.

$$\min E = \sum_{i=1}^n (\hat{u}(i) - u(i))^2 \quad (4.16a)$$

$$s.t. : \hat{u}(i) = \hat{u}(i-1) + \hat{a}(i-1)\Delta t \quad (4.16b)$$

$$\hat{x}(i) = \hat{x}(i-1) + \hat{u}(i-1)\Delta t \quad (4.16c)$$

$$\hat{u}(i), \hat{x}(i) \geq 0 \quad (4.16d)$$

The solution to the optimization problem results in the following model parameters: the maximum throttle level of 1.0 ($T_m = 1.0$), the maximum-throttle $\frac{u}{u_d}$ ratio of 0.6 ($\alpha_m = 0.6$), and $t_1 = 0.190$, $t_2 = 0.152$, $t_3 = 0.050$.

4.2.5.2 Deceleration Model Calibration

The proposed model requires four parameters to be calibrated: θ , u_1 , u_2 , β as illustrated in Equation (4.12). θ characterizes the linear feature of the model, and u_1 , u_2 are the critical conditions upon which the model specification would be determined. β is used to quantify the exponential decay feature.

Likewise, the calibration work can be formulated as a constrained non-linear optimization problem as demonstrated by Equation (4.16). It should be noted that the estimated acceleration (\hat{a}) in the first constraint is negative given the braking manipulation. The resulting model generates 0.0217 as the slope of the linear function ($\theta = 0.0217$), 6 *mi/h* and 21 *mi/h* as the two critical speeds respectively ($u_1 = 6, u_2 = 21$), and 0.10 as the exponential decay parameter ($\beta = 0.10$).

4.2.6 Model Validation

To assess the validity of the dynamics model, the model predictions were compared against the instantaneous field observations in conjunction with an exponential smoothing procedure, as shown in Equation (4.17), where \hat{a} is the exponentially smoothed acceleration/deceleration, a is the instantaneous acceleration/deceleration estimates, and α is the smoothing parameter. The model was also tested in the domains of acceleration/deceleration versus speed and acceleration/deceleration versus distance in order to evaluate the robustness of the model in capturing the train dynamics behavior.

$$\hat{a}(t) = \alpha \cdot a(t) + (1 - \alpha)\hat{a}(t-1) \quad (4.17)$$

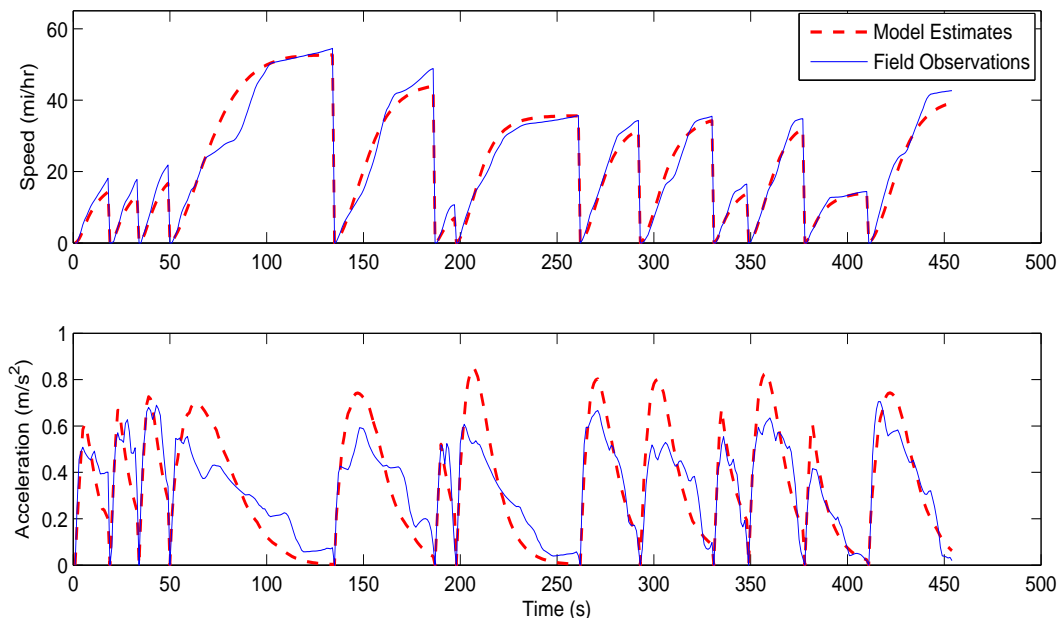


Figure 4.5: Instantaneous model validation (acceleration)

4.2.6.1 Acceleration Modeling Results

A smoothing factor of 0.10 appeared to produce an optimum fit (minimum error of estimated trajectory) to field data by having the coefficient of determination (R^2) of 0.96. As illustrated in Figure 4.5, the acceleration model generates the results consistent with the empirical measurements. Although the model occasionally either overestimates or underestimates at some time instants; in general, however, the predicted trajectory follows the major trend of the measured data.

Figure 4.6 evaluates the model performance in the domains of acceleration versus speed and acceleration versus distance, demonstrating good fits to the field observations. Specifically, acceleration, in general, varies as a concave function of speed and decreases with the increasing distance, which is similar to previous studies on motor vehicles [88, 90, 91, 105]. It is worth noting that, unlike the studies of motor vehicles, there are valleys in the domain of acceleration vs. speed at the speed levels of 10 - 20 *mi/h* and 30 - 40 *mi/h* respectively, implying that higher speed levels may achieve higher acceleration, or vice versa. This is attributed to the fact that acceleration (or throttle level) is determined not only by the instantaneous speed level but also by the segment desired speed. For instance, a train running at 40 *mi/h* on the track segment (desired speed: 50 *mi/h*) may achieve higher acceleration levels than when it is running at 35 *mi/h* yet on the segment with lower desired speed (e.g. 35 *mi/h*), given that the lower desired speed results in higher $\frac{u}{u_d}$ ratio (1.0) and thus

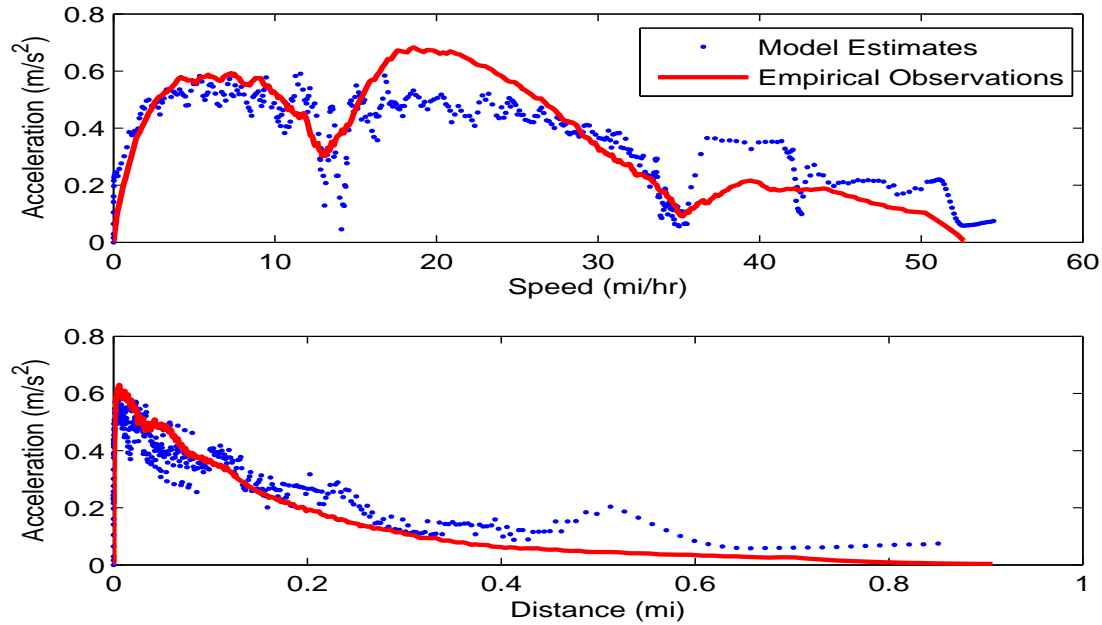


Figure 4.6: Model evaluation: acceleration versus speed and acceleration versus distance

generates significantly lower throttle levels (λ^*).

4.2.6.2 Deceleration Modeling Results

Through minimizing the model error, a smoothing factor of 0.26 was achieved to provide the optimum fit to the field observations, demonstrating a coefficient of determination of 0.94. Figure 4.7 demonstrates a good model fit to field observations by following the peaks and valleys of the measured data.

The evaluation in the domains of deceleration versus speed and deceleration versus distance, as illustrated in Figure 4.8, also demonstrates a good fit to the field measurements. Deceleration, likewise, varies as a concave function of speed and decreases with the cumulative distance. The model goodness-of-fit demonstrates its strong ability to capture deceleration behavior precisely.

4.2.7 Simulation Test

The proposed model has been demonstrated to adequately capture train dynamics. The objective of the model development is to support railway simulation and trip energy estimation.

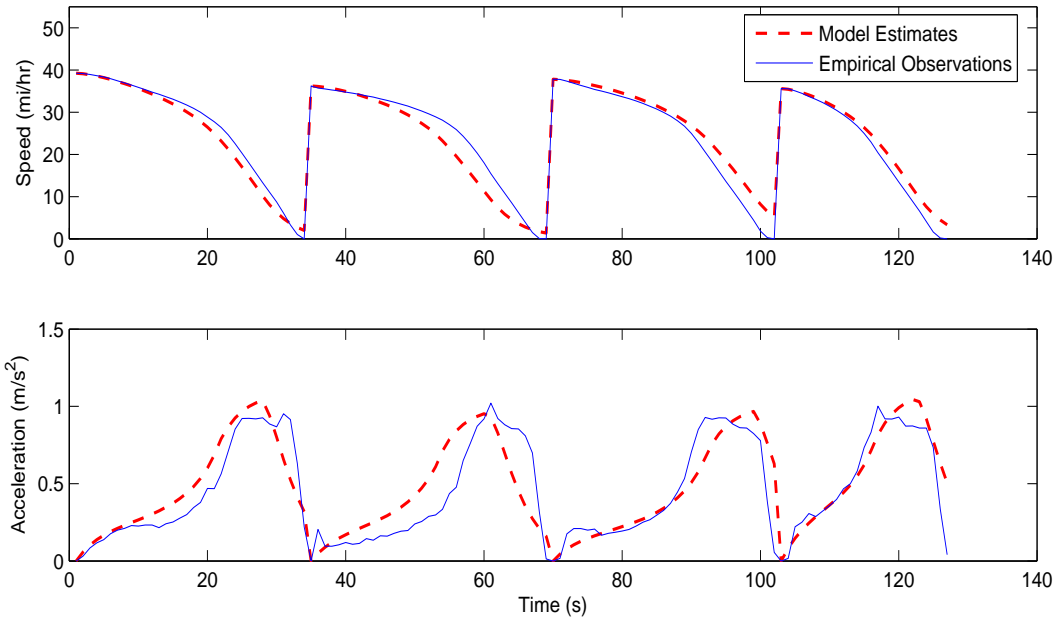


Figure 4.7: Instantaneous model validation (deceleration)

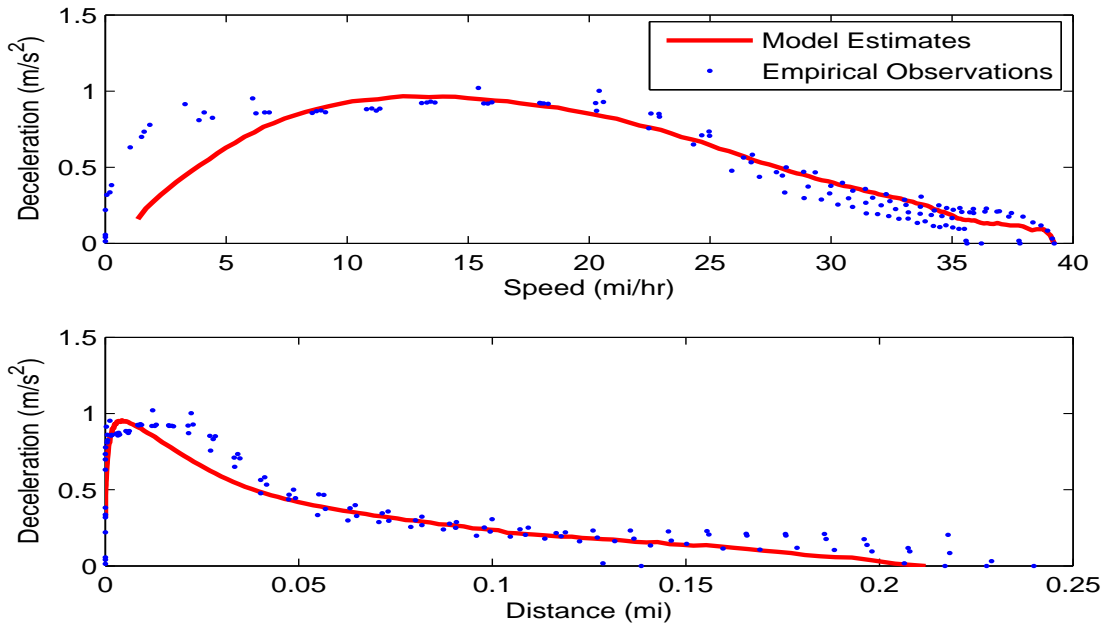


Figure 4.8: Model evaluation: deceleration versus speed and deceleration versus distance

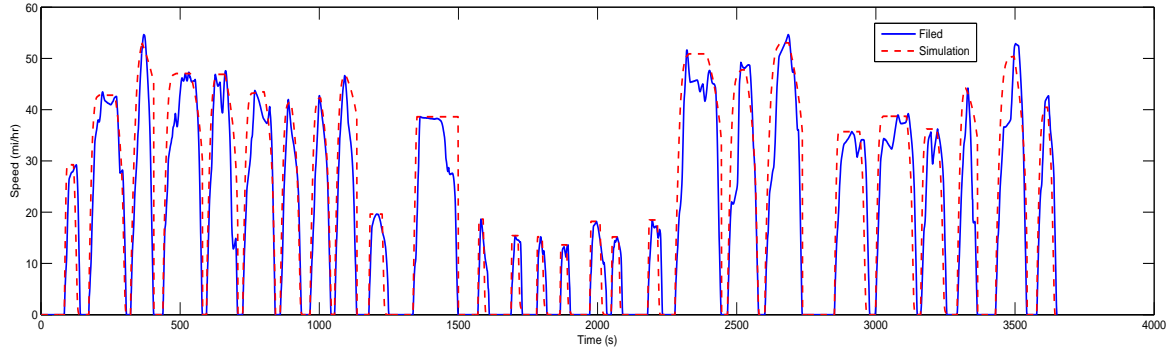


Figure 4.9: Instantaneous simulation test

Thus, the adequacy of the model for simulator development was tested in this section.

Two important parameters are needed for testing purposes, namely: the segment target speed and the average deceleration which were used to determine where a train should start to decelerate in order to ensure a complete stop upon arrival at the various stations. According to the Newton Motion Law, the distance required by complete a stop can be computed by the quadratic difference of the initial speed (target speed) and the final speed (0) divided by double the average deceleration level, as illustrated in Equation (4.18), where D is the distance required for a complete stop, u_d and \bar{a}_d are the segment target speed and average deceleration level respectively. Each micro-trip in Figure 4.4 respectively represents the motions on a track segment, so that, for simplicity, the target speed for each segment can be assumed to be the maximum speed of each micro-trip trajectory. Likewise, the average deceleration of each micro-trip was taken as the segment-specific average deceleration rate (\bar{a}_d).

$$D = \frac{u_d^2}{2\bar{a}_d} \quad (4.18)$$

Through a combination of the proposed dynamics model and the determined segment-specific target speeds and average deceleration, the test was conducted by comparing the simulated trajectories against the field observations on a second-by-second basis. Figure 4.9 demonstrates a good fit of the simulation results to the field trajectories, with a R^2 value of 0.86. Combined with the energy consumption model developed in section 4.3, the proposed subway system will be used to estimate rail trip energy consumption.

4.3 Energy Consumption Modeling

The proposed model was developed based on the VT-CPEM framework [13], characterizing electric power as two piece-wise functions as demonstrated in Equation (4.19) (energy consumption) and Equation (4.20) (energy regeneration). The description of the model parameters is summarized in Table 4.3. Basically, the energy is computed on a second-by-second basis. When the train is in traction mode, the energy flows from the electricity power system to the wheels with the power at the wheels being positive ($P > 0$). Alternatively, when the train is in regenerative braking mode, the energy flows from the wheels back to the power system and the power at the wheels is negative ($P < 0$). Noteworthy here is that, to compute regenerated energy (EC_{re}), only negative power is considered.

($\alpha_{01} \times \beta_1 + \alpha_{02} \times \beta_2$) in Equation (4.19) refers to the head-end power (HEP) in which β_1 and β_2 are dummy variables equal to either 0 or 1. α_{01} , in most cases, is applied to HEP ($\beta_1 = 1$ and $\beta_2 = 0$) except when a train is about to start moving and waiting at the initial route station where only a small fraction of HEP (α_{02}) is applied ($\beta_1 = 0$ and $\beta_2 = 1$). This accounts for the fact that trains only keep the ventilation system and lights on while waiting to load passengers before a trip begins and thus only consumes a small fraction of HEP.

$$EC(t) = \begin{cases} \alpha_{01} \times \beta_1 + \alpha_{02} \times \beta_2 + P(t), & \forall P(t) > 0 \\ \alpha_{01} \times \beta_1 + \alpha_{02} \times \beta_2, & \forall P(t) \leq 0 \end{cases} \quad (4.19)$$

$$EC_{re}(t) = \begin{cases} P(t) \times \eta_{rb}(t), & \forall P(t) < 0 \\ 0, & \forall P(t) \geq 0 \end{cases} \quad (4.20)$$

The aggregated energy consumption for an entire trip is then estimated by summing the instantaneous energy rates and then dividing by the trip length, as illustrated in Equation (4.21), with d being the trip length (km).

$$EC_d \left[kWh/V \cdot km \right] = \frac{\sum_t [EC(t) + EC_{re}(t)]}{d} \quad (4.21)$$

4.3.1 Tractive Power and Tractive Effort

Tractive power is computed using Equation (4.22) in which u is the instantaneous speed (km/h), 0.746 is used to convert the power from horsepower to kilowatt. F is the tractive effort as formulated in Equation (4.23) [56]. The first four terms, $(0.6 + \frac{20}{w_p} + \frac{0.01u(t)}{1.61} +$

Table 4.3: Description of model parameters

Name	Description	Unit
E	Annual energy consumption	kWh
E_p	Annual energy consumed per passenger kilometer	$kWh/P \cdot km$
E_s	Annual energy consumed per seating kilometer	$kWh/S \cdot km$
E_v	Annual energy consumed per vehicle kilometer	$kWh/V \cdot km$
M_p	Annual passenger kilometer	$P \cdot km$
M_s	Annual seating kilometer	$S \cdot km$
M_v	Annual vehicle kilometer	$V \cdot km$
C	Train capacity	-
β	Line loss factor	-
$EC(t)$	Instantaneous energy consumption	kW
$EC_{re}(t)$	Instantaneous energy regeneration	kW
$P(t)$	Instantaneous tractive power	kW
α_{01}	Head-end power (HEP)	kW
α_{02}	Fraction of HEP (0.05 is suggested by [57])	kW
β_{01}, β_{02}	Dummy variable	-
η_{re}	Instantaneous regenerative efficiency	-
EC_d	Trip energy consumption per unit distance	$kWh/V \cdot km$
$F(t)$	Instantaneous tractive force	N
$u(t)$	Instantaneous speed	km/h
w_p	Weight per railcar axle	ton
n_p	Number of axles per railcar	-
K	Train drag coefficient (0.07 suggested by [56])	-
θ	Road grade	%
L	Distance a train moved in one second	m
M	Total train weight	ton
α	Regenerative efficiency model parameter	-
$a(t)$	Instantaneous deceleration level	m/s^2
d	distance covered by the entire driving cycle	km
EC_{NTD}	NTD energy rate	$kWh/V \cdot km$

$\frac{K(u(t)/1.61)^2}{w_p n_p}$), in the model are the modified Davis equation [172], referring to the train resistance comprised of rolling, journal, track, flange and aerodynamic resistance. w_p is the railcar weight per axle (*ton*), including passenger weight (an average of 68 *kg* is assumed for each passenger in this study). The Davis equation was tested through a large amount of field experiments [172, 173, 174]. In addition, as demonstrated by [56, 57, 175], only positive gradient contributes to the grade resistance with an increase of 20 *lbs/ton* (0.01 *N/kg*) per percentage grade. It should be noted that curve resistance has been converted to the equivalent grade resistance by assuming that unit resistance of a 1° curve is the same as the resistance that a 0.04% grade would offer [56]. The last term in the bracket is the force exerted for acceleration or braking. M is the average weight of the moving train (*ton*), including the train curb weight and total passenger weight. 4.4482 is used to convert the tractive effort from *lbs* to *N*.

$$P = \frac{Fu}{375 \times 1.61} \times 0.746 \quad (4.22)$$

$$F(t) = \left[\left(0.6 + \frac{20}{w_p} + \frac{0.01u(t)}{1.61} + \frac{K(u(t)/1.61)^2}{w_p n_p} + 20\theta \right) + 70 \frac{u(t)^2 - u(t-1)^2}{8.4 \times L} \right] \times M \times 4.4482 \quad (4.23)$$

4.3.2 Starting Tractive Effort

It is worth noting that the tractive force in Equation (4.23) only addresses the effort exerted to move the train while in motion. However, a different tractive force is needed to move a train from a complete stop. The starting tractive effort typically consists of the grade resistance, bearing resistance, track resistance, weather resistance, and the resistance resulting from poor track conditions. When a train is starting from a complete stop, the tractive effort is estimated as the sum of these resistance forces rather than using Equation (4.23).

The grade resistance can be estimated as set forth. The typical values of other resistance forces were suggested by [57]. Specifically, the bearing resistance is 10 *lb/ton* (0.005 *N/kg*) at 122 °C (50 °F), and increases by 0.1 *lb/ton* (0.0005 *N/kg*) for 1 °F decrease below 50 °F and decreases by 0.1 *lb/ton* (0.00005 *N/kg*) for 1 °F increase above 50 °F. Track resistance depends on track type. There is no resistance force for 130 *lb* (59 *kg*) rail, and 1 *lb/ton* (0.0005 *N/kg*) resistance for 115 *lb* (52 *kg*) rail and 2 *lb/ton* (0.001 *N/kg*) for 100 *lb* (45 *kg*) rail. Weather resistance is affected by the humidity of the rail. Basically, there is no weather resistance for dry rail, while the wet rail produces a 2 *lb/ton* (0.001 *N/kg*) resistance. The resistance of icy or snowy rail goes up to 10 *lb/ton* (0.005 *N/kg*). The resistance relative to track conditions is 2 *lb/ton* (0.001 *N/kg*) for poor rails and fair cross ties, and 7 *lb/ton*

(0.0035 N/kg) for poor rails and poor cross ties. There is no such resistance if both rails and cross ties are in good condition.

4.3.3 Regenerative Braking Efficiency

Regenerative braking efficiency accounts for the portion of the total braking energy available for recovering. It determines the amount of the energy recovered by a regenerative braking system. The trains operating on an urban rail transit system frequently accelerate and decelerate given the short distance between two stations, so that a large amount of energy may potentially be recovered. Failing to account for energy recovery may thus result in large deviation in energy prediction for trains with regenerative braking.

The regenerative efficiency (η_{re}) is characterized as an exponential function of the deceleration level for electric vehicles [13, 176], as formulated in Equation (4.24). The model demonstrates that higher deceleration levels result in larger regenerative efficiency and thus more energy recovery. This functional form was used in the proposed model to compute the train regenerative energy. The calibration of the model parameter (α) is presented in Section 4.3.4.

$$\eta_{re}(t) = \begin{cases} \frac{1}{e^{|\alpha a(t)|}}, & \forall a(t) < 0 \\ 0, & \forall a(t) \geq 0 \end{cases} \quad (4.24)$$

4.3.4 Model Calibration

Having introduced the modeling framework, the next step is to calibrate the proposed model, which requires only one parameter to be calibrated.

The data required for calibration were classified into four categories: train information, travel activity data, route characteristics, and the information required to estimate the starting tractive effort. The data were provided by researchers at Georgia Tech who requested the data from the Tri-County Metropolitan Transportation District of Oregon (TriMet), the public agency that operates mass transit in the Portland Metropolitan area. TriMet responded with the information for the Metropolitan Area Express (MAX) Blue Line.

The MAX light rail trains are powered by built-in-place electric substations (ESS) located along the system route using the overhead contact line [177] with a nominal Voltage of 825 VDC . The system under study is similar to that investigated by [178, 179]. As illustrated in Figure 4.10, the electric power is transferred from ESS to trains through the contact line. The brake system of the MAX trains is a blending of regenerative braking and friction braking. The regenerative braking is the primary method of braking used when the train is

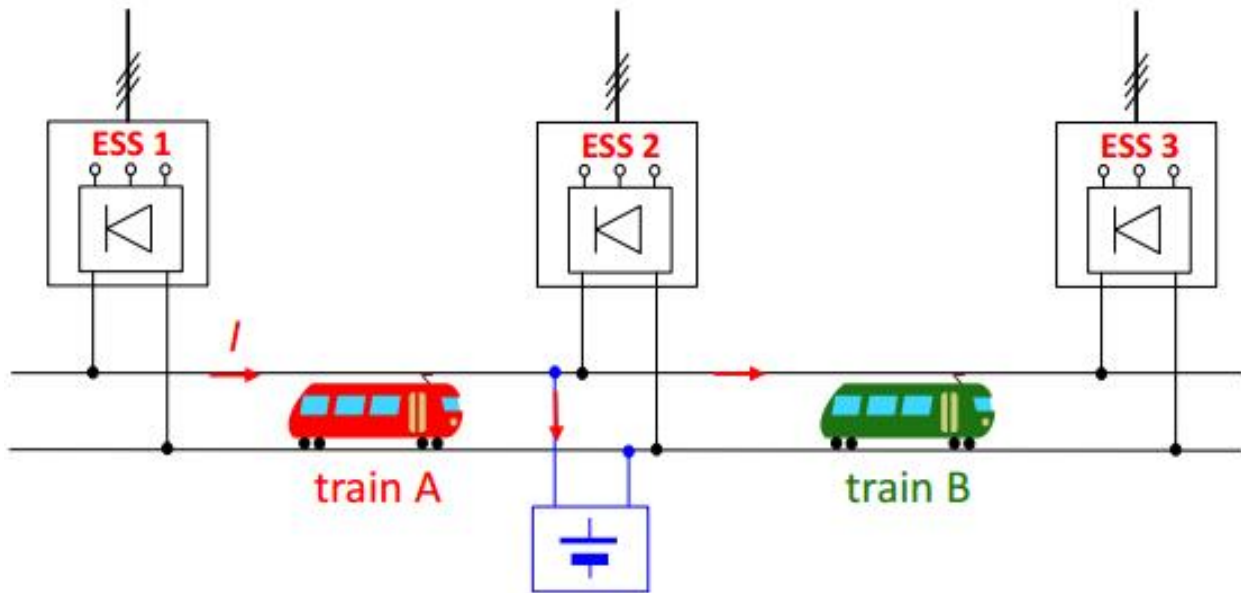


Figure 4.10: A simplified representation of the MAX light rail traction system

going faster than 3 *mph* (4.8 *km/h*), and the friction braking is also applied when the speed of the train is slower than 4.8 *km/h* to ensure sufficient power supply for emergency stopping. In addition, when the train is in braking mode, the electric motors operate like generators, taking the forward motion of the train and converting it into electricity. The regenerated electricity is then partly sent to other trains and partly stored in lineside storage systems for later usage, which significantly improves the system power efficiency. For example, as demonstrated by Figure 4.10, the braking power from train A is partly sent to train B and partly stored in the storage system around ESS 2.

A typical train model (SD 660), as shown in Figure 4.11, manufactured by Siemens, was tested in the field by TriMet to construct the calibration dataset. The test vehicle had two connecting cars each of which provided with 64 seats. The specific information of the testing rolling stock is illustrated in Table 4.4, including the empty railcar weight, number of axles per rail car, drag coefficient, seating capacity, passenger loading, number of cars per train, and HEP. The HEP was simplified to three operational levels: normal, high and maximum. The normal level operates at one-third of the maximum load (25 *kW*), and the high level functions at two-thirds followed by the maximum level that operates at full load. It should be noted that the Chicago train in the table was used for validation purposes.

The characteristics of the testing route are provided in Table 4.5 in terms of station name, milepost, elevation and gradient profiles (the curvature has been converted to its equivalent grade as mentioned in section 4.3.1). The trip starts from the Hatfield Government Center Station and ends at Cleveland station, covering an entire trip of the line with a total distance



Figure 4.11: Portland MAX light rail vehicle

Table 4.4: Test train characteristics

Parameter	Values	
	MAX blue	Chicago Brown
Weight of empty car (<i>ton</i>)	54.5	27.15
Number of axles per car	6	4
Drag coefficient	0.07	0.07
Seating capacity per car	64	49
Percentage loading (peak period)	na	87.5%
Percentage loading (off-peak period)	na	25%
Daily percentage loading	43%	45%
Number of cars per train (peak period)	2	6
Number of cars per train (off-peak period)	2	4
Maximum HEP per car (<i>kW</i>)	25	25
HEP operating level	Normal	Normal

of 32.4 *miles* (52.16 *km*). The vertical layout of the section demonstrates a combination of upgrade (up to 4.26%) and downgrade (up to -4.46%) sections.

Table 4.5: Track information for the MAX Blue Line

Station Name	Milepost		Elevation		Grade to Next Station
	<i>mile</i>	<i>kilometer</i>	<i>foot</i>	<i>meter</i>	
Hatfield Government Center Station	0.000	0.000	200.000	60.960	0.00049
Hillsboro Central /SE 3rd TC	0.360	0.579	200.940	61.247	-0.00122
Tuality Hospital/SE 8th	0.701	1.128	198.745	60.577	-0.00580
Washington/SE 12th	1.117	1.799	185.995	56.691	0.00320
Fair Complex/Hillsboro Airport	2.348	3.781	206.789	63.029	-0.00079
Hawthorn Farm	3.116	5.016	203.609	62.060	0.00310
Orenco/NW 231st	3.845	6.190	215.559	65.702	-0.00095
Quatama/NW 205th	5.265	8.477	208.439	63.532	0.00095
Willow Creek/SW 185th	6.250	10.063	213.379	65.038	0.00047
Elmonica/SW 170th	7.273	11.709	215.894	65.804	0.00210
Merlo/SW 158th	7.860	12.654	222.419	67.793	0.00037
Beaverton Creek	8.409	13.539	223.499	68.122	-0.00532
Millikan Way	9.110	14.667	203.829	62.127	0.00122
Beaverton Central	9.848	15.856	208.594	63.579	-0.00124
Beaverton TC	10.170	16.374	206.494	62.939	0.02039
Sunset TC	12.197	19.637	424.711	129.452	0.00325
Washington Park	15.426	24.836	480.081	146.329	-0.04455
Goose Hollow/SW Jefferson	16.818	27.077	152.648	46.527	-0.01191
Kings Hill/SW Salmon	17.045	27.443	138.358	42.171	0.00804
JELD-WEN Field	17.159	27.626	143.183	43.642	0.00690
13 th st	17.424	28.053	152.838	46.585	-0.02200
Galleria/SW 10th	17.557	28.266	137.438	41.891	-0.02200
Pioneer Square North	17.727	28.541	117.638	35.856	-0.02200
Mall/SW 5th	17.841	28.724	104.438	31.833	-0.01100
SW 3rd	18.030	29.029	93.438	28.480	-0.00895
Oak/SW 1st	18.220	29.334	84.488	25.752	-0.00117
Skidmore Fountain	18.447	29.700	83.088	25.325	0.00334
Old Town/Chinatown	18.574	29.904	85.328	26.008	0.03266
Rose Quarter TC	19.085	30.727	173.498	52.882	0.04261
Convention Center	19.218	30.941	203.328	61.974	0.01174
NE 7th	19.545	31.468	223.638	68.165	0.00500
Lloyd Center/NE 11th	19.634	31.611	225.988	68.881	0.00051
Hollywood/NE 42nd TC	21.377	34.417	230.673	70.309	0.00681
NE 60th	22.381	36.033	266.773	81.312	0.00398

NE 82nd	23.782	38.289	296.213	90.286	0.02047
Gateway/NE 99th TC	24.559	39.540	380.133	115.864	-0.01174
E 102nd	25.402	40.896	327.873	99.936	0.00250
E 122nd	26.585	42.802	343.468	104.689	0.00331
E 148th	27.708	44.610	363.068	110.663	-0.00660
E 162nd	28.371	45.678	339.968	103.622	-0.00808
E 172nd	28.864	46.470	318.968	97.221	-0.00552
E 181st	29.299	47.172	306.268	93.350	0.00275
Rockwood/E 188th	29.678	47.782	311.768	95.027	0.00584
Ruby Junction/E 197th	30.227	48.666	328.718	100.193	0.00866
Gresham City Hall	31.610	50.892	391.918	119.456	0.01529
Gresham Central TC	32.121	51.715	433.198	132.039	0.01419
Cleveland	32.538	52.386	464.408	141.551	0.01419

Table 4.6: Parameter set for starting tractive effort

Parameter	Values	
	MAX Blue	Chicago Brown
Ambient temperature (°F)	74	74
Weather condition	Dry	Dry
Track type	115 <i>lb</i> (52 <i>kg</i>) rail	115 <i>lb</i> (52 <i>kg</i>) rail
Track condition	Good rails and crossties	Good rails and crossties

The information required to estimate the starting tractive effort, as illustrated in Table 4.6, consists of weather condition, ambient temperature, track type and conditions. The test runnings in Portland and Chicago were both conducted on 115-lb good rails with good cross ties at normal temperature on sunny days. The test in Portland delivered the MAX Blue Line driving cycle with a maximum operational speed of 88 *km/h* and a total duration of around 6000 *s*, as illustrated in Figure 4.4. For each between-station running, the train, in general, was first accelerated from a complete stop at one station to a specified target speed, then cruised at the target speed for a spell, and decelerated until achieving a complete stop at the next station.

The exponential feature of the regenerative efficiency in Equation (4.24) results in a non-linear energy consumption model, and thus the calibration procedure was formulated as an unconstrained non-linear optimization problem as shown in Equation (4.25), where D is the model prediction difference relative to the NTD estimates, and EC_{NTD} is the NTD average energy rate. The NTD energy rate was used to calibrate the model because the field energy consumption was unavailable at the moment of model development. The data in the NTD 2011 demonstrated an average energy consumption of 13.57 *kWh/V · mi* (8.48 *kWh/V · km*). The model was calibrated by varying the model parameter (α) value to achieve the minimum prediction error.

$$\min D = (EC_d - EC_{NTD})^2 \tag{4.25}$$

The calibration result generates the optimum model parameter of 0.65 ($\alpha = 0.65$). The resulting regenerative efficiency, as demonstrated in Figure 4.12, exponentially decays with a decrease in the deceleration level. In particular, the decay becomes dramatic when the deceleration level is less than 2 *m/s*².

4.3.5 Model Validation

The model was validated using the data from the Chicago heavy rail system. The validation effort was first made by comparing model predictions against the NTD 2011 estimates,

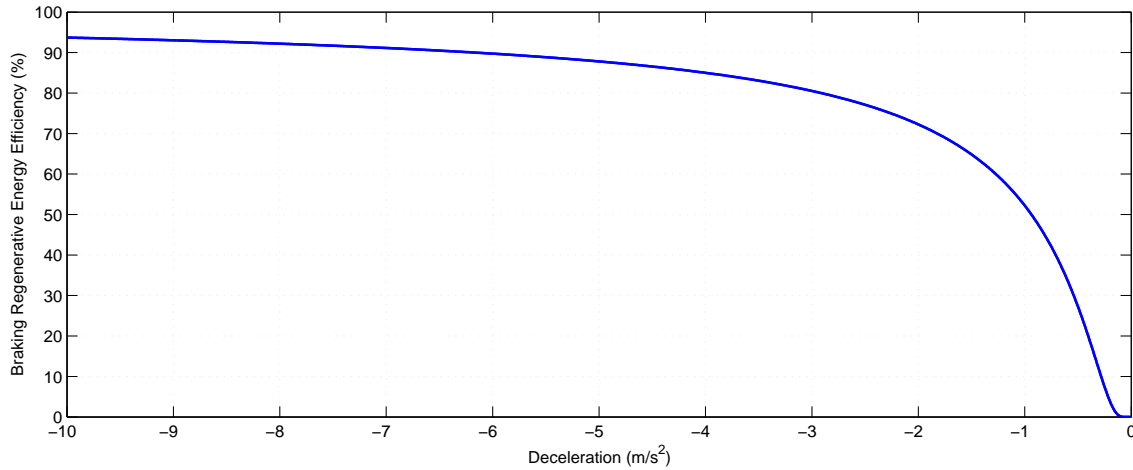


Figure 4.12: Regenerative braking efficiency varies as a function of the deceleration level

followed by a further discussion of modeling results. The NTD energy consumption for the Chicago rail system was $36.44 \text{ kWh}/VM$ ($22.63 \text{ kWh}/V \cdot km$) and $0.13 \text{ kWh}/SM$ ($0.08 \text{ kWh}/S \cdot km$). A train on the Chicago “L” system was tested by Georgia Tech researchers to collect the trajectory data for energy prediction. The Chicago rail has the similar traction and brake system, track infrastructure and vehicle aerodynamics compared to the Portland rail system. The information for the testing vehicle is illustrated in Table 4.3. Compared to the train running on the MAX Blue Line, the Chicago train has lower empty car weight, seating capacity and the number of axles while more connecting cars. The testing route, as demonstrated in Table 4.7, starts from the Kimball station and ends at the Merchandise Mart station, covering 8.7 mi (14.01 km) section of the Chicago Brown Line. The vertical layout of the section demonstrates a combination of upgrade (up to 2.37%) and downgrade (up to -2.55%). The test was completed under the same weather and rail conditions as those on the MAX Blue Line in order to ensure the identical bearing, track and weather resistance between calibration and validation processes. The test results in the Chicago Brown Line driving cycle with a maximum operational speed of $75 \text{ km}/h$ and a total duration of around 2000 s , as illustrated in Figure 4.13. It is worth noting that the number of cars and passenger load differ between the peak and the off-peak periods, resulting in different train weights at different periods. Consequently, energy consumption was first estimated for each period respectively, and then the average of the two periods was compared against the NTD data.

Table 4.8 demonstrates that the model predictions are consistent with the NTD estimates, generating a predicted error of 1.87% ($\text{kWh}/V \cdot mi$) and -2.31% ($\text{kWh}/S \cdot mi$). Not modeling regenerative braking (“No regeneration” as shown in Table 4.8) results in a significant prediction error (27.39% and 21.54%). Modeling the regenerative efficiency as a constant also produces much higher prediction errors compared to the proposed model (16.11% and

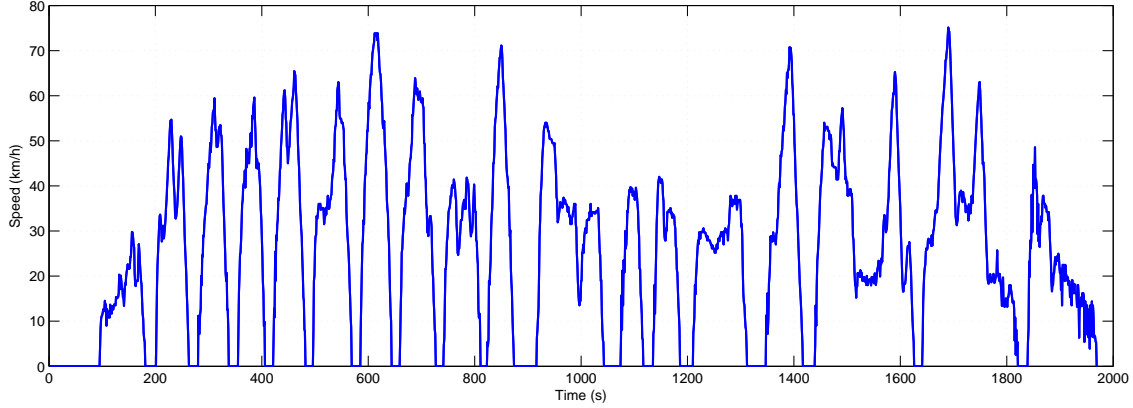


Figure 4.13: The driving cycle for the Chicago Brown line

Table 4.7: Track information for the Chicago Brown Line

Station Name	Milepost		Elevation		Grade to Next Station
	<i>mile</i>	<i>kilometer</i>	<i>foot</i>	<i>meter</i>	
Kimball	0.000	0.000	548.314	167.126	-0.0255
Kedzie	0.252	0.406	514.337	156.770	-0.0169
Francisco	0.626	1.008	481.030	146.618	-0.0011
Rockwell	0.983	1.583	479.016	146.004	0.0094
Western	1.322	2.128	495.863	151.139	0.0025
Damen	1.766	2.844	501.795	152.947	0.0106
Montrose	2.245	3.614	528.681	161.142	0.0196
Irving Park	2.747	4.423	580.702	176.998	-0.0223
Addison	3.222	5.187	524.777	159.952	0.0072
Paulina	3.592	5.784	538.858	164.244	0.0067
Southport	3.955	6.368	551.759	168.176	-0.0030
Belmont	4.692	7.554	539.964	164.581	0.0125
Wellington	4.897	7.885	553.511	168.710	-0.0052
Diversey	5.155	8.300	546.453	166.559	-0.0187
Fullerton	5.642	9.084	498.304	151.883	-0.0071
Armitage	6.106	9.831	480.804	146.549	0.0237
Sedgwick	7.180	11.560	615.272	187.535	-0.0110
Chicago	8.230	13.250	554.058	168.877	0.0091
Merchandise Mart	8.711	14.024	577.077	175.893	0.0091

Table 4.8: Validation on Energy Prediction

	NTD estimates	Instantaneous regeneration		Constant regeneration		No regeneration	
		Predicted energy	Error	Predicted energy	Error	Predicted energy	Error
$kWh/V \cdot mi$	36.44	37.12	1.87%	42.31	16.11%	46.42	27.39%
$kWh/V \cdot km$	22.63	23.06		26.28		28.83	
$kWh/S \cdot mi$	0.13	0.127	-2.31%	0.144	10.77%	0.158	21.54%
$kWh/S \cdot km$	0.08	0.079		0.089		0.098	

10.77%). Furthermore, the constant assumption deems the model incapable of capturing instantaneous energy regeneration so it is not suitable for a microscopic level analysis.

Figure 4.14 demonstrates the adequacy of the model at an instantaneous level. The light blue area represents the energy consumed for the entire cycle. The area delimited by the blue edge line refers to the energy consumption without energy regeneration during braking, and the red edge line represents the case considering energy regeneration. When the train is in traction mode, the electric power is positive and the energy flows from the overhead catenary to the wheels; alternatively, when the train is in brake mode, the power is negative and the energy is sent back to the overhead catenary. The instantaneous variation in the cumulative energy consumption demonstrates the ability of the model in adequately predict electric consumption and energy recovery on an instantaneous basis. Figure 4.14 also reveals that energy recovery significantly reduces the overall power consumption.

4.3.6 Discussion of Modeling Results

The model predictions in Table 4.8 also demonstrate that regenerative braking achieves an energy saving of 20% by reducing the energy consumption from 46.42 $kWh/V \cdot mi$ (28.83 $kWh/V \cdot km$) to 37.12 $kWh/V \cdot mi$ (23.06 $kWh/V \cdot km$). This predicted energy saving is consistent with what is reported in the literature [180, 181, 182], which demonstrated an energy saving of up to 30%.

Furthermore, the proposed modeling approach is able to account for the impact of train parameters (number of cars, seating capacity) on energy consumption. A comparative analysis of predicted energy consumption between the MAX Blue Line and the Chicago Brown Line demonstrates that the Chicago train consumes approximately 174% more energy in

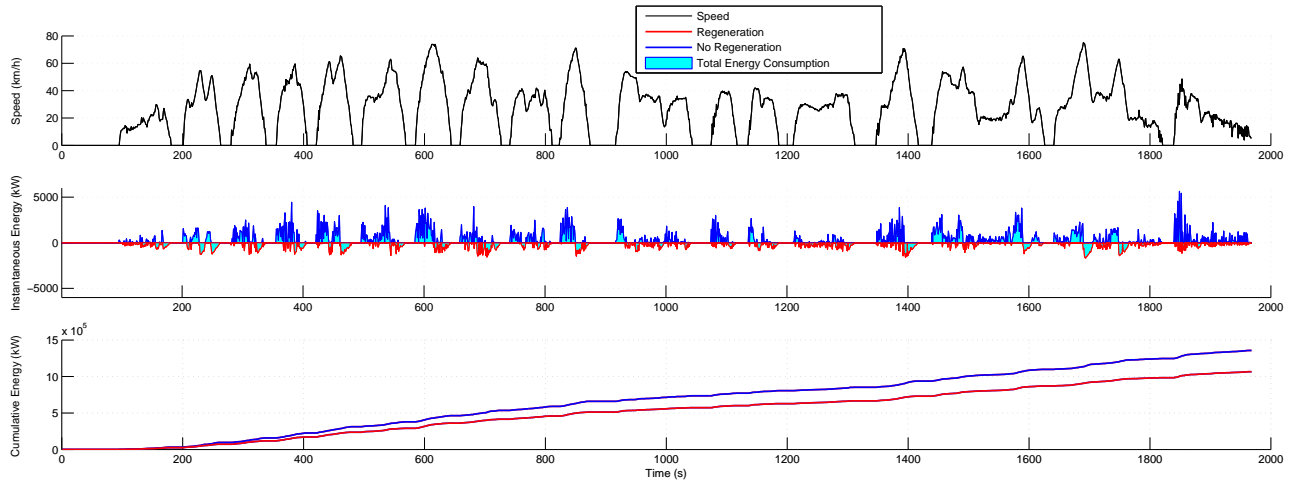


Figure 4.14: Chicago Brown Line: speed and electric power on the entire cycle

$kWh/V \cdot mi$ (13.57 vs. 37.12), while only consumes 20% more for per seating mile (0.106 vs. 0.127). This demonstrates that the Chicago train has significantly more per-train seats. The Chicago train has lower car seating capacity (49 as shown in Table 4.3) yet more connecting cars, resulting in higher per-train seating.

In addition, the sensitivity of the model predictions to train weight and road grade was analyzed. It should be noted that the energy consumption increments in Table 4.9 and Table 4.10 are relative to the base case in which the empty car weight is 27.15 *tons* and the number of cars is 6 for the peak period and 4 for the off-peak period; and the increments in Table 4.11 are relative to the case with level grade. As illustrated in Table 4.9, the original empty car weight (27.15 *tons*) was either decreased or increased by 5 and 10 *tons*, respectively, generating an identical energy consumption increase of 5.6 $kWh/V \cdot mi$ (3.48 $kWh/V \cdot km$) for every 5 *ton* increment. For the original car weight, the number of cars for the base case was either decreased or increased by 1 at a time. The increasing number of cars results in an identical electric consumption increment of 6.19 $kWh/V \cdot mi$ (3.84 $kWh/V \cdot km$), as demonstrated in Table 4.9. Either increasing car weight or adding more connecting cars leads to linear and identical growth of energy consumption. However, increasing the road grade, from 0% to 4% as illustrated in Table 4.11, produces a non-linear feature by having higher energy consumption increments on steeper roads. For example, the energy consumption increases by 9.2% (from 27.11 to 29.61 $kWh/V \cdot km$) with the grade varying from 3% to 4%, while increases by only 5.3% (from 22.25 to 23.44 $kWh/V \cdot km$) with the grade varying from 0% to 1%. This implies that, on steeper roads, the identical gradient increase results in larger energy consumption increases. The sensitivity analysis demonstrates the model's ability to capture energy consumption differences associated with vehicle weight and route characteristics.

Table 4.9: Sensitivity of model predictions to railcar empty weight

Car weight increment (<i>ton</i>)	Empty car weight (<i>ton</i>)	Predicted energy consumption		Energy consumption increment	
		$kWh/V \cdot mi$	$kWh/V \cdot km$	$kWh/V \cdot mi$	$kWh/V \cdot km$
-10	17.15	25.92	16.10	-11.20	-6.96
-5	22.15	31.52	19.58	-5.60	-3.48
0	27.15	37.12	23.06	0.00	0.00
5	32.15	42.72	26.53	5.60	3.48
10	37.15	48.32	30.01	11.20	6.96

Table 4.10: Sensitivity of model predictions to the number of railcars

Number of cars increment	Number of cars		Predicted energy consumption		Energy consumption increment	
	Peak	Off-peak	$kWh/V \cdot mi$	$kWh/V \cdot km$	$kWh/V \cdot mi$	$kWh/V \cdot km$
-2	4	2	24.74	15.37	-12.38	-7.68
-1	5	3	30.93	19.21	-6.19	-3.84
0	6	4	37.12	23.06	0.00	0.00
1	7	5	43.31	26.90	6.19	3.84
2	8	6	49.50	30.75	12.38	7.68

Table 4.11: Sensitivity of model predictions to road grade

Road grade	Predicted energy consumption		Energy consumption increment	
	$kWh/V \cdot mi$	$kWh/V \cdot km$	$kWh/V \cdot mi$	$kWh/V \cdot km$
0%	35.83	22.25	0.00	0.00
1%	37.74	23.44	1.91	1.19
2%	40.31	25.04	4.48	2.78
3%	43.65	27.11	7.82	4.86
4%	47.68	29.61	11.85	7.36

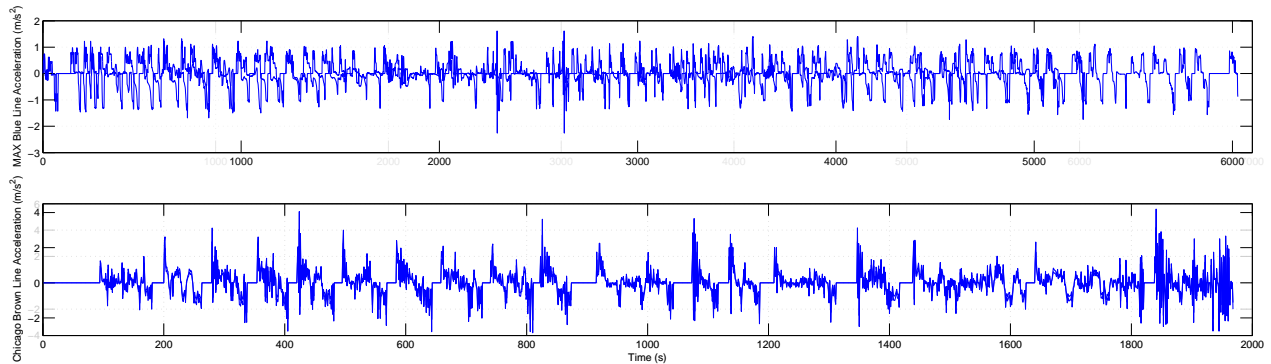


Figure 4.15: Instantaneous acceleration levels

Finally, the MAX Blue Line driving cycle was applied to the Chicago train, generating an average energy consumption of $23.10 \text{ kWh}/V \cdot \text{mi}$ ($14.35 \text{ kWh}/V \cdot \text{km}$), which is significantly lower than that for the Chicago Brown Line cycle ($37.12 \text{ kWh}/V \cdot \text{mi}$). A further analysis, as illustrated in Figure 4.15, demonstrates that the higher electric consumption for the Chicago driving cycle is attributed to more aggressive running that produces higher acceleration levels. The model thus can reflect the energy consumption differences between rail lines by accounting for the impact of operational conditions on energy prediction, which is very important for multi-modal transit planning purposes.

Although the model was calibrated against the Portland light rail, it was demonstrated to have good performance for the Chicago heavy rail as well, implying that similar levels of model accuracy could be expected for other transit systems if there is no significant difference in the energy consumption-related system components, such as propulsion technologies, brake systems, train aerodynamics and track infrastructure.

4.4 Conclusions

The chapter develops electric train dynamics and energy consumption models in support of rail-induced trip energy estimation. Both models can be easily calibrated using non-engine data and implemented in simulation systems and eco-transit applications. The dynamics model varies throttle and brake level with running speed rather than assuming constants as is done by previous studies. The energy consumption model considers instantaneous energy regeneration by formulating regenerative efficiency as an exponential function of deceleration level. Model calibration work is formulated as non-linear optimization problems. The dynamics model is tested on an instantaneous basis, and also evaluated in the domains of acceleration/deceleration versus speed and acceleration/deceleration versus distance. The energy consumption model is tested through comparing model estimates against NTD data

given a lack of instantaneous field energy measurements.

The results of dynamics modeling demonstrate that the proposed model can adequately capture instantaneous acceleration/deceleration behavior and thus produce realistic train trajectories. The model is also demonstrated to provide good fit in the domains of acceleration/deceleration versus speed and acceleration/deceleration versus distance. Furthermore, simulation results provide a good fit between the simulated trajectories and the field data, demonstrating the adequacy of the proposed dynamics model in support of railway simulation system.

The results of the energy consumption modeling demonstrate that the model estimates are consistent with the NTD results, resulting in a predicted error of 1.87% and -2.31%. Not modeling regenerative braking produces a significant prediction error (27.39% and 21.54%). It is also found that energy recovery reduces the overall power consumption by 20%, significantly improving the system energy efficiency. The results also demonstrate that the proposed modeling approach is able to capture the energy consumption differences associated with train, route and operational characteristics, and thus is applicable for project-level analysis.

The resulting models will be used to estimate rail trip energy consumption and thus significantly support route decision-making in the multi-modal eco-routing system.

Chapter 5

Comparison of car-following Models: An Energy and Environmental Perspective

This chapter is based on the paper:

Wang, J., Rakha, H., and Fadhloun, K. Comparison of car-following Models: A Vehicle Fuel Consumption and Emissions Estimation Perspective. *Transportation Research Part D: Transport and Environment*. (In Review).

The multimodal eco-routing system is proposed to be developed and tested in a simulation testbed before it can be used in real application. INTEGRATION was identified in chapter 2 as the micro-simulator that outperformed VISSIM, AIMSUM, PARAMICS and CORSIM in terms of the accuracy and simplicity of the built-in energy consumption and emissions models (VT-CPFM and VT-CPEM). However, the validity of INTEGRATION simulated vehicle trajectories for energy and environmental analysis has not been investigated yet. This chapter aims to address this research need. The car-following model of a micro-simulator controls longitudinal vehicle motions and thus determines the resulting vehicle trajectories. Therefore, the research effort in this chapter mainly focuses on the performance of the car-following model in INTEGRATION from the energy and environmental perspective.

5.1 Introduction

Coupling microscopic traffic simulation models with fuel consumption and emission (FC/EM) models has become increasingly attractive in evaluating the environmental impact of trans-

portation management strategies. However, recent studies [109, 183] have empirically disputed the validity of traffic simulation models in representing realistic driving characteristics, arguing that instantaneous vehicle trajectories derived from a simulation model could not accurately capture the real operating conditions associated with vehicle dynamics and thus fail to guarantee the accuracy of simulated FC/EM profiles.

The car-following model, as the internal mechanism of a traffic simulation model, has been demonstrated to be a major error source given its unrealistic acceleration and inappropriate regime thresholds [21, 22, 23]. Although Song et al. [22] proposed improving the procedure by optimizing the maximum acceleration model and regime thresholds, their solutions could not guarantee a global optima and the results remain to be further verified. Another study conducted by [90] also pointed out that most state-of-the-practice car-following models could not ensure realistic acceleration, which is the FC/EM's most sensitive parameter.

To the authors' best knowledge, the RPA car-following model, embedded in INTEGRATION, is, to date, the only model capable of simulating actual acceleration behavior by incorporating a realistic vehicle dynamics mechanism [88]. The validity of the model for FC/EM estimation, however, has not been studied. This chapter is primarily concerned with investigating the applicability of the model for FC/EM estimation and with a comparison of its performance in that regard with the most widely-used car-following models.

As the best explanatory variable of FC/EM, VSP distribution was thoroughly compared between real world and model numerical simulation in order to capture the ability of each car-following model to represent realistic vehicle trajectories associated with FC/EM. An additional study was subsequently conducted to investigate how much FC/EM estimation error was induced by unrealistic VSP distributions.

The chapter proceeds as follows. Section 5.2 thoroughly investigates the internal mechanisms of car-following models. Section 5.3 introduces data preparation work and the method of VSP distribution comparison, followed by the comparative results illustrated in section 5.4. The estimation of FC/EM error is analyzed in section 5.5, followed by a discussion in section 5.6, and the final section presents the conclusions and implications of the study.

5.2 State-of-the-practice Car-following Models

A car-following model, as the core component of a microsimulator, characterizes the longitudinal motion of vehicles, modeling steady-state and non-steady-state behavior. The steady-state car-following mechanism controls the overall traffic stream behavior, determining the desired speed at different levels of congestion and roadway capacity, as well as the spatial qualities of queues [184]. The non-steady-state mechanism governs the transition from one steady-state to another through the use of acceleration and deceleration models. Accordingly, the car-following model embedded within a microsimulator dominates the sim-

ulated traffic operating conditions associated with vehicle dynamics, and thus governs the validity of the vehicle trajectories as the input to FC/EM models.

Numerous car-following models have been proposed since the 1950's, such as the Pipes model [108], the General Motors (GM) model [185], the Gazis-Herman-Rothery (GHR) model [186], the optimal velocity model (OVM) [187], the full velocity difference model (FVDM) [188], the Newell model [189], the intelligent-driver model (IDM) [170], the Wiedemann model [107], [113], the Fritzsche model [115], and the RPA model [121]. Some of these have been incorporated into commercial traffic simulation software. Specifically, the models developed by [107] and [115] have been used in VISSIM and PARAMICS respectively, which are two of the most prevalently-used traffic micro-simulators. The Gipps model has been integrated into AIMSUN [190], which has thousands of licensed users in government agencies, consultancies and universities worldwide. The RPA model was coupled with INTEGRATION, which is a trip-based microscopic traffic assignment, simulation, and optimization model capable of tracing vehicle movements at a level of resolution of one deci-second. This study selects the most widely-used car-following models – Wiedemann, Gipps, and Fritzsche – as the state-of-the-practice controls of the RPA model. The internal mechanism of each model is discussed in the following subsections.

5.2.1 Wiedemann Model

The Wiedemann car-following model is essentially a psycho-physical model that indicates certain thresholds on relative speed (Δv) and distance (Δx) for drivers of the lagging vehicle to take an action. When approaching a slower leading vehicle, some action points are recognized by the driver for conscious reaction. There are four stages (four regimes) of following a lead vehicle, as defined by five action points (regime thresholds) in Equations (5.1)-(5.5). $RND1$, $RND2$, $RND3$, $RND4$ and $NRND$ are normally distributed driver dependent parameters; AX is the desired distance between stationary vehicles consisting of the physical length (L_{n-1}) of the lead vehicle and the desired front-to-rear distance, AX_{add} and AX_{mult} are model parameters; ABX is the desired minimum following distance at low speed differences computed by Equation (5.2) where $BX = (BX_{add} + BX_{mult} \times RND1)\sqrt{u}$ with BX_{add} , BX_{mult} the model parameters and $u = \min(u_n, u_{n-1})$; SDX is the maximum following distance varying between 1.5 and 2.5 times ABX as specified in VISSIM, formulated in Equation (5.3) where $EX = EX_{add} + EX_{mult} \times (NRND - RND2)$ with EX_{add} , EX_{mult} the model parameters; SDV is the approaching point where a driver has awareness of approaching a slower vehicle ahead, and CX is assumed to be 40 [191]; $CLDV$ is the decreasing speed difference modeling perception of small speed differences at short and decreasing distances, and is typically assumed to equal SDV , as is done in VISSIM; $OPDV$ is the increasing speed difference describing the point where a driver realizes that they are traveling at a slower speed than the preceding vehicle, $OPDV_{add}$ and $OPDV_{mult}$ are model

parameters.

$$AX = L_{n-1} + AX_{add} + RND1 \times AX_{mult} \quad (5.1)$$

$$ABX = AX + BX \quad (5.2)$$

$$SDX = AX + EX \times BX \quad (5.3)$$

$$SDV = \left(\frac{\Delta x - L_{n-1} - AX}{CX} \right)^2 \quad (5.4)$$

$$OPDV = CLDV \times (-OPDV_{add} - OPDV_{mult} \times NRND) \quad (5.5)$$

Figure 5.1a illustrates the regimes of the Wiedemann model. Specifically, when front-to-rear distance $(\Delta x - L_{n-1})$ is smaller than ABX , the vehicle operates in the “Emergency” regime in which the deceleration d_n is assigned, as formulated in Equation (5.6) where d_{n-1} is the deceleration of the leading vehicle and $d_{max} = -BMIN_{add} - BMIN_{mult} \times RND3 + BMIN_{mult} \times u_n$ with $BMIN_{add}$ and $BMIN_{mult}$ the model parameters. When $\Delta x - L_{n-1} \geq ABX$ and $\Delta v \geq SDV$, the vehicle is in the regime of “Closing in”, and a deceleration of d'_n is assigned as defined in Equation (5.7). The combination of the thresholds of ABX , SDX , $OPDV$ and SDV constitutes the “Following” regime, for which the acceleration $-a_{null}$ is assigned when a vehicle is passing from either SDV or ABX into this regime and a_{null} is assigned when passing from either $OPDV$ or SDX . a_{null} is computed by Equation (5.8) where $BNULL_{mult}$ is the calibration parameter. For “Free Driving,” namely $\Delta x - L_{n-1} \geq SDX$ and $\Delta v \leq SDV$, the maximum acceleration a_{max} is initially assigned to achieve the desired speed; after the desired speed is reached, either a_{null} or $-a_{null}$ is used. The maximum acceleration is computed by Equation (5.9) where u_{max} is the maximum speed and $BMAX_{mult}$ and $FAKTORV$ are model constants.

$$d_n = 0.5 \times \frac{\Delta v^2}{ABX - (\Delta x - L_{n-1})} + d_{n-1} + d_{max} \times \frac{ABX - (\Delta x - L_{n-1})}{BX} \quad (5.6)$$

$$d'_n = 0.5 \times \frac{\Delta v^2}{ABX - (\Delta x - L_{n-1})} + d_{n-1} \quad (5.7)$$

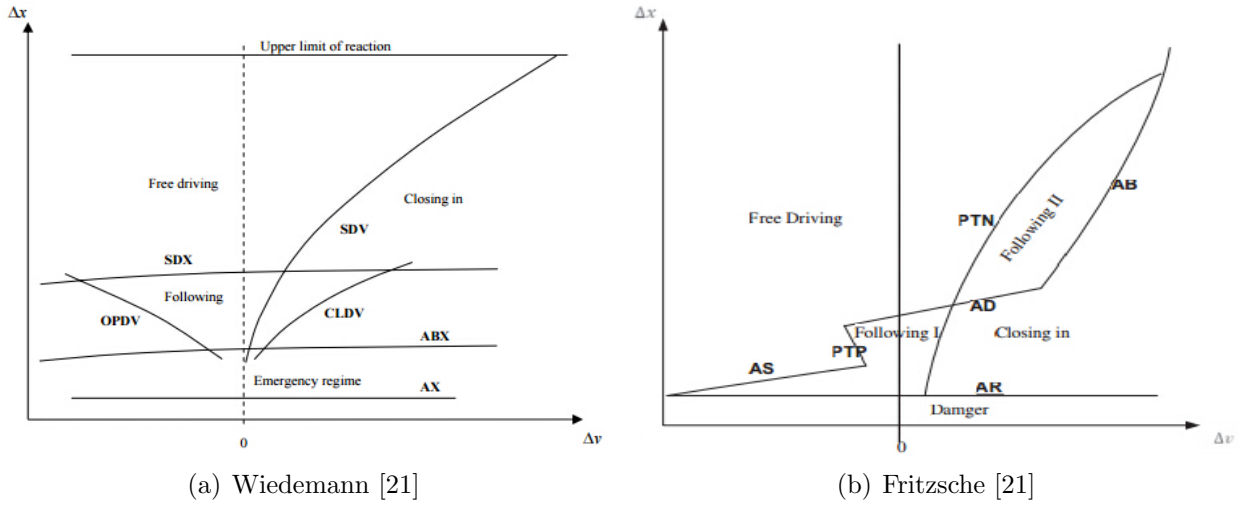


Figure 5.1: Regime of car-following models

$$a_{null} = BNULL_{mult}(RND4 + NRND) \quad (5.8)$$

$$a_{max} = BMAX_{mult} \times (u_{max} - u_n \times FAKTORV) \quad (5.9)$$

Noticeably, both maximum acceleration and deceleration models are linear decay functions. As specified in [191], $3.5 - \frac{3.5}{40}u$ is used to determine the maximum acceleration, and $-20 + \frac{1.5}{60}u$ is used to determine the maximum deceleration level. These calculations are therefore used in this study.

5.2.2 Gipps Model

The Gipps model [113] is constrained by a combination of three conditions. The first condition ensures that the vehicle speed does not exceed the facility free-flow speed; the second assumes that acceleration initially increases with vehicle speed and then decreases to zero when approaching the desired speed; and the third introduces a safety mechanism for collision avoidance. The combination of the first two conditions controls the vehicle acceleration when vehicles are distant from each other. When a vehicle is traveling close to the leader vehicle, the third condition becomes dominant and controls acceleration behavior of the follower vehicle. In such a case, the speed of the follower vehicle is affected by driver reaction time, spacing headway between the leader and follower vehicles, the speed of the leader and follower vehicles, and the deceleration rates the drivers are willing to use [113, 184].

Considering the aforementioned constraints, the speed of the following vehicle can be determined by:

$$u_n(t) = \min \left[u_n(t - \Delta t) + 2.5a_{max}^{des} \Delta t \left(1 - \frac{u_n(t - \Delta t)}{u_f} \right) \sqrt{0.025 + \frac{u_n(t - \Delta t)}{u_f}}, \right. \\ \left. d_{max}^{des} \Delta t + \sqrt{(d_{max}^{des} \Delta t)^2 - d_{max}^{des} \left(2(\Delta x(t - \Delta t) - s_{n-1}) - u_n(t - \Delta t) \Delta t - \frac{u_{n-1}^2(t - \Delta t)}{\hat{d}} \right)} \right] \quad (5.10)$$

where a_{max}^{des} and d_{max}^{des} are the desired maximum acceleration and deceleration respectively (m/s^2); s_{n-1} is the effective length of the lead vehicle (physical vehicle length plus safety margin); \hat{d} is the estimate of the maximum deceleration of the lead vehicle (for \hat{d} estimation, see [113]). Basically, if a vehicle is traveling in an unconstrained traffic situation where the vehicle can travel at its desired speed, the first component of the model dominantly determines the vehicle speed. Alternatively, in congested traffic conditions, the second argument of the model is applied to limit the speed estimated by the first argument.

5.2.3 Fritzsche Model

The Fritzsche car-following model is also a psycho-physical model which has a modeling framework similar to the Wiedemann model. The actions taken by drivers of follower vehicles also depend on the defined thresholds relative to speed difference (Δv) and spacing headway (Δx). The Fritzsche model defines five regimes (i.e., danger, closing in, following I, following II, and free driving) based on six regime thresholds, as illustrated in Equations (5.11)-(5.16).

$$AR = s_{n-1} + T_r u_{n-1} \quad (5.11)$$

$$AS = s_{n-1} + T_s u_n \quad (5.12)$$

$$AD = s_{n-1} + T_D u_n \quad (5.13)$$

$$AB = AR + \frac{\Delta v^2}{\Delta b_m} \quad (5.14)$$

$$PTP = -k_{PTP}(\Delta x - s_{n-1})^2 - f_x \quad (5.15)$$

$$PTN = k_{PTN}(\Delta x - s_{n-1})^2 + f_x \quad (5.16)$$

where AR , AS , AD , AB , PTP , and PTN are the regime thresholds; k_{PTP} , k_{PTN} , f_x , T_r , T_s , T_D and Δb_m are model parameters; and Δv is speed difference. Other parameters were defined hereinbefore.

Figure 5.1b presents a general view of the Fritzsche model. Specifically, when $\Delta x \leq AR$, the vehicle operates in the regime of “Danger” and the driver has to adopt the maximum deceleration (d_{max}) for collision avoidance. When $AR < \Delta x \leq AD$ and $\Delta v > PTN$ or $AR < \Delta x \leq AB$ and $\Delta v > PTN$, the vehicle is in the regime of “Closing in”, and acceleration a_n is assigned as formulated in Equation (5.17), where $d_c = \Delta x - AR + u_{n-1}\Delta t$. In the “Following I” regime, namely $AR < \Delta x \leq AD$ and $PTP < \Delta v \leq PTN$ or $AR < \Delta x \leq AS$ and $\Delta v < PTP$, the model constant a_{null} or $-a_{null}$ is assigned as the acceleration. In the “Following II” regime, namely $\Delta x > AD$ and $\Delta v > PTN$ or $\Delta x > AB$ and $\Delta v > PTN$, the vehicle takes no action given the large spacing headway. For the “Free Driving” regime in which $\Delta x > AD$ and $\Delta v \leq PTN$ or $\Delta x > AS$ and $\Delta v \leq PTP$, the vehicle takes the maximum acceleration (a_{max}) to reach the desired speed and thereafter is assigned a_{null} or $-a_{null}$ to be responsible for the inadequate control over the acceleration and brake pedal.

$$a_n = \frac{u_{n-1}^2 - u_n^2}{2d_c} \quad (5.17)$$

It should be noted that, as demonstrated by [115], the maximum acceleration is assumed to be a given constant, which is not realistic.

5.2.4 Rakha-Pasumathy-Adjerid Model

The RPA model is a simplified behavioral vehicle longitudinal motion model comprised of three components: steady-state car-following behavior, a collision avoidance mechanism, and vehicle dynamics constraint. The steady-state component controls vehicle speed based on the relative speed and distance between the follower and leader vehicles. When the follower vehicle is traveling close to the leader vehicle, the collision avoidance model becomes more important to determine speed in order to maintain a minimum safe distance when the leader vehicle suddenly comes to a complete stop. The acceleration derived from the first two components is constrained by vehicle dynamics given that, at each speed level, the realistic acceleration cannot exceed the maximum acceleration that is allowed by vehicle dynamics.

Consequently, the minimum speed of the three components is finally taken as the velocity for a given instant in time.

The steady-state component of RPA was first proposed by [119] and [120] as formulated as a single-regime non-linear functional form in Equation (5.18):

$$\Delta x = c_1 + c_3 u'_n + \frac{c_2}{u_f - u'_n} \quad (5.18)$$

where Δx is the spacing headway (m) between the following vehicle n and its predecessor $n-1$; u'_n is the velocity of the follower determined by the steady-state model (m/s); u_f is the facility free-flow speed (m/s); c_1 is a fixed distance headway constant (m); c_2 is a variable headway constant (m^2/s); c_3 is a variable spacing headway constant (s). Considering the boundaries [192] that the derivative of traffic flow with respect to speed equals 0 at speed-at-capacity (u_c) and that speed equals 0 at jam density (k_j), c_1 , c_2 , c_3 can be computed using Equation (5.19):

$$c_1 = \frac{u_f}{k_j u_c^2} (2u_c - u_f); c_2 = \frac{u_f}{k_j u_c^2} (u_f - u_c)^2; c_3 = \frac{1}{q_c} - \frac{u_f}{k_j u_c^2} \quad (5.19)$$

where q_c is the facility capacity (veh/s). To clarify the speed formulation, Equation (5.18) generates a variant as computed by Equation (5.20):

$$u'_n(t) = \frac{-c_1 + c_3 u_f + \Delta x(t) - \sqrt{(c_1 - c_3 u_f - \Delta x(t))^2 - 4c_3(\Delta x(t)u_f - c_1 u_f - c_2)}}{2c_3} \quad (5.20)$$

Noticeably, to ensure the validity of Equation (5.20), the square root term should be non-negative. Namely, $(c_1 - c_3 u_f - \Delta x(t))^2 - 4c_3(\Delta x(t)u_f - c_1 u_f - c_2) \geq 0$, assuming that

$$\begin{aligned} A &= (c_1 - c_3 u_f - \Delta x)^2 - 4c_3(\Delta x u_f - c_1 u_f - c_2) \\ &= (c_1 - c_3 u_f)^2 + \Delta x^2 - 2(c_1 - c_3 u_f)\Delta x - 4c_3 u_f \Delta x + 4c_1 c_3 u_f + 4c_2 c_3 \\ &= (\Delta x - (c_1 + c_3 u_f))^2 + 4c_2 c_3 \end{aligned} \quad (5.21)$$

The first term of Equation (5.21) ensures non-negativity by having a quadratic component; however, the sign of the second term $4c_2 c_3$ remains to be determined given that c_2 is a non-negative, while c_3 may either be positive or negative. Therefore, the conditions that make $A < 0$ would be $4c_2 c_3 < 0$ and $-4c_2 c_3 > (\Delta x - (c_1 + c_3 u_f))^2$. The speed formulation (Equation (5.20)) should guarantee that the spacing headway is $\Delta x \notin (c_1 + c_3 u_f - \sqrt{-4c_2 c_3}, c_1 + c_3 u_f + \sqrt{-4c_2 c_3})$ in order to ensure its validity. To this concern, the next objective is to find

the maximum possible value of the term $B = c_1 + c_3 u_f + \sqrt{-4c_2 c_3}$ in order to achieve $\Delta x > B_{max}$. Assuming that the first-order and second-order derivatives of B with respect to c_3 equal 0, B is found to reach its maximum at the point $c_3 = -\frac{c_2}{u_f^2}$. Substituting c_3 by $-\frac{c_2}{u_f^2}$ in $c_1 + c_3 u_f + \sqrt{-4c_2 c_3}$:

$$\begin{aligned} B_{max} &= c_1 - \frac{c_2}{u_f^2} u_f + \sqrt{4c_2 \frac{c_2}{u_f^2}} \\ &= \frac{u_f}{k_j u_c^2} (2u_c - u_f) + \frac{\frac{u_f}{k_j u_c^2} (u_f - u_c)^2}{u_f} \\ &= \frac{1}{k_j} = \Delta x_j \end{aligned} \tag{5.22}$$

where Δx_j is the spacing headway at jam density (m). Consequently, the condition $\Delta x \geq \Delta x_j$ ensures the validity of the model. Specifically, $\Delta x = c_1 + c_3 u_n' + \frac{c_2}{u_f - u_n} \geq \Delta x_j = c_1 + \frac{c_2}{u_f}$, so that $c_3 \geq -\frac{c_2}{u_f(u_f - u_n')}$. The final condition for model validity is therefore given by Equation (5.23) formulated as:

$$\begin{aligned} \frac{1}{q_c} - \frac{u_f}{k_j u_c^2} &\geq -\frac{\frac{u_f}{k_j u_c^2} (u_f - u_c)^2}{u_f^2} \\ q_c &\leq \frac{k_j u_f u_c}{2u_f - u_c} \end{aligned} \tag{5.23}$$

Equation (5.23) ensures that the minimum spacing occurs at jam density [123]. The model calibration effort requires the estimation of four traffic stream parameters (q_c, u_c, u_f, k_j). For a detailed calibration procedure, see [124].

The aforementioned steady-state model (Equation (5.20)) cannot guarantee safe driving given that the velocity estimated by the model may exceed the permissible maximum value at which the follower is capable of maintaining a minimum safe distance behind a lead vehicle when coming to a complete stop. For safety purposes, the steady-state model is improved by adding a collision avoidance constraint as formulated in Equation(5.24):

$$u_n''(t) = \sqrt{u_{n-1}(t)^2 + 2d_{max}(\Delta x(t) - \Delta x_j)} \tag{5.24}$$

where $u_n''(t)$ is the maximum speed of the follower required to avoid collision (m/s); $u_{n-1}(t)$ is the speed of the leading vehicle (m/s); d_{max} is the maximum deceleration level (m/s^2). This constraint applies only when the following vehicle travels at a higher speed than the lead vehicle.

An accurate acceleration model is the requirement of a car-following model in simulating realistic vehicle activity. Various kinematic acceleration models have been developed and applied by researchers, such as the dual-regime model [193], the linear decay model, and the polynomial model [168]. However, none of these models can adequately capture realistic acceleration behavior given that they do not explicitly model the actual components – tractive force and resistance force opposing a vehicle’s motion – which affect the motion of a vehicle. Rakha et al. [90] developed a vehicle dynamics model as the second constraint of the RPA model, demonstrating that the model can provide a better fit to field observations than kinematic models. The model is formulated in Equation (5.25) where a_{max} is the maximum acceleration level associated with vehicle dynamics (m/s^2); M is the vehicle mass (kg); R is the total resistance force (N) being a combination of aerodynamic, rolling and grade resistance; and F is the residual force (N), computed by Equation (5.26) where η is engine efficiency; β is the variable power factor (estimation of β see [90]); P is the vehicle power (kW); M_{ta} is the mass of vehicle on tractive axles (kg); g is the gravitational acceleration ($9.8066 m/s^2$); and μ is the coefficient of friction between tires and pavement.

$$a_{max}(t) = \frac{F(t) - R(t)}{M} \quad (5.25)$$

$$F(t) = \min\left(3600\eta\beta\frac{P}{u_n(t)}, gM_{ta}\mu\right) \quad (5.26)$$

Constrained by vehicle dynamics, the maximum speed that a vehicle could reach for a given time interval Δt is formulated in Equation (5.27):

$$u_n'''(t) = u_n(t - \Delta t) + \gamma a_{max}(t - \Delta t)\Delta t \quad (5.27)$$

where u_n''' is the maximum speed level that a vehicle could reach during Δt (Δt taken as 1 s in this study); γ is the throttle level that a driver wishes to take (ranging from 0.0 to 1.0).

Consequently, the velocity of the follower vehicle (u_n) is the minimum of the speeds determined by the steady-state model (u_n'), collision avoidance model (u_n'') and vehicle dynamics model (u_n'''); namely, $u_n = \min(u_n', u_n'', u_n''')$.

5.3 Test Scenario

The ability of the four car-following models (RPA, Gipps, Fritzsche, and Wiedemann) in generating realistic vehicle trajectories associated with FC/EM estimation was thoroughly investigated. First, the field car-following trajectory was identified from a naturalistic database. Secondly, the simulated trajectory of each car-following model was generated by numerical simulation. Finally, the consistency of simulated VSP distributions with field observations was analyzed, and the error of distributions was compared between models.

5.3.1 Field Data Preparation

The field car-following trajectory was identified from the 100-Car Naturalistic Driving Study database. This study was conducted by Virginia Tech Transportation Institute (VTTI) in the Washington D.C. metropolitan area between 2002 and 2004, and is the first instrumented vehicle study designed to collect a large volume of naturalistic driving data for a large number of drivers over an extended period of time [194]. Test vehicles were equipped with instruments and sensors and driven as ordinary vehicles. Drivers, without any experimenters accompanying them, were not given any instructions during test driving. For more details about data collection, see [194]. Statistically, a total of nearly 337,000 hours of data were collected across 207,000 trips, resulting in more than 12 billion observations at a frequency of 10 *Hz*. The data used in this study is a subset of the naturalistic data gathered along an 8.75 mi (14-km) section of Dulles Airport Access Road (with a speed limit of 55 *mph*), ensuring facility homogeneity. The car-following events were identified via visual inspection, see [195], with a total of 1,732 events identified (789 minutes of trajectories collected by four test vehicles).

The identified trajectories were used to estimate VSP distributions. VSP, referring to the vehicle power per unit mass of the vehicle, can be formulated by dividing the power by vehicle mass, as formulated in Equation (5.28) with all parameters defined in Equation (2.3). Grade is assumed to be zero in this study given that the test terrain is flat.

$$VSP(t) = \left(g \cdot \cos(\theta) \cdot \frac{C_r}{1000} (c_1 v(t) + c_2) + g \cdot \sin(\theta) + a(t) + 0.5 \rho_{air} \frac{A_f C_D}{m} v^2(t) \right) \cdot v(t) \cdot \frac{1}{\eta_d} \quad (5.28)$$

5.3.2 Numerical Simulation

For numerical simulation, the identical field trajectory was applied as the input of the leading vehicle to each car-following model, ensuring that the follower's driving course of events constrained by the same leader. The facility free-flow speed (u_f) was estimated specific to each car-following event, instead of configuring a constant, given the great heterogeneity of the driver behavior during free driving, resulting in a distribution illustrated in Figure 5.2. Specifically, most free-flow speeds range between 55 and 75 *mph*; namely, free driving may occur when speed is higher than 55 *mph* (speed limit). To maintain the homogeneity of road facility and driver behavior, each car-following model employs the same desired speed distribution provided by Figure 5.2. Jam density (k_j), capacity (q_c) and speed-at-capacity (u_c) were estimated in order to generate RPA simulated trajectory. For estimation procedure, see [124]. The throttle level γ in Equation (5.27) is taken as 0.6 based on field observations. The vehicle-specific parameter values used by RPA can be obtained from manufacturer website, as illustrated in Table 5.1 (the identified car-following trajectories were collected by the four vehicles as shown in the table). The parameter values relative to Gipps, Fritzsche,

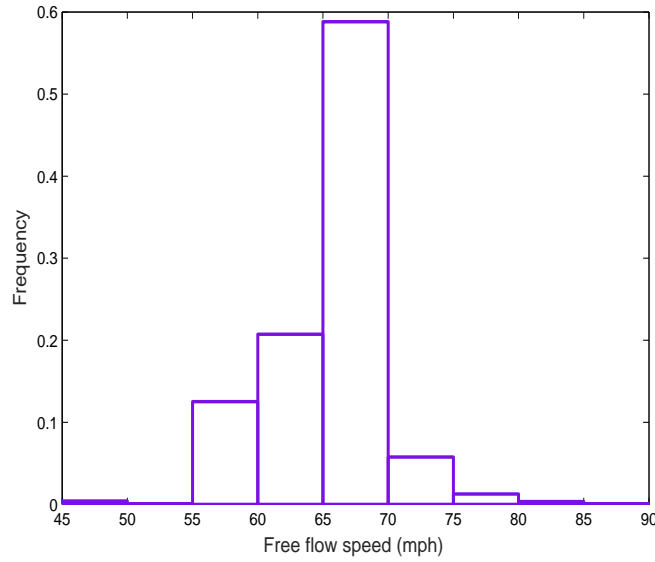


Figure 5.2: Desired speed distribution

Wiedemann were obtained according to test vehicles and references [113, 115, 190, 191], as illustrated in Table 5.2.

Again, the VSP values were estimated using Equation (5.28) on a second-by-second basis as a simulated counterpart of the field observations.

5.3.3 Comparison of VSP Distribution and Vehicle Dynamics

Given that average speed is the only factor affecting the peak of VSP distribution for a given facility and vehicle type [196], the vehicle trajectories were grouped into various speed bins

Table 5.1: Testing vehicle characteristics

Test vehicle	Power (P (kW))	Mass (M (kg))	Drag Co- efficient (C_D)	Frontal area ($A_f(m^2)$)	Engine effi- ciency (η)	Maximum tractive force ($g\mu M_{ta}$ (N))
Vehicle 1	90	1190	0.36	2.06	0.86	3.24
Vehicle 2	90	1090	0.40	2.00	0.86	3.24
Vehicle 3	145	1375	0.40	2.18	0.86	3.24
Vehicle 4	119	1900	0.50	2.94	0.86	3.24

Table 5.2: Model parameter values for Gipps, Fritzsche and Wiedemann

Model	Parameter	value	Parameter	value	Parameter	value
Gipps	a_{max}^{des}	2.5 m/s^2	d_{max}^{des}	-5.0 m/s^2	\hat{d}	-4.0 m/s^2
	τ	1 s	s_{n-1}	6 m		
Fritzsche	k_{PTN}	0.001	k_{PTP}	0.002	f_x	0.5
	T_r	0.5 s	T_s	1.0 s	T_D	1.8 s
	a_{max}	2.0 m/s^2	Δb_m	0.4 m/s^2	a_{null}	0.2 m/s^2
Wiedemann	s_{n-1}	6 m	d_{max}	-6.0 m/s^2		
	$RND1$	N(0.5,0.15)	$RND2$	N(0.5,0.15)	$RND3$	N(0.5,0.15)
	$RND4$	N(0.5,0.15)	$NRND$	N(0.5,0.15)	AX_{add}	1.25
	AX_{mult}	2.5	BX_{add}	2.0	BX_{mult}	1.0
	EX_{add}	1.5	EX_{mult}	0.55	$OPDV_{add}$	1.5
	$OPDV_{mult}$	1.5	CX	40	$BNULL_{mult}$	0.1
	a_{max}	$3.5 - \frac{3.5}{40}u$	d_{max}	$-20 + \frac{1.5}{60}u$	L_{n-1}	4.5 m

in order to investigate the consistency of speed-specific VSP distributions. Specifically, 766 pieces of 60-s speed segments were identified and grouped based on the average speed of each segment into 14 speed bins ranging between 0 and 70 *mph* (few over-70 *mph* data samples) with an identical speed interval of 5 *mph*. VSP distribution is defined as Equation (5.29), with n the integer from -30 to 30 kW/ton given that 98% of the VSP values belongs to this range.

$$VSP \in (n - 0.5, n + 0.5), VSPbin = n \quad (5.29)$$

Acceleration behavior was also evaluated to capture the error of VSP distribution associated with vehicle dynamics, as defined in Equation (5.30) with m restricted between -2 and 2 m/s^2 varying with an interval of 0.1 m/s^2 given 99% of acceleration levels within this range.

$$Acceleration \in (m - 0.05, m + 0.05), AccelerationBin = m \quad (5.30)$$

Furthermore, Root Mean Square Error (RMSE) was computed to quantify the accuracy of simulated VSP- and acceleration- distribution, as defined in Equation (5.31) and Equation (5.32) where $RMSEVSP_k$ and $RMSEACC_k$ are respectively the RMSE of VSP- and acceleration- distribution for speed bin of k ; $SimuVSP_{i,k}$ and $ObsVSP_{i,k}$ are the fraction of simulated and field VSP distribution for VSP bin i of speed bin k ; $SimuACC_{j,k}$ and $ObsACC_{j,k}$ are the fraction of simulated and field acceleration distribution for acceleration bin j of speed bin k . Basically, lower RMSE demonstrates higher consistent distributions

between real world and numerical simulation.

$$RMSEVSP_k = \sqrt{\left(\sum_{i=1}^n \frac{(SimuVSP_{i,k} - ObsVSP_{i,k})^2}{n}\right)}, k = 1, 2, \dots, 14. \quad (5.31)$$

$$RMSEACC_k = \sqrt{\left(\sum_{j=1}^m \frac{(SimuACC_{j,k} - ObsACC_{j,k})^2}{m}\right)}, k = 1, 2, \dots, 14. \quad (5.32)$$

5.4 Results for VSP Distribution and Vehicle Dynamics

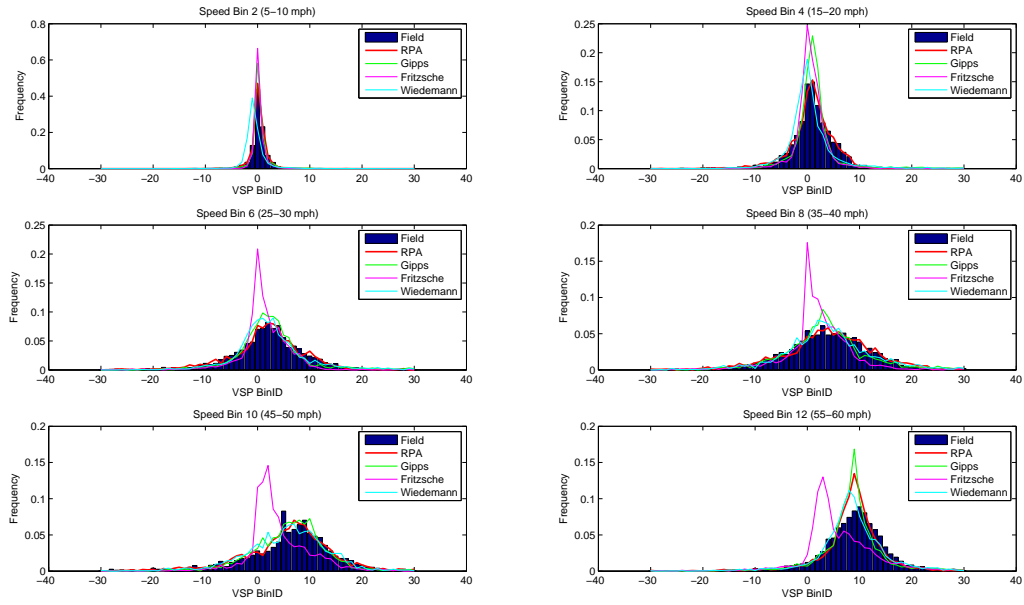
Given the space limitation, six speed bins covering various speed levels (5-10, 15-20, 25-30, 35-40, 45-50, and 55-60 mph) were selected to visually illustrate the consistency of simulated VSP- and acceleration- distributions with field observations. RMSE was then analyzed for the entire speed range as the quantitative metrics of the consistency.

5.4.1 VSP Distribution

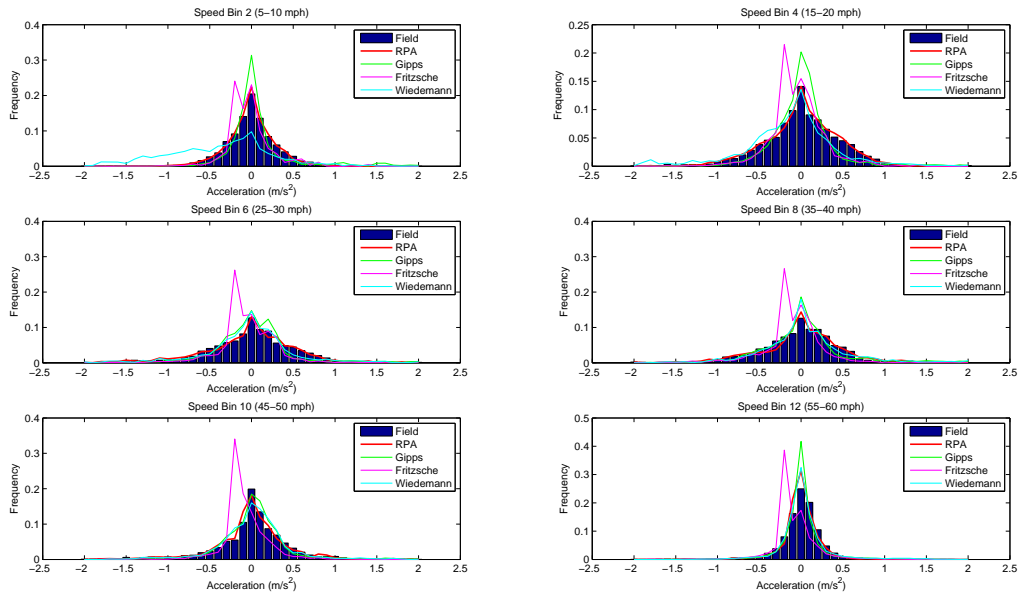
The resulting field VSP distributions, as illustrated in Figure 5.3a, are approximately normally distributed and present consistent behavior with [196] by having VSP mean values move towards the positive direction with the increase of vehicle speed. RPA, in general, provides more consistent VSP behavior than the other models, although relatively less consistent for free driving (speed bin 12: 55-60 mph). Given that drivers behave highly heterogeneously during free driving, it is hard for a car-following model to capture realistic free driving behavior. Gipps, at low speed levels, overestimates VSP distributions in the central area and underestimates in other areas; during free driving, the model also cannot generate realistic VSP distributions. However, relative to Fritzsche and Wiedemann, Gipps captures the VSP behavior more consistent with that of RPA. Wiedemann behaves inconsistently at low speed levels ($speed \leq 20mph$) by differing VSP means but presents a good fit with the increasing speed level. Fritzsche behaves worst among the four models.

5.4.2 Acceleration Behavior

Given that acceleration is the most sensitive parameter to vehicle power, the acceleration behavior was thus thoroughly investigated to uncover the underlying error source of VSP distribution induced by the internal mechanism of a car-following model.



(a)



(b)

Figure 5.3: Comparison of VSP and acceleration distributions: (a) VSP distribution and (b) Acceleration distribution

Figure 5.3b presents the consistency of acceleration distributions across various speed levels. Specifically, RPA generates highly consistent acceleration distributions but a poorer fit for free driving (speed bin 12). Gipps, with a consistency similar to that of VSP distributions, appears to overestimate in the central area and underestimate in other areas for the low-speed operation as well as free driving; this model also provides a relatively better match with RPA than the other two models. Wiedemann offers highly inconsistent distributions at low speed ranges while producing a better fit at moderate- and high- speed levels. Fritzsche generates the most inconsistent acceleration behavior by differing means of distributions for the entire speed range. In summary, the inconsistency of acceleration distributions provides an overriding explanation of inadequate representation of realistic VSP behavior.

Because they impose unrealistic vehicle dynamics constraints on acceleration behavior, the majority of state-of-the-practice car-following models cannot ensure realistic acceleration. Figure 5.4 gives the acceleration behavior derived from the internal acceleration model embedded in each car-following model. Intuitively, RPA, incorporating the realistic vehicle dynamics model (Equation (5.25)), generates highly consistent acceleration behavior with field observations. Conversely, the other three models do not provide a good fit. Although Gipps presents a similar concave-shaped curve varying maximum acceleration with vehicle speed, the peak shifts to the negative direction. Fritzsche employs a constant to constrain the acceleration behavior, resulting in behavior that is inconsistent for the entire speed range. Wiedemann applies a linear decay model having the maximum acceleration decrease monotonously with vehicle speed, resulting in large acceleration behavior error, especially for low speed levels.

Acceleration model, however, is not the only factor that results in unrealistic acceleration behavior. According to recent studies [22, 23], the regime structure of the Wiedemann and Fritzsche models is another major error source given the unsmooth transition of acceleration between regimes. For the Gipps model, it offers a suboptimal fit of the speed-flow relationship to the field data [184] so that results in less accurate steady-state car-following behavior compared to the RPA model which has been demonstrated to reflect the field data fairly well for both steady-state and non-steady-state behavior [122, 124].

5.4.3 Root Mean Square Error

To obtain quantitative clarification, RMSE was computed, as illustrated in Figure 5.5. In general, the variation of VSP RMSE with speed is highly consistent with that of acceleration RMSE, quantitatively demonstrating that unrealistic acceleration behavior is the primary trigger of inadequate representation of VSP distribution. In particular, RPA overall outperforms the other models by having the lowest level of RMSE (no more than 1%) for both VSP and acceleration distributions in the car-following regime (speed bin ≤ 11 , speed $\leq 55mph$), although the increasing error observed for free driving (speed bin ≥ 12 , speed $> 55mph$). Gipps, compared to RPA, produces larger error especially at low speed levels (speed bin

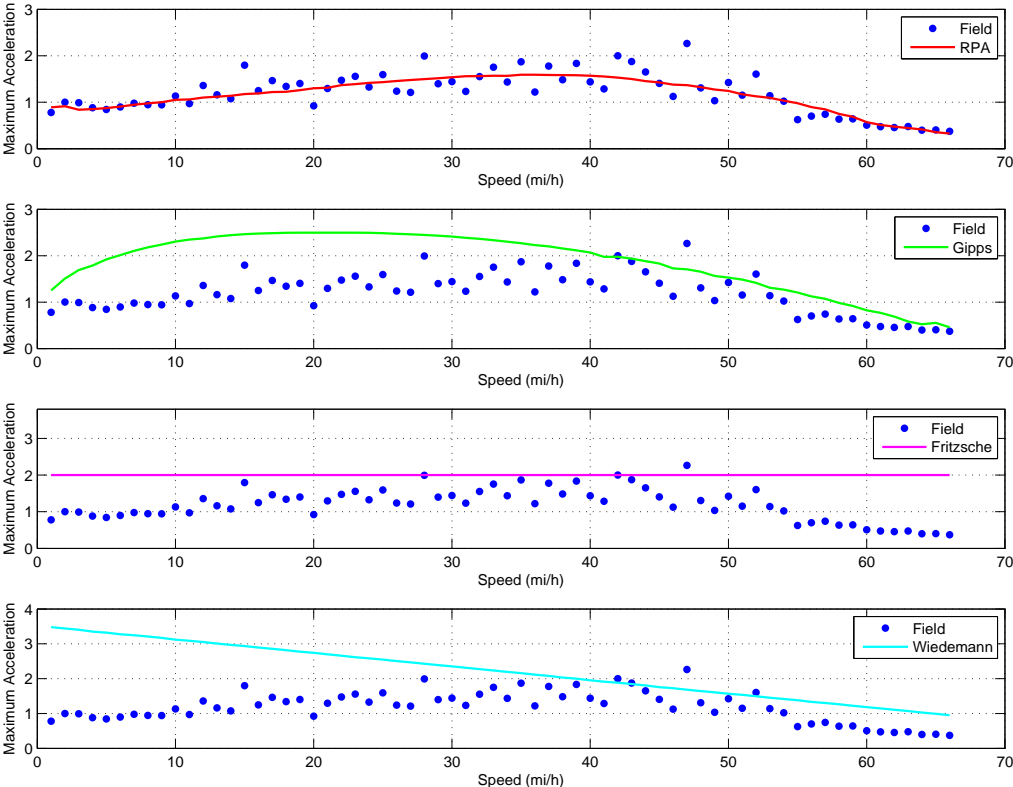


Figure 5.4: Maximum acceleration behavior (m/s^2)

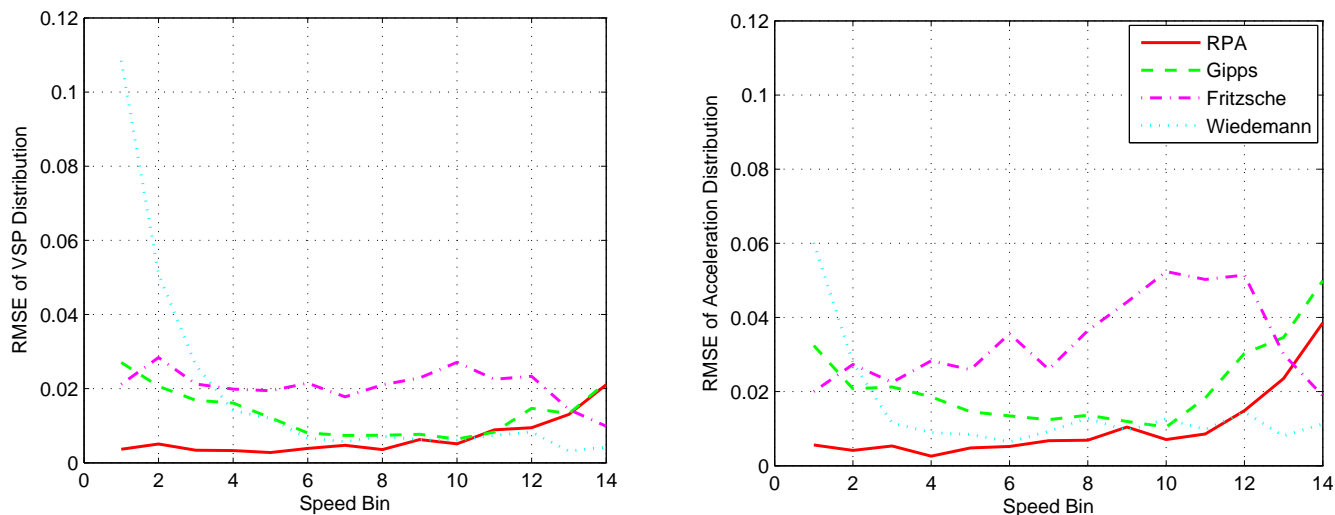


Figure 5.5: Root mean square error

smaller than 6; i.e., $0 - 30\text{mph}$); and the error is asymptotically consistent with that of RPA with the increase of speed. This is attributable to the fact that Gipps shifts the peak of the acceleration behavior to the negative direction, as demonstrated in Figure 5.4. Fritzsche has overall higher RMSE compared to other models except under low speed levels where Wiedemann produces extremely high RMSE given the tremendous deviation of acceleration behavior. Further, Wiedemann’s RMSE differs insignificantly from that of RPA when the speed bin is larger than 6 (speed $> 30\text{mph}$). In a nutshell, RPA outperforms the other models for FC/EM estimation especially in the low speed range ($0 - 30\text{mph}$).

Figure 5.6 quantifies how much more error of VSP distribution induced by other models relative to that of RPA. Intuitively, Gipps and Fritzsche initially generate 5 times the RPA RMSE while Wiedemann approximately 30 times. The difference of the error overall decreases with the increasing speed level. Specifically, RMSE of Gipps and Wiedemann differs insignificantly from that of RPA with the speed higher than 30mph (speed bin higher than 6), whereas Fritzsche produces significantly higher error except for free driving. Accordingly, RPA outperforms the other three models in terms of FC/EM analysis especially at low speed levels.

5.5 Fuel Consumption and Emissions

To gain insight into how much error the VSP distribution may introduce to FC/EM estimation, the Environmental Protection Agency (EPA) MOVES was utilized to generate FC/EM

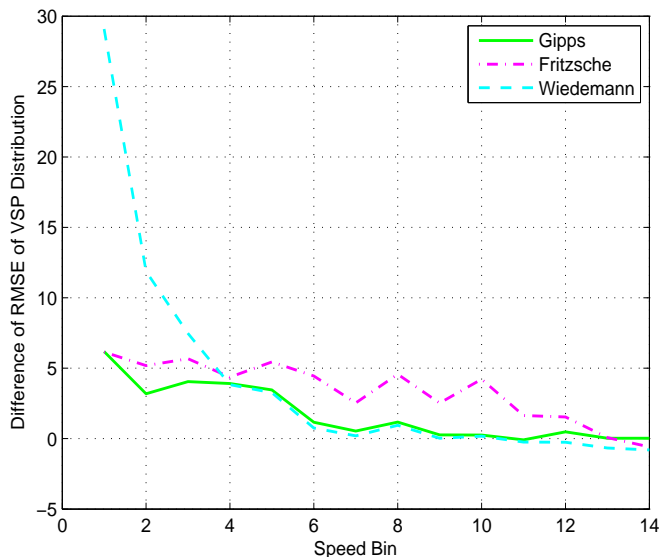


Figure 5.6: Relative difference of VSP distribution RMSE between RPA and other car-following models

profiles. Given that passenger cars collected the field trajectory, light duty gasoline vehicle with conventional internal combustion engine technology was selected in MOVES. According to [194], the test vehicles for the naturalistic driving study were manufactured between 1995 and 2003, and 1999 was thus selected as an average of the model years. Further, as a point of comparison to older cars, the model year 2015 was chosen as representative of new cars in order to achieve an insight into how sensitive the applicability of simulated trajectories for FC/EM estimation is to vehicle model year. Table 5.3 and Table 5.4 show the generated energy and emission inventories for each model year. Carbon monoxide (CO), Hydrocarbon (HC) and Nitric Oxide (NO_x) were also analyzed as representative of emissions.

FC/EM were analyzed primarily relative to the car-following regime given that the major concern of a car-following model is the ability to emulate car-following behavior; results for free driving were employed as a control. As illustrated in Figure 5.2, speed limit ($55mph$) is the demarcation of car-following ($u < 55mph$) and free driving ($u \geq 55mph$) regimes. Accordingly, the field trajectory, along with each simulated trajectory, were divided respectively into two speed bins: $u < 55mph$ and $u \geq 55mph$, generating a total of 10 trajectories. The instantaneous FC/EM rates relative to each trajectory were first estimated based on MOVES mean base rates (Table 5.3 and Table 5.4) for each model year, and then averaged across the specific trajectory.

As a follow-up, the absolute values of the relative differences between simulated average rates and field rates were computed, resulting in Table 5.5. Basically, RPA generates the most accurate FC/EM estimates for both model years with a relative error of, at most, 2.97%

Table 5.3: MOVES energy/emission rate (model year: 1999)

Operating mode ID	Energy rate (KJ/hr)	HC (g/hr)	CO (g/hr)	NO _x (g/hr)
0	50080.5	1.23	6.96	1.13
1	44269.9	0.30	1.20	0.48
11	68600	0.84	23.92	1.67
12	90758	0.64	39.06	2.55
13	136573	1.22	36.01	5.98
14	178006	1.65	51.67	10.55
15	219270	2.31	74.93	18.71
16	278661	3.68	126.43	39.01
21	85709.5	1.26	31.18	3.31
22	105849	1.15	41.32	5.37
23	137124	1.24	53.13	8.12
24	179231	2.37	77.67	13.69
25	229004	2.37	88.15	19.20
27	301831	3.74	132.38	30.23
28	406833	5.67	232.03	47.25
29	557151	10.06	491.40	82.96
30	699354	16.61	1725.90	109.15
33	135268	1.21	23.41	7.05
35	215174	1.68	39.98	19.45
37	280198	2.15	58.85	27.18
38	365379	3.83	212.67	40.12
39	486672	5.55	224.40	59.73
40	621048	7.26	659.51	75.23

Table 5.4: MOVES energy/emission rate (model year: 2015)

Operating mode ID	Energy rate (KJ/hr)	HC (g/hr)	CO (g/hr)	NO _x (g/hr)
0	42199.5	0.10	1.98	0.07
1	39039.4	0.02	0.34	0.03
11	61388.6	0.07	6.80	0.10
12	84766.5	0.05	11.11	0.16
13	117806	0.09	10.24	0.37
14	148855	0.13	14.69	0.65
15	177506	0.18	21.31	1.15
16	214392	0.29	35.95	2.40
21	83515.7	0.10	8.87	0.20
22	95064.2	0.09	11.75	0.33
23	115783	0.10	15.11	0.50
24	148541	0.18	22.09	0.84
25	198229	0.18	25.07	1.18
27	261323	0.29	37.65	1.86
28	352244	1.96	126.33	6.86
29	482576	3.47	267.54	12.04
30	606011	5.73	939.67	15.84
33	118985	0.09	6.66	0.43
35	190794	0.13	11.37	1.20
37	248541	0.17	16.73	1.68
38	324084	1.32	115.79	5.82
39	431674	1.92	122.18	8.67
40	550281	2.51	359.07	10.92

Table 5.5: The FC/EM estimation error (%) by numerical simulation

Fuel and emission type	Model year	<i>Speed < 55mph (car-following)</i>				<i>Speed ≥ 55mph (free driving)</i>			
		RPA	Gipps	Fritzsche	Wiedemann	RPA	Gipps	Fritzsche	Wiedemann
Fuel	1999	0.90	3.98	15.50	2.37	2.33	0.98	6.26	5.28
	2015	0.89	3.96	14.81	2.95	2.32	0.94	6.34	5.36
<i>HC</i>	1999	0.76	8.71	16.31	7.53	3.82	2.54	0.14	9.70
	2015	2.97	42.02	19.75	33.58	16.15	12.80	21.95	41.43
<i>CO</i>	1999	0.52	36.25	14.45	21.21	9.45	6.29	15.50	35.12
	2015	2.88	62.14	13.48	40.79	14.82	10.64	31.01	56.28
<i>NO_x</i>	1999	1.15	13.19	25.32	4.91	3.37	0.96	10.12	8.92
	2015	2.77	28.89	26.12	18.59	9.43	6.36	1.98	23.85

in the car-following regime. For free driving, RPA gives relatively high yet tolerant error given the increasing RMSE of the VSP distribution. It is worth noting that three paradoxes have been identified. First, Gipps somehow provides higher emission error than Fritzsche does; however, the RMSE of VSP distributions for Gipps is lower than that for Fritzsche in most cases illustrated by Figure 5.5. Secondly, Wiedemann generates lower FC/EM error for car-following than for free driving, which contradicts the fact that higher RMSE of VSP distributions is observed for car-following, demonstrated in Figure 5.5. Thirdly, for free driving, Wiedemann, in most cases, produces higher FC/EM error than other models do, although the model captures a lower RMSE of VSP distributions. On the one hand, these issues can be attributed to an offset that is achieved between overestimating VSP distribution in some areas and underestimating in other areas. On the other hand, as demonstrated by Table 5.3 and Table 5.4, some of the operating modes gain more weights to determine FC/EM estimates by having significantly higher mean base rates than other modes, such as $ID = 28, 29, 30, 38, 39, 40$ where VSP is at a high level. It was found, through the inspection of operating mode distributions, that the inconsistencies in these distributions at high weight operating modes (high VSP levels) were the major trigger for lower VSP RMSE leading to higher FC/EM error. In addition, the emission error is amplified from model year 1999 to 2015, given that the high weight operating modes gain more weights for the new vehicle, which intensifies the associated error. An exception is observed in the emission error induced by Fritzsche (for the car-following regime), which is insensitive to the model year; this may be attributed to the offset of overestimation and underestimation. In addition, the variation in fuel consumption error is insensitive to model year given that, for energy rate, the weights of high VSP levels differ insignificantly with the variation of the model year, as demonstrated in Table 5.3 and Table 5.4.

To validate the robustness of RPA model performance, the VT-CPFM model was applied. The model has been demonstrated, by recent studies [12, 40, 41, 160, 197], to generate

Table 5.6: Comparison of simulated fuel consumption error (%) between MOVES and VT-CPFM

Fuel consumption model	<i>Speed < 55mph (car-following)</i>				<i>Speed ≥ 55mph (free driving)</i>			
	RPA	Gipps	Fritzsche	Wiedemann	RPA	Gipps	Fritzsche	Wiedemann
MOVES	0.89	3.96	14.81	2.95	2.32	0.94	6.34	5.36
VT-CPFM (Toyota)	0.60	0.91	18.42	5.20	3.66	4.19	3.05	4.09
VT-CPFM (Ford)	0.25	1.84	21.71	8.47	3.93	5.09	1.84	3.79

more robust and realistic fuel estimates at a microscopic level compared to other state-of-the-practice fuel consumption models. It should be noted that, to date, validation has been made only for fuel consumption given a lack of VT-CPFM based emission models. Additionally, two model year 2015 LDVs, a Toyota Corolla and a Ford Taurus, were selected as the representatives of small- and large- displacement passenger cars respectively. The comparison of fuel consumption error between MOVES and VT-CPFM was conducted only for the model year 2015. Table 5.6 presents consistent results between MOVES and VT-CPFM, showing that RPA generates the lowest level of fuel consumption error in the car-following regime although the error values differ, demonstrating that the applicability of RPA for fuel estimation is robust to different fuel consumption models. The deviation of error values results from the differences of fuel estimates and vehicle types employed between the two models; specifically, MOVES employs a composite LDV stored in EPA database while VT-CPFM employs two specific LDVs, namely Toyota and Ford.

5.6 Discussion

A calibration procedure, similar to that of the RPA model, was used to improve the performance of the Gipps, Fritzsche and Wiedemann models. After calibration, it is demonstrated, in Figure 5.7, that the RMSE of the Gipps and Fritzsche models decreases compared to the results before calibration as illustrated in Figure 5.5. For the Wiedemann model, however, the RMSE decreases only at low speeds (0-20 *mph*: speed bin smaller than 4) while increases at most speed levels. The improvement of the Gipps and Fritzsche models partly results from the enhancement of acceleration behavior, as shown in Figure 5.8 which presents better model fits to the field observations (except for the Wiedemann model) compared to Figure 5.4 (before calibration).

Notwithstanding that the Gipps and Fritzsche models have been improved after calibration, the prediction error resulted from the models is yet at significantly higher levels relative to

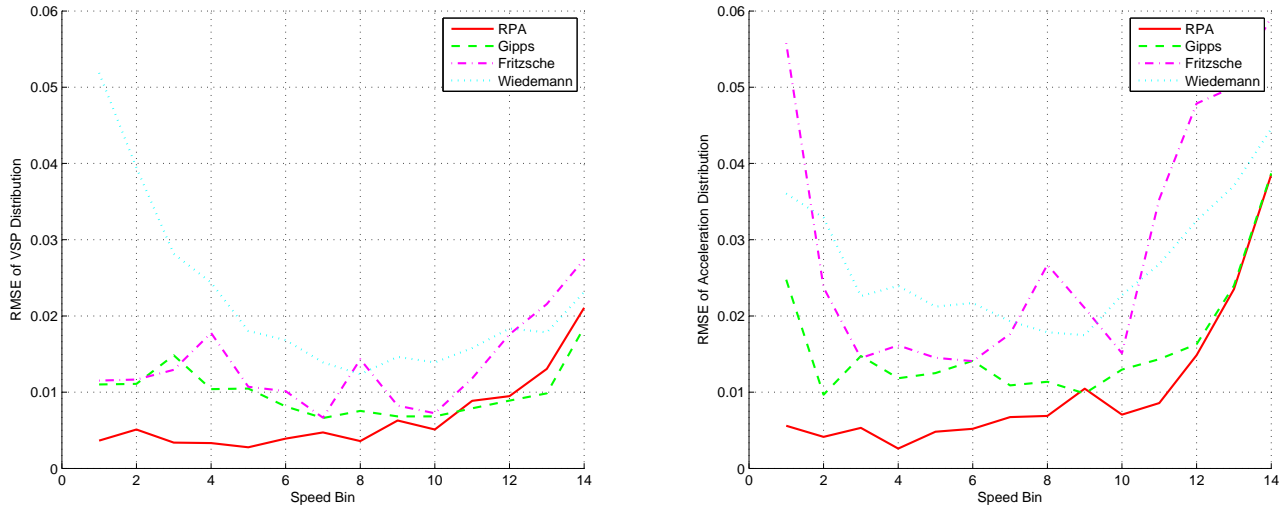


Figure 5.7: Root mean square error (after model calibration)

the RPA model. Furthermore, although they present a good model fit in terms of acceleration behavior, the high prediction error empirically demonstrates that the acceleration model is not the only factor that results in unrealistic vehicle trajectories and thus VSP behavior. In addition, the Wiedemann model produces the highest level of prediction error without significant improvement by calibration.

5.7 Conclusions

The RPA car-following model has been demonstrated to provide realistic acceleration behavior by incorporating a vehicle dynamics model; however, as of yet no research has been undertaken to assess its validity for FC/EM estimation. This chapter thoroughly investigates the ability of the RPA model to generate realistic vehicle trajectory for FC/EM analysis and compares its performance in this regard with the most widely-used car-following models: Gipps, Fritzsche and Wiedemann. VSP distributions are compared between real world and numerical simulations, and the consistency of VSP behavior is thoroughly analyzed. Finally, the FC/EM error is computed to quantify the implications of car-following models for FC/EM estimation.

The results demonstrate that the RPA model outperforms the Gipps, Fritzsche and Wiedemann car-following models in generating realistic VSP distributions, especially at low speed levels ($0 - 30\text{mph}$) where car-following is most common, and is the most robust model for FC/EM analysis. The study also suggests that the built-in acceleration model is one of the

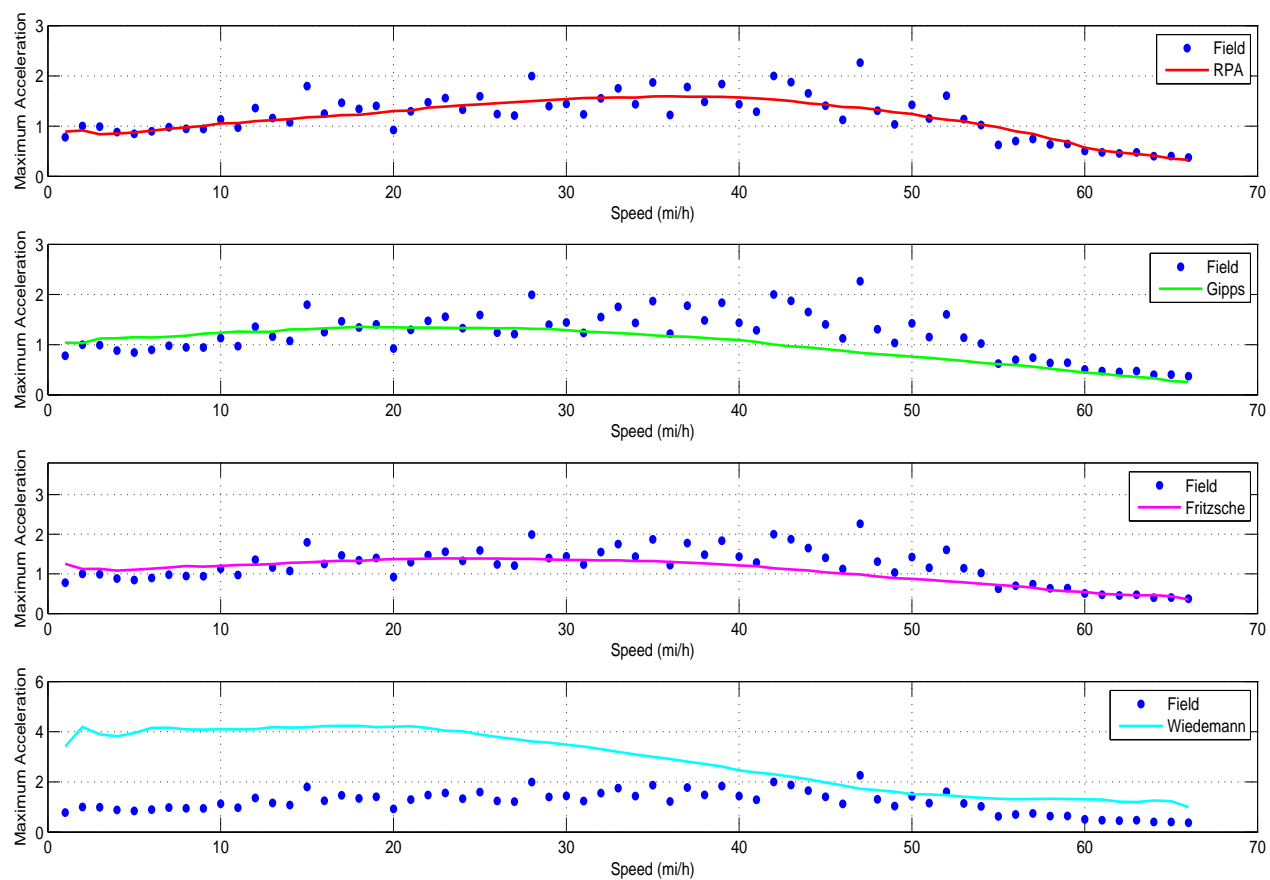


Figure 5.8: Maximum acceleration behavior (m/s^2)(after model calibration)

major factors in determining the adequacy of simulated VSP distributions. Furthermore, the study demonstrates that aggregated results may produce erroneous conclusions given that second-by-second errors may cancel each other out thus producing a low overall error. Lower VSP distribution errors occasionally may result in greater bias in FC/EM estimates given the large deviation of the distribution at high VSP levels. Finally, it is found that sophisticated calibration improves the performance of the Gipps and Fritzsche models while not significantly enhancing the Wiedemann model. However, the Gipps and Fritzsche models produce significantly higher prediction error as ever relative to the RPA model.

Given that the RPA model is used in the INTEGRATION software, the results of this study demonstrate the validity of the INTEGRATION software in generating realistic vehicle trajectories, and thus in FC/EM estimations. Due to the adequacy of the resulting VSP distribution as well as the accuracy and simplicity of the built-in energy consumption and emissions models, INTEGRATION is selected as the simulation testbed for the multimodal eco-routing system.

Chapter 6

Eco-routing Formulation and System Development for On-board Navigation Applications

This chapter is based on the papers:

1. Wang, J. and Rakha, H. An Eco-Routing Model for Multi-Modal Transportation Systems. (Working Paper).
2. Wang, J., Rakha, H., and Elbery, A. Dynamic Multi-modal Eco-routing System: Model Development and Testing. (Working Paper).

This chapter aims to develop an eco-routing system for in-vehicle navigation applications that is able to comprehensively incorporate microscopic elements and route vehicles in real time while at the same time differentiate eco-routes between vehicle models. The proposed system in this chapter, as mentioned before, is a submodule of the multi-modal eco-routing system, and only applies to the on-road vehicles which do not have fixed routes. A link cost function was first developed, followed by the eco-routing formulation. The system was then developed and tested in the INTEGRATION simulation testbed.

6.1 Link Cost Function

The majority of the existing eco-routing systems utilized the parameters such as average speed and fixed link-specific grade as the inputs of link cost function, and thus cannot produce accurate link cost factors given the inadequacy in considering microscopic elements.

Our approach to estimating link cost factors is built on the VT-CPFM and VT-CPEM models. The VT-CPFM model is used to estimate the fossil fuel consumption for conventional gasoline and diesel vehicles, and the VT-CPEM model is applied to estimate electric power for electric vehicles. These models are used because they provide robust energy estimates instantaneously and also can be easily implemented in the in-vehicle eco-routing systems given their simple model specifications. The VT-CPFM model is demonstrated in Equation (3.1). A variant of the model is generated for the formulation purpose, as illustrated in Equation (6.1). The VSP in the model refers to the vehicle specific power as defined in Equation (5.28). Likewise, the VT-CPEM model is also formulated based on VSP, as demonstrated in Equation (6.2). It should be noted that during deceleration the VSP is negative and a portion of electric power can be recovered given the regenerative braking. The regenerative efficiency η_{re} is defined in Equation (2.1).

$$FC(t) = \begin{cases} \alpha_0 + \alpha_1 \frac{mVSP(t)}{1000} + \alpha_2 \left(\frac{mVSP(t)}{1000} \right)^2, & \forall VSP(t) \geq 0 \\ \alpha_0, & \forall VSP(t) < 0 \end{cases} \quad (6.1)$$

$$EC(t) = \begin{cases} \frac{mVSP(t)}{1000}, & \forall VSP(t) \geq 0 \\ \frac{mVSP(t)}{1000} \times \eta_{re}(t), & \forall VSP(t) < 0 \end{cases} \quad (6.2)$$

Equations (6.1) and (6.2) estimate energy consumption at an instantaneous level. The link-level energy cost is thus calculated by accumulating the instantaneous model estimates, as illustrated in Equations (6.3) and (6.4) respectively:

$$FC_{link} = TT \times \alpha_0 + \alpha_1 \frac{m}{1000} \sum_t VSP^{(+)}(t) + \alpha_2 \left(\frac{m}{1000} \right)^2 \sum_t VSP^{2(+)}(t) \quad (6.3)$$

$$EC_{link} = \frac{m}{1000} \left(\sum_t VSP^{(+)}(t) + \sum_t (VSP^{(-)}(t) \times \eta_{re}(t)) \right) \quad (6.4)$$

where FC_{link} and EC_{link} are link-based conventional fuel (l) and electric energy (Wh) consumption respectively, TT is the link travel time (s), $VSP^{(+)}$ and $VSP^{(-)}$ are positive and negative power respectively, and $VSP^{2(+)}$ is the power square for the positive power condition. Four link-based parameters are generated by the equations: TT , $\sum_t VSP^{(+)}(t)$, $\sum_t VSP^{2(+)}(t)$, and $\sum_t (VSP^{(-)}(t) \times \eta_{re}(t))$. The VSP-based link parameters successfully include microscopic characteristics, given that the VSP generated by the engine is a function of the forces acting on a vehicle which include aerodynamic, rolling, grade and acceleration forces so that is able to adequately capture traffic conditions, road attributes, vehicle specifications and the interactions between them.

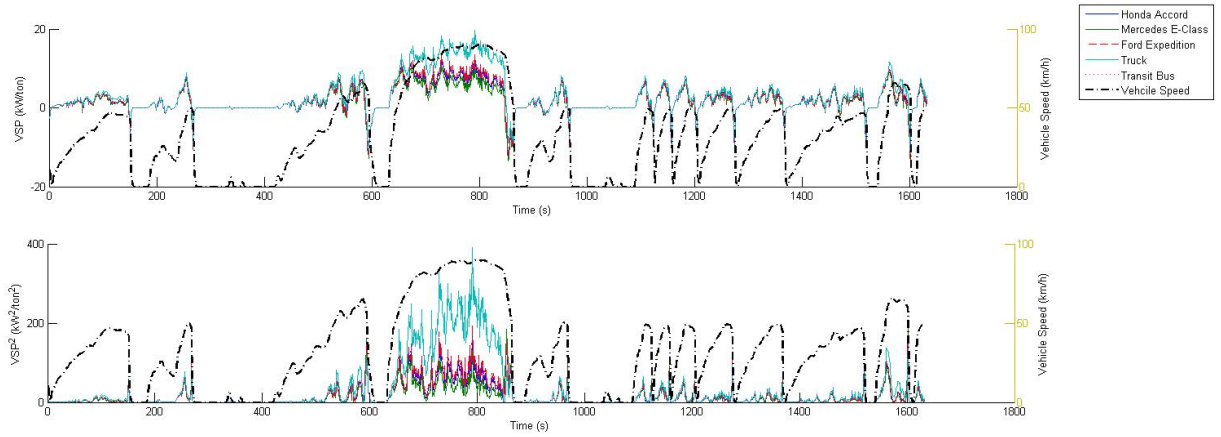


Figure 6.1: Comparison of vehicle power between vehicle models

Nonetheless, the eco-routing based on the three VSP-based parameters cannot differentiate vehicle power between different vehicle models, which may also result in estimation bias in link energy cost. This is because power behavior, similar to energy consumption, also differs between vehicle models. Namely, under the same traffic and road conditions, different vehicle models may require different levels of power to overcome resistance forces and move forward. Specifically, the result in Figure 6.1, resulted from test running different vehicle models on the identical driving cycle, demonstrates that the truck produces significantly higher power level than the other tested vehicles, especially at high speeds. That is because higher aerodynamic force is generated for the truck which requires more power exerted to overcome. The tested Mercedes passenger car produces the lowest level of power given its small drag coefficient. Intuitively, to avoid estimation bias, the three VSP-based parameters, similar to energy consumption, should be estimated and updated relative to vehicle models for each link. However, this would result in that the vehicle model-specific link parameters are updated only when a vehicle within this model departs from the link, implying that eco-routing relative to a specific vehicle model is only affected by the operation conditions of the vehicles within this model but irrelevant to other vehicles. This results in that link cost and eco-route updating is not based on real time information. In summary, the vehicle model-specific parameters (e.g. energy consumption and the three VSP-based parameters) are not suitable for being link cost factors in the dynamic eco-routing system.

In adequately achieving real time applications, it is critically important to identify the link parameters that are irrelevant to vehicle specifications and can be dynamically updated without leading to energy estimation bias. Noticeably, VSP consists of four components: 1. the power to overcome rolling resistance ($g \cdot \cos(\theta) \cdot \frac{C_r}{1000}(c_1 v(t) + c_2) \times \frac{v(t)}{\eta_d}$); 2. the power to overcome grade resistance ($g \cdot \sin(\theta) \times \frac{v(t)}{\eta_d}$); 3. the power exerted to accelerate the vehicle ($\frac{a(t)v(t)}{\eta_d}$); and 4. the power to overcome aerodynamic resistance ($0.5\rho_{air} \frac{A_f C_D}{m} v^2(t) \times \frac{v(t)}{\eta_d}$).

It is interesting to see that the summation of the first three components, denoted as VSP_{rga} , of the VSP function is irrelevant to vehicle specifications. Specifically, gravitational acceleration (g) is a constant relative to a specific geographical location. Road grade (θ) depends on the terrain of the road network. The rolling coefficients (C_r , c_1 and c_2) are determined by pavement type and vehicle tyre which could be assumed to be a constant for the majority of vehicle fleet. Speed (v) and acceleration (a) are related to traffic conditions, and driveline efficiency (η_d) is also assumed to be a constant (0.9 is suggested by the literature [12, 88, 198]) for most of vehicle models. For the fourth component, $\frac{A_f C_D}{m}$ is the term relevant to vehicle specifications. ρ_{air} is the air density only affected by the air pressure of the test location (1.2256 kg/m^3 is suggested for the sea level air density in this study). For simplicity, Equation (5.28) is re-formulated as demonstrated by Equation (6.5) which separates VSP into two components: 1. the first component VSP_{rga} is irrelevant to vehicle model; and 2. the second part $0.5 \frac{\rho_{air}}{\eta_d} \frac{A_f C_D}{m} \cdot v^3(t)$ is related to vehicle model.

$$VSP(t) = VSP_{rga}(t) + 0.5 \frac{\rho_{air}}{\eta_d} \frac{A_f C_D}{m} \cdot v^3(t) \quad (6.5)$$

Substituting Equation (6.5) into Equations (6.3) and (6.4), the three VSP-based link parameters are re-formulated as demonstrated in Equations (6.6)-(6.8) with (+) and (-) the positive and negative power conditions respectively. It is worth noting that seven link aggregated parameters irrelevant to vehicle models are identified in Equations (6.6)-(6.8): $\sum_t v^3(t)^{+}$, $\sum_t v^6(t)^{+}$, $\sum_t VSP_{rga}^{(+)}(t)$, $\sum_t VSP_{rga}^{2(+)}(t)$, $\sum_t (VSP_{rga}^{(+)}(t) \cdot v^3(t)^{+})$, $\sum_t (VSP_{rga}^{(-)}(t) \cdot \eta_{re}(t))$, $\sum_t (v^3(t)^{-} \cdot \eta_{re}(t))$. These parameters as well as link travel time (TT), namely, a total of eight parameters, can be dynamically updated without triggering the bias in eco-route calculation, and thus are suitable for dynamic eco-routing that differentiates vehicle models.

$$\sum_t VSP^{(+)}(t) = \sum_t VSP_{rga}^{(+)}(t) + 0.5 \frac{\rho_{air}}{\eta_d} \frac{A_f C_D}{m} \cdot \sum_t v^3(t)^{+} \quad (6.6)$$

$$\begin{aligned} \sum_t VSP^{2(+)}(t) &= \sum_t \left(VSP_{rga}^{(+)}(t) + 0.5 \frac{\rho_{air}}{\eta_d} \frac{A_f C_D}{m} \cdot v^3(t)^{+} \right)^2 \\ &= \sum_t \left[VSP_{rga}^{2(+)}(t) + \left(0.5 \frac{\rho_{air}}{\eta_d} \frac{A_f C_D}{m} \right)^2 \cdot v^6(t)^{+} \right. \\ &\quad \left. + \frac{\rho_{air}}{\eta_d} \frac{A_f C_D}{m} \cdot VSP_{rga}^{(+)}(t) \cdot v^3(t)^{+} \right] \\ &= \sum_t VSP_{rga}^{2(+)}(t) + \left(0.5 \frac{\rho_{air}}{\eta_d} \frac{A_f C_D}{m} \right)^2 \cdot \sum_t v^6(t)^{+} \\ &\quad + \frac{\rho_{air}}{\eta_d} \frac{A_f C_D}{m} \cdot \sum_t \left(VSP_{rga}^{(+)}(t) \cdot v^3(t)^{+} \right) \end{aligned} \quad (6.7)$$

$$\begin{aligned}
\sum_t (VSP^{(-)}(t) \times \eta_{re}(t)) &= \sum_t \left[\left(VSP_{rga}^{(-)}(t) + 0.5 \frac{\rho_{air}}{\eta_d} \frac{A_f C_D}{m} \cdot v^3(t)^{(-)} \right) \cdot \eta_{re}(t) \right] \\
&= \sum_t \left(VSP_{rga}^{(-)}(t) \cdot \eta_{re}(t) \right) + 0.5 \frac{\rho_{air}}{\eta_d} \frac{A_f C_D}{m} \cdot \sum_t \left(v^3(t)^{(-)} \cdot \eta_{re}(t) \right)
\end{aligned} \tag{6.8}$$

The up-to-date eight parameters are taken as the input of energy consumption models to estimate vehicle model-specific link energy costs and eco-routes. The resulting link cost functions are demonstrated in Equations (6.9) and (6.10). In the functions, $(\cdot)_p$ represents the parameters relative to vehicle model p , and $(\cdot)_l$ refers to the parameters specific to link l ; $FC_{l,p}$ and $EC_{l,p}$ are the aggregated conventional fuel and electric energy costs for vehicle model p on link l . Consequently, the use of the eight parameters enables link energy costs and eco-routes to be updated based on most recent information and simultaneously provides realistic eco-routing suggestions that are able to differentiate vehicle models.

$$\begin{aligned}
FC_{l,p} &= TT_l \times \alpha_{0,p} + \alpha_{1,p} \frac{m_p}{1000} \left[\left(\sum_t VSP_{rga}^{(+)}(t) \right)_l + 0.5 \frac{\rho_{air}}{\eta_d} \frac{A_{f,p} C_{D,p}}{m_p} \cdot \left(\sum_t v^3(t)^{(+)} \right)_l \right] \\
&\quad + \alpha_{2,p} \left(\frac{m_p}{1000} \right)^2 \left[\left(\sum_t VSP_{rga}^{2(+)}(t) \right)_l + \left(0.5 \frac{\rho_{air}}{\eta_d} \frac{A_{f,p} C_{D,p}}{m_p} \right)^2 \cdot \left(\sum_t v^6(t)^{(+)} \right)_l \right] \\
&\quad + \frac{\rho_{air}}{\eta_d} \frac{A_{f,p} C_{D,p}}{m_p} \cdot \left(\sum_t (VSP_{rga}^{(+)}(t) \cdot v^3(t)^{(+)}) \right)_l
\end{aligned} \tag{6.9}$$

$$\begin{aligned}
EC_{l,p} &= \frac{m_p}{1000} \left[\left(\sum_t VSP_{rga}^{(+)}(t) \right)_l + 0.5 \frac{\rho_{air}}{\eta_d} \frac{A_{f,p} C_{D,p}}{m_p} \cdot \left(\sum_t v^3(t)^{(+)} \right)_l \right] \\
&\quad + \frac{m_p}{1000} \left[\left(\sum_t (VSP_{rga}^{(-)}(t) \cdot \eta_{re}(t)) \right)_l + 0.5 \frac{\rho_{air}}{\eta_d} \frac{A_{f,p} C_{D,p}}{m_p} \cdot \left(\sum_t (v^3(t)^{(-)} \cdot \eta_{re}(t)) \right)_l \right]
\end{aligned} \tag{6.10}$$

6.2 Eco-routing Model

With the developed link cost functions, the eco-routing model is formulated in this section in support of the proposed dynamic eco-routing system. Consider a network $G(\mathcal{N}, \mathcal{L})$ that

consists of a set of nodes \mathcal{N} and a set of links \mathcal{L} , assuming that there are \mathcal{P} vehicle models in the network. The objective of the proposed eco-routing problem is to find a route between an origin (O) and a destination (D) that minimizes the trip energy cost for each specific vehicle model, as demonstrated in Equation (6.11).

$$\text{Min } Z = \sum_{l \in \mathcal{L}} \left(FC_{l,p} x_p + EC_{l,p} (1 - x_p) \right) y_l \quad (6.11a)$$

$$\text{subject to } \eta_{re}(t) = \begin{cases} \frac{1}{e^{\frac{0.0411}{|a(t)|}}}, & \forall a(t) < 0 \\ 0, & \forall a(t) \geq 0 \end{cases} \quad (6.11b)$$

$$|a(t)| \leq 6 \quad (6.11c)$$

$$x_p \in (0, 1), \forall p \in \mathcal{P} \quad (6.11d)$$

$$y_l \in (0, 1), \forall l \in \mathcal{L} \quad (6.11e)$$

In this formulation, the vehicle model-specific link costs $FC_{l,p}$ and $EC_{l,p}$ are calculated using Equations (6.9) and (6.10). Constraint (6.11b) demonstrates that energy regeneration only occurs during deceleration. Constraint (6.11c) limits acceleration level to 6 m/s^2 to ensure realistic acceleration behavior. x_p is used to specify whether a vehicle is an electric vehicle or a conventional vehicle (0 for electric vehicle; otherwise conventional vehicle). y_l is the dummy variable that depicts routing decisions.

Upon the proposed eco-routing model, the optimum routes can be generated relative to each vehicle model. Therefore, the vehicles within different categories may be assigned to different routes. Also, the model enables electric vehicle eco-routing which has not been investigated in traditional eco-routing systems. In addition, give that the minimum path is calculated based on the most recent information (eight parameters updated by every vehicle's departure from a link), the model is suitable for real time navigation system.

6.3 Numerical Experiment

6.3.1 Sample Network

In this section, a numerical experiment is designed to test the proposed eco-routing model. A sample network with 4 nodes and 5 links was constructed as illustrated in Figure 6.2. Each node refers to a location where vehicles depart or arrive. Each of the links represents a roadway street and all of the streets in the network are one-way streets. It is also assumed that there is only one O-D pair in the network. Node 1 is the origin and node 4 is the destination, and all vehicles travel from node 1 to node 4. No traffic control was considered in order to simplify traffic conditions in the network.

Table 6.1 presents network characteristics. Specifically, all of the links are one-lane roads

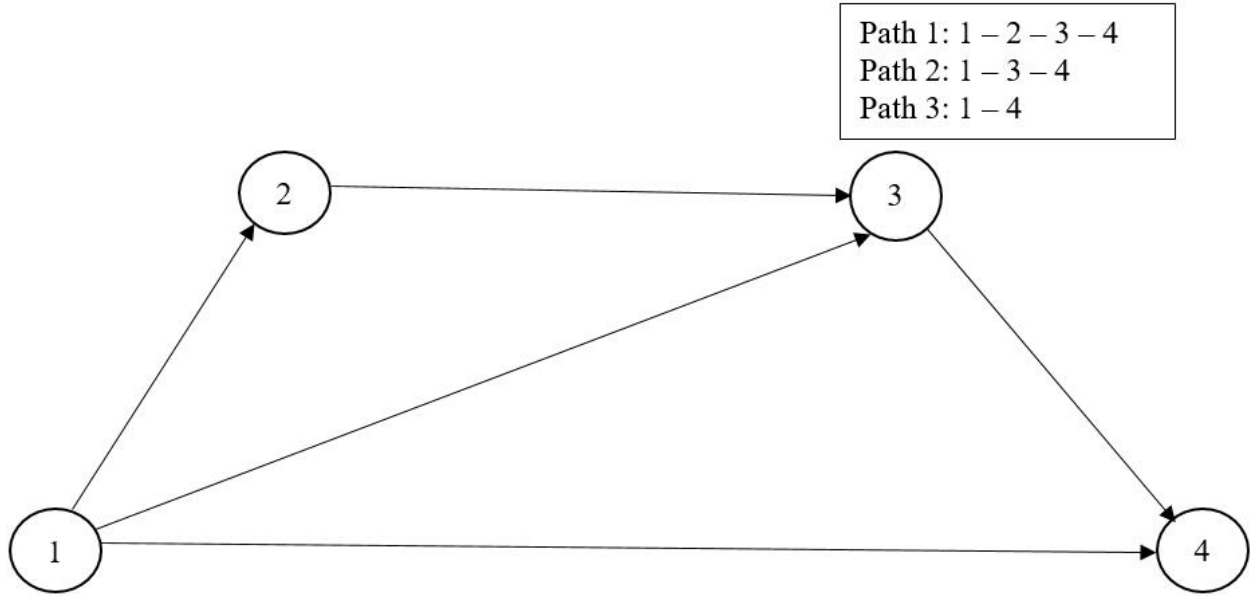


Figure 6.2: A sample network

Table 6.1: Network characteristics

Link ID	Starting Node	Ending Node	Number of Lanes	Link Length (<i>km</i>)	Speed Limit (<i>km/h</i>)
1	1	2	1	2	45
2	1	3	1	4	70
3	1	4	1	6	100
4	2	3	1	2	45
5	3	4	2	2	45

except for link 5 which has two lanes. Given that there are two links converging at node 3, two lanes were designed for link 5 in order to eliminate bottleneck. Three of the links (link 1, 4, 5) have an identical length of 2 *km*, and link 2 has a length of 4 *km* and link 3 is 6 *km* long. The configuration of the link length ensures an identical distance of 6 *km* for each path. The network contains three paths. Path 1 (1-2-3-4), consisting of link 1, link 4 and link 5, has a speed limit of 45 *km/h*, which is typically considered as a local street route. Path 2 (1-3-4), however, conceives an arterial link with a speed limit of 70 *km/h* followed by a local street link (link 5). Path 3 (1-4), with a speed limit of 100 *km/h*, is a freeway route. In short, the network conceives three route alternatives: local street, arterial and freeway.

Table 6.2: Tested vehicle specifications

Vehicle Model	Mass (<i>kg</i>)	Nominal power (kW)	C_D	A_f	C_r	c_1	c_2
Honda Accord	1469	138	0.325	2.3	1.75	0.0328	4.575
Mercedes C300	1550	180	0.24	2.2	1.75	0.0328	4.575
Ford Expedition	2626	272	0.41	3.88	1.75	0.0328	4.575
Truck (International/ 9800 SBA)	7239	261	0.78	8.9	1.75	0.0328	4.575
Transit Bus (19XX)	12864	336	0.78	8.8	1.75	0.0328	4.575
Tesla S	2108	310	0.24	2.67	1.75	0.0328	4.575
BMW i3	1477	80	0.28	2.33	1.75	0.0328	4.575
Nissan Leaf	1297	125	0.29	2.38	1.75	0.0328	4.575

6.3.2 Test Scenario

In order to achieve link traffic data, a simulation run was conducted to the sample network using INTEGRATION. 8 vehicle models were loaded to the network, covering a wide range of energy consumption behavior. The specifications of the tested vehicles are provided in Table 6.2. Honda Accord and Mercedes C300 are the representatives of sedan passenger car, and Ford Expedition is the full size sport utility vehicle (SUV). One of the modeled trucks in section 3.3, International/ 9800 SBA, was tested to represent typical truck fuel consumption behavior. A bus within the series 19XX was selected as the representative of transit bus. It should be noted that the bus was tested here only for the purpose of demonstrating the ability of the proposed eco-routing model in differentiating eco-routes between vehicle models, but not used in the dynamic eco-routing system given that buses cannot be re-routed in real time. Tesla S, BMW i3 and Nissan Leaf are three of the most widely used electric vehicles.

A total demand of 6400 *veh/h* traveling from node 1 to node 4 was loaded onto the simulation network for the first 1200 *s*. Each vehicle model has an equal demand of 800 *veh/h*. After the simulation run, the eight link parameters experienced by each vehicle exiting a link were calculated based on the simulated trajectory data. Upon each of the five links, there were multiple sets of eight parameters (each vehicle generates a set of eight parameters) which were sorted according to the departure time of each vehicle. The sorted parameters of each link were then smoothed respectively through an exponential smoothing procedure, and the last set of the parameters of each link were exactly the most recent information at the end of simulation run. Assuming that eco-routes were updated at the moment of simulation end, the real time eight parameters were used as the input of energy consumption models to generate the vehicle model-specific link energy costs and eco-routes.

Upon the simulated trajectory data, link energy costs and eco-routes were also calculated using the traditional eco-routing method (Rakha’s eco-routing [24]) in order to compare the performance of the traditional and proposed eco-routing. The traditional eco-routing model basically utilizes energy consumption (instead of eight parameters) as the real time information which is also updated by every vehicle’s departure from a link. The model assumes that all vehicle types have the same link energy cost and eco-route.

Furthermore, a discussion on the traditional eco-routing model was proposed based on the assumption that link energy cost relative to a specific vehicle model was only affected by the vehicles within this category. Namely, the vehicle model-specific link costs and eco-routes are updated only when a vehicle within the same type departs from the link and irrelevant to the vehicles of other categories. This assumption, as discussed in section 6.1, may result in that eco-routing relative to a specific vehicle model is only affected by the operation conditions of the vehicles within this type but irrelevant to the vehicles within other categories. Consequently, the resulting eco-routes may not be based on real time information, given the probably ever-changing traffic conditions during the time gap in which the two vehicles within the same type successively depart from a link. The link costs and eco-routes resulted from this method were also compared with those from the proposed model.

In addition, the results derived from the four parameters-based approach ($TT, \sum_t VSP^{(+)}(t), \sum_t VSP^{2(+)}(t)$ and $\sum_t (VSP^{(-)}(t) \times \eta_{re}(t))$), were investigated as well to identify the bias in eco-routing calculation resulted from not considering the effect of vehicle specifications on vehicle power.

6.3.3 Results Analysis

The resulting link energy costs and eco-routes were compared between different vehicle models and eco-routing methods, as demonstrated in Tables 6.3-6.5. Method 1 in the tables refers to the proposed eco-routing method, Method 2 is the traditional eco-routing method, Method 3 represents the approach assuming that the eco-routing relative to a specific vehicle model is only affected by the vehicles within the same category, and Method 4 is the four parameters-based approach.

Table 6.3 demonstrates that, for Methods 1, 3 and 4, link energy costs differ between different vehicle models with the same method. For example, for the conventional fuel-powered vehicles, the truck and bus produce significantly higher fuel consumption levels than the LDVs: Honda Accord, Mercedes C300 and Ford Expedition; and for the electric vehicles, Tesla in general requires more power consumption than BMW i3 and Nissan Leaf. Also, the electric power is in the unit of Wh resulting in significantly different numerical values relative to conventional fuel in l . Therefore, Method 2 in this study generated energy costs for conventional and electric vehicles respectively rather than mixing them up, resulting in that conventional vehicles are routed separately from electric vehicles. However, all vehicle models in either the cluster of conventional vehicles or the cluster of electric vehicles yet have the same link cost and cannot be differentiated for eco-routing. For a specific vehicle model, Methods 2, 3 and 4 produce different link costs relative to the proposed method, demonstrating that failing to use real time information or to capture the effect of vehicle model on either energy consumption or vehicle power results in the estimation error in link cost factors.

Table 6.3: Link energy cost

Link ID	Vehicle Model	Link Energy Cost (Conventional fuel in l , electric power in Wh)			
		Method 1	Method 2	Method 3	Method 4
Link 1	Honda Accord	0.129	0.312	0.125	0.13
	Mercedes C300	0.119	0.312	0.115	0.122
	Ford Expedition	0.153	0.312	0.147	0.153
	Truck (International/ 9800 SBA)	0.52	0.312	0.516	0.49
	Transit Bus (19XX)	0.663	0.312	0.659	0.671
	Tesla S	154.547	117.649	162.881	177.198
	BMW i3	116.043	117.649	116.465	124.156
	Nissan Leaf	106.375	117.649	109.281	109.025
Link 2	Honda Accord	0.183	0.475	0.177	0.182
	Mercedes C300	0.182	0.475	0.179	0.189
	Ford Expedition	0.252	0.475	0.252	0.241
	Truck (International/ 9800 SBA)	1.066	0.475	1.091	0.873
	Transit Bus (19XX)	1.379	0.475	1.4	1.329
	Tesla S	407.844	366.064	422.723	471.068
	BMW i3	323.31	366.064	343.146	330.061
	Nissan Leaf	305.562	366.064	331.348	289.837
Link 3	Honda Accord	0.242	1.162	0.244	0.246
	Mercedes C300	0.26	1.162	0.261	0.299
	Ford Expedition	0.437	1.162	0.454	0.414
	Truck (International/ 9800 SBA)	2.062	1.162	2.089	1.539
	Transit Bus (19XX)	2.608	1.162	2.742	2.589
	Tesla S	848.627	769.088	854.441	1109.99
	BMW i3	708.914	769.088	732.037	777.731
	Nissan Leaf	688.441	769.088	706.085	682.95
Link 4	Honda Accord	0.107	0.439	0.001	0.11
	Mercedes C300	0.102	0.439	0.001	0.112
	Ford Expedition	0.134	0.439	0.135	0.143
	Truck (International/ 9800 SBA)	0.506	0.439	0.515	0.503
	Transit Bus (19XX)	0.653	0.439	0.004	0.751
	Tesla S	174.147	171.696	171.696	253.851
	BMW i3	134.198	171.696	2.998	177.864
	Nissan Leaf	124.867	171.696	2.789	156.188
Link 5	Honda Accord	0.082	0.354	0.082	0.085
	Mercedes C300	0.086	0.354	0.087	0.1
	Ford Expedition	0.135	0.354	0.127	0.136
	Truck (International/ 9800 SBA)	0.626	0.354	0.612	0.51
	Transit Bus (19XX)	0.799	0.354	0.764	0.844
	Tesla S	254.889	196.126	229.275	352.266
	BMW i3	209.863	196.126	198.048	246.82
	Nissan Leaf	202.321	196.126	186.678	216.741

Table 6.4: Path energy cost

Vehicle Model	Path ID	Method 1	Method 2	Method 3	Method 4
Honda Accord ¹	1	0.3179	1.1052	0.2076	0.3253
	2	0.2651	0.8284	0.2589	0.2672
	3	0.2421	1.1624	0.2439	0.2458
Mercedes C300 ¹	1	0.3075	1.1052	0.2025	0.3348
	2	0.2686	0.8284	0.266	0.2899
	3	0.2599	1.1624	0.2611	0.2989
Ford Expedition ¹	1	0.4219	1.1052	0.4084	0.4314
	2	0.3874	0.8284	0.3791	0.3772
	3	0.4369	1.1624	0.4544	0.4138
Truck (International/ 9800 SBA) ¹	1	1.6518	1.1052	1.643	1.5023
	2	1.6922	0.8284	1.7031	1.3825
	3	2.0621	1.1624	2.0888	1.5394
Transit Bus (19XX) ¹	1	2.1152	1.1052	1.4276	2.2658
	2	2.178	0.8284	2.164	2.1726
	3	2.6083	1.1624	2.742	2.5891
Tesla S ²	1	583.5833	485.4716	563.8517	783.3154
	2	662.7326	562.1901	651.9976	823.3346
	3	848.6269	769.0876	854.4408	1109.9905
BMW i3 ²	1	460.1037	485.4716	317.511	548.841
	2	533.173	562.1901	541.1933	576.8811
	3	708.9137	769.0876	732.0366	777.7305
Nissan Leaf ²	1	433.5625	485.4716	298.747	481.9545
	2	507.8838	562.1901	518.0252	506.5773
	3	688.4415	769.0876	706.0848	682.9495

¹Conventional fuel: l . ²Electric energy: Wh .

The link cost error leads to the differences in path costs between the proposed method and the other three methods, as demonstrated in Table 6.4. Likewise, for Methods 1, 3 and 4, path costs differ between vehicle models, while Method 2 cannot differentiate vehicle model-specific path costs.

The eco-routes were calculated based on the path costs, as illustrated in Table 6.5. In general, either different vehicle models or eco-routing methods may result in different eco-routes. Specifically, according to the results of the proposed method, Honda Accord and Mercedes C300 (sedan passenger car) are suggested to choose path 3 (freeway route: 1 - 4) to minimize their fuel consumption levels; while Ford Expedition (SUV) is provided with path 2 (arterial route: 1 - 3 - 4) as the optimum route, and the truck and bus (HDVs) as well as Tesla S, BMW i3 and Nissan Leaf (electric vehicles) are routed to path 1 (local street: 1 - 2 - 3 - 4). The routing results are reasonable, given that Honda Accord and Mercedes C300 have an optimum fuel economy cruise speed of around 80 km/h which is higher than those of Ford Expedition (58 km/h), HDVs ($30\text{-}50 \text{ km/h}$) and electric vehicles ($15\text{-}25 \text{ km/h}$, [199]). Therefore, the

Table 6.5: Comparison of eco-routes

Vehicle Model	Method 1		Method 2		Method 3		Method 4	
	Minimum Path	Minimum cost	Minimum Path	Minimum cost	Minimum Path	Minimum cost	Minimum Path	Minimum cost
Honda Accord ¹	1-4	0.2421	1-3-4	0.8284	1-2-3-4	0.2076	0.2458	1-4
Mercedes C300 ¹	1-4	0.2599	1-3-4	0.8284	1-2-3-4	0.2025	0.2899	1-3-4
Ford Expedition ¹	1-3-4	0.3874	1-3-4	0.8284	1-3-4	0.3791	0.3772	1-3-4
Truck (International/ 9800 SBA) ¹	1-2-3-4	1.6518	1-3-4	0.8284	1-2-3-4	1.643	1.3825	1-3-4
Transit Bus (19XX) ¹	1-2-3-4	2.1152	1-3-4	0.8284	1-2-3-4	1.4276	2.1726	1-3-4
Tesla S ²	1-2-3-4	583.5833	1-2-3-4	485.4716	1-2-3-4	563.8517	783.3154	1-2-3-4
BMW i3 ²	1-2-3-4	460.1037	1-2-3-4	485.4716	1-2-3-4	317.511	548.841	1-2-3-4
Nissan Leaf ²	1-2-3-4	433.5625	1-2-3-4	485.4716	1-2-3-4	298.747	481.9545	1-2-3-4

¹Conventional fuel: *l.* ²Electric energy: *Wh.*

tested passenger cars are assigned to the freeway route which generates a prevailing speed closer to their optimum cruise speeds; while the arterial route, consisting of two links with the speed limits of 70 *km/h* and 45 *km/h* respectively, provides the prevailing speed closer to the optimum speed of Ford Expedition. HDVs and electric vehicles, however, are routed to local streets given their significantly lower optimum cruise speeds. It should be noted that, to simplify traffic operations, no traffic control occurred in the sample network, so that the prevailing speed of each route dominantly determines the resulting energy consumption. In reality, however, traffic operations are more complex, and the route with the prevailing speed closer to the optimum cruise speed may not always be the environmentally best. For example, the freeway route may become the best for Ford Expedition if there are many traffic signals on the arterial route with frequent stop-and-go activities.

For the specific vehicle model, the other three methods, however, produce different routing results relative to the proposed method. Specifically, method 2 assigns all conventional vehicles to the arterial route (1 - 3 - 4) given the inability of differentiating eco-routes between vehicle models. Also, method 3 assigns Honda Accord and Mercedes C300 to the local street given that the resulting eco-routes are not based on real time information. Method 4 also provides inconsistent results by routing Mercedes C300, the truck and bus to the arterial route, given that the method is unable to capture the effect of vehicle specifications on vehicle power.

6.4 Dynamic Eco-routing System

With the resulting eco-routing model, this section is primarily to develop the proposed dynamic eco-routing system for in-vehicle navigation applications. The INTEGRATION framework for routing logic is first introduced. The architecture of the proposed system is then developed, followed by the testing work.

6.4.1 INTEGRATION Framework for Traffic Assignment

INTEGRATION is basically an agent-based microscopic traffic assignment and simulation software. Within the software, the selection of the next link to be taken by a vehicle is determined by the model's internal routing logic [200, 201]. Before the study of this dissertation, there were 10 built-in routing methods in INTEGRATION as illustrated below:

1. Time-Dependent Method of Successive Averages (MSA)
2. Time-Dependent Sub-Population Feedback Assignment (SFA)
3. Time-Dependent Agent Feedback Assignment (AFA)
4. Time-Dependent Dynamic Traffic Assignment (DTA)
5. Time-Dependent Frank-Wolf Algorithm (FWA)
6. Time-Dependent External Routing 1 – File 8 (ER1)
7. Time-Dependent External Routing 2 – File 9 (ER2)
8. Distance Based Routing
9. ECO-Subpopulation Feedback Assignment (ECO-SFA)
10. ECO-Agent Feedback Assignment (ECO-AFA)

Some of these methods are static and deterministic (e.g. MSA, FWA, Distance Based Routing), and some of them are dynamic and stochastic (e.g. SFA, AFA, ECO-SFA, ECO-AFA). Regardless of the particular method that is used to route vehicles, the selection of the next link that a vehicle should take is done using a vehicle-specific array that lists for the vehicle the entire sequence of links from its origin to its destination. Upon the completion of any link, a vehicle simply queries this array to determine which link it should utilize next to reach its ultimate destination in the most efficient manner. When traveling across this next link is in turn completed, the selection process is then repeated until a link whose downstream node is the vehicle's ultimate trip destination is reached [24].

Among these routing options, ECO-SFA and ECO-AFA are the eco-routing algorithms that dynamically estimate and update eco-routes based on the feedback information reported by the vehicles departing from each link. Specifically, ECO-SFA is a subpopulation-based routing logic which equally divides all routing vehicles into five sub-populations. The minimum paths for each of the five subpopulations are updated by every user-specified time interval, which demonstrates that path updates may often be several seconds or minutes old and thus not based on the most recent information. Alternatively, ECO-AFA assigns vehicles individually. Link costs and eco-routes are updated by every vehicle's departure

from a link, rather than by average time interval. This agent-based routing logic enables the resulting eco-routes to be generated based on the most recent information. Consequently, the proposed eco-routing system is built at the agent-based level.

6.4.2 System Architecture

The routing logic of the proposed system is similar to ECO-AFA. However, ECO-AFA cannot differentiate vehicle models given that the system utilizes energy consumption as the real time information being updated by every vehicle's departure from a link regardless of vehicle models. This demonstrates that all vehicle models share the same link-specific energy costs to calculate eco-routes, resulting in that all vehicles have the same eco-route. This is not realistic in reality. The proposed system, alternatively, was developed using the eco-routing model as proposed in section 6.2 which is able to estimate and update the eight link parameters to achieve real time information as the input of energy consumption model and thus to generate vehicle model-specific link costs and eco-routes. Also, the eight parameters, as mentioned, comprehensively incorporate microscopic characteristics into the link cost function.

The general architecture of the proposed system is presented in Figure 6.3. The system was developed in the INTEGRATION simulation framework which requires the input of road characteristics, signal information, OD demands and vehicle specifications for the simulation run. The eco-routing logic starts from an initialization procedure in which routes are selected based on the energy consumption estimated using facility's free flow speed. The use of free flow speed is attributed to the fact that the network is initially empty without experienced traffic information reported. Upon the initial vehicle routing, the traffic is assigned to the network. Once the route is selected, INTEGRATION updates the vehicle longitudinal and lateral motions every deci-second using the built-in RPA car-following model and lane changing model respectively. The RPA car-following model has been demonstrated in chapter 5 to generate realistic vehicle trajectories that result in accurate VSP distributions and energy estimates. The lane changing logic was described and validated against field data in an earlier publication [202], demonstrating an adequate capture of vehicle lateral motions. The vehicle locations and speeds are recorded on an instantaneous basis while at the same time input to the power module to estimate the instantaneous eight parameters. Once a vehicle departs from the origin or from a link, the instantaneous eight parameters of that vehicle are accumulated to achieve link-level statistics: $\sum_t VSP_{rga}^{(+)}(t)$, $\sum_t v^3(t)^{+}$, $\sum_t VSP_{rga}^{2(+)}(t)$, $\sum_t v^6(t)^{+}$, $\sum_t (VSP_{rga}^{(+)}(t) \cdot v^3(t)^{+})$, $\sum_t (VSP_{rga}^{(-)}(t) \cdot \eta_{re}(t))$, $\sum_t (v^3(t)^{-} \cdot \eta_{re}(t))$. These aggregated parameters are then updated respectively to serve as the real time information through an exponential smoothing procedure using Equation (6.12), where $[\cdot]'_{n,l}$ is the smoothed link parameters when vehicle n is departing from link l , $[\cdot]'_{n-1,l}$ is the smoothed link parameters when vehicle $n - 1$ is departing from link l , and $[\cdot]_{n,l}$ is the observed link parameters for vehicle n going through link l . It should be noted that the eight parameters as well as the optimum routes are only updated upon a vehicle's departure from the origin or from a link; otherwise, route selection is based on the original routing solutions.

$$\left[\sum_t VSP_{rga}^{(+)}(t) \right]'_{n,l} = (1 - \alpha) \left[\sum_t VSP_{rga}^{(+)}(t) \right]'_{n-1,l} + \alpha \left[\sum_t VSP_{rga}^{(+)}(t) \right]_{n,l} \quad (6.12a)$$

$$\left[\sum_t v^3(t)^{(+)} \right]'_{n,l} = (1 - \alpha) \left[\sum_t v^3(t)^{(+)} \right]'_{n-1,l} + \alpha \left[\sum_t v^3(t)^{(+)} \right]_{n,l} \quad (6.12b)$$

$$\left[\sum_t VSP_{rga}^{2(+)}(t) \right]'_{n,l} = (1 - \alpha) \left[\sum_t VSP_{rga}^{2(+)}(t) \right]'_{n-1,l} + \alpha \left[\sum_t VSP_{rga}^{2(+)}(t) \right]_{n,l} \quad (6.12c)$$

$$\left[\sum_t VSP_{rga}^{2(+)}(t) \right]'_{n,l} = (1 - \alpha) \left[\sum_t VSP_{rga}^{2(+)}(t) \right]'_{n-1,l} + \alpha \left[\sum_t VSP_{rga}^{2(+)}(t) \right]_{n,l} \quad (6.12d)$$

$$\begin{aligned} \left[\sum_t (VSP_{rga}^{(-)}(t) \cdot \eta_{re}(t)) \right]'_{n,l} &= (1 - \alpha) \left[\sum_t (VSP_{rga}^{(-)}(t) \cdot \eta_{re}(t)) \right]'_{n-1,l} \\ &+ \alpha \left[\sum_t (VSP_{rga}^{(-)}(t) \cdot \eta_{re}(t)) \right]_{n,l} \end{aligned} \quad (6.12e)$$

$$\begin{aligned} \left[\sum_t (VSP_{rga}^{(-)}(t) \cdot \eta_{re}(t)) \right]'_{n,l} &= (1 - \alpha) \left[\sum_t (VSP_{rga}^{(-)}(t) \cdot \eta_{re}(t)) \right]'_{n-1,l} \\ &+ \alpha \left[\sum_t (VSP_{rga}^{(-)}(t) \cdot \eta_{re}(t)) \right]_{n,l} \end{aligned} \quad (6.12f)$$

$$\begin{aligned} \left[\sum_t (v^3(t)^{(-)} \cdot \eta_{re}(t)) \right]'_{n,l} &= (1 - \alpha) \left[\sum_t (v^3(t)^{(-)} \cdot \eta_{re}(t)) \right]'_{n-1,l} \\ &+ \alpha \left[\sum_t (v^3(t)^{(-)} \cdot \eta_{re}(t)) \right]_{n,l} \end{aligned} \quad (6.12g)$$

$$TT'_{n,l} = (1 - \alpha)TT'_{n-1,l} + \alpha TT_{n,l} \quad (6.12h)$$

The up-to-date eight parameters are introduced to the built-in energy consumption model (VT-CPFM and VT-CPEM) to estimate vehicle model-specific link energy costs using Equations (6.9)-(6.10). The outputs from the energy module are then used to compute eco-routes relative to each vehicle model in the module of the shortest path algorithm. Routes are selected based on the resulting eco-routing suggestions, assuming that all drivers would always choose the best routes. Therefore, the proposed system is essentially a deterministic routing method.

The routing results change traffic conditions in the network, and the new traffic conditions may in turn affect the eco-routing solutions of the next iteration, and so forth. Accordingly, the system is essentially a loop which is able to generate routing suggestions in real time adaptable to the evolution of traffic conditions.

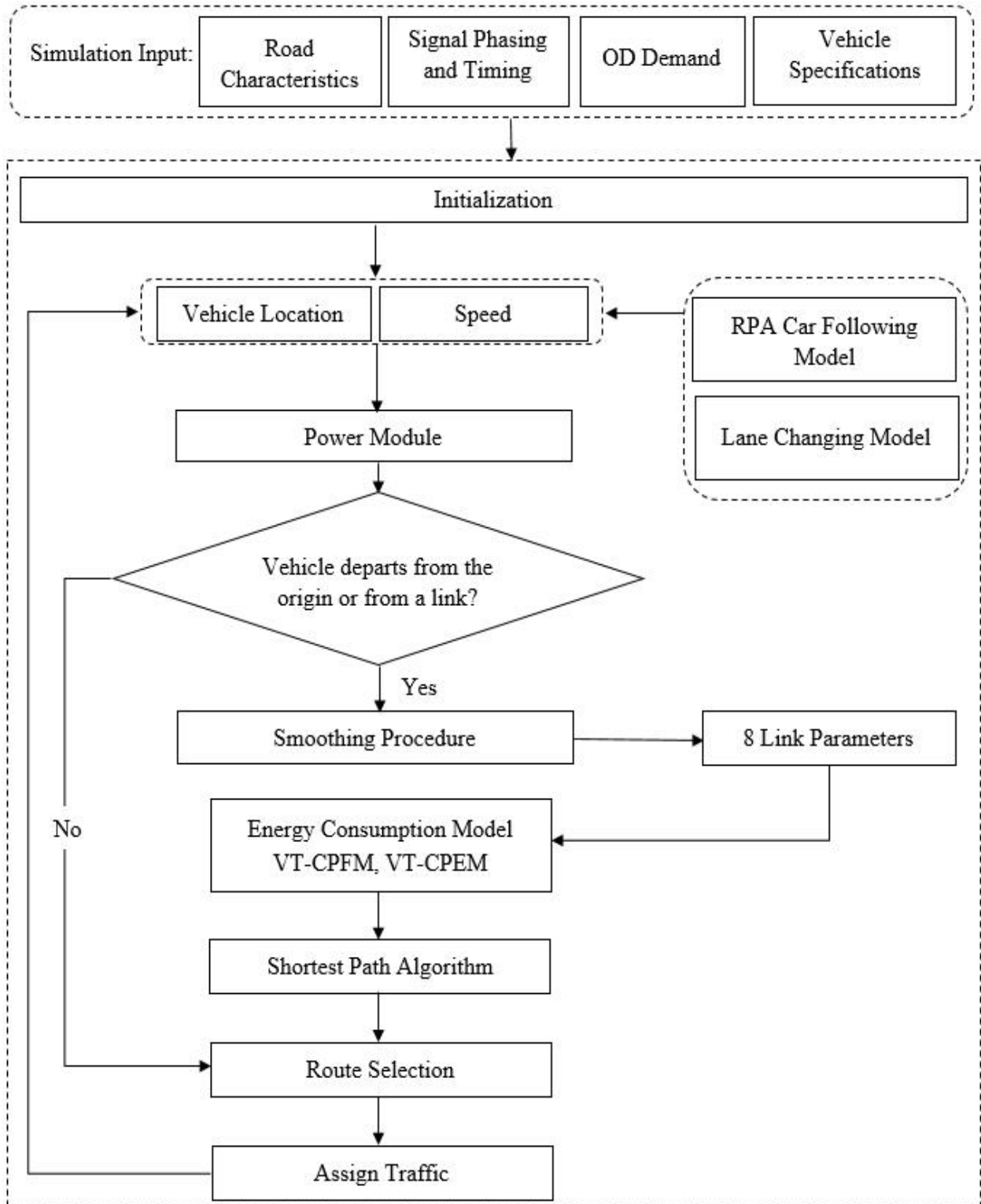


Figure 6.3: INTEGRATION framework for the dynamic eco-routing system

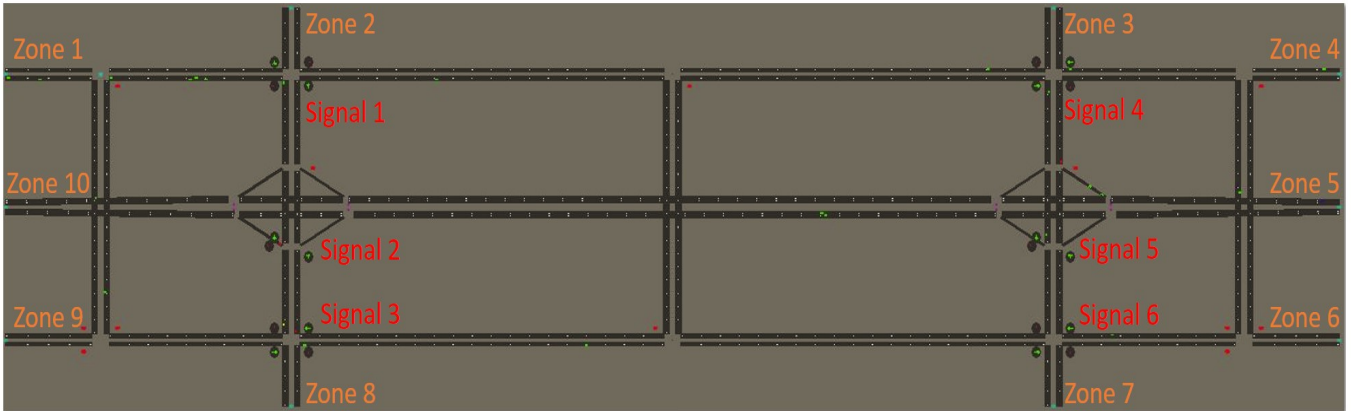


Figure 6.4: QNET sample network configuration

6.4.3 System Testing

The proposed system was tested in a sample network and a real world network respectively which were built in INTEGRATION. Four vehicle models were selected as the representatives of typical vehicle fleet: Honda Accord (gasoline sedan car), Ford Expedition (gasoline SUV), International/ 9800 SBA (diesel truck), and Tesla S (electric LDVs). It should be noted that transit bus is not selected in this chapter given that buses operate on fixed routes and cannot be dynamically re-routed based on real time traffic conditions. The performance of the system in terms of energy consumption, travel time and distance traveled was compared to Rakha’s traditional eco-routing system (ECO-AFA) and travel time (TT) routing logic (AFA) both of which are built-in agent-based routing methods in INTEGRATION as mentioned before. In addition, the resulting measures of effectiveness (MOEs) from the three routing systems as a function of congestion level have been investigated as well.

6.4.3.1 System Testing in Sample Network

The testing effort was first conducted in a sample network which was entitled “QNET”. QNET consists of 10 zones, 32 nodes, 68 links, and 196 O-D pairs. The network includes traffic control infrastructures such as traffic signals and stop signs and thus covers the impact of traffic control on vehicle operations. As illustrated in Figure 6.4, the two central horizontal roads are freeways with a free flow speed of 110 km/h and other roads are arterial roads with the free flow speed of 60 km/h . The freeways have 3 lanes in each direction connected by one-lane on-ramps and off-ramps, and each of the arterial roads has 2 lanes per direction.

An original demand of 2513 veh/h was loaded onto the network for the first 1800 s, and the simulation was continued until all of the loaded vehicles cleared the network. This

resulted in a total of 1257 vehicles being simulated. Noticeably, the demand for each O-D pair was equally shared by the four tested vehicle models in order to exclude the impact of disproportionate vehicle lineup on testing results. The simulation was run with ten random seeds for each of the three routing methods to eliminate the perturbation of simulation stochasticity. The MOEs relative to each routing system were calculated by dividing the total network statistics by total number of vehicles, and then averaged over the ten random seeds, as demonstrated in Table 6.6 that summarizes the network-wide average statistics including travel distance (km), travel time (s), conventional petroleum fuel consumption (l), and electric energy consumption (Wh). The negative relative differences (Relative Diff.) in the table demonstrate the savings from the proposed eco-routing in either energy consumption or travel time or distance.

According to the mean values in Table 6.6, the proposed eco-routing system on average produces the conventional fuel of 0.453 l and an electric energy of 88.907 Wh . This results in the energy savings of 4.5% (conventional fuel) and 10.32% (electric power) respectively compared to the ECO-AFA system, and 4.22% (conventional fuel) and 22.09% (electric power) respectively compared to the TT-AFA system. Furthermore, the lower and upper 95% confidence intervals (CIs) between the proposed eco-routing and the other two routing systems do not overlap, demonstrating that the proposed eco-routing significantly improves energy efficiency. In addition, the TT-AFA routing results in lower travel time and fewer distances traveled yet more energy consumption, implying that the minimum travel time or shortest distance route may instead produce higher energy consumption levels. This result is consistent with [6].

The proposed eco-routing was also tested at multiple demand levels in order to quantify the impact of congestion level on the system performance. Specifically, nine demand levels were tested varying from 5% to 200% of the original demand. At each demand level, the simulation was run with ten random seeds for each of the three routing methods (a total of 30 simulation runs were completed for each demand level). The MOEs were then averaged over the random seeds. The average statistics were compared between the proposed eco-routing and the other two routing methods.

The results are presented in Table 6.7 in which the negative relative differences also demonstrate an either energy saving or travel time or distance saving by the proposed system. Basically, the proposed eco-routing produces lowest levels of energy consumption for both conventional and electric vehicles at all demand levels, demonstrating that the system in general outperforms the traditional eco-routing and travel time routing systems in terms of energy saving. In particular, with the increasing demand level, the conventional fuel savings on average vary from 3.33% to 9.57% relative to the Eco-AFA system and from 6.92% to 0.76% relative to the TT-AFA system. The decreasing fuel savings relative to the TT-AFA routing are mainly attributed to the fact that fewer route alternatives are available for conventional vehicles when the network is getting congested. In addition, relative to the Eco-AFA routing, although more fuel savings are observed with the increasing demands for the proposed system, it is not secure to draw the conclusion that the proposed eco-routing

Table 6.6: Network-wide impacts of the proposed eco-routing system (sample network: QNET)

MOEs	Proposed Eco-routing (Pro-Eco)			Traditional ECO-AFA (Tra-Eco)			Travel Time AFA (TT-AFA)			Relative Diff.	
	Mean	Lower 95% CI	Upper 95% CI	Mean	Lower 95% CI	Upper 95% CI	Mean	Lower 95% CI	Upper 95% CI	(Pro-Eco vs. Tra-Eco: %)	(Pro-Eco vs. TT-AFA: %)
Distance (<i>km</i>)	3.298	3.292	3.304	3.488	3.454	3.523	3.177	3.166	3.187	-5.46	3.82
Travel time (<i>s</i>)	221.077	220.006	222.149	248.981	242.971	254.991	179.541	178.824	180.258	-11.21	23.13
fuel (<i>l</i>)	0.453	0.450	0.456	0.474	0.471	0.477	0.473	0.470	0.476	-4.50	-4.22
energy (<i>Wh</i>)	88.907	87.700	90.113	99.142	95.688	102.597	114.109	113.398	114.820	-10.32	-22.09

achieves more fuel savings in a congested network. This is because the higher fuel consumption levels for the Eco-AFA routing are resulted from the fact that the traditional eco-routing system cannot differentiate link costs between vehicle models and thus may generate incorrect link costs and eco-routes which may route vehicles to the sub-optimal paths. Such estimate error is not monotonously related to the demand level.

For the electric power, the increasing demand level does not demonstrate monotonous increase or decrease in energy saving. Specifically, the savings relative to the Eco-AFA system in general increase at first and then decrease with the increasing demand level. Alternatively, the savings relative to the TT-AFA system do not significantly change with the variation of demand level. This is, on the one hand, attributed to the fact that, in an uncongested network, electric vehicles in most cases would choose local roads to minimize their energy consumption levels given the significantly low optimum energy economy cruise speed (15-25 *km/h*, [199]), while choose the routes with high prevailing speeds such as freeway to minimize travel time. This may result in significant differences in prevailing speeds and thus energy consumption between the two routing methods. On the other hand, in a congested network, electric vehicles enable more energy regenerated given frequent deceleration events. Accordingly, electric vehicles may achieve significant energy savings at both low and high demand levels. This implies that the electric vehicle eco-routing that only considers minimizing energy consumption may assign vehicles to congested networks, which makes traffic conditions even worse. Some constraints on other factors such as travel time are thus needed in the future study.

Despite the energy savings, the proposed system requires significantly more trip travel time compared to the travel time routing (20% to 30% more travel time as illustrated in Table 6.7). Consequently, energy saving may be at the cost of travel time in some networks.

6.4.3.2 System Testing in Real World Network

The proposed system is also tested in a real world network. Figure 6.5 shows the testing area located in the downtown of Doha city in Qatar which was originally built in INTEGRATION to evaluate transportation operational strategies. The Doha network consists of 48 zones, 174 nodes, 302 links, and 54144 OD pairs. The network can reflect real-world traffic conditions in large metropolitan areas and also includes a large amount of traffic control infrastructures. There are three road types in the network, including the freeway with a free flow speed of 105 *km/h* and the arterial roads with the free flow speeds of 80 and 65 *km/h* respectively. The two central horizontal roads are freeways and other roads are arterial roads. The testing area has relatively flat terrain and thus the grade was assumed to be zero in this study.

For the base test scenario, the realistic one-hour traffic demand was loaded onto the network, and the simulation was continued until all vehicles cleared the network. Again, the demand for each O-D pair was equally shared by the four tested vehicle models. The simulation was run with ten random seeds for each of the three routing methods, and the resulting MOEs

Table 6.7: Impacts of congestion levels (sample network: QNET)

MOEs	Routing Methods	Demand Levels									
		5%	25%	50%	75%	100%	125%	150%	175%	200%	
Fuel (<i>l</i>)	Pro-Eco	0.472	0.443	0.449	0.452	0.453	0.458	0.464	0.472	0.48	
	Tra-Eco	0.488	0.46	0.465	0.471	0.474	0.485	0.5	0.517	0.53	
	TT-AFA	0.507	0.475	0.474	0.473	0.473	0.473	0.476	0.478	0.483	
	Relative Diff.	-3.33	-3.66	-3.56	-4.1	-4.5	-5.46	-7.05	-8.78	-9.57	
	(Pro-Eco Vs. Tra-Eco) (%)	-6.92	-6.73	-5.26	-4.52	-4.22	-3.16	-2.51	-1.31	-0.76	
	Relative Diff.										
Electric Energy (<i>Wh</i>)	(Pro-Eco Vs. TT-AFA) (%)										
	Pro-Eco	91.653	93.698	92.972	91.503	88.907	88.38	86.06	83.395	80.837	
	Tra-Eco	92.838	100.595	99.796	99.746	99.142	101.561	96.872	88.979	88.136	
	TT-AFA	120.641	117.369	114.72	115.502	114.109	112.692	111.431	111.286	110.081	
	Relative Diff.	-1.28	-6.86	-6.84	-8.26	-10.32	-12.98	-11.16	-6.28	-8.28	
	(Pro-Eco Vs. Tra-Eco) (%)	-23.05	-20.17	-18.96	-20.78	-22.09	-21.57	-22.77	-25.06	-26.57	
Travel Time (<i>s</i>)	Relative Diff.										
	(Pro-Eco Vs. TT-AFA) (%)										
	Pro-Eco	217.826	211.751	215.353	218.257	221.077	224.566	230.301	236.548	245.27	
	Tra-Eco	214.014	224.872	228.762	240.489	248.981	260.205	286.571	319.344	352.9	
	TT-AFA	174.792	175.808	177.186	177.629	179.541	180.385	182.988	185.112	188.952	
	Relative Diff.	1.78	-5.83	-5.86	-9.24	-11.21	-13.7	-19.64	-25.93	-30.5	
Distance (<i>km</i>)	(Pro-Eco Vs. Tra-Eco) (%)										
	Relative Diff.										
	(Pro-Eco Vs. TT-AFA) (%)										
	Pro-Eco	24.62	20.44	21.54	22.87	23.13	24.49	25.86	27.79	29.81	
	Tra-Eco	3.407	3.302	3.306	3.308	3.298	3.286	3.277	3.258	3.245	
	TT-AFA	3.275	3.206	3.190	3.178	3.177	3.162	3.163	3.162	3.169	
Distance (<i>km</i>)	Relative Diff.	3.408	3.444	3.446	3.487	3.488	3.513	3.509	3.491	3.490	
	(Pro-Eco Vs. Tra-Eco) (%)	-0.02	-4.12	-4.07	-5.13	-5.46	-6.47	-6.61	-6.69	-7.04	
	Relative Diff.										
	(Pro-Eco Vs. TT-AFA) (%)										
	Pro-Eco	4.05	2.98	3.63	4.08	3.82	3.90	3.63	3.03	2.38	
	Relative Diff.										
(Pro-Eco Vs. TT-AFA) (%)											

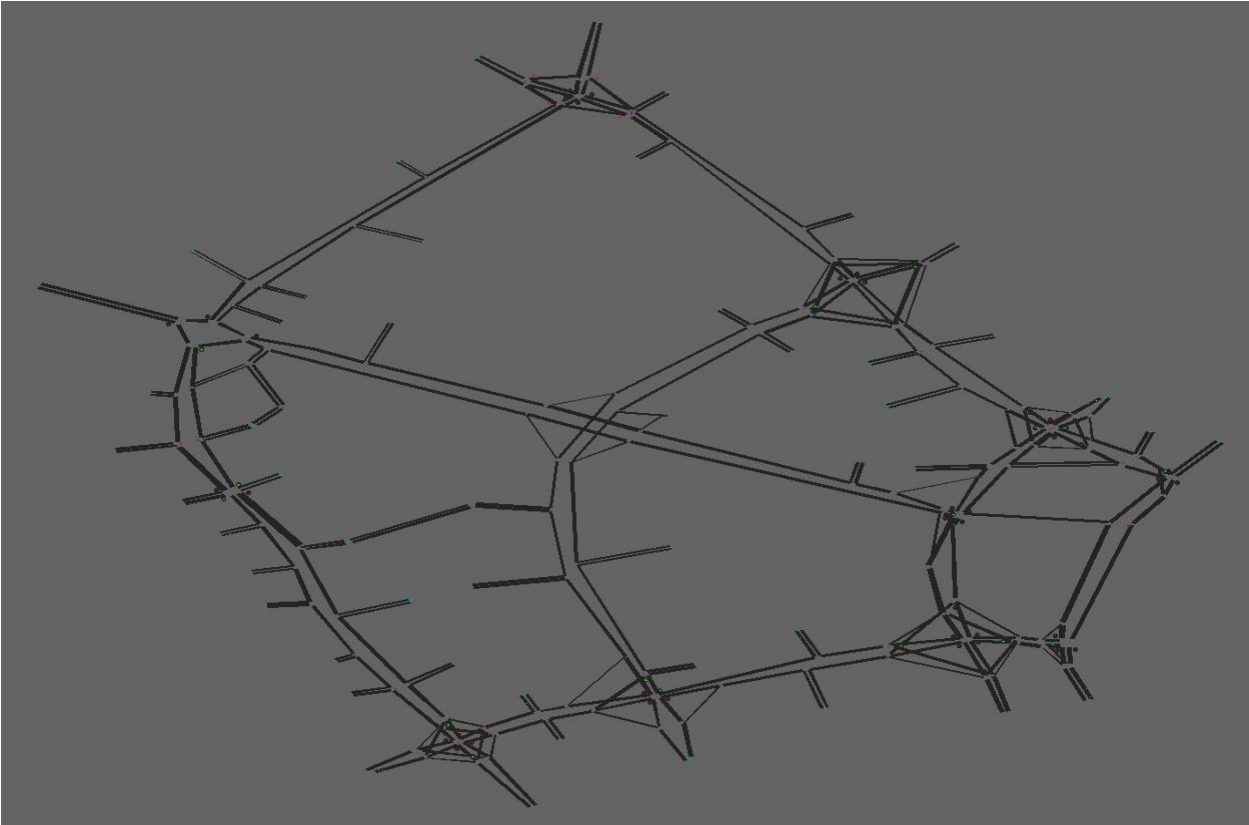


Figure 6.5: Doha network configuration

were generated by averaging the statistics over the random seeds.

Table 6.8 presents the simulation results. The proposed eco-routing on average produces the conventional fuel consumption of 0.49 *l* and electric power of 67.822 *Wh*, resulting in the energy savings of 2.04% (conventional fuel) and 7.57% (electric energy) respectively relative to the ECO-AFA system, and 6.12% (conventional fuel) and 12.53% (electric energy) respectively relative to the TT-AFA system. Furthermore, similar to the QNET sample network, the non-overlapped CIs demonstrate a significant improvement by the proposed system in terms of energy efficiency. It is worth noting that, compared to the TT-AFA routing, the proposed eco-routing also results in shorter distance and the travel time without significant difference (0.04%). This result is different from that generated in the QNET network in which the proposed eco-routing results in longer distance and higher travel time. This implies that, in some of the networks, the shortest distance or the minimum travel time could be achieved on the most energy-efficient routes; while this might not be the case in other networks. Consequently, network configuration significantly affects the eco-routing benefits.

The testing effort was also conducted at multiple demand levels. Again, nine congestion levels were tested varying from 5% to 200% of the realistic demand. At each demand level, the simulation was run with ten different random seeds for each of the routing systems. The MOEs were then averaged over the random seeds and compared between routing methods. The results are illustrated in Table 6.9.

Similar to the results in the sample network, the proposed eco-routing achieves energy savings for both conventional and electric vehicles at all demand levels. In particular, the conventional fuel savings on average vary from 1.68% to 10.2% relative to the Eco-AFA system and from 0.83% to 7.69% relative to the TT-AFA system; the electric energy savings vary from 1.02% to 9.09% relative to the Eco-AFA system and from 2.44% to 15.44% relative to the TT-AFA system. With the increasing congestion level, the conventional fuel savings relative to the travel time routing in general decrease although slight fluctuation is observed at some of the demand levels; while for electric vehicles, the energy savings in general increase given that more deceleration events occur to regenerate energy in a congested network. Noticeably, with the increasing demands, the conventional fuel savings relative to the Eco-AFA system do not demonstrate a monotonous increase as is the case in the sample network. This confirms that the energy saving of the proposed system relative to the traditional eco-routing is not monotonously related to demand level.

It is worth noting that the electric energy savings relative to the TT-AFA system are significantly more in the QNET network (shown in Table 6.7) than in the Doha network (shown in Table 6.9). This is probably attributed to the difference in network configuration. Specifically, there are three road types in the Doha network with the difference in free flow speed (65 *km/h*, 80 *km/h*, and 105 *km/h*) less significant than that in the QNET network which conceives only two road types (60 *km/h* and 110 *km/h*). As demonstrated by a recent study [199], electric power was highly sensitive to cruise speed as illustrated in Figure 6.6. The

Table 6.8: Network-wide impacts of the proposed eco-routing system (Doha network)

MOEs	Proposed Eco-routing (Pro-Eco)			Traditional ECO-AFA (Tra-Eco)			Travel Time AFA (TT-AFA)			Relative Diff. (Pro-Eco vs. Tra-Eco: %)	Relative Diff. (Pro-Eco vs. TT-AFA: %)
	Mean	Lower 95% CI	Upper 95% CI	Mean	Lower 95% CI	Upper 95% CI	Mean	Lower 95% CI	Upper 95% CI		
Distance	2.455	2.452	2.459	2.540	2.528	2.552	2.625	2.614	2.636	-3.33	-6.47
Travel time	227.639	226.611	228.667	236.280	233.623	238.937	227.723	224.589	230.857	-3.66	-0.04
fuel	0.490	0.486	0.494	0.500	0.497	0.503	0.522	0.516	0.527	-2.04	-6.12
energy	67.822	66.909	68.735	73.379	72.124	74.634	77.537	76.298	78.775	-7.57	-12.53

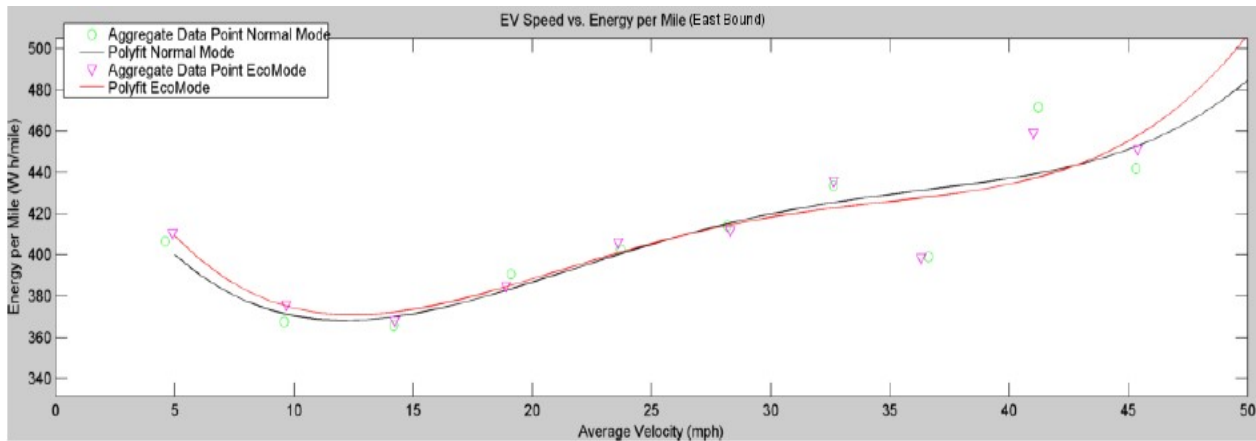


Figure 6.6: Electric energy consumption vs. cruise speed

vehicles cruising on freeways thus produce significantly higher energy consumption levels than those cruising on arterial roads with lower prevailing speeds. In the QNET network, the majority of vehicles traveled on freeways as suggested by the travel time routing while traveled on arterial routes during eco-routing, resulting in significant difference in energy consumption between the two routing methods. In the Doha network, however, the less significant difference in prevailing speeds results in lower energy savings.

For the conventional fuel savings, there is no significant difference between the two networks. This is because conventional fuel consumption is less sensitive to cruise speed compared to the electric power. Specifically, as demonstrated in Figures 3.9 and 3.15, fuel consumption produces a milder variation with the cruise speed at most of the speed levels, compared to the electric power as demonstrated in Figure 6.6.

However, network configuration also significantly affects conventional fuel savings of eco-routing systems. For example, a grid network, given more route alternatives, may generate more fuel savings compared to a freeway corridor network [126]. Also, the steep roads with high grade levels may be less attractive than the flat roads with level grade. In addition, as demonstrated in Table 6.9, the proposed eco-routing also results in shortest distances and minimum travel time, which is different from the QNET results illustrated in Table 6.7. Consequently, in some of the networks, the most energy-efficient routes may also achieve minimum travel time and distances traveled; while in some other networks, energy saving may be at the cost of longer distances or higher travel time.

Table 6.9: Impacts of congestion levels (Doha network)

MOEs	Routing Methods	Demand Levels									
		5%	25%	50%	75%	100%	125%	150%	175%	200%	
Fuel (<i>l</i>)	Pro-Eco	0.252	0.410	0.454	0.474	0.490	0.508	0.527	0.558	0.598	
	Tra-Eco	0.268	0.420	0.463	0.482	0.500	0.520	0.542	0.622	0.621	
	TT-AFA	0.266	0.445	0.488	0.502	0.522	0.539	0.558	0.580	0.603	
	Relative Diff.	-5.84	-2.23	-1.92	-1.68	-2.04	-2.30	-2.64	-10.20	-3.74	
	(Pro-Eco Vs. Tra-Eco) (%)										
	Relative Diff.	-5.28	-7.69	-7.02	-5.60	-6.12	-5.69	-5.43	-3.77	-0.83	
	(Pro-Eco Vs. TT-AFA) (%)										
	Pro-Eco	38.790	66.961	70.580	70.097	67.822	65.494	63.203	61.258	58.294	
	Tra-Eco	39.190	72.123	76.965	76.374	73.379	71.912	69.135	65.812	64.120	
	TT-AFA	40.172	74.925	79.286	79.641	77.537	74.250	72.734	70.951	68.941	
Relative Diff.	-1.02	-7.16	-8.30	-8.22	-7.57	-8.92	-8.58	-6.92	-9.09		
(Pro-Eco Vs. Tra-Eco) (%)											
Relative Diff.	-2.44	-10.63	-10.98	-11.98	-12.53	-11.79	-13.10	-13.66	-15.44		
(Pro-Eco Vs. TT-AFA) (%)											
Pro-Eco	126.580	189.919	206.711	218.189	227.639	240.925	259.587	303.469	392.192		
Tra-Eco	130.099	192.410	211.831	224.627	236.280	253.878	281.916	414.346	466.813		
TT-AFA	133.052	198.566	213.447	219.518	227.723	240.938	263.723	317.186	396.323		
Relative Diff.	-2.70	-1.29	-2.42	-2.87	-3.66	-5.10	-7.92	-26.76	-15.99		
(Pro-Eco Vs. Tra-Eco) (%)											
Relative Diff.	-4.86	-4.35	-3.16	-0.61	-0.04	-0.01	-1.57	-4.32	-1.04		
(Pro-Eco Vs. TT-AFA) (%)											
Pro-Eco	1.211	2.116	2.343	2.405	2.455	2.486	2.511	2.543	2.582		
Tra-Eco	1.240	2.162	2.412	2.482	2.540	2.585	2.612	2.638	2.675		
TT-AFA	1.252	2.284	2.511	2.566	2.625	2.645	2.673	2.711	2.747		
Relative Diff.	-2.32	-2.16	-2.85	-3.07	-3.33	-3.84	-3.86	-3.60	-3.48		
(Pro-Eco Vs. Tra-Eco) (%)											
Relative Diff.	-3.24	-7.38	-6.68	-6.25	-6.47	-6.02	-6.06	-6.17	-6.01		
(Pro-Eco Vs. TT-AFA) (%)											
Pro-Eco	126.580	189.919	206.711	218.189	227.639	240.925	259.587	303.469	392.192		
Tra-Eco	130.099	192.410	211.831	224.627	236.280	253.878	281.916	414.346	466.813		
TT-AFA	133.052	198.566	213.447	219.518	227.723	240.938	263.723	317.186	396.323		
Relative Diff.	-2.70	-1.29	-2.42	-2.87	-3.66	-5.10	-7.92	-26.76	-15.99		
(Pro-Eco Vs. Tra-Eco) (%)											
Relative Diff.	-4.86	-4.35	-3.16	-0.61	-0.04	-0.01	-1.57	-4.32	-1.04		
(Pro-Eco Vs. TT-AFA) (%)											
Pro-Eco	1.211	2.116	2.343	2.405	2.455	2.486	2.511	2.543	2.582		
Tra-Eco	1.240	2.162	2.412	2.482	2.540	2.585	2.612	2.638	2.675		
TT-AFA	1.252	2.284	2.511	2.566	2.625	2.645	2.673	2.711	2.747		
Relative Diff.	-2.32	-2.16	-2.85	-3.07	-3.33	-3.84	-3.86	-3.60	-3.48		
(Pro-Eco Vs. Tra-Eco) (%)											
Relative Diff.	-3.24	-7.38	-6.68	-6.25	-6.47	-6.02	-6.06	-6.17	-6.01		
(Pro-Eco Vs. TT-AFA) (%)											

6.5 Conclusions

This chapter first formulates the eco-routing problem which is able to comprehensively consider microscopic elements and calculate eco-routes based on most recent information while at the same time differentiate eco-routes between vehicle models. A numerical experiment is designed to test the benefit of the model. With the developed eco-routing model, the dynamic eco-routing system is then constructed, and tested in the INTEGRATION simulation testbed at different congestion levels. To test the eco-routing benefit, the MOEs of the proposed eco-routing are compared to those derived from the traditional eco-routing and travel time routing systems.

The results of the numerical experiment demonstrate that the proposed eco-routing model is able to generate reasonable routing suggestions based on real time information and also differentiate vehicle models. The eco-routing methods that fail to capture the effect of vehicle specifications on energy consumption and vehicle power may produce incorrect routing results. In addition, the method, assuming that the vehicle model-specific link energy costs and eco-routes are only affected by the vehicles within the same type, may also generate unrealistic routing suggestions given that the routing results are not based on real time information.

The testing results of the dynamic eco-routing system demonstrate that the proposed eco-routing achieves lower network-wide energy consumption levels compared to the traditional eco-routing and travel time routing at all congestion levels. It is also found that the conventional fuel savings relative to the travel time routing decrease with the increasing congestion level given fewer route alternatives in a congested network. For the electric power, however, the savings relative to travel time routing do not monotonously vary with congestion level given that significant energy savings could be achieved at both low and high demand levels. Furthermore, the energy savings relative to the traditional eco-routing are also not monotonously related to congestion level. In addition, the results also demonstrate that network configuration significantly affects the eco-routing benefit. For example, in some of the networks, energy savings may be achieved at the cost of more travel time or distances traveled; while in other networks, the most energy-efficient routes simultaneously minimize travel time and distances.

The proposed system in this chapter will be integrated into the higher-level multimodal eco-routing system in the future study in support of intermodal routing suggestions. Although the system is developed in the simulation environment, it is also applicable for real application where the network-wide vehicle-to-vehicle (V2V) communication is available. With the extensive development of connected vehicle techniques, the application of the proposed system in reality is anticipated to be realized in the near future.

Additionally, as mentioned before, the proposed system is a deterministic routing method with the assumption that all drivers would always choose the best routes. However, whether

would drivers completely conform to the routing suggestions in reality? How does the real time route information affect drivers' route choice behavior? The following chapter attempts to answer these questions.

Chapter 7

Effect of Dynamic Route Information on Driver Route Choice Behavior

This chapter is based on the papers:

1. Wang, J. and Rakha, H. Empirical Study of Effect of Dynamic Travel Time Information on Driver Route Choice Behavior. *Transportation Research Part F: Traffic Psychology and Behaviour*. (In Review).
2. Wang, J. and Rakha, H. Impact of Dynamic Route Information on Day-to-Day Driver Route Choice Behavior. Presented at *94th Transportation Research Board Annual Meeting*, Washington D.C. 2015.

The chapter aims to study how drivers response to the received real time route information and how the information affects their route choice behavior. The study is a follow-up experiment of Tawfik's study [148] in which participants were not provided with information. The results of the two studies are compared to provide significant implications to the behavioral effect of route information. The achievements of this chapter will be insightful for the enhancement to the design of routing systems.

7.1 Experimental Design

As aforementioned, Tawfik et al. identified four route choice patterns observed in a real world experiment. This chapter attempts to quantify the influence of route information on traveler route choice behavior by comparing the choice patterns between Tawfik et. al.'s experiment and the experiment conducted in this study. Occasionally, drivers prefer a route they frequently choose instead of switching to the actually faster route; or may deviate

from the habitual route to the alternative route which is on average worse, only because the performance of the usually-taken route becomes bad on a random day. These irrational behaviors may probably be caused by a lack of precise information. Travel time information was provided to participants in this study given that travel time is easily collected in real world. The study attempts to address a number of questions: will travel time information make drivers behave more rationally? Will the effect of information be different among individuals? What type of information will be most effective?

A total of 20 participants were recruited within two age groups (18-33 and 55-75)¹, 10 male and 10 female. Each of them was required to accomplish three sectors of the experiment: a pre-run questionnaire, on-road test and a post-run questionnaire. The pre-run questionnaire was conducted before the beginning of the on-road test, which gathered the participants' demographics, driving experiences, preferences, habits, information usage and the perception of route performance. Noticeably, each participant was demonstrated to have little knowledge of the route performance according to the results of pre-run questionnaire. The on-road test was conducted around the areas in Blacksburg and Christiansburg, VA for the morning, noon and evening peak from October 2013 to April 2014. The participants were asked to drive as if² they were commuting in order to ensure that travel time was an important consideration when they were to make choices. Each participant was asked to drive 10 trials, 5 of which provided participants with strict information (average travel time) and 5 provided with range information (travel time variability). It should be noted that the information was provided one time with average travel time and one time with travel time variability in order to eliminate the bias on each of the information type. The average travel time information provided to each trial was estimated by averaging the experienced travel time of three previous trials³, and travel time variability was estimated using the average value and standard deviation (*average travel time* $\pm 2 * \textit{standard deviation}$), so that the information could be dynamically updated each day to enhance the reliability of the information. For each trial, there were five O-D trips each of which had two alternative routes, one route was on average faster in travel time than the other. The characteristics of each route are specified in Table 7.1. The participants' task was to repeatedly make choices between the two alternatives on each trip. Statistically, 55 choice observations were collected for each participant, 100 observations by each trial and 220 on each trip. Upon the completion of 10 trials of the on-road test, the post-run questionnaire was thereafter conducted, whereby the participants were asked whether the provided information was beneficial. The accuracy of

¹These two age groups were selected because the authors wanted to investigate the impact of drivers' age on the information effectiveness in changing choice behavior. The big difference of drivers' age in the two age groups may more easily distinguish the difference of information effect resulted from drivers' age.

²When drivers were doing the test, they were asked to drive from one predefined origin to the destination during every trip, and they actually did not commute during the test. But the researchers wanted to emulate the trip as a commute trip on which travel time may probably be the first consideration by the drivers. So "as if" here means that drivers were asked to behave like commute.

³The experienced travel time was recorded by GPS during the testing; three previous trials were selected to be averaged because the trails before has little impact on the decision based on the literature [148]; information used for the first trail was obtained from the experiment in [148]

travel time perception would be compared between the two questionnaires in order to have a knowledge of whether the participants' perception was improved as a result of providing them with information.

The logical choice rate—the proportion of times in which the faster route is chosen as a function of time (trial number), participant and trip, respectively—was selected as the indicator of the positive role of information in facilitating rational behavior. The inertial choice rate—the proportion of participants remaining on their habitual but slower route—served to evaluate whether the information contributed to enhancing participant attitudes of risk seeking in the gain domain. The choice data collected by Tawfik was applied to estimate the choice rates specified as “without information” group. Tawfik's experiment was conducted on the same trips in Blacksburg and Christiansburg in 2012, which was also a day-to-day commuting test in which participants were asked to repeatedly make choice between the two alternative routes on each trip. The difference between the two experiments was that the proposed study provided participants with travel time information. For more details of Tawfik's study, see [148].

7.2 Results Analysis

By comparing the perceived travel time of the pre-run questionnaire to the actual travel time collected during the on-road tests, it was demonstrated that the accuracy of participants' perception of travel time ranged from 5% to 55% for all five trips, with an average accuracy of only 38%. Consequently, it would be safe to conclude that the participants had limited knowledge of the route performance prior to the start of the experiment. Based on the results of participants' perception in the post-run questionnaire, the average accuracy increased from 38% to 62% with an increase of 24%. Consequently, it would be interesting to see whether participants behave more rationally with higher perception accuracy.

Figure 7.1 presents the proportions of logical- and inertial- choices as a function of time, identified as trial number. As expected, the logical choice rates are on average around 10% higher in the “with-information” group than “without-information” group, especially for the first two trials in which the enhancement is up to 15%. This demonstrates that the positive effect of information becomes more evident when travelers have limited knowledge of route performance. Although there are some oscillations at some of the trails, in general, the logical rates between the two groups are getting closer from the beginning to the end. The inertial choice rates are basically lower with the provision of information, implying that it is more likely for travelers to risk switching to the faster route when they are informed. However, regardless of being informed or not being informed, the inertial behavior is not reduced in day-to-day variation, which is different from the results in the simulation study [135]. This may be attributed to the habit or other decision considerations.

In reality, the behavioral effect of information varies from person to person. One may

Table 7.1: Trip characteristics

Trip No.	Route No.	Average Travel Time	No. of Intersections		No. of Left Turns	Route Description
			Signalized	Unsignalized		
1	1	9.2	10	3	3	Mostly a high speed (65 mi/h) freeway
	2	9.3	5	4	4	High speed (45 mi/h) urban highway
2	3	15.8	5	2	3	Mostly a shorter, low speed (30 mi/h) back road with a lot of curves
	4	18.2	2	2	2	Mostly a longer, high speed (55 mi/h) rural highway
3	5	8.6	5	3	3	A longer high speed (65 mi/h) freeway followed by a low speed (25 mi/h) urban road
	6	9.4	8	3	2	A shorter urban route (40 and 35 mi/h)
4	7	10.4	5	3	4	A short urban route that passes through campus (25 and 35 mi/h)
	8	10.3	6	2	2	Primarily a long high speed (65 mi/h) freeway and low speed (25 mi/h) urban roads
5	9	10.5	8	4	4	A long urban road that passes through town (35 mi/h)
	10	8.5	3	1	3	A short low speed (25 and 35 mi/h) rural road that passes by a small airport, and more direct

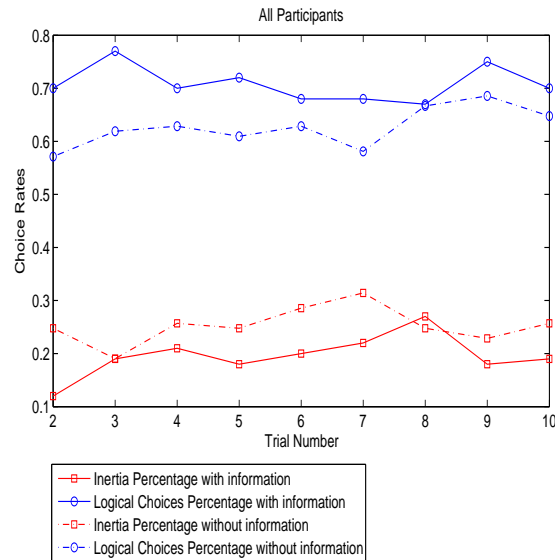
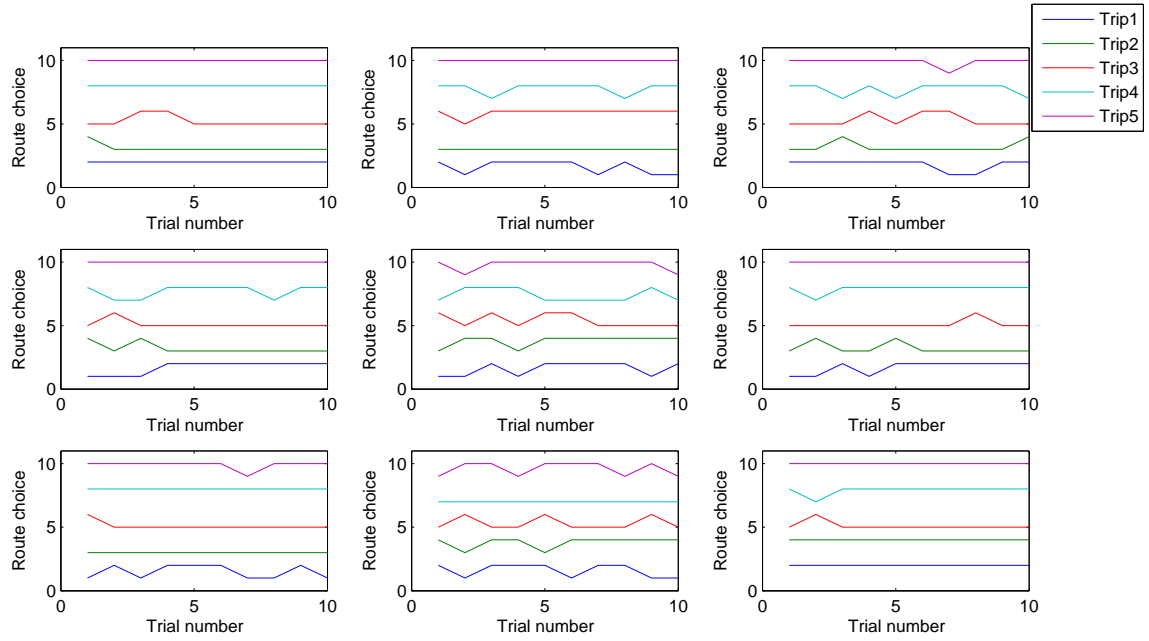


Figure 7.1: Logical- and inertial- choice rates over trials.

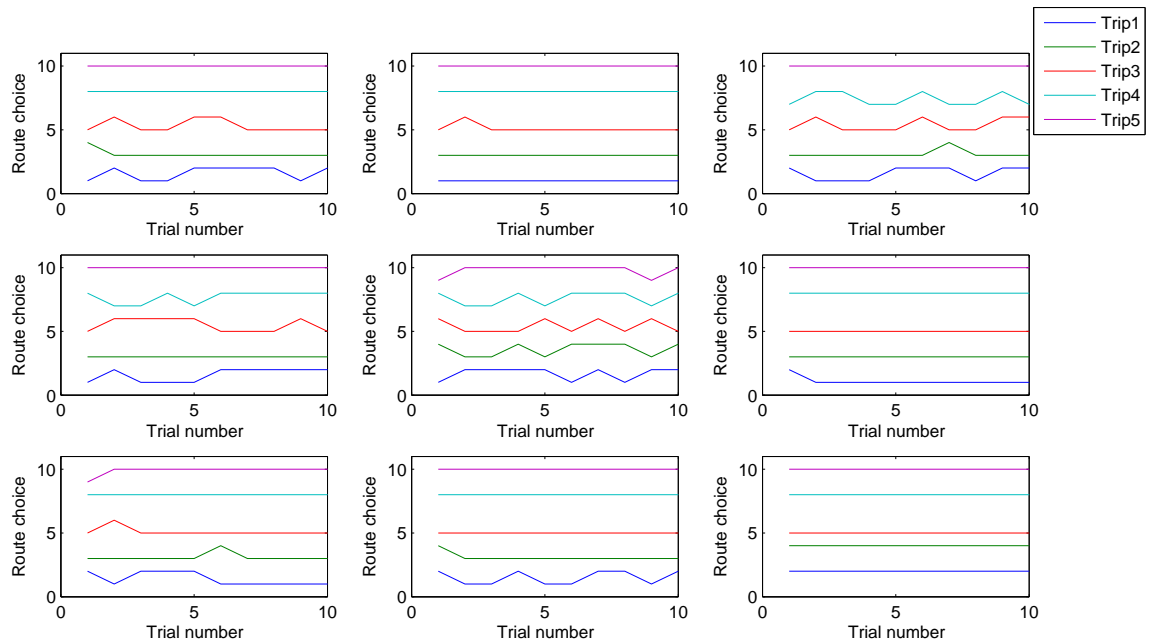
probably have more confidence in his/her experiences than the acquired information; or travel time is not his/her top consideration. Accordingly, the insights gained from previous analyses are needed. Nine of the participants in this study attended Tawfik and Rakha’s experiment. The choice results of these participants were specifically compared between the two experiments in order to see how the effect of information differentiated individually and how well they learned from the information. Figure 7.2 compares the behavioral types (introduced in Table 2.1 which was proposed by [140]) for each of the nine participants between with- and without-information. The degree of the fluctuation of each line gives an explicit generalization of participants’ behavioral aggressiveness. The more fluctuated in the lines, the more aggressively the participants behave. In general, the information significantly changes behavioral types either from risk-seeking to risk-aversion or vice versa. Some of the participants exhibited a high preference for one route when information was not provided and switched frequently when they were informed; whereas some switched more without information and maintained a single route when informed. Overall, the effect of information significantly differs at an individual level.

Figure 7.3 summarizes the behavioral tendency of participants. According to Figure 7.3a, participants 1, 2, 3, 5, 8 basically moved their choices towards rationality with the assistance of information, whereas participants 4, 6, 7, 9 behaved more irrationally when they were informed. In Figure 7.3b, participants 6, 7, 9 instead have higher inertial rates with the provision of information, implying that they behaved even more risk averse when they were provided with information.

Based on the results of the post-run questionnaire, participants 6, 7 and 9 mentioned that



(a) Choice patterns without route information



(b) Choice patterns with route information

Figure 7.2: Participants choice patterns without vs. with route information.

travel time information had little impact on their route choices. Specifically, participant 6 preferred rural roads due to his preference on route scenery, although travel time was important to him as well. Participant 7 held the point that, instead of travel time, the number of intersections was the overriding factor she considered for route choice decisions. Participant 9 preferred to stick to her current route without any route-switching, which is the first type of the typical behavior shown in Table 2.1. Noticeably, participant 4 had both logical and inertial rates decreased with the provision of travel time information. That was because travel time was not the only consideration to this participant. Based on the results of the questionnaire, “avoid traffic lights” was the other equally important factor to him, which highly impacted his choice behavior. Occasionally, participant 4 switched to the slower route instead in order to avoid traffic lights even though he was informed the alternative route was better in terms of travel time, which increased the proportion of compromising behavior (the other type of illogical choice other than inertial choice) and decreased the logical choice rate. In general, travel time may have little effectiveness in enabling drivers to behave logically when drivers do not take travel time as their foremost factor in planning their routes. Additionally, participants 4, 6, 7, 9 are all senior persons from the age group of 55-75 year old. This implies that elder drivers are preferable to make choices based on their preferences or habits rather than received information, which confirms the results in [136].

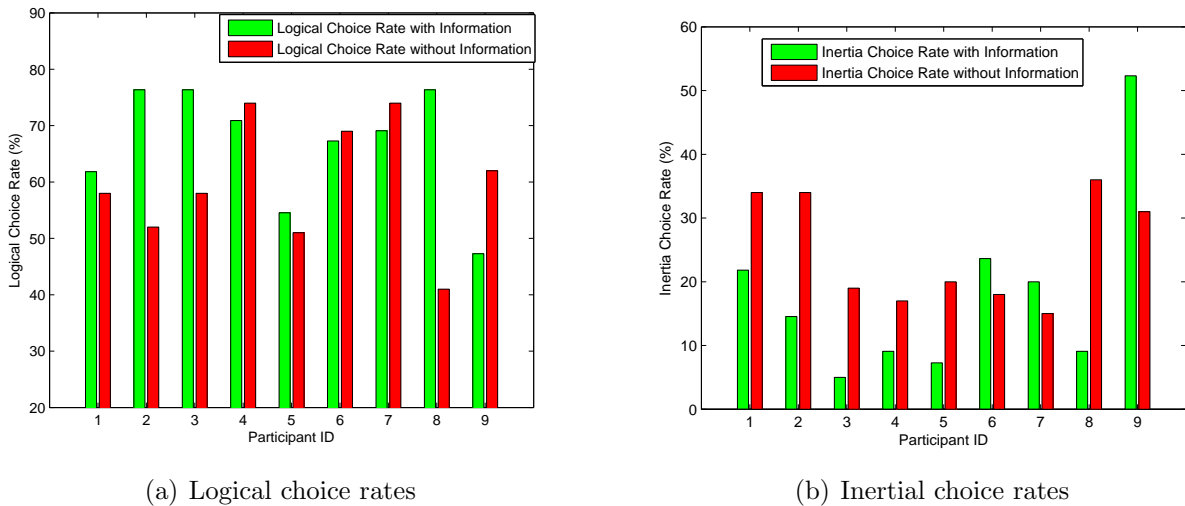


Figure 7.3: Logical- and inertial- choice rates over participants.

In addition to individual traits, trip characteristics may also affect the positive role of information. To study such effects, the choice rates were aggregated by trips. As illustrated in Figure 7.4, information enhances behavioral rationality only for the first three trips. For trip 4, logical rates decrease while inertial rates increase when information is provided. On trip 5, the choice rates do not change significantly between with- and without- information. According to the route characteristics addressed in Table 7.1, route 7 and route 8 (on trip

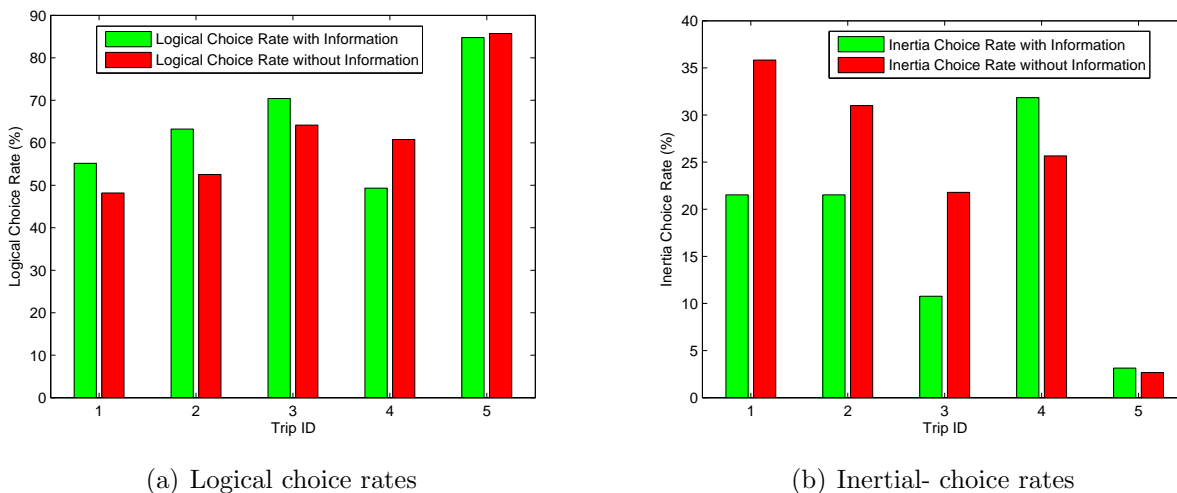


Figure 7.4: Logical- and inertial- choice rates over trips

4) are almost identical in travel time, whereas many participants pointed out that they were reluctant to take route 7 even though it occasionally took less travel time since they did not want to risk being caught on campus by pedestrian flows. The provided information was considered to be less reliable for this trip. Interestingly, travel time is very close as well between the two routes on trip 1; however, the effect of information appears to be very positive. That is because there is no distinct advantage for one route over the other on this trip. Although route 1 is on a highway system with a 20 km/h higher speed limit than route 2, there are five more signalized intersections on it. The provided travel time information for this trip was considered reliable by participants. For trip 5, route 10 distinctively outperforms route 9 in terms of travel time, directness, less traffic and fewer intersections. Tawfik et al. [148] clearly indicated that drivers were able to precisely perceive the route performance and to make correct decisions on this trip without any assistance of information. Overall, information provides little benefit if one route visibly outperforms the other.

Figure 7.5 and Figure 7.6 provide a broad view of the effect of different information types on route choice behavior. In Figure 7.5, the comparative analysis was performed between strict information (average travel time) and range information (variability). According to Figure 7.5a, strict information results in higher logical rates with lower inertial rates for the first trial, demonstrating that strict information is more effective than range information when drivers are lack of experience. For the following trials, however, there is no significant distinctiveness between the two scenarios. This may be attributed to the fact that the effect of information type tends to be identical after drivers gain experience. As illustrated in Figure 7.5b, strict information results in higher logical rates and lower inertial rates on average. Nonetheless, to some of the participants, range information performs better, implying that the responses to different information types, to a large extent, are dependent on individual traits, although

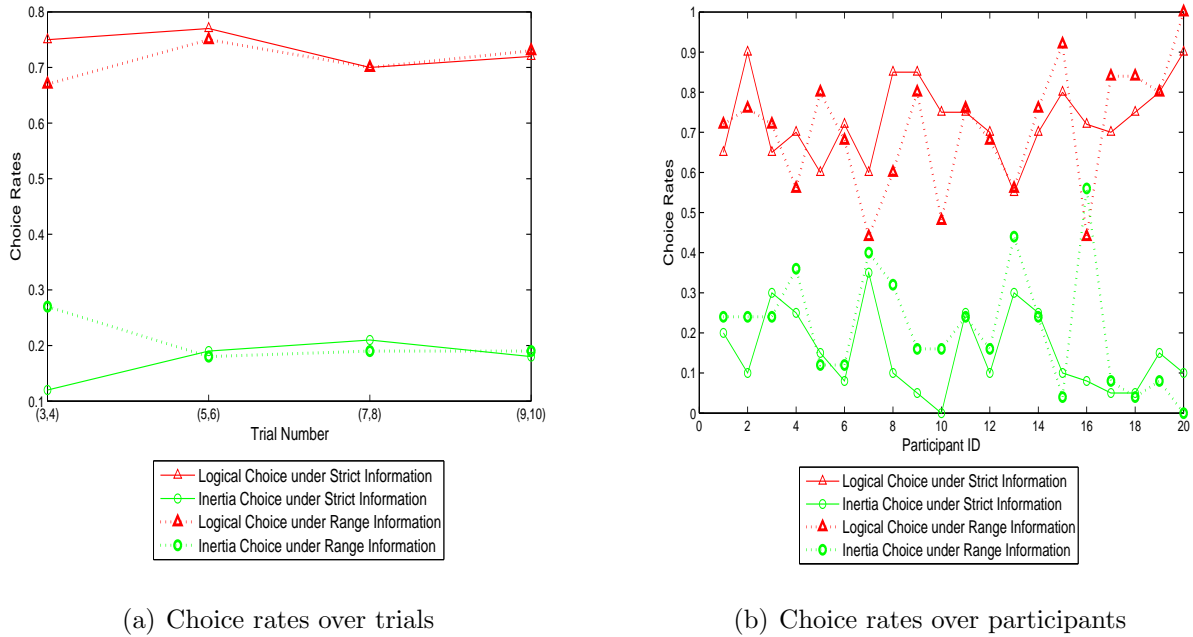


Figure 7.5: Choice rates with strict information vs. with range information

strict information overall performs better in this study.

Figure 7.6 presents the effect of different range information scenarios. As illustrated in Figure 7.6a, “Risky-fast” scenario refers to the faster route (lower average travel time) with higher variability while “safer-fast” represents the faster route with lower variability. Interestingly, the risky-fast scenario appears to have higher logical rates and lower inertial rates in the first two trials; whereas the positive effect decreases in the following three trials. This implies that, when drivers have limited knowledge of route performance, the faster route with high variability is more attractive and subject to make drivers take risk in the gain domain. Once drivers gather experience, however, they are reluctant to risk seeking in the gain domain under higher uncertainty; instead, the safer-fast route becomes preferable. This confirms the results of [131, 132, 133, 134]. Figure 7.6b demonstrates that there is no consensus between participants on which scenario is more effective. Some of the participants have higher logical rates and lower inertial rates for the risky-fast scenario while some exhibit the opposite pattern.

7.3 Conclusions

This chapter empirically investigates the effect of dynamic travel time information on day-to-day commuter route choice behavior by designing and running a real world experiment.

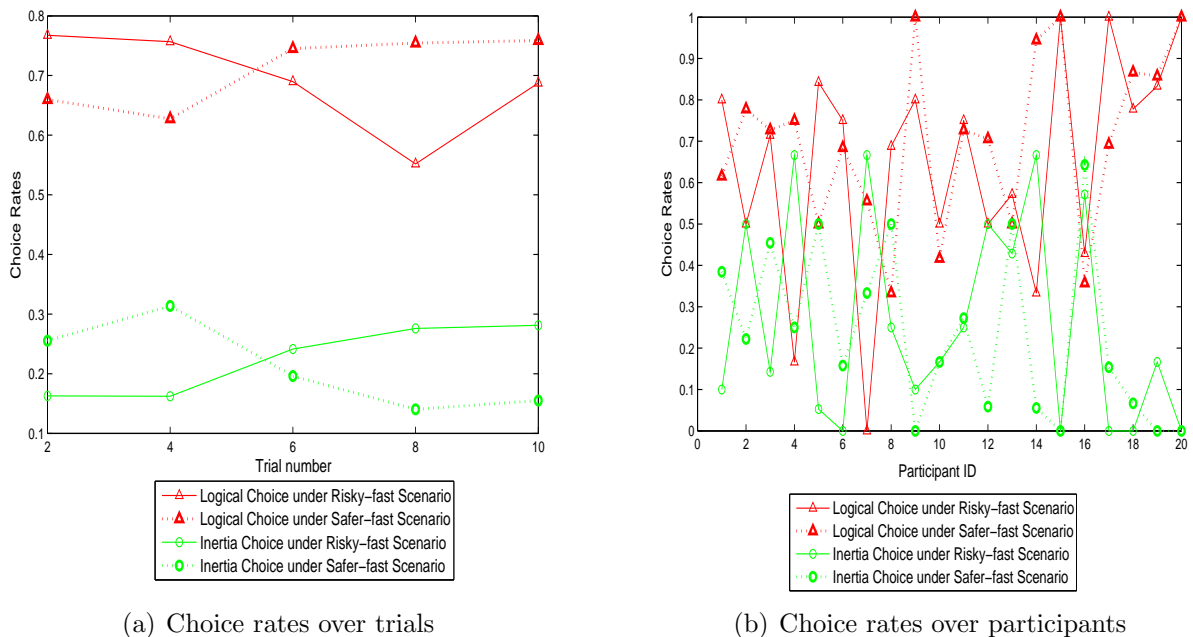


Figure 7.6: Choice rates with risky-fast scenario vs. safer-fast scenario

The experiment confirms some of the results obtained from previous simulation studies, demonstrating that, in general, real-time information significantly enhances behavioral rationality especially when drivers lack long-term experience. Simultaneously, inertial choice rates decrease with information provision, demonstrating that drivers are more willing to risk switching to faster routes when they have more information about these routes. Nonetheless, the positive role of information is, to a large extent, dependent upon the individual's age, preferences, and route characteristics. The results demonstrate that travel time information may not have positive impacts on driver route choice behavior if they value other factors in making their decisions, such as route scenery, habit, number of intersections and traffic signals. The results also reveal that the information effect is less evident for elder drivers, which is consistent with [136]. In addition to personal traits, route characteristics are found to be another important factor influencing the effectiveness of information. Specifically, information may not add value if one route is significantly better than the other given that drivers would be able to identify the optimum route on their own through their experiences.

The effect of the information type on route choice behavior was also studied. The experiment generates the results consistent with the results of simulation studies, demonstrating that, when drivers have limited experiences, information on expected travel times is in general more effective than information on travel time variability in enhancing rational behavior. After drivers gain sufficient knowledge of the alternative routes, however, the benefit of providing strict information appears to diminish. The results also demonstrate that drivers prefer to

take the faster less reliable route as opposed to the slower more reliable route when they lack historical experience. However, as drivers accumulate experience, they become more willing to take the more reliable route, demonstrating that they become less risk seeking in the gain domain at higher uncertainty once experience is gained. In addition, the effect of information types significantly differentiates from person to person. The subject that which type of information is most effective to what group of travelers remains to be investigated in future research.

The experiment also demonstrates that, regardless of being informed or not being informed, the drivers' inertial behavior does not reduce in day-to-day variation, which is different from the results obtained by simulation studies. This may be attributed to the habit or much more decision considerations in actual driving conditions.

The results of this chapter will be used to model route choice behavior under information environment, and thus enable to adequately consider choice stochasticity in routing systems.

Chapter 8

Conclusions and Recommendations for Further Research

This chapter summarizes the main findings of the dissertation. Also, the recommendations for the future research are proposed.

8.1 Dissertation Conclusions

The dissertation is a building block of a multi-modal energy-efficient routing system, attempting to develop four submodules of the system including energy consumption modeling, subway system module, on-road vehicles dynamic eco-routing system, and information effect on route choice behavior. Towards this goal, the study first models energy consumption in support of link cost and eco-route calculation. Given that gasoline LDVs and electric vehicles had been modeled in previous studies [12, 13], this dissertation mainly focuses on the HDDV and train modeling. Secondly, the study develops a railway simulation system through modeling train dynamics, which will be combined with the train energy model to estimate rail-induced trip energy consumption. Thirdly, given that the system is proposed to be developed and tested in the simulation environment before it can be used in real applications, the most suitable microsimulation testbed is identified. The eco-routing problem for the on-road vehicles dynamic eco-routing system is then formulated, followed by a numerical experiment designed to test the benefit of the model. With the developed eco-routing model, the dynamic eco-routing system is developed for in-vehicle navigation applications, and tested at multiple congestion levels. Finally, the dissertation investigates the effect of dynamic route information on route choice behavior in order to provide significant implications to route choice modeling under information environment and thus to enhance the routing system in terms of choice stochasticity.

The research findings are presented as follows:

The conventional fuel consumption models are developed in chapter 3 for HDDTs, conventional diesel and hybrid-electric buses. The model circumvents the bang-bang type of control, and also can be easily calibrated and implemented in traffic simulation software, in-vehicle or smartphone eco-routing and eco-driving applications. It is found that the estimates of the proposed VT-CPFM model are consistent with field observations as well as the estimates of CMEM and MOVES, and that the models can provide realistic driving suggestions in control systems. The optimum fuel economy cruise speed ranges between 32 and 52 *km/h* for the tested trucks and between 39 and 47 *km/h* for the tested buses on grades varying from 0% to 8%. The results also demonstrate that steeper roads (uphill) and heavier vehicles result in lower optimum cruise speeds. These optimum cruise speeds are significantly lower than those of LDVs (60-80 *km/h*). In addition, a recent study [199] on electric vehicle eco-routing generated the optimum cruise speed ranging between 15 and 25 *km/h* which is significantly lower than the conventional vehicles. Consequently, optimum cruise speeds differ between vehicle models, and may result in different vehicle model-specific eco-routes.

Chapter 4 develops electric train dynamics and energy consumption models in support of railway microsimulator development and trip energy estimation. Both models can be easily calibrated using non-engine data and implemented in simulation systems and eco-transit applications. The dynamics model varies throttle and brake level with running speed rather than assuming constants as was done by previous studies. The energy consumption model considers instantaneous energy regeneration by formulating regenerative efficiency as an exponential function of deceleration level. The results of the dynamics modeling demonstrate that the proposed model can adequately capture instantaneous acceleration/deceleration behavior and thus produce realistic train trajectories. The model is also demonstrated to provide good fit in the domains of acceleration/deceleration versus speed and acceleration/deceleration versus distance. In addition, simulation results provide a good fit to the field data, demonstrating the adequacy of the proposed dynamics model in support of railway simulation system. The results of the energy consumption modeling demonstrate that the model estimates are consistent with the NTD results. Significant prediction error is observed without modeling regenerative braking. It is also found that the proposed energy model is able to capture the energy consumption differences associated with train, route and operational characteristics, and thus is applicable for project-level analysis.

Chapter 5 identifies the applicability of the state-of-the-art microsimulation models (INTEGRATION, VISSIM, AIMSUM, PARAMICS) to serve as the testbed for the proposed study. Given that the car-following model of a micro-simulator controls longitudinal vehicle motions and thus determines the resulting vehicle trajectories, the research efforts in this chapter mainly focus on the performance of the built-in car-following models from the energy and environmental perspective. The VSP distributions resulted from the car-following models used in each of the microsimulation software are compared to the field observations. The results demonstrate that the RPA model (INTEGRATION) outperforms the Gipps (AIMSUM), Fritzsche (PARAMICS) and Wiedemann (VISSIM) models in generating realistic VSP distributions, especially at low speed levels (0 – 30*mph*) where car-following is most

common. It is also found that the RPA model produces the lowest level of prediction error in terms of fuel consumption and emissions. The conclusions of this chapter demonstrate the advantage of the INTEGRATION software over the other three widely-used simulation models for energy and environmental analysis. Accordingly, INTEGRATION is used to develop and test the proposed eco-routing system.

Chapter 6 formulates an eco-routing model for in-vehicle routing applications. The model comprehensively considers microscopic elements and is able to calculate eco-routes based on most recent information while at the same time differentiate eco-routes between vehicle models. A numerical experiment is designed to test the benefit of the model. With the developed eco-routing model, the dynamic eco-routing system is then constructed, and tested in the INTEGRATION simulation testbed at different congestion levels. The results of the numerical experiment demonstrate that the proposed eco-routing model is able to generate reasonable routing suggestions based on real time information and also differentiate vehicle models. The testing results of the dynamic eco-routing system demonstrate that the proposed eco-routing achieves lower network-wide energy consumption levels compared to the traditional eco-routing and travel time routing at all congestion levels. The results also demonstrate that the conventional fuel savings relative to the travel time routing decrease with the increasing congestion level given fewer route alternatives in a congested network. For the electric power, however, the savings relative to travel time routing do not monotonously vary with congestion level given that significant energy savings could be achieved at both low and high demand levels. Furthermore, the energy savings relative to the traditional eco-routing are also not monotonously related to congestion level. In addition, network configuration is demonstrated to significantly affect the eco-routing benefits.

In order to enhance the design of the eco-routing system from the choice stochasticity perspective, Chapter 7 empirically investigates the effect of dynamic route information on day-to-day commuter route choice behavior by designing and running a real world experiment. The experiment confirms some of the results obtained from previous simulation studies, demonstrating that, in general, route information significantly enhances behavioral rationality especially when drivers lack long-term experience. The results also demonstrate that the effectiveness of information in routing rationality depends upon individual's preferences, age, and route characteristics. Specifically, the provided information may not have positive impacts on choice rationality if travelers value other considerations in decision-making such as route scenery, habit, number of intersections and traffic signals. It is also found that the information effect is less evident for elder drivers. Furthermore, information may not add value if one route is significantly better than the other given that drivers would be able to identify the optimum route on their own through their experiences. The results also demonstrate that the strict information is, in general, more effective than the variability information when travelers have limited experiences, and that the difference becomes insignificant with experience accumulation. Finally, the results reveal that the faster less reliable route is more attractive than the slower more reliable route when drivers lack experience, while with cumulative experiences, travelers become more willing to take the more reliable route given

that they are reluctant to become risk seekers once experience is gained.

8.2 Recommendations for Further Research

To extend the research work of this dissertation, several efforts should be made in the future which are presented in this section.

First, the dissertation develops four submodules as partial fulfillment of the multimodal eco-routing system. Other submodules such as pedestrian and bicycle modeling should be investigated in the future study. Upon the completion of all submodules, the system will be used to estimate door-to-door trip energy consumption in support of intermodal route planning. After simulation testing, the system will be proposed for real applications.

Secondly, the eco-routing system developed in this dissertation is deterministic assuming that travelers always choose the actually best route as suggested, which is not realistic in reality. Based on the results in chapter 7, travelers may not always choose the suggested optimum routes. For example, some of the travelers do not prefer the routes traversing downtown areas or university campus even though they are informed that these routes are the best; some of them prefer to choose habitual routes or rural routes. These stochastic factors may significantly affect eco-routing benefits. Incorporating behavioral stochasticity into the proposed system would be an important concern in the future.

Furthermore, the dynamic eco-routing system developed in Chapter 6 ultimately achieves the User Equilibrium (UE) in which all drivers minimize their own energy consumption rather than achieving the System Optimum (SO). UE is more realistic in capturing real-world route choice behavior given that drivers in reality always consider minimizing their own travel costs instead of trying to optimize system-level measure of effectiveness. However, investigating the SO solutions will be providing insightful implications to moving routing rationality towards system-wide optimum.

Another issue is that the minimum energy consumption does not necessarily guarantee the optimum in pollutant emissions such as CO , NO_x , HC , given that these emissions are nonlinearly related to energy consumption [203]. Consequently, further study should be recommended specifically on emission-optimized routing to reduce air pollutants from the route planning perspective.

Finally, the proposed eco-routing system in this study takes energy consumption as the single objective without considering other factors such as travel time. In reality, travelers may not be willing to either spend significantly more travel time or make a big detour to minimize their energy consumption levels. Consequently, some constraints with respect to travel time or distance should be added to the optimization problem, so that users are able to specify their tolerance of extra travel time and distances traveled in reducing energy consumption. Another way of constraining the eco-routing problem is to consider more objectives and

achieve a compromise solution through superimposing weight on each objective. Both approaches enable travelers to reduce their energy consumption within reasonable travel time or distances traveled.

Bibliography

- [1] Stacy C Davis, Susan W Diegel, and Robert G Boundy. *Transportation energy data book*. Oak Ridge National Laboratory, 2015.
- [2] EPA. Inventory of US greenhouse gas emissions and sinks: 1990-2013. Technical report, EPA 430-R-15-004, 2015.
- [3] U.S. Energy Information Administration (EIA). Energy consumption by sector. Technical report, 2014.
- [4] Fatemeh Baratian-Ghorghi and Huaguo Zhou. Investigating women’s and men’s propensity to use traffic information in a developing country. *Transportation in developing economies*, 1(1):11–19, 2015.
- [5] Matthias Prandtstetter, Markus Straub, and Jakob Puchinger. On the way to a multi-modal energy-efficient route. In *Industrial Electronics Society, IECON 2013-39th Annual Conference of the IEEE*, pages 4779–4784. IEEE, 2013.
- [6] Kyounggho Ahn and Hesham Rakha. The effects of route choice decisions on vehicle energy consumption and emissions. *Transportation Research Part D: Transport and Environment*, 13(3):151–167, 2008.
- [7] Eva Ericsson, Hanna Larsson, and Karin Brundell-Freij. Optimizing route choice for lowest fuel consumption–potential effects of a new driver support tool. *Transportation Research Part C: Emerging Technologies*, 14(6):369–383, 2006.
- [8] Matthew Barth, Kanok Boriboonsomsin, and Alex Vu. Environmentally-friendly navigation. In *Intelligent Transportation Systems Conference*, pages 684–689. IEEE, 2007.
- [9] Richard Cook and Edward L Glover. Technical description of the toxics module for MOBILE 6. 2 and guidance on its use for emission inventory preparation. *US EPA, Office of Transportation and Air Quality, Ann Arbor, MI*, 2002.
- [10] CARB EMFAC2007 Version. 2.30 user guide: calculating emission inventories for vehicles in California. *California Air Resource Board*, 2006.

- [11] Hesham Rakha, Huanyu Yue, and Francois Dion. VT-Meso model framework for estimating hot-stabilized light-duty vehicle fuel consumption and emission rates. *Canadian Journal of Civil Engineering*, 38(11):1274–1286, 2011.
- [12] Hesham A Rakha, Kyounggho Ahn, Kevin Moran, Bart Saerens, and Eric Van den Bulck. Virginia tech comprehensive power-based fuel consumption model: model development and testing. *Transportation Research Part D: Transport and Environment*, 16(7):492–503, 2011.
- [13] Chiara Fiori, Kyounggho Ahn, and Hesham A Rakha. Power-based electric vehicle energy consumption model: Model development and validation. *Applied Energy*, 168:257–268, 2016.
- [14] X Perpinya. *Reliability and safety in railway*. InTech, 2012.
- [15] István Zobory, Hans G Reimerdes, Elemér Békefi, Jens Marsolek, and István Németh. Longitudinal dynamics of train collisions–crash analysis. In *7th Mini Conference on Vehicle System Dynamics, Identification and Anomalies*, pages 89–110, 2000.
- [16] Andrew Nash and Daniel Huerlimann. Railroad simulation using opentrack. *WIT Transactions on The Built Environment*, 74, 2004.
- [17] Mao Baohua, Jia Wenzheng, Chen Shaokuan, and Liu Jianfeng. A computer-aided multi-train simulator for rail traffic. In *Vehicular Electronics and Safety. IEEE International Conference on*, pages 1–5. IEEE, 2007.
- [18] Tadeusz Piechowiak. Pneumatic train brake simulation method. *Vehicle System Dynamics*, 47(12):1473–1492, 2009.
- [19] QianSuo Yang, JunHao Song, Duo Li, Jie Zhang, and GuoWei Yang. Train model acceleration and deceleration. *Science China Technological Sciences*, 56(3):642–647, 2013.
- [20] Qing Wu, Maksym Spiriyagin, and Colin Cole. Longitudinal train dynamics: an overview. *Vehicle System Dynamics*, pages 1–27, 2016.
- [21] Guohua Song, Lei Yu, and Long Xu. Comparative analysis of car-following models for emissions estimation. *Transportation Research Record: Journal of the Transportation Research Board*, (2341):12–22, 2013.
- [22] Guohua Song, Lei Yu, and Zhongbo Geng. Optimization of wiedemann and fritzsche car-following models for emission estimation. *Transportation Research Part D: Transport and Environment*, 34:318–329, 2015.
- [23] Hongyu Lu, Guohua Song, and Lei Yu. A comparison and modification of car-following models for emission estimation. In *Transportation Research Board 95th Annual Meeting, No. 16-3329, Washington D.C.*, 2016.

- [24] Hesham A Rakha, Kyoungcho Ahn, and Kevin Moran. Integration framework for modeling eco-routing strategies: Logic and preliminary results. *International Journal of Transportation Science and Technology*, 1(3):259–274, 2012.
- [25] Gwo Hshiung Tzeng and Chien-Ho Chen. Multiobjective decision making for traffic assignment. *IEEE Transactions on Engineering Management*, 40(2):180–187, 1993.
- [26] Anna Nagurney. Congested urban transportation networks and emission paradoxes. *Transportation Research Part D: Transport and Environment*, 5(2):145–151, 2000.
- [27] Anna Nagurney and June Dong. A multiclass, multicriteria traffic network equilibrium model with elastic demand. *Transportation Research Part B: Methodological*, 36(5):445–469, 2002.
- [28] Laurence R Rilett and Christine M Benedek. Traffic assignment under environmental and equity objectives. *Transportation Research Record: Journal of the Transportation Research Board*, (1443):92–99, 1994.
- [29] Christine M Benedek and Laurence R Rilett. Equitable traffic assignment with environmental cost functions. *Journal of Transportation Engineering*, 124(1):16–22, 1998.
- [30] Satoshi Sugawara and D Niemeier. How much can vehicle emissions be reduced?: exploratory analysis of an upper boundary using an emissions-optimized trip assignment. *Transportation Research Record: Journal of the Transportation Research Board*, (1815):29–37, 2002.
- [31] Kanok Boriboonsomsin, Matthew J Barth, Weihua Zhu, and Alexander Vu. Eco-routing navigation system based on multisource historical and real-time traffic information. *IEEE Transactions on Intelligent Transportation Systems*, 13(4):1694–1704, 2012.
- [32] Jaap Vreeswijk, Tom Thomas, Eric van Berkum, and Bart van Arem. Drivers’ perception of route alternatives as indicator for the indifference band. *Transportation Research Record: Journal of the Transportation Research Board*, 2383(1):10–17, 2013.
- [33] Mathew Barth, Feng An, Theodore Younglove, George Scora, Carrie Levine, Marc Ross, and Thomas Wenzel. Comprehensive modal emission model (CMEM), version 2.0 user’s guide. *University of California, Riverside*, 2000.
- [34] Bart Saerens, Moritz Diehl, and Eric Van den Bulck. Optimal control using pontryagin’s maximum principle and dynamic programming. In *Automotive Model Predictive Control*, pages 119–138. Springer, 2010.
- [35] S Hausberger, M Rexeis, M Zallinger, and R Luz. PHEM user guide for version 10. *TUG/FVT Report*, pages 1–57, 2010.

- [36] Alessandra Cappiello, Ismail Chabini, Edward K Nam, Alessandro Lue, and M Abou Zeid. A statistical model of vehicle emissions and fuel consumption. In *Proceedings of the IEEE 5th International Conference on Intelligent Transportation Systems*, pages 801–809. IEEE, 2002.
- [37] Hesham Rakha, Kyoungcho Ahn, and Antonio Trani. Development of VT-Micro model for estimating hot stabilized light duty vehicle and truck emissions. *Transportation Research Part D: Transport and Environment*, 9(1):49–74, 2004.
- [38] Luc Pelkmans, Patrick Debal, Tom Hood, Günther Hauser, and Maria-Rosa Delgado. Development of a simulation tool to calculate fuel consumption and emissions of vehicles operating in dynamic conditions. Technical report, SAE Technical Paper, 2004.
- [39] Motor Vehicle Emission Simulator. User guide for MOVES2014a. *Assessment and Standards Division, Office of Transportation and Air Quality, US Environmental Protection Agency. EPA-420-B-12-001b*, 2014.
- [40] Jinghui Wang and Hesham A Rakha. Heavy-duty diesel truck fuel consumption modeling. In *Transportation Research Board 95th Annual Meeting, No. 16-2147, Washington D.C.*, 2016.
- [41] Jinghui Wang and Hesham A Rakha. Fuel consumption model for conventional diesel buses. *Applied Energy*, 170:394–402, 2016.
- [42] Robin Smit, Richard Smokers, and Elke Rabé. A new modelling approach for road traffic emissions: Versit+. *Transportation Research Part D: Transport and Environment*, 12(6):414–422, 2007.
- [43] Sangjun Park, Hesham Rakha, Kyoungcho Ahn, and Kevin Moran. Virginia tech comprehensive power-based fuel consumption model (VT-CPFM): model validation and calibration considerations. *International Journal of Transportation Science and Technology*, 2(4):317–336, 2013.
- [44] Jinghui Wang and Hesham A Rakha. Electric train energy consumption modeling. *Applied Energy*, 193:346–355, 2017.
- [45] David Wenzhong Gao, Chris Mi, and Ali Emadi. Modeling and simulation of electric and hybrid vehicles. *Proceedings of the IEEE*, 95(4):729–745, 2007.
- [46] John G Hayes, R Pedro R de Oliveira, Sean Vaughan, and Michael G Egan. Simplified electric vehicle power train models and range estimation. In *Vehicle Power and Propulsion Conference (VPPC)*, pages 1–5. IEEE, 2011.
- [47] Matteo Muratori, Michael J Moran, Emmanuele Serra, and Giorgio Rizzoni. Highly-resolved modeling of personal transportation energy consumption in the united states. *Energy*, 58:168–177, 2013.

- [48] Xinkai Wu, David Freese, Alfredo Cabrera, and William A Kitch. Electric vehicles' energy consumption measurement and estimation. *Transportation Research Part D: Transport and Environment*, 34:52–67, 2015.
- [49] Rami Abousleiman and Osamah Rawashdeh. Energy consumption model of an electric vehicle. In *Transportation Electrification Conference and Expo (ITEC)*, pages 1–5. IEEE, 2015.
- [50] John G Hayes and Kevin Davis. Simplified electric vehicle powertrain model for range and energy consumption based on epa coast-down parameters and test validation by argonne national lab data on the nissan leaf. In *Transportation Electrification Conference and Expo (ITEC)*, pages 1–6. IEEE, 2014.
- [51] Aoife Foley, Barry Tyther, Patrick Calnan, and Brian Ó Gallachóir. Impacts of electric vehicle charging under electricity market operations. *Applied Energy*, 101:93–102, 2013.
- [52] Keith B Wipke, Matthew R Cuddy, and Steven D Burch. Advisor 2.1: A user-friendly advanced powertrain simulation using a combined backward/forward approach. *IEEE transactions on vehicular technology*, 48(6):1751–1761, 1999.
- [53] Reed T Doucette and Malcolm D McCulloch. Modeling the prospects of plug-in hybrid electric vehicles to reduce CO₂ emissions. *Applied Energy*, 88(7):2315–2323, 2011.
- [54] Phillip J Kollmeyer, Larry W Juang, and TM Jahns. Development of an electromechanical model for a corbin sparrow electric vehicle. In *Vehicle Power and Propulsion Conference (VPPC)*, pages 1–8. IEEE, 2011.
- [55] How subway works, 2007, <http://science.howstuffworks.com/engineering/civil/subway3.htm>.
- [56] William W Hay. *Railroad engineering*, volume 1. John Wiley & Sons, 1982.
- [57] Franklin Gbologah, Yanzhi Xu, Michael Rodgers, and Randall Guensler. Demonstrating a bottom-up framework for evaluating energy and emissions performance of electric rail transit options. *Transportation Research Record: Journal of the Transportation Research Board*, (2428):10–17, 2014.
- [58] Christopher Puchalsky. Comparison of emissions from light rail transit and bus rapid transit. *Transportation Research Record: Journal of the Transportation Research Board*, (1927):31–37, 2005.
- [59] Christina Messa. Comparison of emissions from light rail transit, electric commuter rail, and diesel multiple units. *Transportation Research Record: Journal of the Transportation Research Board*, (1955):26–33, 2006.
- [60] FTA, U.S. department of transportation. *National Transit Annual Database*, <http://www.ntdprogram.gov/ntdprogram/data.htm>.

- [61] Ram K Mittal. Energy intensity of intercity passenger rail. Technical report, Department of Transportation, Washington, DC (USA). Office of Univ. Research, 1977.
- [62] J. B. Hopkins. Railroads and the environment estimation of fuel consumption in rail transportation, volume 1: Analytical model. Technical report, Federal Railroad Administration. Final Report FRA-OR-D-75-74.I. Washington, DC, 1975.
- [63] Jyh-Cherng Jong and En-Fu Chang. Models for estimating energy consumption of electric trains. *Journal of the Eastern Asia Society for Transportation Studies*, 6:278–291, 2005.
- [64] Ricardo Barrero, Xavier Tackoen, and Joeri Van Mierlo. Quasi-static simulation method for evaluation of energy consumption in hybrid light rail vehicles. In *2008 IEEE Vehicle Power and Propulsion Conference*, pages 1–7. IEEE, 2008.
- [65] Rongfang Rachel Liu and Iakov M Golovitcher. Energy-efficient operation of rail vehicles. *Transportation Research Part A: Policy and Practice*, 37(10):917–932, 2003.
- [66] Edward J Lombardi. Engineering tests performed on the x2000 and ice high speed trainsets. In *Railroad Conference Proceedings of the 1994 ASME/IEEE Joint (in Conjunction with Area 1994 Annual Technical Conference)*, pages 13–21. IEEE, 1994.
- [67] Alberto Álvarez. Energy consumption and emissions of high-speed trains. *Transportation Research Record: Journal of the Transportation Research Board*, (2159):27–35, 2010.
- [68] Kitae Kim and Steven I-Jy Chien. Optimal train operation for minimum energy consumption considering track alignment, speed limit, and schedule adherence. *Journal of Transportation Engineering*, 137(9):665–674, 2010.
- [69] Carlos Sicre, Asunción P Cucala, Antonio Fernández, and Piotr Lukaszewicz. Modeling and optimizing energy-efficient manual driving on high-speed lines. *IEEJ Transactions on Electrical and Electronic Engineering*, 7(6):633–640, 2012.
- [70] Shuai Su, Xiang Li, Tao Tang, and Ziyong Gao. A subway train timetable optimization approach based on energy-efficient operation strategy. *IEEE Transactions on Intelligent Transportation Systems*, 14(2):883–893, 2013.
- [71] A González-Gil, R Palacin, P Batty, and JP Powell. A systems approach to reduce urban rail energy consumption. *Energy Conversion and Management*, 80:509–524, 2014.
- [72] Xiang Li and Hong K Lo. An energy-efficient scheduling and speed control approach for metro rail operations. *Transportation Research Part B: Methodological*, 64:73–89, 2014.

- [73] Iakov M Golovitcher. Energy efficient control of rail vehicles. In *Systems, Man, and Cybernetics, 2001 IEEE International Conference on*, volume 1, pages 658–663. IEEE, 2001.
- [74] Christopher W. Jenks, Lawrence D Goldstein, Anthony P Avery, Eileen P Delaney, and Sharon Lamberton. National cooperative rail research program (ncrrp) report 3: Comparison of passenger rail energy consumption with competing modes. Technical report, Transportation Research Board, Washington DC, 2015.
- [75] Argonne national laboratory. autonomie, 2015.
- [76] Anne Marie Lewis, Jarod C Kelly, and Gregory A Keoleian. Evaluating the life cycle greenhouse gas emissions from a lightweight plug-in hybrid electric vehicle in a regional context. In *2012 IEEE International Symposium on Sustainable Systems and Technology (ISSST)*, pages 1–6. IEEE, 2012.
- [77] Anne Marie Lewis, Jarod C Kelly, and Gregory A Keoleian. Vehicle lightweighting vs. electrification: Life cycle energy and ghg emissions results for diverse powertrain vehicles. *Applied Energy*, 126:13–20, 2014.
- [78] Alfons Radtke and Dirk Hauptmann. Automated planning of timetables in large railway networks using a microscopic data basis and railway simulation techniques. *WIT Transactions on The Built Environment*, 74, 2004.
- [79] JB Bahn. Simulation of railway and streetcar networks. [http : //www.jbss.de/hpgeng.htm](http://www.jbss.de/hpgeng.htm), 2010.
- [80] Pablo Grube, Felipe Núñez, and Aldo Cipriano. An event-driven simulator for multi-line metro systems and its application to santiago de chile metropolitan rail network. *Simulation Modelling Practice and Theory*, 19(1):393–405, 2011.
- [81] Andrea E Rizzoli, Nicoletta Fornara, and Luca Maria Gambardella. A simulation tool for combined rail/road transport in intermodal terminals. *Mathematics and Computers in Simulation*, 59(1):57–71, 2002.
- [82] Massimo Paolucci and Raffaele Pesenti. An object-oriented approach to discrete-event simulation applied to underground railway systems. *Simulation*, 72(6):372–383, 1999.
- [83] Simon Iwnicki. *Handbook of railway vehicle dynamics*. CRC press, 2006.
- [84] T Seifer, D Hauptmann, and L Muller. *A Computer Model for the Simulation of Longitudinal Dynamics in Trains*. World Congress on Railway Research, 1997.
- [85] Vijay Garg. *Dynamics of railway vehicle systems*. Elsevier, 2012.
- [86] Q Wu. *Optimisations of draft gear designs for heavy haul trains*. PhD thesis, Central Queensland University, 2016.

- [87] John Searle. Equations for speed, time and distance for vehicles under maximum acceleration. Technical report, SAE Technical Paper, 1999.
- [88] Hesham Rakha, Ivana Lucic, Sergio Henrique Demarchi, José Reynaldo Setti, and Michel Van Aerde. Vehicle dynamics model for predicting maximum truck acceleration levels. *Journal of Transportation Engineering*, 127(5):418–425, 2001.
- [89] Hesham Rakha and Ivana Lucic. Variable power vehicle dynamics model for estimating truck accelerations. *Journal of Transportation Engineering*, 128(5):412–419, 2002.
- [90] Hesham Rakha, Matthew Snare, and François Dion. Vehicle dynamics model for estimating maximum light-duty vehicle acceleration levels. *Transportation Research Record: Journal of the Transportation Research Board*, (1883):40–49, 2004.
- [91] Karim Fadhloun, Hesham Rakha, Amara Loulizi, and Abdessattar Abdelkefi. Vehicle dynamics model for estimating typical vehicle accelerations. *Transportation Research Record: Journal of the Transportation Research Board*, (2491):61–71, 2015.
- [92] K Fadhloun, H Rakha, A Abdelkefi, and A Loulizi. An enhanced rakha-pasumarthy-adjerid car-following model accounting for driver behavior. In *96st Annual Meeting of the Transportation Research Board, Washington, DC*, 2017.
- [93] Herman John Schrader. The friction of railway brake shoes at high speed and high pressure. *University of Illinois bulletin; v. 35, no. 72*, 1938.
- [94] David G Blaine and Mark F Hengel. Brake-system operation and testing procedures and their effects on train performance. Technical report, 1971.
- [95] BL Karvatski. General theory of automated brakes. *OPED-CFR, Bucharest*, 1950.
- [96] UIC. Uic leaflet 544-1: Brakes - braking power, 4th edition. Technical report, 2004.
- [97] UIC. Uic leaflet 540: Brakes - air brakes for freight trains and passenger trains, 5th edition. Technical report, 2006.
- [98] UIC. Uic leaflet 541-3: Brakes - disc brakes and their application - general conditions for the approval of brake pads, 7th edition. Technical report, 2010.
- [99] Shukai Li, Lixing Yang, Keping Li, and Ziyou Gao. Robust sampled-data cruise control scheduling of high speed train. *Transportation Research Part C: Emerging Technologies*, 46:274–283, 2014.
- [100] Shukai Li, Lixing Yang, and Ziyou Gao. Coordinated cruise control for high-speed train movements based on a multi-agent model. *Transportation Research Part C: Emerging Technologies*, 56:281–292, 2015.

- [101] Pengling Wang and Rob MP Goverde. Multiple-phase train trajectory optimization with signalling and operational constraints. *Transportation Research Part C: Emerging Technologies*, 69:255–275, 2016.
- [102] YV Bocharnikov, AM Tobias, C Roberts, S Hillmansen, and CJ Goodman. Optimal driving strategy for traction energy saving on dc suburban railways. *IET Electric Power Applications*, 1(5):675, 2007.
- [103] Rémy Chevrier, Paola Pellegrini, and Joaquin Rodriguez. Energy saving in railway timetabling: A bi-objective evolutionary approach for computing alternative running times. *Transportation Research Part C: Emerging Technologies*, 37:20–41, 2013.
- [104] Xihui Yan, Baigen Cai, Bin Ning, and Wei ShangGuan. Online distributed cooperative model predictive control of energy-saving trajectory planning for multiple high-speed train movements. *Transportation Research Part C: Emerging Technologies*, 69:60–78, 2016.
- [105] Jinghui Wang, Hesham A Rakha, and Karim Fadhloun. Comparison of car-following models: A vehicle fuel consumption and emissions estimation perspective. In *Transportation Research Board 96th Annual Meeting, No. 17-1158, Washington D.C.*, 2017.
- [106] Loren Bloomberg and Jim Dale. Comparison of VISSIM and CORSIM traffic simulation models on a congested network. *Transportation Research Record: Journal of the Transportation Research Board*, (1727):52–60, 2000.
- [107] R Wiedemann. Simulation of the flow of traffic, the Institute of Transport of the University of Karlsruhe. 1974.
- [108] Louis A Pipes. An operational analysis of traffic dynamics. *Journal of Applied Physics*, 24(3):274–281, 1953.
- [109] Guohua Song, Lei Yu, and Yanhong Zhang. Applicability of traffic microsimulation models in vehicle emissions estimates: Case study of VISSIM. *Transportation Research Record: Journal of the Transportation Research Board*, (2270):132–141, 2012.
- [110] Waleed F Faris, Hesham A Rakha, Raed Ismail Kafafy, Moumen Idres, and Salah Elmoselhy. Vehicle fuel consumption and emission modelling: an in-depth literature review. *International Journal of Vehicle Systems Modelling and Testing*, 6(3-4):318–395, 2011.
- [111] ATMS and Systems Engineering Program Team. Corsim user’s guide version 6.0. *FHWA Office of Operations Research, Development and Technology Federal Highway Administration*, 2006.
- [112] Hesham Rakha and Brent Crowther. Comparison of greenshields, pipes, and van aerde car-following and traffic stream models. *Transportation Research Record: Journal of the Transportation Research Board*, (1802):248–262, 2002.

- [113] Peter G Gipps. A behavioural car-following model for computer simulation. *Transportation Research Part B: Methodological*, 15(2):105–111, 1981.
- [114] PARAMICS Modeller. v4. 0 user guide and reference manual. *Quadstone Ltd*, 2002.
- [115] Hans-Thomas Fritzsche. A model for traffic simulation. *Traffic Engineering and Control*, 35(5):317–21, 1994.
- [116] Michel Van Aerde and Sam Yagar. Dynamic integrated freeway/traffic signal networks: A routing-based modelling approach. *Transportation Research Part A: Policy and Practice*, 22(6):445–453, 1988.
- [117] M Van Aerde and H Rakha. Integration© release 2.30 for windows: User’s guide—volume I: Fundamental model features. *M. Van Aerde & Assoc., Ltd., Blacksburg*, 2007.
- [118] Hesham A Rakha. Integration release 2.30 for windows: User’s guide—volume 1: Fundamental model features and volume 2: Advanced model features, 2002.
- [119] M Van Aerde. Single regime speed-flow-density relationship for congested and uncongested highways. In *74th Annual Meeting of the Transportation Research Board, Washington, DC*, volume 6, 1995.
- [120] Michel Van Aerde and Hesham Rakha. Multivariate calibration of single regime speed-flow-density relationships [road traffic management]. In *Proceedings of Vehicle Navigation and Information Systems Conference*, pages 334–341. IEEE, 1995.
- [121] H Rakha, P Pasumarthy, and S Adjerid. The integration framework for modeling longitudinal vehicle motion. *TRANSTEC, Athens*, 2004.
- [122] Hesham Rakha, Praveen Pasumarthy, and Slimane Adjerid. A simplified behavioral vehicle longitudinal motion model. *Transportation letters*, 1(2):95–110, 2009.
- [123] Hesham Rakha. Validation of Van Aerde’s simplified steady-state car-following and traffic stream model. *Transportation Letters*, 1(3):227–244, 2009.
- [124] Hesham Rakha and Mazen Arafeh. Calibrating steady-state traffic stream and car-following models using loop detector data. *Transportation Science*, 44(2):151–168, 2010.
- [125] Yu Marco Nie and Qianfei Li. An eco-routing model considering microscopic vehicle operating conditions. *Transportation Research Part B: Methodological*, 55:154–170, 2013.
- [126] Kyoung-ho Ahn and Hesham A Rakha. Network-wide impacts of eco-routing strategies: a large-scale case study. *Transportation Research Part D: Transport and Environment*, 25:119–130, 2013.

- [127] William Edwardes and Hesham Rakha. Virginia tech comprehensive power-based fuel consumption model: Modeling diesel and hybrid buses. *Transportation Research Record: Journal of the Transportation Research Board*, (2428):1–9, 2014.
- [128] Guoyuan Wu, Kanok Boriboonsomsin, and Matthew J Barth. Eco-routing navigation system for electric vehicles. Technical report, Center for Environmental Research and Technology, University of California, Riverside, 2014.
- [129] Jerker Denrell and James G March. Adaptation as information restriction: The hot stove effect. *Organization Science*, 12(5):523–538, 2001.
- [130] Daniel Kahneman and Amos Tversky. Prospect theory: An analysis of decision under risk. *Econometrica: Journal of the Econometric Society*, pages 263–291, 1979.
- [131] Konstantinos V Katsikopoulos, Yawa Duse-Anthony, Donald L Fisher, and Susan A Duffy. Risk attitude reversals in drivers’ route choice when range of travel time information is provided. *Human Factors: The Journal of the Human Factors and Ergonomics Society*, 44(3):466–473, 2002.
- [132] Konstantinos V Katsikopoulos, Yawa Duse-Anthony, Donald L Fisher, and Susan A Duffy. The framing of drivers’ route choices when travel time information is provided under varying degrees of cognitive load. *Human Factors: The Journal of the Human Factors and Ergonomics Society*, 42(3):470–481, 2000.
- [133] Eran Ben-Elia, Ido Erev, and Yoram Shiftan. The combined effect of information and experience on drivers’ route-choice behavior. *Transportation*, 35(2):165–177, 2008.
- [134] Eran Ben-Elia and Yoram Shiftan. Which road do i take? a learning-based model of route-choice behavior with real-time information. *Transportation Research Part A: Policy and Practice*, 44(4):249–264, 2010.
- [135] Karthik K Srinivasan and Hani S Mahmassani. Modeling inertia and compliance mechanisms in route choice behavior under real-time information. *Transportation Research Record: Journal of the Transportation Research Board*, 1725(1):45–53, 2000.
- [136] Rong-Chang Jou, Soi-Hoi Lam, Yu-Hsin Liu, and Ke-Hong Chen. Route switching behavior on freeways with the provision of different types of real-time traffic information. *Transportation Research Part A: Policy and Practice*, 39(5):445–461, 2005.
- [137] Amalia Polydoropoulou, Moshe Ben-Akiva, and Isam Kaysi. Influence of traffic information on drivers’ route choice behavior. *Transportation Research Record: Journal of the Transportation Research Board*, 1453:56–65, 1994.
- [138] Karthik K Srinivasan and Hani S Mahmassani. Analyzing heterogeneity and unobserved structural effects in route-switching behavior under atis: a dynamic kernel logit formulation. *Transportation Research Part B: Methodological*, 37(9):793–814, 2003.

- [139] Enide AI Bogers, Francesco Viti, and Serge P Hoogendoorn. Joint modeling of advanced travel information service, habit, and learning impacts on route choice by laboratory simulator experiments. *Transportation Research Record: Journal of the Transportation Research Board*, 1926(1):189–197, 2005.
- [140] Aly M Tawfik and Hesham A Rakha. Latent class choice model of heterogeneous drivers’ route choice behavior based on learning in a real-world experiment. *Transportation Research Record: Journal of the Transportation Research Board*, 2334(1):84–94, 2013.
- [141] Erel Avineri and Joseph N Prashker. The impact of travel time information on travelers’ learning under uncertainty. *Transportation*, 33(4):393–408, 2006.
- [142] Hussein Dia. An agent-based approach to modelling driver route choice behaviour under the influence of real-time information. *Transportation Research Part C: Emerging Technologies*, 10(5):331–349, 2002.
- [143] Karthik K Srinivasan and Hani S Mahmassani. Role of congestion and information in trip-makers’ dynamic decision processes: Experimental investigation. *Transportation Research Record: Journal of the Transportation Research Board*, 1676(1):44–52, 1999.
- [144] Katrien Ramaekers, Sofie Reumers, Geert Wets, and Mario Cools. Modelling route choice decisions of car travellers using combined gps and diary data. *Networks and Spatial Economics*, 13(3):351–372, 2013.
- [145] Dominik Papinski, Darren M Scott, and Sean T Doherty. Exploring the route choice decision-making process: A comparison of planned and observed routes obtained using person-based gps. *Transportation research part F: traffic psychology and behaviour*, 12(4):347–358, 2009.
- [146] Hainan Li, Randall Guensler, and Jennifer Ogle. Analysis of morning commute route choice patterns using global positioning system-based vehicle activity data. *Transportation Research Record: Journal of the Transportation Research Board*, (1926):162–170, 2005.
- [147] Hani S Mahmassani and Rong-Chang Jou. Transferring insights into commuter behavior dynamics from laboratory experiments to field surveys. *Transportation Research Part A: Policy and Practice*, 34(4):243–260, 2000.
- [148] Aly Mohamed Aly Tawfik and Hesham Rakha. A real-world route choice experiment to investigate drivers perceptions and choices. In *Transportation Research Board 91st Annual Meeting, No. 12-3927, Washington D.C.*, 2012.
- [149] Mohamed A Abdel-Aty, Ryuichi Kitamura, and Paul P Jovanis. Using stated preference data for studying the effect of advanced traffic information on drivers’ route choice. *Transportation Research Part C: Emerging Technologies*, 5(1):39–50, 1997.

- [150] Emily Parkany, Ryan Gallagher, and Phillip Viveiros. Are attitudes important in travel choice? *Transportation Research Record: Journal of the Transportation Research Board*, 1894(1):127–139, 2004.
- [151] U.S. EPA and NHTSA. Final rules: Greenhouse gas emissions standards and fuel efficiency standards for medium and heavy-duty engines and vehicles. Technical report, Federal Register 76: 57106, 2011.
- [152] Emily Pindilli. Applications for the environment: Realtime information synthesis (AERIS) benefit-cost analysis. *United States Department of Transportation, Federal Highway Administration Office*, 2012.
- [153] Frank Lattemann, Konstantin Neiss, Stephan Terwen, and Thomas Connolly. The predictive cruise control: A system to reduce fuel consumption of heavy duty trucks. *SAE transactions*, 113(2):139–146, 2004.
- [154] K Dzenisiuk. Eco-driving-changing truck driver behavior to achieve long-term sustainability results. Master’s thesis, Copenhagen Business School, 2012.
- [155] Yutaka Takada, Shigeru Ueki, Akira Saito, Naoya Sawazu, and Yayoi Nagatomi. Improvement of fuel economy by eco-driving with devices for freight vehicles in real traffic conditions. Technical report, SAE Technical Paper, 2007.
- [156] H Christopher Frey, Nagui M Roupail, Haibo Zhai, Tiago L Farias, and Gonçalo A Gonçalves. Comparing real-world fuel consumption for diesel-and hydrogen-fueled transit buses and implication for emissions. *Transportation Research Part D*, 12(4):281–291, 2007.
- [157] Jiadong Guo, Yunshan Ge, Lijun Hao, Jianwei Tan, Zihang Peng, and Chuanzhen Zhang. Comparison of real-world fuel economy and emissions from parallel hybrid and conventional diesel buses fitted with selective catalytic reduction systems. *Applied Energy*, 159:433–441, 2015.
- [158] Matthew Barth, George Scora, and Theodore Younglove. Modal emissions model for heavy-duty diesel vehicles. *Transportation Research Record: Journal of the Transportation Research Board*, (1880):10–20, 2004.
- [159] David R Cocker, Sandip D Shah, Kent Johnson, J Wayne Miller, and Joseph M Norbeck. Development and application of a mobile laboratory for measuring emissions from diesel engines: 1. regulated gaseous emissions. *Environmental Science and Technology*, 38(7):2182–2189, 2004.
- [160] Jinghui Wang and Hesham A Rakha. Modeling fuel consumption of hybrid electric buses: Model development and comparison with conventional buses. *Transportation Research Record: Journal of the Transportation Research Board*, (2539):94–102, 2016.

- [161] Kyounggho Ahn, Hesham Rakha, and Kevin Moran. Eco-cruise control: Feasibility and initial testing. In *Transportation Research Board 90th Annual Meeting, No. 11-1031, Washington D.C.*, 2011.
- [162] Sangjun Park, Hesham Rakha, Kyounggho Ahn, and Kevin Moran. Predictive eco-cruise control: Algorithm and potential benefits. In *Integrated and Sustainable Transportation System (FISTS), 2011 IEEE Forum on*, pages 394–399. IEEE, 2011.
- [163] Shoichiro Watanabe and Takafumi Koseki. Energy-saving train scheduling diagram for automatically operated electric railway. *Journal of Rail Transport Planning & Management*, 5(3):183–193, 2015.
- [164] Arturo González-Gil, Roberto Palacin, and Paul Batty. Sustainable urban rail systems: Strategies and technologies for optimal management of regenerative braking energy. *Energy conversion and management*, 75:374–388, 2013.
- [165] Xuesong Feng. Optimization of target speeds of high-speed railway trains for traction energy saving and transport efficiency improvement. *Energy Policy*, 39(12):7658–7665, 2011.
- [166] Xuesong Feng, Baohua Mao, Xujie Feng, and Jia Feng. Study on the maximum operation speeds of metro trains for energy saving as well as transport efficiency improvement. *Energy*, 36(11):6577–6582, 2011.
- [167] Donald R Drew. Traffic flow theory and control. Technical report, 1968.
- [168] Rahmi Akçelik and DC Biggs. Acceleration profile models for vehicles in road traffic. *Transportation Science*, 21(1):36–54, 1987.
- [169] Michael S Varat and Stein E Husher. Vehicle impact response analysis through the use of accelerometer data. Technical report, SAE Technical Paper, 2000.
- [170] Martin Treiber, Ansgar Hennecke, and Dirk Helbing. Congested traffic states in empirical observations and microscopic simulations. *Physical review E*, 62(2):1805, 2000.
- [171] American Railway Engineering Association et al. *Manual for Railway Engineering*. American Railway Engineering Association, 1995.
- [172] American Railway Engineering Association et al. *Manual for Railway Engineering 1980-1981*. American Railway Engineering Association, 1980-1981.
- [173] Edward Charles Schmidt. *Freight Train Resistance: Its Relation to Car Weight*. Number 43. The University of Illinois, 1934.
- [174] John K Tuthill. *High Speed Freight Train Resistance: Its Relations to Average Car Weight*. Number 32. The University of Illinois, 1948.

- [175] Gregory Gould and Debbie Niemeier. Review of regional locomotive emission modeling and the constraints posed by activity data. *Transportation Research Record: Journal of the Transportation Research Board*, (2117):24–32, 2009.
- [176] Chevy Volt. Chevy volt tech watch: regenerative braking, 2011.
- [177] Kinh D Pham, Ralph S Thomas, and Xavier Ramirez. Traction power supply for the portland interstate max light rail extension. In *Transportation Research Circular E-C058: 9 th National Light Rail Transit Conference*, pages 669–677, 2004.
- [178] M Ceraolo and G Lutzemberger. Stationary and on-board storage systems to enhance energy and cost efficiency of tramways. *Journal of Power Sources*, 264:128–139, 2014.
- [179] Amedeo Frilli, Enrico Meli, Daniele Nocciolini, Luca Pugi, and Andrea Rindi. Energetic optimization of regenerative braking for high speed railway systems. *Energy Conversion and Management*, 129:200–215, 2016.
- [180] International Union of Railways. Regenerative braking for 50 hz, 25 kv systems, 2002, <http://www.railway-energy.org/tfee/index.php>.
- [181] M.D., sudhir, Braking green for mumbai trains, 2012, <http://blog.siemens.co.in/?p=4559>.
- [182] Bombardier. Bombardier environmental technologies help delhi metro achieve world-first under united nations-backed climate change initiative, <http://csr.bombardier.com/en/media-center/csr-news/25-bombardiers-environmental-technologies-help-delhimetro-achieve-world-first-under-united-nations-backed-climate-changeinitiative>. Accessed July 26, 2013.
- [183] Hassan Swidan. Integrating AIMSUN micro simulation model with portable emissions measurement system (PEMS): Calibration and validation case study. Master’s thesis, North Carolina State University, 2011.
- [184] Hesham Rakha and Weidong Wang. Procedure for calibrating Gipps car-following model. *Transportation Research Record: Journal of the Transportation Research Board*, (2124):113–124, 2009.
- [185] Robert E Chandler, Robert Herman, and Elliott W Montroll. Traffic dynamics: studies in car following. *Operations research*, 6(2):165–184, 1958.
- [186] Denos C Gazis, Robert Herman, and Richard W Rothery. Nonlinear follow-the-leader models of traffic flow. *Operations research*, 9(4):545–567, 1961.
- [187] Masako Bando, Katsuya Hasebe, Akihiro Nakayama, Akihiro Shibata, and Yuki Sugiyama. Dynamical model of traffic congestion and numerical simulation. *Physical review E*, 51(2):1035, 1995.

- [188] Rui Jiang, Qingsong Wu, and Zuojin Zhu. Full velocity difference model for a car-following theory. *Physical Review E*, 64(1):017101, 2001.
- [189] Gordon Frank Newell. A simplified car-following theory: a lower order model. *Transportation Research Part B: Methodological*, 36(3):195–205, 2002.
- [190] Irene Soria, Lily Elefteriadou, and Alexandra Kondyli. Assessment of car-following models by driver type and under different traffic, weather conditions using data from an instrumented vehicle. *Simulation modelling practice and theory*, 40:208–220, 2014.
- [191] Reiter Wiedemann and U Reiter. Microscopic traffic simulation: the simulation system mission, background and actual state. *Project ICARUS (V1052) Final Report*, 2:1–53, 1992.
- [192] SH Demarchi. A new formulation for Van Aerde’s speed-flow-density relationship. In *XVI Congress of Research and Education in Transportation*, pages 313–324, 2002.
- [193] GH Bham and RF Benekohal. Development, evaluation, and comparison of acceleration models. In *81st Annual Meeting of the Transportation Research Board, No. 02-3767, Washington, DC*, 2002.
- [194] Thomas A Dingus, Sheila G Klauer, Vicki L Neale, A Petersen, Suzanne E Lee, JD Sudweeks, MA Perez, J Hankey, DJ Ramsey, S Gupta, et al. The 100-car naturalistic driving study, phase II-results of the 100-car field experiment. Technical report, 2006.
- [195] John Sangster, Hesham Rakha, and Jianhe Du. Application of naturalistic driving data to modeling of driver car-following behavior. *Transportation Research Record: Journal of the Transportation Research Board*, (2390):20–33, 2013.
- [196] Guohua Song, Lei Yu, and Zhao Tu. Distribution characteristics of vehicle-specific power on urban restricted-access roadways. *Journal of Transportation Engineering*, 138(2):202–209, 2011.
- [197] Jinghui Wang and Hesham A Rakha. Convex fuel consumption model for diesel and hybrid buses. *Transportation Research Record: Journal of the Transportation Research Board*, No. 2647, 2017.
- [198] James William Fitch. Motor truck engineering handbook. *Training*, 2013:08–05, 1993.
- [199] Guoyuan Wu, Kanok Boriboonsomsin, and Matthew J. Barth. Eco-routing navigation system for electric vehicles. Technical report, University of California, Riverside, 2014.
- [200] LR Rilett, M Van Aerde, G MacKinnon, and M Krage. Simulating the TravTek route guidance logic using the INTEGRATION traffic model. In *Vehicle Navigation and Information Systems Conference*, volume 2, pages 775–787. IEEE, 1991.

- [201] Laurence R Rilett and Michel W Van Aerde. Modelling distributed real-time route guidance strategies in a traffic network that exhibits the braess paradox. In *Vehicle Navigation and Information Systems Conference*, volume 2, pages 577–587. IEEE, 1991.
- [202] Hesham Rakha and Yihua Zhang. INTEGRATION 2.30 framework for modeling lane-changing behavior in weaving sections. *Transportation Research Record: Journal of the Transportation Research Board*, (1883):140–149, 2004.
- [203] Mohamed A Elbadawy Abdelmegeed and Hesham Rakha. Heavy duty diesel truck emission modeling. In *Transportation Research Board 96th Annual Meeting, No. 17-0855, Washington D.C.*, 2017.